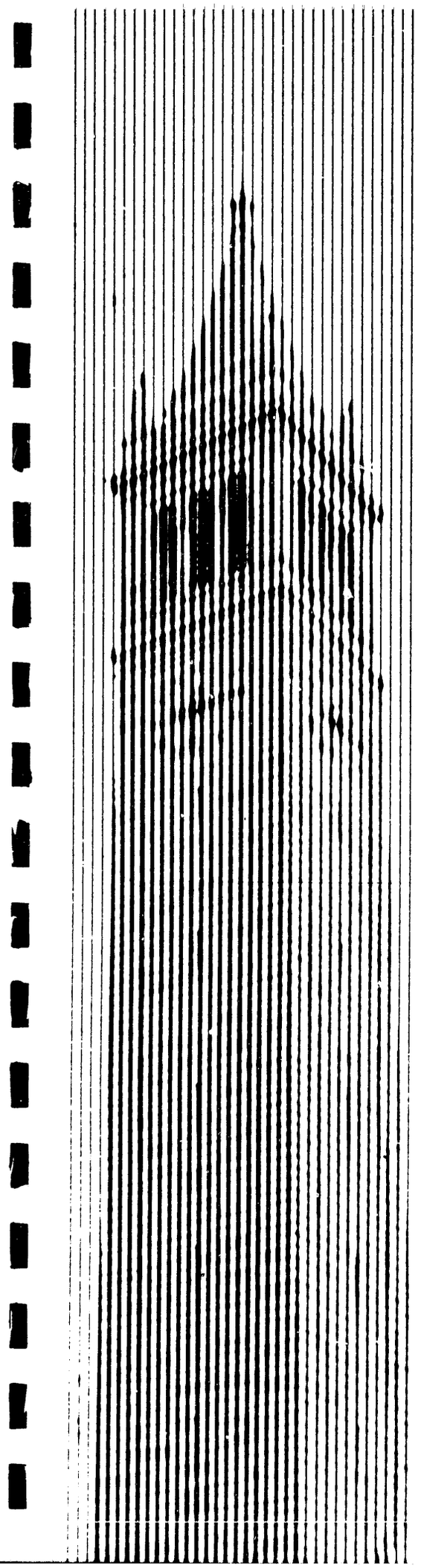

FINAL REPORT

CODE DEVELOPMENT INCORPORATING ENVIRONMENTAL, SAFETY, AND ECONOMIC ASPECTS OF FUSION REACTORS (FY 89-91)

Fusion Environmental and Safety Group,
Berkeley Fusion Engineering

Edited by S.K. Ho, T.K. Fowler, and J.P. Holdren

UC-BFE-027

November 1991

Work Supported by the U.S. Department of Energy
Contract Number DE-FG03-89ER52154

Berkeley Fusion Engineering

University of California at Berkeley

DOE/ER/52154--T4

DE92 004060

FINAL REPORT

CODE DEVELOPMENT INCORPORATING ENVIRONMENTAL, SAFETY, AND ECONOMIC ASPECTS OF FUSION REACTORS (FY 89-91)

Fusion Environmental and Safety Group,
Berkeley Fusion Engineering

Edited by S.K. Ho, T.K. Fowler, and J.P. Holdren

UC-BFE-027

November 1991

Work Supported by the U.S. Department of Energy
Contract Number DE-FG03-89ER52154

List of Project Participants

H.R. Beguiristian[1,5]
S. Brereton[2,6]
F. Brechtel[1,7]
R.B. Campbell[2,6]
Y. Chiba[2,5]
Z. Covaliu[1,8]
U. El-Saied[1,5]
T.K. Fowler[3,5]
E. Greenspan[2,5]
L.M. Grossman[3,5]
P. Hibbard[1,9]
S.K. Ho[4,5]
J.P. Holdren[3,9]
J. James[2,5]
A. Kinzig[1,9]
W. Kozukue[2,5]
R. Levinson[1,7]
Q. Nguyen[1,5,10]
R.M. Oliver[3,8]
F. Osaisai[1,5]
L.J. Perkins[2,6]
D. Sarigiannis[1,9]
H. Yang[1,8]

1. Graduate student
2. Guest participant
3. Professor, UCB
4. Assistant Research Engineer
5. Nuclear Engineering
6. Lawrence Livermore National Laboratory
7. Mechanical Engineering
8. Industrial Engineering and Operations Research
9. Energy and Resources Group
10. Department of Energy Fusion Technology Fellowship

Table of Contents

1. Overview	1
2. Activation Analysis	7
2.1 Computational Codes	7
2.2 Scaling Formulation for the Activation Radioactivity in a Silicon Carbide First Wall	8
2.3 Carbon-14 Analyses	14
3. Tritium Inventory	29
3.1 Dynamic Simulation Model	30
3.2 Simulation Results and Conclusions	38
4. Environmental and Safety Indices and Their Graphical Representation	48
4.1 Extension, Refinement, and Updating of ESECOM ES Indices	49
4.2 Graphical Representation of ES Indices	54
4.3 Streamlining, Modularization, and Automation	60
5. Probabilistic Risk Assessment (PRA) and Decision Analysis	66
5.1 Application of PRA to Fusion Reactor Design	66
5.2 A Simple Model PRA of Tritium Release Accidents	72
5.3 Application of Multi-Objective Decision Analysis to Fusion Reactor Design	80
6. Plasma Burn Control -- Application to ITER	92
6.1 Operating Point Control	92
6.2 Emergency Plasma Shutdown	105
7. Other Applications	115
7.1 Application to ARIES	115
7.2 PCA Case in ESECOM Scheme	120
7.3 Update of ESECOM Comparison of Fusion and Fission: Some Preliminary Considerations	130
8. Program Interactions	164
9. Publications and Theses	165
9.1 Theses Completed	165
9.2 Papers and Reports	165

1. OVERVIEW

This is the Final Report for a three-year (FY 89-91) study of the Environmental, Safety, and Economic (ESE) aspects of fusion energy systems, emphasizing development of computerized approaches suitable for incorporation as modules in fusion system design codes. The work -- which took as its starting point the results of the Senior Committee on Environmental, Safety, and Economic Aspects of Magnetic Fusion Energy (ESECOM), chaired by Holdren -- was funded by contract DE-FG03-89ER52154 ending November 1, 1991. A new proposal has been submitted for funding to continue this work.

The Berkeley Fusion Environmental and Safety group, which was formed to conduct this project, is now well-established. It consists of affiliated professors from three departments on campus (Nuclear Engineering, Energy and Resources Group, Industrial Engineering and Operations Research) and graduate students from these three departments as well as from Mechanical Engineering. Close ties have been established with the ITER design activity through LLNL and the ARIES project through UCLA. Dr. John Perkins of LLNL, active in ITER research, has been a regular participant in our bi-weekly group meetings.

The Berkeley group emphasizes as an ultimate goal the development of fast-running ESE computer models. Heretofore, calculation of radioactive inventories, release fractions, and doses has been so time consuming that only after-the-fact, point-design studies of specific, completed reactor designs have been feasible. Our long-term goal is to develop computationally fast system-code modules to carry out environmental and safety analyses in parallel with other engineering and plasma analyses now incorporated in systems codes. Only then will environmental and safety factors have a direct and interactive impact on fusion reactor design at a system level. It was recognized in the original three-year grant proposal that achieving this ambitious goal might take five or more years. Halfway there, we are now confident that we will indeed achieve system-code application of our computer modeling effort within the next two or three years.

Another function of the Berkeley Fusion Environmental and Safety group is as an independent, academically based group of experts in a field of increasing importance as work proceeds on the International Thermonuclear Experimental Reactor (ITER). In our original grant proposal in 1988, we made the following observation: "The ITER design effort has established an international timetable for confronting fusion reactor engineering issues three to five years from now. One can already anticipate that a decision to proceed or not proceed on a multi-billion dollar engineering test reactor will engender intense debate on the merits of fusion as an energy source, including inevitable comparisons with fission on ESE issues." This has come to pass, as evidenced by the prominence of environmental and safety concerns in the report of the Fusion Policy Advisory Committee (FPAC) in the U.S.; the reports of the European Community study of environmental and economic potential of fusion (EEF) and the European Fusion Programme Evaluation Board (FPEB); and increasingly in the ITER project through U.S. influence on the ITER Scientific and Technical Advisory Committee (ISTAC) and in the recent U.S. ITER review. The Principal Investigators were intimately involved in this process: Fowler as a member of the FPAC and ISTAC, Holdren as a consultant to the EEF study and as a member of the U.S. ITER Review Panel. It can be anticipated that environmental and safety concerns will only intensify during the coming ITER Engineering Design Activity.

Considerable progress has been made on the overall objectives of the original grant proposal. This work has been reported in 26 publications including M.S. theses, journal

publications, conference papers, laboratory reports, and semi-annual reports, as listed in Section 9.

A critical step in the development of environmental and safety (ES) system code modules is the capability to model computationally fast ES modules to allow for many design iterations. During the last two years, we have made considerable progress toward fast radioactive-inventory calculations following two approaches. The first and presently our primary approach is the formulation of approximate scaling equations containing parameters that are determined by regression scaling of numerical data obtained from Monte Carlo transport calculations, much as plasma design formulae are generated from the experimental database. Generating the neutronics database requires numerous calculations and substantial computing time. However, reducing this extensive database to scaling equations would fulfill our goal of constructing fast ESE computer models suitable to be incorporated as integral, interactive components of the systems codes. The initial evaluation of this approach, applied to modeling a silicon carbide first wall (as proposed for ARIES-I), is encouraging. Our second, backup approach, and one that may also speed up neutronics database calculations, is adaptation of an existing discrete-ordinates diffusion code, ANISN.

In addition to computer modules to carry out the primary ESE analysis, we have also made progress on improved indices for characterization of reactor-accident hazards, remote maintenance requirements, and radioactive-waste management burdens. Our improvements include addition of further fusion-relevant isotopes, corrections and refinements to the dispersion and dosimetry models underlying the calculations of indices, computational streamlining of the relevant codes, development of an array of graphical indices of hazard potential more comprehensive and more illuminating than what was available from the ESECOM study, and modularization of the relevant computer codes for ease of execution and integration with fusion-reactor systems codes. These improvements have been put to use in assessing the environmental and safety characteristics of ARIES designs and stainless-steel-structure variants of ESECOM designs, and in comparing these additional cases with the array of designs studied by ESECOM.

We have also made substantial progress on several special topics related to ESE assessment: confirmation of carbon-14 build up observed in some ESECOM cases and identification of the mechanism by which C-14 is produced; development of a fast code for dynamic simulation of tritium inventories in fusion reactors; investigation of potential applications of probabilistic risk assessment and decision analysis in our work; and participation in ITER work on plasma burn control and emergency plasma shutdown.

A simplified overview of our code development efforts is sketched in Fig. 1.1. As already noted, the major environmental and safety tasks include activation analysis, tritium inventory evaluation, radiological dose conversion, development of safety indices, and plasma burn control and emergency shutdown. The integration of these modules into tokamak systems codes and optimization of the resulting package will be implemented after completion of the various tasks. We are also exploring applications of probabilistic risk assessment and decision analysis as reported in Section 5.

We have examined several tokamak systems codes as drivers for the tokamak reactor studies. As a learning exercise, we first became familiar with the simplified GENEROMAK code utilized in ESECOM studies. In doing so a useful output was the conversion of this code into a Fortran version that can run on both PC's and mainframes. This work is documented in publication number 5 (see Section 9.2).

By now we have also become familiar with and utilized more elaborate tokamak systems codes, specifically TETRA and SUPERCODE. The TETRA code was used extensively for the ITER design work, while the SUPERCODE is under development for future ITER design applications. It is expected that these tokamak systems codes will be important vehicles for the integration of our environmental and safety modules in the future.

To date, our current main focus has been on the development of the individual environmental and safety modules compatible with the tokamak systems codes. This involves deriving new models and figures of merit, streamlining and integrating existing computer codes, and testing alternative approaches and calculational algorithms. Our accomplishments thus far will be described in subsequent sections. A summary of the highlights of the program is shown in Table 1.1.

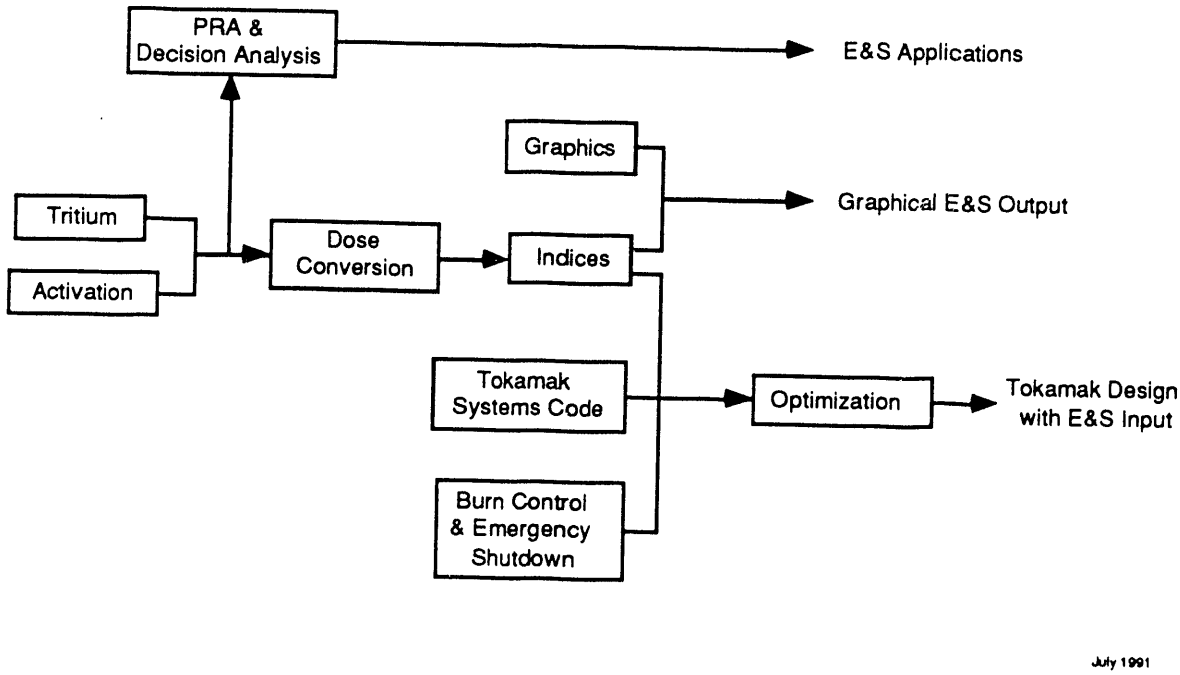

Figure 1.1. Schematic flowchart of the organization and integration of work tasks.

Table 1.1. Program highlights.

Activation Analysis and Tritium Inventory:

Assessment of carbon-14 production in fusion reactor components; survey of control techniques for C-14.

Acquisition of neutron activation codes (TART and ANISN); extensive use of TART to develop activation database.

Derivation, from regression data fitting, of a scaling formulation of the radioactivity inventory of a silicon carbide fusion reactor first wall.

Development of a fast dynamic simulation of tritium inventories in fusion reactors.

Representation of Safety and Environmental Characteristics:

Improvement of computer codes for calculation of environmental and safety indices.

Development of graphical representations of environmental and safety characteristics.

Preliminary investigation of the application of probabilistic risk assessment (PRA) to radiological hazards of fusion reactor accidents.

Programmatic Applications:

ITER--

Studies of ITER operating point control and plasma burn control.

Investigation of plasma emergency shutdown for ITER.

ARIES--

Calculation of radioactive inventories and radiological hazards for an ARIES-I reactor design candidate.

Comparison of environmental and safety performance of an ARIES-I-type fusion reactor (D-T fuel and silicon carbide structure) and an ARIES-III-type fusion reactor (D-^{3}He fuel and ferritic steel structure).

Assessment of fueling schemes for the ARIES-III reactor design.

Code Integration and Other Activities:

Production of a Fortran version of the GENEROMAK code to run on both PCs and mainframes.

Table 1.1 (continued)

	Calculation of environmental and safety indices for PCA stainless steel variant of ESECOM reactor design.
	Preliminary studies of heat conduction for graphite and tungsten divertors.
	Preliminary assessment of environmental and safety characteristics of recent advanced fission reactor designs in relation to fusion characteristics.
	Critique of the December 1989 report of the EEF, Commission of European Community, on "Environmental, Safety-Related, and Economic Potential of Fusion Power."

2. ACTIVATION ANALYSIS

Calculating activation radioactive inventories involves neutron transport calculations in realistic geometry. As stated in Section 1, simply adding conventional Monte Carlo neutron transport codes to systems codes is impractical because of the computer time required, and even diffusion codes such as ANISN may require too much running time. Therefore we have given considerable attention to a different approach in which the accurate Monte Carlo code TART is used to generate a database for various machine design parameters and various choices of materials. Several methods are being evaluated for utilizing this database on-line during the systems design process. As indicated in Figure 1.1, these include graphical displays to provide immediate information for decisions by the designer as well as more ambitious computer optimization procedures that help to guide the design iteratively toward pre-determined objectives. The database information itself can be provided in the form of table look-up; approximate solutions fitted to exact solutions; and finally the regression scaling concept mentioned in Section 1, whereby environmental and safety indices are parameterized and fitted by regression analysis of the many cases that make up the database.

Preliminary analysis indicates that the regression scaling approach is promising. A specific example calculation is discussed in Section 2.2 following a discussion in Section 2.1 of the computer codes used to develop an activation database. Some issues concerning the activation product carbon-14 are discussed in Section 2.3.

2.1 COMPUTATIONAL CODES

The neutron activation problem can be calculated by two conventional types of neutron transport codes, namely, the Monte Carlo and the discrete ordinates schemes. The two types of codes are briefly described here.

In the Monte Carlo approach, a set of computer codes TART,[2.1] ORLIB,[2.2] and FORIG[2.3] and their associated databases are used. These codes were also used in the ESECOM studies in calculating the neutron activation radioactivity.

The tokamak configuration is approximated as a set of concentric cylinders consisting of the plasma, first wall, blanket, and shield regions. The length of the cylinder is determined such that the volumes of the cylindrical layers are approximately equal to that in the real toroidal design configuration.

The neutron transport simulations are calculated by the Monte Carlo code TART. It determines the neutron and gamma spectra in the various regions of the tokamak by following neutrons and tracking their energies in three spatial dimensions. We used 20 samples with 2000 particles per sample in each run.

The neutron spectra in various zones of a tokamak are input into the ORLIB code. The code then integrates the neutron spectra to obtain space- and energy- averaged neutron fluxes. This information is then utilized to evaluate tables of neutron-flux-averaged nuclear reaction cross sections for a very complete list of reactions and materials.

The FORIG code calculates, in each reactor component, the nuclide generation and depletion by the decay, neutron activation, and neutron absorption processes. It uses a point model with the space- and energy- averaged reaction cross sections from ORLIB to solve for a set of coupled differential equations.

Among the three codes, the Monte Carlo code TART consumes the most computer time. It requires about 5 to 10 minutes CPU time for each run on the NERSC Cray computers.

This set of Monte Carlo transport codes is very accurate in computing the activation radioactive inventory, but at the expense of large computer run time. We have used these codes to calculate the activation radioactivity for various tokamak reactor designs. Examples of their application to ARIES-type reactor design candidates will be presented in Section 7.1.

We have also investigated the neutron activation problem by using a discrete ordinates neutron transport code ANISN.[2.4] The code solves the one-dimensional Boltzmann transport equation for neutrons and gamma rays for anisotropic scattering in slab, sphere, or cylinder geometry. The solution is obtained by a discrete-ordinates discretization of the anisotropic multigroup transport equation using step or weighted differencing for the spatial coordinate. The energy-group and space dependent flux generated may then be used to obtain group-weighted cross sections for activation calculations.

A version of ANISN obtained from the RSIC Computer Code Collection of Oak Ridge National Laboratory called ANISN-ORNL-CCC-254[2.4] is used for this project. The running time for sample problems on a PC 386 varied from several minutes to a maximum of thirty minutes. Special forms of cross-section library for materials of interest to fusion reactor systems are being investigated.

2.2 SCALING FORMULATION FOR THE ACTIVATION RADIOACTIVITY IN A SILICON CARBIDE FIRST WALL

In this work, we study the feasibility of formulating approximate scaling equations to evaluate the neutron activation radioactivity inventory in a fusion reactor. As a first step, we have studied the activation of the silicon carbide composite as the first wall of a fusion reactor.

Evaluating the activation of the first wall is comparatively simpler than that of the blanket because the range of the thickness of a first wall is very small, hence the variations of radioactivity is not too drastic. All the incoming neutrons have the same fusion-born energy at 14 MeV. Silicon carbide (SiC) is studied primarily for two reasons: (1) its low activation property and the corresponding interest in it in reactor design studies such as the ARIES work, and (2) a relatively small number of nuclides make up the majority of the radiological hazards, therefore minimizing the amount of data regression required to determine the scaling equations.

Since all other figures of merit can be derived from the radioactivity inventories of all the activation products, the scaling equations are a potentially powerful tool for comparing different tokamak designs. Of course, the usefulness of the scaling equations is

directly proportional to their generality. Significant progress has been made in this direction.

2.2.1 Activation Physics

In this section, we briefly look at the neutron activation physics to have some qualitative understanding of the functional form of the activation radioactivity. The neutron activation processes in general are schematically shown in the following sequences:

$$n + A \longrightarrow B \xrightarrow{\lambda_B} D$$

$$n + B \longrightarrow C \xrightarrow{\lambda_C} E$$

Nuclide B is produced by a direct neutron activation with a target material nuclide A, whereas nuclide C is generated by involving two-step activation reactions with an intermediate activation product B. Both nuclides D and E result from decays after the nuclear reactions. There are many possible reactions or chains of reactions to generate various radionuclides.

The equations governing these sequences of reactions and the solutions of the number of nuclides B and C are as follows:

$$\frac{dN_B}{dt} = \Phi \sigma_{AB} N_A - \lambda_B N_B - \Phi \sigma_{BC} N_B \qquad (2.1)$$

$$\frac{dN_C}{dt} = \Phi \sigma_{BC} N_B - \lambda_C N_C \qquad (2.2)$$

$$N_B = \frac{\Phi \sigma_{AB} N_A}{\lambda_B + \Phi \sigma_{BC}} (1 - \exp\{ -(\lambda_B + \Phi \sigma_{BC}) t \}) \qquad (2.3)$$

$$N_C = \frac{\Phi^2 \sigma_{AB} \sigma_{BC} N_A}{(\lambda_B + \Phi \sigma_{BC}) \lambda_C} F(\Phi, \sigma_{BC}, \lambda_B, \lambda_C, t) \qquad (2.4)$$

where N_i and λ_i denote the number and decay constant of nuclide i, σ_{ij} is the reaction cross section for transforming nuclide i into nuclide j, Φ is the neutron flux, and F is a time dependent function for nuclide C.

For simplicity, we neglect the time dependence by assuming conditions at a very long time for the following analysis. We observe that the radioactivity of nuclide B ($\lambda_B N_B$) is simply $\Phi \sigma_{AB} N_A$ if $\Phi \sigma_{BC} << \lambda_B$. This can be the case for a low neutron flux irradiation and/or if nuclide B has a relatively higher decay rate than activation reaction. On the other hand, if the neutron flux is high and/or the decay rate is low, the radioactivity of nuclide B is independent of the flux. Similarly for the multi-process activation product nuclide C, the radioactivity may depend on the flux, square of the flux, or non-linear combinations of the flux, depending on the properties of the individual nuclides and the irradiation conditions.

Hence, it is very helpful to have some prior knowledge of the radioactive properties of the activation target nuclides and the relevant nuclear reactions. This will enhance the regression fitting and the formulation of simplified scaling equations to evaluate radioactivity as discussed in later sections.

2.2.2 Neutronics Results

We have generated numerical results for the neutron activation of SiC from the neutron transport and activation codes TART, ORLIB, and FORIG by varying the input variables in order to determine the functional form of the dependent variables. The variations of the neutron flux and reaction cross sections with the tokamak input parameters (thickness and density of the various first wall and blanket materials, tokamak geometrical factors, and neutron wall loading, etc) are studied from this database.

We illustrate here, using the silicon carbide first wall activation cross section of Si-28 to Al-28 as an example, the application of the neutronics database to the task of constructing a scaling equation. The activation cross section for a particular nuclear reaction is only a function of the neutron energy, which in turn depends mainly on the first wall density ρ and thickness δ. Hence, it can be represented as

$$\sigma = g_1(\rho)\, g_2(\delta) \tag{2.5}$$

The variations of the neutron activation cross section with both the first wall density and thickness in the relevant range anticipated in a reactor design can be calculated by the neutron transport codes. We can then use regression fitting to correlate this data in some simple power formulations. The activation cross section for Si^{28} is found to vary as:

$$\sigma \propto \rho^{-0.117} \tag{2.6}$$

$$\sigma \propto \delta^{-0.121} \tag{2.7}$$

The Si-28 activation cross section is larger at higher neutron energy in the range of interest. There are more neutrons slowing down for increasing first wall density or thickness, resulting in a slightly lower neutron energy spectrum. This is reflected in the reduction of the averaged activation cross section for increasing first wall density and thickness. However, the difference is not very large because the range of variations is limited by the nature of the first wall.

We have also verified numerically the theoretical prediction that the neutron flux is linearly proportional to the neutron source strength S_n, and inversely proportional to the plasma radius r_p and the tokamak major radius R in our cylindrical-geometry model. Hence, the neutron flux in the first wall has the functional dependence,

$$\Phi = S_n\ f_1(\rho)\, f_2(\delta) / r_p\, R \tag{2.8}$$

The functions $f_1(\rho)$ and $f_2(\delta)$ include the variations of the average neutron flux due to both the first wall density and thickness. These functions can be determined similarly as illustrated above for the activation cross section.

2.2.3 Scaling Equations

The first step in the study is to determine the activation products contributing most significantly to dose. In particular, we are interested in evaluating the critical, chronic, and intruder doses (see ESECOM[2.5] report), as well as afterheat. The various doses can be calculated as:

$$\text{Dose}_j = \Sigma_i \, (DC)_{ij} \, A_i \tag{2.9}$$

where $(DC)_{ij}$ is the dose conversion factor for the i-th radionuclide to the j-th dose, which has to be evaluated by a radiological dose conversion code.[2.6] The summation in Eq. (2.9) is over all the activation product radionuclides. By checking the various contributions of the individual nuclides to the doses, we can find out the dominant nuclides that should be included. For the SiC first wall, only the eight nuclides listed in Table 2.1 contribute significantly to the four hazard indices mentioned above.

The saturated radioactivity of a single-step reaction can be expressed as,

$$A = \Phi \, \sigma \, N_p \tag{2.10}$$

where σ is the microscopic reaction cross section for the activation reaction, N_p is the number of target material atoms. The number of target material atoms can be found simply from the multiplication of the first wall volume and density, with a weight-to-atom number conversion factor C,

$$N_p = C \, R \, (2 \, r_p \, \delta + \delta^2) \, \rho \tag{2.11}$$

It is assumed that the variations in blanket design have negligible effect on the first wall radioactivity except for the thermal neutron reactions, which are accounted for by correction factors to the first wall scaling equations. We have used a 0 - 40% by atom ratio of tritium breeding materials, the balance consisting of structural materials and coolants.

We can combine the analytical results and the numerically fitted equations, and replace the neutron source strength with its equivalent fusion power. Hence, we can formulate scaling equations which calculate the per-nuclide contribution to the radioactivity in the first wall as a function of fusion power (P_{fus}), first wall thickness (δ) and density (ρ), tokamak major and minor radii (R and r_p), and a data-fitting constant (K) as shown in Eq. (2.12). The radionuclides Na-24 and Al-26 are produced from two-step activation-reactions, so the relation describing their activity is slightly different as indicated in Eq. (2.13). The values of K, x, and y for each nuclide are listed in Table 2.1.

$$A = K \, P_{fus} \, \delta^x \, \rho^y \, (1 + \delta / 2 \, r_p) \tag{2.12}$$

$$A = K \, P_{fus}^2 \, \delta^x \, \rho^y \, (1 + \delta / 2 \, r_p) / (r_p \, R) \tag{2.13}$$

where A is in Ci, P_{fus} is in MW, δ and r_p are in cm, and ρ is in g/cm^3. The constants in these scaling equations are obtained by averaging the numerical data.

Table 2.1. Significant activation products in a SiC first wall and the associated empirical coefficients and exponents from data regression in Eqs. (2.12) and (2.13).

Nuclide	x	y	K
Be-10	0.85	0.84	4.60e-4
C-14	0.93	0.96	8.67e-4
Mg-27	0.81	0.84	9.71e2
Al-28	0.83	0.85	1.07e5
Al-29	0.83	0.85	5.13e3
Co-60	1.18	1.19	5.60e-2
Na-24*	0.62	0.68	2.86e-2
Al-26*	0.58	0.65	6.76e-9

* Radioactivity of these nuclides are determined from Eq. (2.13), all other radioactivities are calculated from Eq. (2.12).

We have also studied the effects of changing other system parameters, like the blanket or divertor modules, on the activation radioactivity of the first wall. These effects will be incorporated as higher order correction factors to the above scaling equations. The coupling of the first wall with either the blanket or divertor modules is through the modification of the resulting neutron spectrum in the first wall. The magnitude of the neutron flux and the neutron-energy dependent reaction cross sections within the first wall are changed in the process.

In general, the fast neutron spectrum is not much affected by the blanket region. On the other hand, the thermal neutron spectrum is very sensitive to the blanket configuration, as many neutrons are thermalized and reflected back into the first wall by the blanket. As a result, fast-neutron activation reactions are almost independent of the blanket design while the thermal-neutron activation processes are strongly dependent on the geometry and composition of the blanket. Among the major nuclides listed in Table 2.1, only C-14 and Co-60 are mainly produced by thermal-neutron activations. Hence, modifications to the scaling equations are required for C-14 and Co-60 with respect to the blanket system parameters. We have also studied the effect of divertors attenuating the incoming neutron flux into the first wall. Correction factors are also formulated to include this effect.

As an example, we illustrate the variations of Co-60 activity in a SiC first wall due to changes in thickness and lithium composition in the blanket. Figure 2.1 indicates that the radioactivity of Co-60 in the first wall is quite sensitive to changes in the relative abundance of lithium in the blanket. This is due to the fact that lithium has a very large thermal neutron absorption cross section. The presence of lithium in the blanket can greatly reduce the thermal neutron population. We also find that there is a threshold blanket thickness beyond which the effect of blanket thickness is negligible for any given lithium composition. The moderating and scattering processes are saturated at this threshold thickness, and the neutron transport behaves like that in an infinite medium.

Using the data shown in Fig. 2.1, we have constructed correction factor to quantify the modifications in the first wall radioactivity from Co-60 due to the variations of the composition of lithium (c, Li fraction in atom ratio) in the blanket and the blanket thickness (δB, in cm). The radioactivity of Co-60 is then given by,

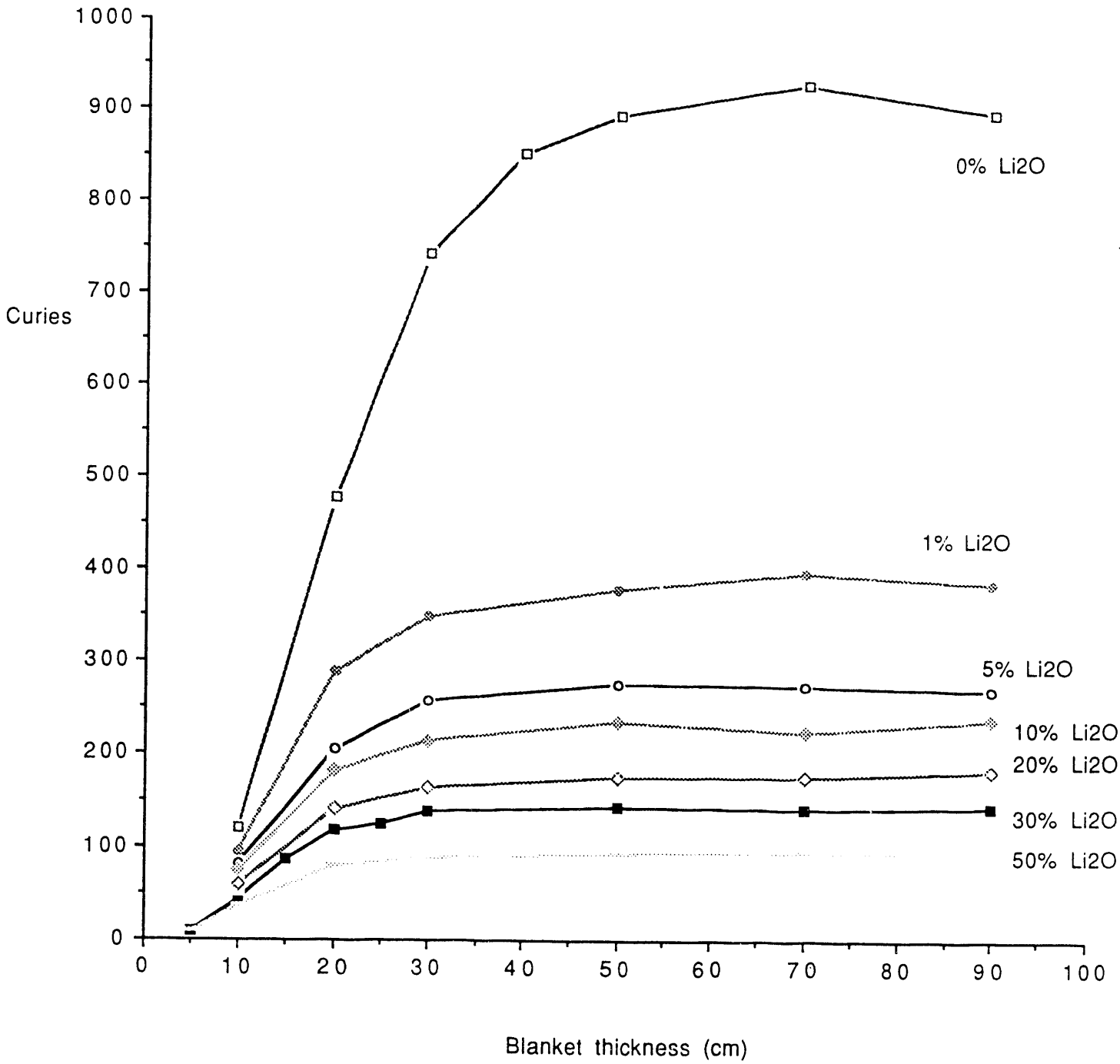

Figure 2.1. Variations of radioactivity of Co-60 in a SiC first wall with blanket thickness and lithium composition.

$$A_{Co\text{-}60}(c, \delta B) = A_{ref}\ CF(c, \delta B) \qquad (2.14)$$

where A_{ref} is given by Eq. (2.12) and $CF(c, \delta B)$ is calculated from,

$$CF(c, \delta B) = \text{Minimum}\ (CF_{sat}, S\ \delta B) \qquad (2.15)$$

with
$$CF_{sat} = \begin{cases} 5.583 & c = 0 \\ 2.362\ (1 - 6.45\times10^{-2}\ c + 2.46\times10^{-2}\ c^2 - 3.18\times10^{-5}\ c^3) & c > 0 \end{cases}$$

$$S = \begin{cases} 0.1616 & c = 0 \\ 0.08836\ (1 - 4.49\times10^{-2}\ c + 8.64\times10^{-4}\ c^2) & 10 \geq c > 0 \\ 0.07247\ (1 - 2.53\times10^{-2}\ c + 3.02\times10^{-4}\ c^2) & c > 10 \end{cases}$$

By analyzing the data for various system parameters, we can formulate correction factors to account for the effects due to these system parameters in our approximation of first wall radioactivity. We are currently working on data regression to generate equations describing these trends. A complete set of scaling equations for fast computational purpose of the silicon carbide first wall activation radioactivity will be issued in a future report.

2.2.4 Summary

Conventionally, the neutron activation reactions are calculated by large computer codes, which cannot be implemented into a systems code due to their long running time. We have examined various alternative approaches to overcome this problem. We find a promising scheme of regression fitting of numerical neutronics data from detailed activation calculations into some approximate scaling equations.

We used the silicon carbide first wall as an example to demonstrate the methodology and feasibility of such a scaling formulation approach. Simple scaling equations are obtained to evaluate the radioactivity in the silicon carbide first wall with good accuracy.

Future work will be extended to study radioactivity inventories in other materials and various reactor components. A collection of these scaling equations will enable efficient calculations of activation radioactivity in a reactor systems code. Hence we can have the ability to treat various reactor component materials as design input variables to evaluate environmental and safety issues in the systems studies phase of a design.

2.3 CARBON-14 ANALYSES

The neutron-activation calculations done for a range of conceptual fusion-reactor designs in the ESECOM study[2.5] yielded a widely varying set of production rates for carbon-14 in different designs and components, exceeding reactor totals of 200 Ci/year in four of the designs. These ESECOM results for carbon-14 production are summarized in Table 2.2. For comparison, calculated C-14 production rates for contemporary fission reactors -- pressurized-water reactors (PWRs) and boiling-water reactors (BWRs) -- fall in

the range of 15 to 45 Ci per 1-GWe reactor-year.[2.7] The distribution of these production figures by component and reaction is shown in Table 2.3.

Table 2.2. ESECOM results for C-14 production.

Reactor	Component	Materials	Ci C-14 per year
V-Li tokamak	breeder	Li	not calculated
	other blanket	V-Cr-Ti, Fe-Cr-V alloys	167
	shield	Fe-Cr-V alloy	64
RAF-He tokamak	breeder	Li_2O	282
	other blanket	ferritic steel	4
	shield	Fe-Cr-V alloy	35
RAF-LiPb RFP	breeder	LiPb	73
	other blanket	ferritic steel	10
	shield	Fe-Cr-V alloy	1
V-Li RFP	breeder	Li	not calculated
	other blanket	V-Cr-Ti alloy	8
	shield	V-Cr-Ti, Fe-Cr-V alloys	351
SiC-He tokamak	breeder	Li_2O	237
	other blanket	SiC	7
	shield	Al	0.2
V-FLiBe tokamak	breeder	FLiBe	32
	other blanket	V-Cr-Ti alloy	6
	shield	Ni-Fe-Cr alloy	0.01
D-^{3}He tokamak	breeder	none	0
	other blanket	V-Cr-Ti alloy	1.2
	shield	Fe-Cr-V alloy	0.054

Table 2.3. C-14 production rates in fission reactors (Ci/GWe-yr).

Reactor Type	Production rate in coolant from reactions on		Production rate in fuel from reactions on		Total Product Rate
	N-14	O-17	N-14	O-17	
BWR	0.3-1.3	9-12	11-21	3-11	30-44
PWR	0.1-1.3	3-10	8-18	3-7	20-30

When C-14 is released to the environment, the isotope mixes gradually with the carbon reservoirs in the atmosphere, hydrosphere, and biota; estimates of the ultimate population dose, which is delivered on a timescale of a few C-14 half-lives or some tens of thousands of years, are in the range of 500 rem per curie released.[2.8] Although the corresponding dose rates are extremely low, consideration of the cumulative effect under the assumption of a linear dose-response relation has led to regulatory interest in restricting the emissions of C-14 even from fission reactors. If the ESECOM calculations of C-14 production in fusion reactors are correct, those fusion designs with the higher C-14 production rates are therefore quite likely to require technologies for capturing and sequestering the C-14.

In the present work, therefore, we sought to confirm that the ESECOM figures for C-14 production are realistic and not the result of some artifact or flaw in the neutronics codes and cross-section libraries, and we surveyed the techniques available for capturing C-14 in order to avoid its release.

2.3.1 Explanation of C-14 Production Rates in ESECOM Cases

The reactions that can account for the production of C-14 involve neutron bombardment of isotopes of carbon, nitrogen, and oxygen, as shown in Table 2.4.[2.9] Clearly, the most important reaction in air is that on N-14. The most important reaction in H_2O or Li_2O is that on O-17 (isotopic abundance 3.9e-4) except when N is present as a contaminant at greater than 40 ppm. The reaction on N-14 can also be important in metallic alloys containing N as a contaminant.

Table 2.4. Effective cross sections for C-14 formation.

	Effective Cross Section (barns = 10^{-24} cm^2)			
Reaction	thermal neutrons	LWR spectrum	HTGR spectrum	LMFBR spectrum
13C(n,g)14C	9.0e-4	1.0e-3	4.0e-4	5.0e-7
14N(n,p)14C	1.8	1.5	1.0	1.3e-2
15N(n,d)14C	0	0	0	1.0e-3
16O(n,3He)14C	0	0	0	5.0e-8
17O(n,4He)14C	0.24	0.18	0.11	1.2e-4

Examination of the neutronics calculations for the ESECOM cases showed that, indeed:

(a) in cases not containing oxygen in the breeder, the C-14 comes almost entirely from reactions on N-14 present in metals as a contaminant (e.g., the VCrTi alloy used in several ESECOM blankets was assumed to contain 100 ppm N and the FeCrV alloy 150 ppm);
(b) in cases with Li_2O breeder, the reaction on O-17 accounts for most of the C-14.

The high C-14 production in the shield of the V/Li reversed-field pinch results from the combination of N in the shield alloys and the high neutron flux remaining at the shield because of the unusual thinness of the blanket in this case.

The results for two ESECOM cases examined in detail -- the reduced-activation-ferritic (RAF)/He tokamak, and the SiC/He tokamak -- are shown in Table 2.5. Close inspection of these results shows that the ESECOM figures for C-14 production are correct and not the results of errors or idiosyncrasies in the neutronics codes.

2.3.2 Chemical Form of Carbon-14 in Lithium Oxide

In attempting to investigate the pathways of carbon-14 produced within the lithium oxide breeder to the environment, it is pertinent to understand the chemical form in which it exists, because its mobility depends on its chemical state. In a lithium oxide matrix, depending on the oxygen potential, carbon could be in any of three possible states—C, CO and CO_2.

For every lithium atom destroyed, one-half of an oxygen atom is dislodged. The oxygen atom could exist in the atomic state until it sees a like atom to form O_2 gas. It may also combine with other atomic species to form oxides depending on the energetics and kinetics of the reaction. Species in the matrix which could react with oxygen are C-14 and tritium.

Assuming a breeder temperature of 700°C, the Gibb's free energy of formation of CO_2 from carbon and oxygen is -230 kcal/mole, while the equivalent value for formation of H_2O (in this case, T_2O) is -92 kcal/mole.[2.10] In view of the relative amounts of oxygen and carbon-14 produced in the breeder, the thermodynamics strongly favors oxidation of the carbon. However, the constraints imposed by kinetics limitations cannot be adequately addressed here due to the lack of data on diffusion properties of carbon and its oxides in lithium oxide. Even if all the carbon-14 produced in the lithium oxide matrix was in the oxide form, we cannot meaningfully estimate how fast and how much of it could be released from the breeder.

Therefore, in this analysis we assume that all of the carbon-14 produced in the Li_2O stays in the breeder until the Li_2O is processed to recover the tritium. The carbon-14 in this scenario will therefore be off-gassed as carbon dioxide. The treatment systems evaluated here are therefore those based on isolation of the carbon dioxide from the gaseous effluents.

Table 2.5a. Carbon-14 production in the RAF-He/TOK.

Zone	Material	volume fraction of mat'l	Zone Volume (cm3)	Flux (#/s*cm2)	Reaction	x-sect (barns)	#dens of reaction isotope in mat'l (#/cm3)	14C Production (Ci/yr)	Total 14C Production (Ci/yr)	ESECOM Production (Ci/yr)
3 First Wall	modht9	0.12	4.131E+07	1.207E+15	13C(n,g)14C	1.936E-05	6.426E+18	0.002		
					14N(n,p)14C	2.103E-02	3.297E+18	1.36	Included In blanket	
					17O(n,a)14C	9.117E-02	7.707E+15	0.014		
	He	0.88			13C(n,g)14C					
					14N(n,p)14C					
					17O(n,a)14C					
4 Blanket 1	modht9	0.08	3.359E+08	4.816E+14	13C(n,g)14C	1.752E-05	6.426E+18	0.00		
					14N(n,p)14C	1.551E-02	3.297E+18	2.16	Included In blanket	
					17O(n,a)14C	5.306E-02	7.707E+15	0.02		
	He	0.11			13C(n,g)14C					
					14N(n,p)14C					
					17O(n,a)14C					
	LI2O	0.81			13C(n,g)14C					
					14N(n,p)14C				Included in coolant/ breeder	
					17O(n,a)14C	5.306E-02	1.227E+19	279		
5 Blanket 2	modht9	0.29	9.733E+07	8.093E+13	13C(n,g)14C	1.385E-05	6.426E+18	0.001		
					14N(n,p)14C	9.576E-03	3.297E+18	0.24	Included In blanket	
					17O(n,a)14C	1.915E-02	7.707E+15	0.001		
	He	0.08			13C(n,g)14C					
					14N(n,p)14C					
					17O(n,a)14C					
	LI2O	0.63			13C(n,g)14C					
					14N(n,p)14C				coolant/ breeder	
					17O(n,a)14C	1.915E-02	1.228E+19	3.82	283	282
6 Manifold	modht9	0.2	1.869E+08	4.290E+13	13C(n,g)14C	1.950E-05	6.426E+18	0.001		
					14N(n,p)14C	2.359E-02	3.297E+18	0.408		
					17O(n,a)14C	1.660E-02	7.707E+15	0.001		
	He	0.8			13C(n,g)14C					
					14N(n,p)14C					
					17O(n,a)14C				blanket	
									4.2	4
8 Shield	Fe2Cr1V	0.8	2.795E+08	8.071E+12	13C(n,g)14C	6.469E-05	4.590E+18	0.002		
					14N(n,p)14C	1.237E-01	4.817E+19	35.16		
					17O(n,a)14C					
	H2O	0.2			13C(n,g)14C					
					14N(n,p)14C					
					17O(n,a)14C	2.698E-02	1.271E+19	0.51	shield 35.7	35

Table 2.5b. Carbon-14 production in the SiC-He/TOK.

Zone	Material	volume fraction of mat'l	Zone Volume (cm3)	Flux (#/s*cm2)	Reaction	x-sect (barns)	#dens of reaction isotope in mat'l (#/cm3)	14C Production (Ci/yr)	Total 14C Production (Ci/yr)	ESECOM Production (Ci/yr)
3 First Wall	SiC	1	6.287E+06	1.025E+15	13C(n,g)14C 14N(n,p)14C 17O(n,a)14C	2.037E-05	5.332E+20	0.23	included in blanket	
4 Blanket	SiC	0.16	3.632E+08	4.151E+14	13C(n,g)14C 14N(n,p)14C 17O(n,a)14C	1.849E-05	5.330E+20	0.78		
	He	0.2			13C(n,g)14C 14N(n,p)14C 17O(n,a)14C				Included in blanket	
	Li2O	0.64			13C(n,g)14C 14N(n,p)14C 17O(n,a)14C	6.121E-02	1.227E+19	237	coolant/ breeder 237	237
5 Manifold	SiC	0.1339	2.394E+08	7.513E+13	13C(n,g)14C 14N(n,p)14C 17O(n,a)14C	3.892E-05	5.332E+20	0.16		
	He	0.4804			13C(n,g)14C 14N(n,p)14C 17O(n,a)14C					
	BeO	0.0629			13C(n,g)14C 14N(n,p)14C 17O(n,a)14C	2.516E-02	2.195E+19	2.04		
	C	0.3229			13C(n,g)14C 14N(n,p)14C 17O(n,a)14C	3.892E-05	1.252E+21	0.93	blanket 4	7
7 Shield	Al	0.124	1.161E+09	8.402E+11	13C(n,g)14C 14N(n,p)14C 17O(n,a)14C					
	B4C	0.18			13C(n,g)14C 14N(n,p)14C 17O(n,a)14C	1.851E-05	2.745E+19	0.00		
	SiC	0.425			13C(n,g)14C 14N(n,p)14C 17O(n,a)14C	1.851E-05	5.332E+20	0.01		
	H2O	0.109			13C(n,g)14C 14N(n,p)14C 17O(n,a)14C	4.191E-02	1.271E+19	0.17		
	W	0.103			13C(n,g)14C 14N(n,p)14C 17O(n,a)14C				shield 0.19	0.2

2.3.3 Methods of C-14 Isolation and Containment

This section summarizes the available information on removal techniques for ^{14}C in the LWR and chemical industry that may be applicable to the treatment of ^{14}C produced in fusion reactor systems. Several methods of ^{14}C removal which are theoretically suitable for application to gaseous effluents from LWR systems have been extensively described in the literature.[2.11] The most prominent is caustic scrubbing, followed by fluorocarbon absorption and molecular sieve absorption. Other techniques include ethanolamine scrubbing, lime bed scrubbing, and cryogenic distillation. Although most of these methods were primarily developed for ^{14}C control at fuel reprocessing plants or high temperature gas-cooled reactors, they are general enough to be modified for application to other systems with proper considerations for size and concentration of carbon compounds.

2.3.3.1 Double Alkaline Scrubbing

Double akaline scrubbing[2.11-12] is one of two methods of CO_2 removal which involves scrubbing a gas stream with a caustic solution. The other method, direct scrubbing, is discussed in the the next section. Double alkaline entails the scrubbing of the gas stream with an aqueous solution of sodium hydroxide in a packed column. The CO_2 is stripped from the gas by the following reaction:

$$2NaOH + CO_2 \longrightarrow Na_2CO_3 + H_2O$$

The clean gas stream exits through the top of the column.

At intervals the aqueous solution is transferred to a mix tank where calcium hydroxide is added. The calcium carbonate precipitates out of the solution according to the following reaction:

$$Na_2CO_3 + Ca(OH)_2 \longrightarrow 2NaOH + CaCO_3$$

The resulting calcium carbonate is filtered out. The purified sodium hydroxide is recycled to the column. A schematic of the double alkaline system is shown in Fig. 2.2.

The process is a chemical reaction and therefore the rate is concentration dependent. A pilot facility at Oak Ridge National Laboratory (ORNL) has shown efficiencies up to 99.99% at CO_2 concentrations of 10 ppm and above. Note that the normal CO_2 concentration in air is 330 ppm by volume.

Treatment of LWR gaseous effluents with a double alkaline caustic scrubber is simple. For a boiling water reactor (BWR), the feed gas to the system diagrammed in Fig. 2.2 is the discharge from the recombiner, with an average flow rate of 30–40 standard cubic feet per minute (SCFM). The annual discharge of total radioactive and nonradioactive CO_2 is about 189,000 g/yr. Assuming 100% removal of the CO_2 in the form of $CaCO_3$ results in 854,000 grams or 1900 lb per year of filter sludge.

For a pressurized water reactor (PWR), the stream from the gaseous waste treatment tanks is mixed with air (dilution ratio of about 10) and routed through the recombiner. It is then fed into the treatment system with an average flow rate of about 22 SCFM at about 300 ppm of CO_2. This translates into an annual discharge of 94,000 grams/yr. With 100% removal of the CO_2 in the form of $CaCO_3$ there is 428,000 grams or 950 lbs per year of sludge.

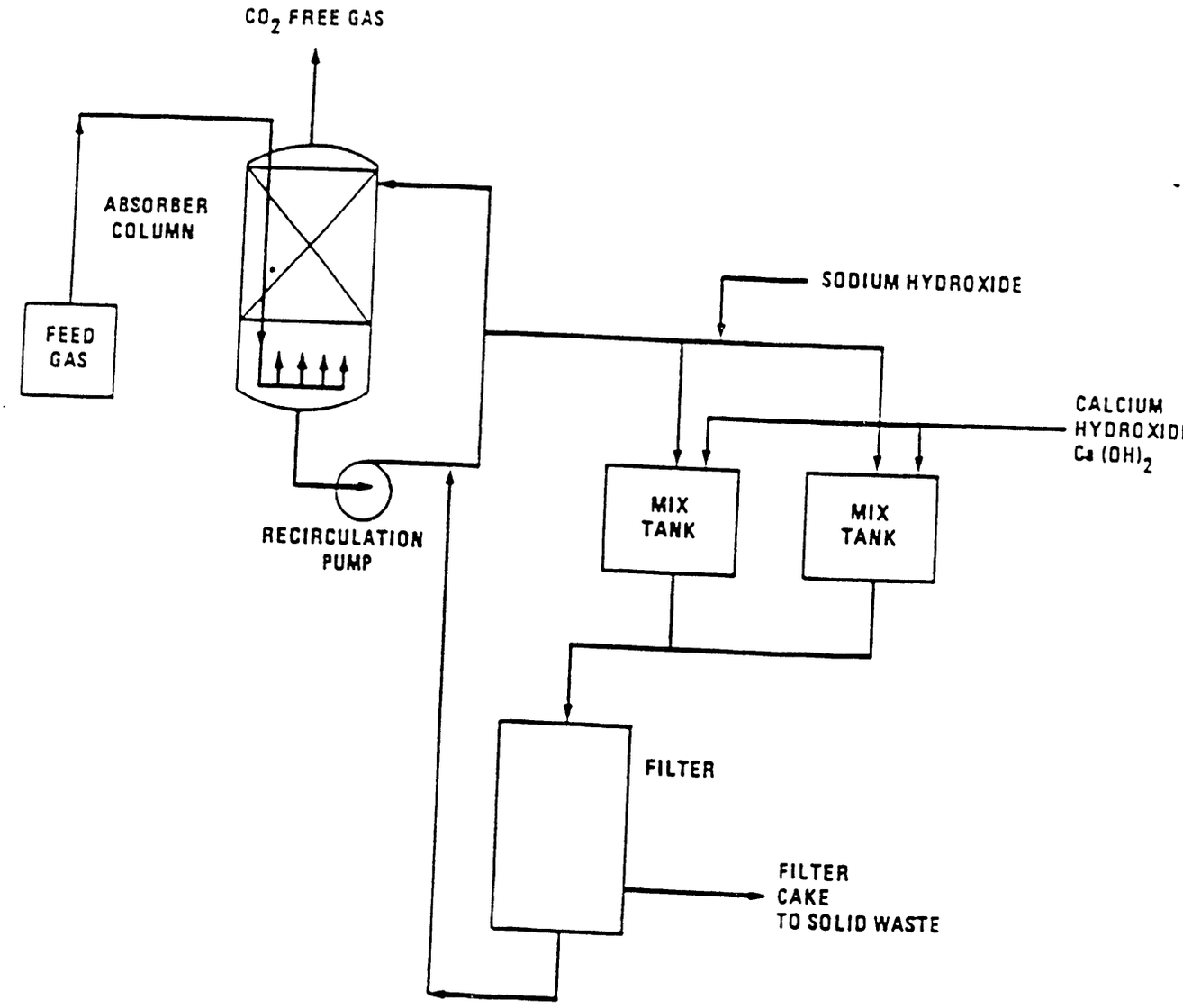

Figure 2.2. CO_2 removal by double alkaline process.

The filter sludge, which requires special handling for disposal, is de-watered to 50% by weight water and mixed with cement. This results in about 41 ft^3 and 20.4 ft^3 of waste for the BWR and PWR, respectively, with a specific carbon-14 activity of about 8 μCi/cc.

2.3.3.2 Direct Alkaline Scrubbing (Lime Bed Scrubbing)

Direct alkaline scrubbing is a process in which the CO_2 reacts directly with calcium hydroxide in a packed vessel to form calcium carbonate according to the following chemical equation:

$$Ca(OH)_2 + CO_2 \longrightarrow CaCO_3 + H_2O$$

A schematic diagram of the direct alkaline system is shown in Figure 2.3.

The $Ca(OH)_2$ solution is made by adding quicklime (CaO) to water. However, this process is limited by the possibility of plugging of the bed due to the precipitation of the insoluble $CaCO_3$. Experiments at ORNL[2.13] have been very successful in removing CO_2 by the direct scrubbing method using barium hydroxide in an agitated tank.

Various other alkalis and combinations of alkalis have been suggested for use; removal efficiencies range from 99.7% to 99.99%. Fixed bed and fluidized bed experiments have also been performed using dry hydrated barium hydroxide. In these studies, a reduction in removal efficiency with the length of continuous flow of CO_2 through the fixed bed was observed. This was due to the partial coverage of the hydroxide bed by the product carbonate.

Currently, there is no data base to evaluate the system performance of the fixed bed and fluidized bed variants. However, for the agitated contactor using $Ca(OH)_2$ with or without NaOH, the final products are expected to be similar to the final products of the double alkaline scrubber system.

2.3.3.3 Fluorocarbon Absorption

The fluorocarbon absorption process[2.11, 2.14] was developed for commercial application at the Oak Ridge Gaseous Diffusion Plant (ORGDP) and is known as FASTER (Fluorocarbon Absorption System for Treating Effluents from Reprocessors). The technology should be applicable to processors of the lithium oxide breeder. The pilot facility consists of four packed columns. The first three are the absorber and two strippers. Figure 2.4 shows a schematic of of the system. The various gaseous separations take place in these columns based on the gas-liquid solubility differences between the solvent and the volatile constituents of the feed gas. The last column is used to purify the solvent for recycling.

In contrast to the caustic scrubbing systems, which are based on chemical reactions, fluorocarbon absorption is a process which takes advantage of the physical properties of the feed gas, the contaminants, and the solvent. It is therefore not dependent on the concentration of CO_2 in the feed gas. The ORGDP pilot plant has reported CO_2 removal efficiencies of 99.99% at concentrations as low as 100 ppb.

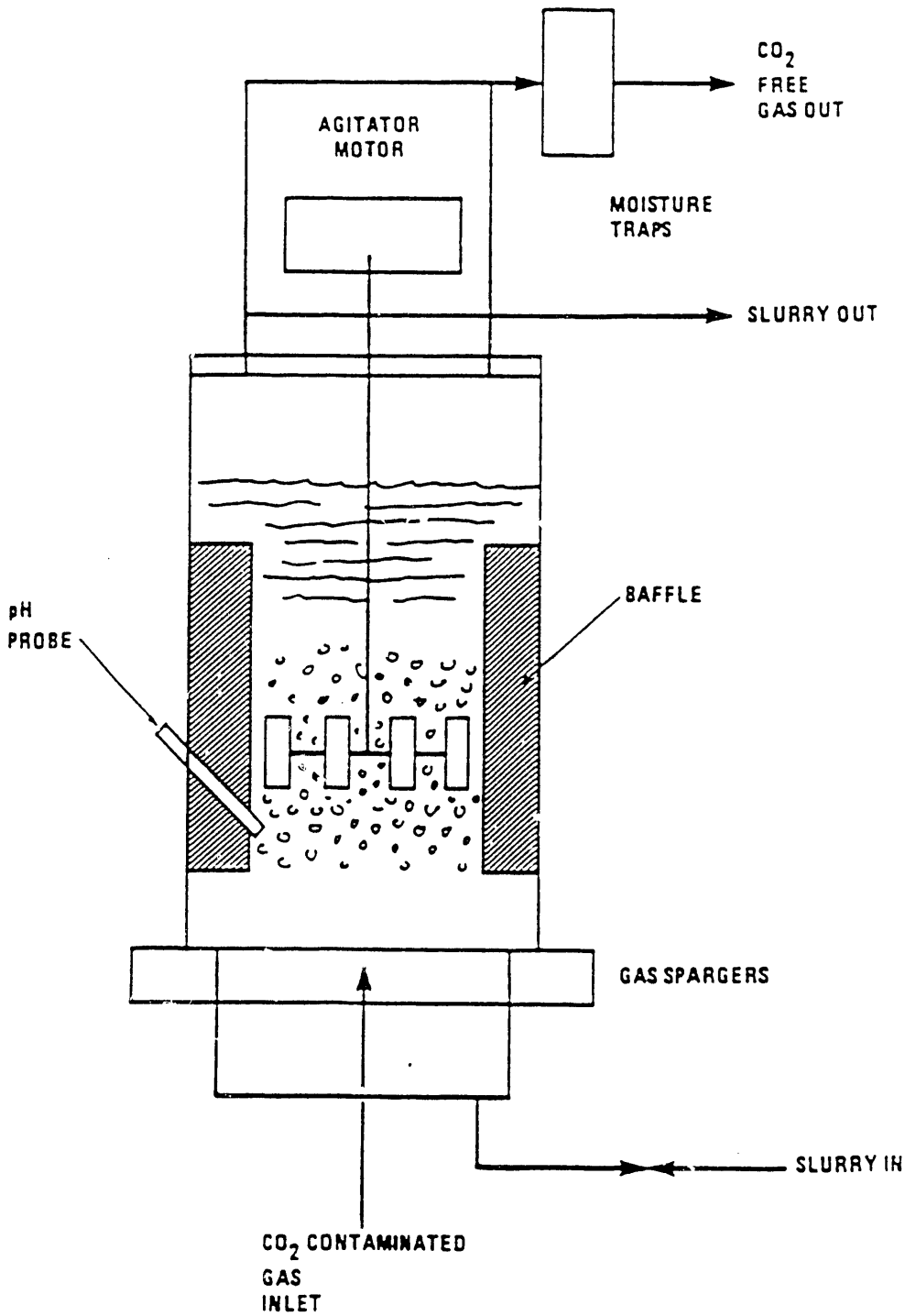

Figure 2.3. CO_2 removal by direct alkaline process.

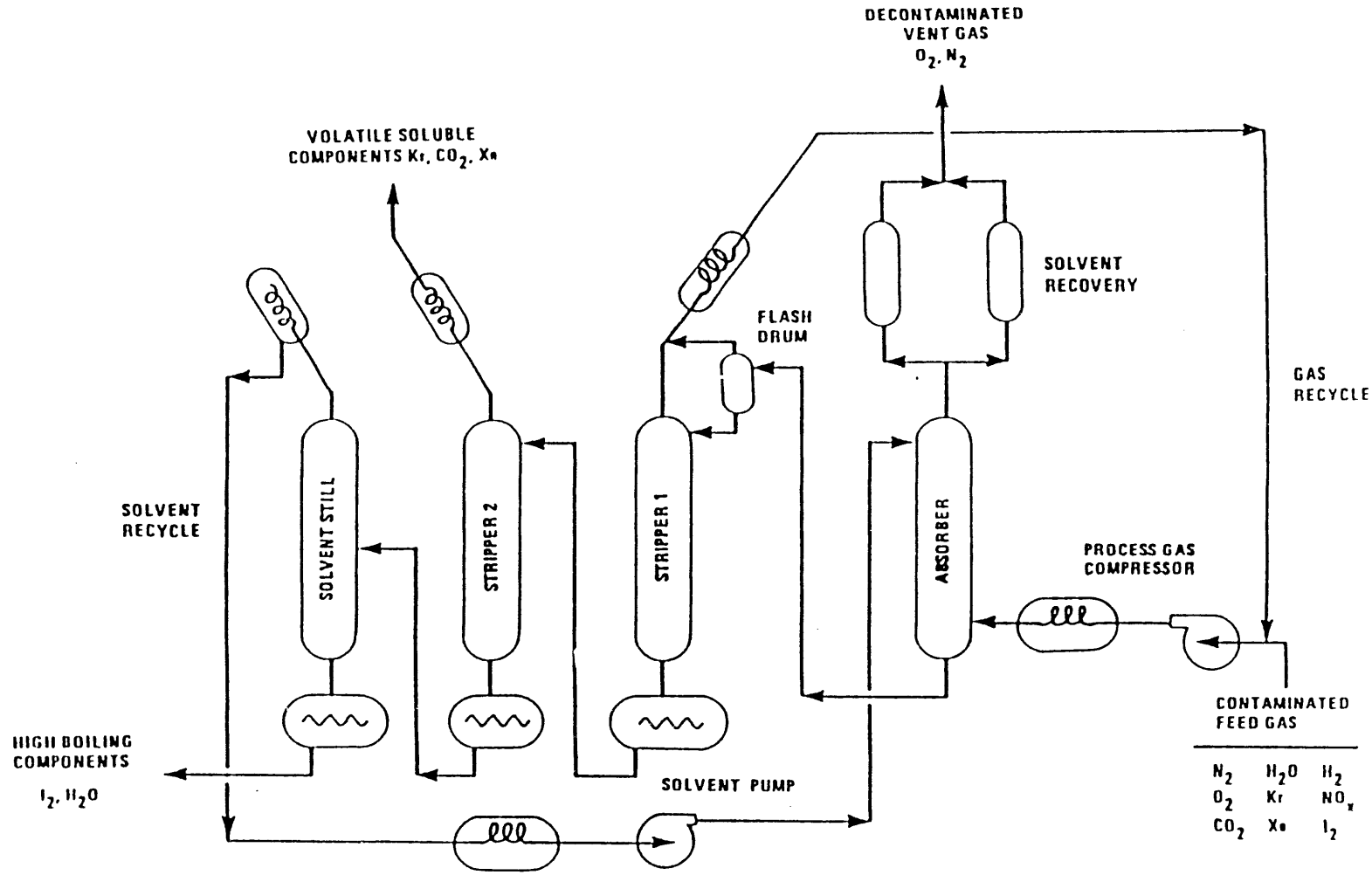

Figure 2.4. Fluorocarbon absorption system.

The CO_2 removal efficiency is high enough for the system to be effective even at very low concentrations of carbon dioxide. However, this fraction is still in the gaseous form and must be immobilized. Therefore, for compaction and long term storage, the separated gaseous effluent from the fluorocarbon absorption plant has to be fed into the caustic scrubber system to form $CaCO_3$ and subsequent immobilization as described in section 2.3.3.4.

2.3.3.4 Other Methods

Other methods for carbon-14 removal, such as molecular sieve absorption, ethanolamine scrubbing, and cryogenic distillation, have been extensively reviewed in the literature.[2.11-12, 2.15-16] Figure 2.5 is a schematic diagram of the molecular sieve absorption method. In most cases, these methods are still limited to laboratory scale experimental work, and do have various limitations respectively. The common drawback in all three is the fact that the CO_2 in its separated form is still a gas and requires some method of fixation. Table 2.6 summarizes the advantages and disadvantages of all the removal systems.

Table 2.6. Advantages and disadvantages of ^{14}C removal techniques.

Removal Technique	Advantages	Disadvantages
Double Caustic Scrubbing	Well-established technology Simplicity of operation High removal efficiency Removes nitrogen dioxide	Requires lime precipitation Nitrate salt by-product Liquid effluent for disposal Needs multistage processing
Direct Caustic Scrubbing (Lime Bed Absorption)	Well-established technology Removes nitrogen dioxide High removal efficiency	Sludge scaling in scrubber Nitrate salt by-product Liquid effluent for disposal
Fluorocarbon Absorption	Integrates with krypton removal High removal efficiency Concentration independent	Releases solvent vapor Needs product purification Needs product solidification
Molecular Sieve Adsorption	Simplicity of operation High removal efficiency	Potential fire hazard Final product still a gas
Ethanolamine Scrubbing	Well-established technology High removal efficiency Produces purified CO_2 gas stream	Odorous solvent release Solvent disposal needed Requires stripping system Final product still a gas Solvent easily oxidized to corrosive acid
Cryogenic Distillation	Proven technology Integrates with krypton removal	Potential plugging problem Operates at elevated pressure High power requirement Final product still a frozen gas

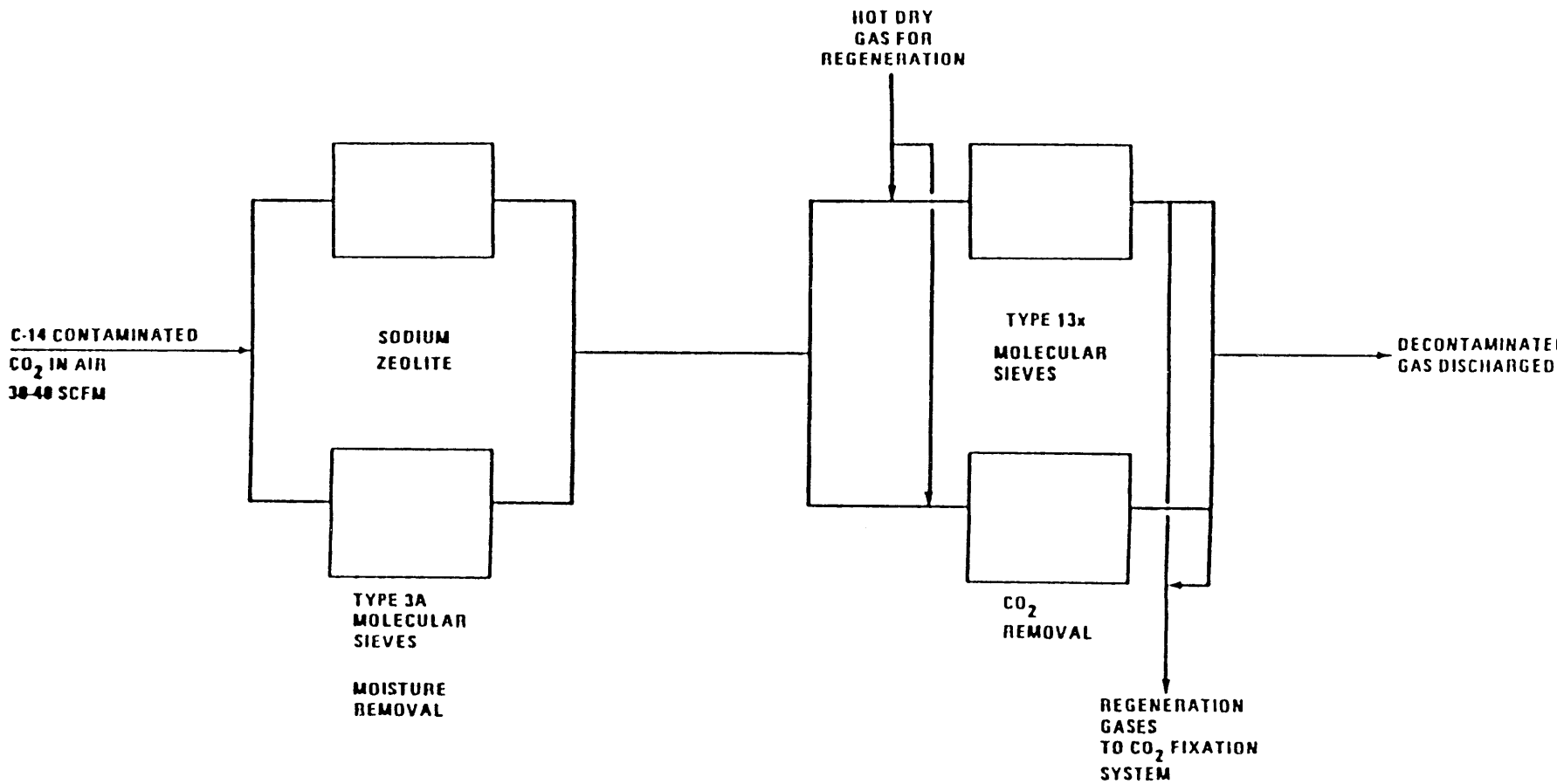

Figure 2.5. CO_2 removal by absorption on molecular sieves.

2.3.3.5 Cost of Removal Systems

Cost information is rather scanty and highly uncertain for some of the systems. In most cases, the data is just nonexistent. Table 2.7 is compilation of the available cost data as obtained from Ref. 2.17.

Table 2.7. Cost of ^{14}C control.

Reactor	System	Capital Cost (k$)	Annual Cost (k$)
BWR	Caustic Scrubbing	100 - 960	53 - 210
	Molecular Sieve	525	180
	Mol. Sieve/Caustic Scrub	629	196
PWR	Caustic Scrubbing	855 - 1150[a]	180 - 257

(a) Includes cost of recombiner which was not included in BWR case.

References

2.1. E.F. Plechaty and J.R. Kimlinger, "TARTNP: A Coupled Neutron-Photon Monte Carlo Transport Code," Lawrence Livermore National Laboratory, Report UCRL-50400 (1976).

2.2. J.A. Blink, R.E. Dye, and J.R. Kimlinger, "ORLIB: A Computer Code that Produces One-Energy-Group, Time- and Spatially Averaged Neutron Cross Sections," Lawrence Livermore National Laboratory, UCRL-53262 (1981).

2.3. J.A. Blink, "ORLIB: A Computer Code for Calculating Radionuclides Generation and Depletion in Fusion and Fission Reactors," Lawrence Livermore National Laboratory, UCRL-53633 (1981).

2.4. "ANISN-ORNL: A One Dimensional Discrete Ordinates Transport Code System with Anisotropic Scattering," RSIC Computer Code Collection, No. CCC-254, Radiation Shielding Information Center, Oak Ridge National Laboratory, April 1991.

2.5. J.P. Holdren, D.H. Berwald, R.J. Budnitz, J.G. Crocker, J.G. Delene, R.D. Endicott, M.S. Kazimi, R.A. Krakowski, B.G. Logan, and K.R. Schultz, "Exploring the Competitive Potential of Magnetic Fusion Energy: The Interaction of Economics with Safety and Environmental Characteristics," Fusion Technol. **13**, 7 (1988).

2.6. S.A. Fetter, "Radiological Hazards of Fusion Reactors: Models and Comparisons," PhD Thesis, University of California, Berkeley (1985).

2.7. A.W. Fairhall, "Potential Impact of Radiocarbon Releases by the Nuclear Power Industry," California Energy Commission, Sacramento, CA (1980).

2.8. J.B. Cannon, Ed., "Background Information and Technical Basis for Assessment of Environmental Implications of Magnetic Fusion Energy," DOE/ER-0170, Office of Energy Research, U.S. Department of Energy, Washington, DC (1983).

2.9. NCRP Report No. 81, "Carbon-14 in the Environment," Bethesda, MD (1985).

2.10. D.R. Olander and Aus Bafi "Computer Generation of Janaf Thermodynamic Tables," Nuclear Engineering Department, U. C. Berkeley (1987).

2.11. D.T. Pence, "Draft Report on the Assessment and Cost Estimates for Applying Removal Techniques for Tritium, Carbon-14, Krypton-85 and Iodine-129," Science Applications Inc., May 1978.

2.12. Gary R. Bray, Charles L. Miller, Tien D. Nguyen, and John W. Rieke, "Assessment of Carbon-14 Control Technology and Costs for the LWR Fuel Cycle," (EPA S20/4-77-013), Prepared by Science Applications Inc. for the U.S. Environmental Protection Agency, Office of Radiation Programs, September 1977.

2.13. D.W. Holliday and G.L. Haag, "Removal of ^{14}C-contaminated CO_2 from Simulated LWR Reprocessing Off-Gas by Utilizing the Reaction between CO_2 and Alkaline Hydroxide in either Slurry or Solid Form," presented at the 15th DOE Nuclear Air Cleaning Conference.

2.14. M.J. Stephenson and R.S. Eby, "Development of a Faster Process for Removing Krypton-85, Carbon-14, and Other Contaminants from the Off-Gas of Fuel Reprocessing Plants," presented at the 14th ERDA Air Cleaning Conference.

2.15. H.B.H. Cooper, "A Technical and Economic Evaluation of the Atmospheric Containment Technology for Radioactive Isotope Releases from Nuclear Fuel Reprocessing," Testimony before the GESMO Hearing Board on behalf of the states of Texas and New York, Docket No. RM-50-5, May 4, 1977.

2.16. George Rand, Union Carbide Corp. Molecular Sieve Department, personal communication with J. W. Phillips, March 20, 1979.

2.17. J. Wynn Phillips, "An Evaluation of removal techniques applicable to gaseous effluents from Light-water-Cooled Reactors," prepared for the California Energy Commission, 1980.

3. TRITIUM INVENTORY

Dynamic simulation of the tritium stocks and flows in the complex environment of a fusion power plant is essential for analyzing the tritium hazard potential. The present work aims to include tritium inventory calculations in a general safety-assessment scheme to be integrated with fusion-reactor design codes.

Tritium is the principal radioactive substance that will be released during routine operation of the plant as well as one of the most likely radionuclides to be released in significant quantities in a fusion reactor accident. Tritium is one of the least hazardous radionuclides. The ionizing radiation it produces is of low energy. It is not concentrated in the food chain. Nonetheless, the considerable tritium inventory in the power plant, combined with a propensity to diffuse through certain metals and the difficulty of separating tritiated water from ordinary water, poses non-negligible problems for fusion-reactor designers. The aqueous forms of tritium (T_2O, HTO or DTO) are more hazardous than its gaseous forms (T_2, HT, DT). Aqueous forms do not disperse as readily as gaseous forms, and they can enter tissue more easily.[3.1] If gaseous HT, DT, or T_2 comes in contact only with skin, it would pose little hazard, because the emitted β particles (18 keV maximum, 5.7 keV average) cannot penetrate the exterior dead skin layer (energy threshold for penetration is 70 keV). However, if the HT, DT or T_2 is inhaled, it may be transformed into HTO, DTO or T_2O and stays in the body in aqueous form, posing a significant hazard. Thus, a detailed analysis of the fraction of tritium that is released in gaseous or liquid form is crucial to the determination of the Biological Hazard Potential (BHP) of the use of tritium in fusion reactors.

There are two main pathways by which tritium in a fusion reactor could leak to the environment during normal operation. The first is through the heat exchangers into the steam system, from which the tritium can escape into the condensor coolant and thus into the environment (as liquid HTO). The second pathway for tritium escape is diffusion through the various containment-system boundaries into the air surrounding the plant as HT or gaseous HTO. The tritium inventory most difficult to reduce seems not to be the inventory in the breeder, however, but rather the inventory associated with recycling tritium that has been injected as fuel but escapes from the reaction region without burning. The lower the fractional burnup, the more severe this problem.[3.2] Other pathways of tritium outflow from the reactor include the vacuum pumping system (leakages) and permeation through the fueling chamber walls.

Most technologies envisioned to provide the extraordinary degree of tritium control required in fusion reactors remain to be proven in practice. How difficult it will be to keep track of kilograms of tritium to an accuracy of 1 ppm (part per million) per day, through a complex system of leaky valves, faulty seals, scratched diffusion barriers, and so on, remains to be seen. In many cases, computer-aided simulation of the tritium inventory in the reactor system can provide useful information as to the relative tritium hazard potential of the different components of the fusion power plant. This information can subsequently be used to improve the reactor design in advance (at the conceptualization stage), integrating safety and environmental considerations in the design process.

To date, computer codes aiming to calculate tritium inventories have been either long detailed models that correspond to a specific point design, with little provision for

tracking major design alterations, or extremely crude, steady-state estimates that may not correspond to a self-consistent model at all and do not provide any insight on the dynamic behavior and control of the tritium system.[3.2]

The aim of this work is an intermediate level of detail, requiring and using considerable design information to generate an internally consistent picture of the tritium inventories and their dynamics, yet simple enough to be recalculated quickly in response to changes in design parameters. The ultimate goal of the project, then, is the development of a flexible computer code that will serve as an on-line expert system in: (a) showing the designer the impact of the design on the tritium inventory and (b) allowing exploration of possible design changes that would tend to minimize the vulnerable tritium inventory in the fusion power plant.

The code consists of the following sections:
1. Data input referring to the initial point design, proposed by the reactor designer.
2. Analytical relations between the design parameters and the parameters used as input to the tritium inventory model.
3. Model parameters initialization and consistency checks on the parameter set in saving much computer time by avoiding meaningless simulations.
4. Main part of the code including calculation of the tritium inventory using a deterministic model.
5. Graphical display of the dynamic behavior of the tritium system providing easily accessible information that can be used in an on-line process.

The parts of the code that have already been finished and are presented in this paper include parts 3, 4 and 5 of the above list. The reason for having to start with construction of the model and then proceed to the user-interface is the need to have an accurate and fast simulation code that could provide in an informative way the dynamic behavior of the tritium fuel cycle. Parts 1 and 2 of the list, although highly time-consuming tasks, rely heavily on the simulation model. The latter took therefore priority over all the other parts of the code.

3.1 DYNAMIC SIMULATION MODEL

3.1.1. Theory of Tritium System Modeling

A survey of the tritium literature showed that the major elements of the tritium-processing system have been thoroughly investigated, both in terms of the process-engineering aspects and in terms of the elements of material science involved in tritium research. More specifically, mathematical models and techniques calculating the operating parameters of particular components of the tritium fuel cycle (e.g., the isotope separation system,[3.3] the fuel cleanup system,[3.4] and the tritium permeation and diffusion problems arising in the blanket[3.5] or the first wall of the reactor[3.6]) have been developed, providing the reactor designer with considerable information on the specific details of the above processes. There is, however, a lack of an integrated approach to the tritium system as a whole.

Two models, developed independently by Abdou et al. (1985)[3.7] and by Gabowitch and Spannagel (1988)[3.8] attempt to address this situation, adopting a systems analysis approach. Since several distinct processing stations can be identified within the

tritium fuel cycle, it is only natural to simulate the cycle with compartment models (dynamic systems) in which each processing station is represented by one compartment. Each of the models cited, however, corresponds to only a single reactor design. The non-flexibility of those models renders them unsuitable for our intended application matched to exploratory reactor-design codes. The fundamental concept underlying our approach is the fact that the tritium fuel cycle can be characterized as a set of distinct components or levels of operation, each one of which may be characterized with different classes of states. These subsystems may or may not coincide with the aggregation levels described in the above mentioned models, depending on the reactor design that our code is called upon to simulate. Such an approach allows us to simulate tritium cycles of future technologically advanced reactors with high availability (deterministic case -- steady-state operation is a good approximation of the actual behavior of the system), as well as the first generation of research reactors (possible feasible application on the ITER advanced design) with limited availability. The dynamic simulation provides useful information on the kinds of behavior to be expected over the time horizon of reactor operation. Moreover different strategies of operation can be investigated.

3.1.2. Mathematical Model

The tritium processing system in fusion reactor plants can be crudely represented as a linear dynamic system, assuming that there are no coupling effects induced by disruptions in the fuel cycle. Time-dependent variables $Y_0,...,Y_n$ in such a model describe the tritium inventories in the compartments $S_0,...,S_n$ of the tritium processing system S. The level of aggregation of the models varies for different designs found in the literature. But in all cases, the mathematical model is a linear system of first-order ordinary differential equations of the form

$$dY_i/dt = \phi_i(t) + \Sigma f_{ij}(t)Y_j(t), \quad \text{where} \quad i = 0,1,...,n \; ; \; j = 0,1,...,n \tag{3.1}$$

The coefficients f_{ij} are calculated from the primary design parameters through an expert-system that can transform the latter to the parameters required by the model. The terms ϕ_i represent non-conventional process fluid flow into compartment i respectively They account for processes like tritium breeding [Eq. (3.4)], or the amount of tritium gas flowing from the plasma chamber to the exhaust processing unit [Eq. (3.7)].

This type of equation describes a donor-controlled process as the tritium flow within the process system is assumed to be. The mean residence time of tritium in each compartment is the parameter that controls the relative flow rate from the one subsystem to the next.

The modularized approach that is adopted in this work can save significant amounts of computer time and allows for easy changes to the design parameters by the operator of the system. The dynamics of all inventories $Y_0,...,Y_n$ can be simulated if the initial conditions are defined :

$$Y_0(0) = I_0 \, , \, ... \, , \, Y_n(0) = I_n \tag{3.2}$$

The model that is developed in this paper corresponds to the box-model in Fig. 3.1. The detailed mathematical system is as follows:

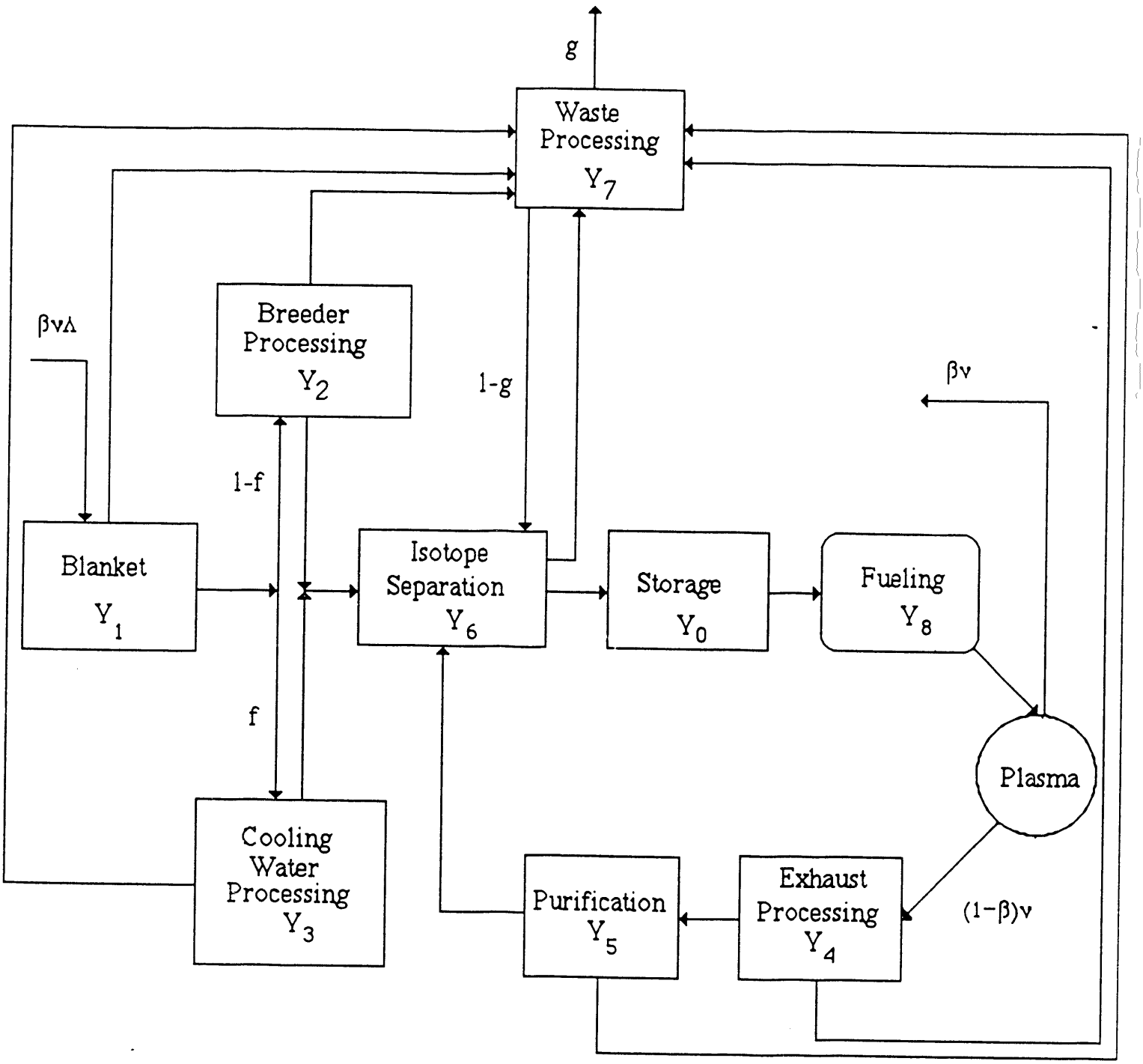

Fig. 3.1 : Tritium fuel cycle simplified flowsheet

$$dY_0/dt = r_6Y_6 - \lambda_0Y_0 \qquad Y_0(0) = I_0 \qquad (3.3)$$

$$dY_1/dt = \beta\nu\Lambda - \lambda_1Y_1 \qquad Y_1(0) = I_1 \qquad (3.4)$$

$$dY_2/dt = (1 - f)r_1Y_1 - \lambda_2Y_2 \qquad Y_2(0) = I_2 \qquad (3.5)$$

$$dY_3/dt = fr_1Y_1 - \lambda_3Y_3 \qquad Y_3(0) = I_3 \qquad (3.6)$$

$$dY_4/dt = (1 - \beta)\nu - \lambda_4Y_4 \qquad Y_4(0) = I_4 \qquad (3.7)$$

$$dY_5/dt = r_4Y_4 - \lambda_5Y_5 \qquad Y_5(0) = I_5 \qquad (3.8)$$

$$dY_6/dt = r_2Y_2 + r_3Y_3 + r_5Y_5 - \lambda_6Y_6 + r_7(1 - g)Y_7 \qquad Y_6(0) = I_6 \qquad (3.9)$$

$$dY_7/dt = \Sigma\,\varepsilon_iY_i - \lambda_7Y_7 \qquad Y_7(0) = I_7 \qquad (3.10)$$

$$dY_8/dt = r_0Y_0 - \lambda_8Y_8 \qquad Y_8(0) = I_8 \qquad (3.11)$$

$$\nu = r_8Y_8 = N \qquad (3.12)$$

The sets of parameters used in the above model are the following :

(A) Design parameters :

r_i = rate of transfer of a tritium unit from compartment *i* to all other compartments (day^{-1}),

ν = rate of tritium injection into the plasma chamber (kg/day)

N = theoretical requirement of tritium supply rate to the plasma chamber (kg/day)

Λ = tritium breeding ratio = N+ /N- , where N+ is the rate of tritium production in the system (usually in the blanket) and N- is the rate of burning tritium in the plasma. Λ is dimensionless.

f = fraction of the blanket tritium inventory that permeates to the coolant.

g = fraction of the tritium inventory in the waste processing system that is released or leaks to the environment surrounding the facility.

β = tritium fractional burnup [0.05 - 0.06]. This range of values for β represent the typical range introduced in the so far suggested designs.

ε_i = rate of the loss of a tritium unit to the atmosphere (usually in the form of tritium gas, in day^{-1})

μ_i=rate of the loss of a tritium unit to the metallic body of the reactor, treated as solid waste (day^{-1})

ω_i = rate of leakage/permeation of a tritium unit into liquid waste (coolant water, oil, etc.), usually as HTO or T_2O (day^{-1})

(B) Dependent parameters :

$\lambda_i = \lambda + r_i + \varepsilon_i + \mu_i + \omega_i$

(C) Independent parameters :

t = time variable (day)

λ = radioactive decay constant for tritium.

An underlying assumption of the simulation model is that the tritium residence time in the plasma chamber is negligible compared with the residence time in the rest of the fuel cycle. The parameters f and g vary between 0 and 1, representing the fractions of the inventories that circulate on one of the 2 possible routes (see Fig.3.1). An analysis of its major components and modelling concepts will immediately follow.

0-Storage System (Y_0)

The tritium storage system is fed in the course of the reactor operation with tritium from the Isotope Separation System (ISS--system 6). Following the donor-controlled approach, the tritium input will be described by the term $r_6 Y_6$. Tritium outflow from storage is described by $\lambda_0 Y_0$, where λ_0 is a lumped expression of coefficients corresponding to the various routes through which tritium flows out of subsystem (0).

1-Reactor Blanket (Y_1)

There are two main processes that determine the tritium inventory in the blanket of the reactor :

(a) Tritium breeding; it is a function of the tritium that is burned up in the plasma ($\beta\nu$) and the breeding ratio (Λ)--the ratio of tritium produced in the reactor over the total tritium consumed. The aggregate term ($\beta\nu\Lambda$) represents the amount of tritium that is bred during each fuel cycle.

(b) Tritium flows out of the blanket through three main routes :

-- leakages (solid, liquid or gaseous, passing through the waste processing unit);

-- breeder processing : the part of the system that processes tritium coming from the blanket and drives it to the ISS and the Waste Processing Unit (WPU);

-- coolant processing : some of the tritium generated in the blanket passes to the coolant (in the form of HTO or T_2O).

After being processed, it is forwarded to the ISS (after having mixed with the tritium coming from the Breeder Processing Unit (BPU)) or "caught" by the WPU for further processing before it is released to the environment. The aggregate tritium outflow from the blanket is expressed by the term $\lambda_1 Y_1$ that includes radioactive decay in the blanket, wastes and leakages as well as transfer to other parts of the fuel system.

2-Breeder Processing (Y_2)

As described above, tritium is transferred from the blanket to the rest of the system through the breeder and the coolant processing. A separation coefficient (f) is used to denote the fraction of tritium that is directed to the coolant processing unit. The rest of the tritium, which is directed to the BPU, is expressed by the term $(1 - f)r_2 Y_2$. Again, all outflows from the breeder processing (leakages, wastes, isotope separation system) are lumped in the term $\lambda_2 Y_2$.

3-Coolant Processing Unit (Y_3)

The tritium inflow from the blanket is expressed by the term fr_1Y_1, where the outflows, similarly as above, are captured in the term $\lambda_3 Y_3$.

4-Exhaust Processing Unit (Y_4)

This is the first unit where tritium is driven after it leaves the plasma. This amount of tritium will be equal to $(1 - \beta)v$, that is the amount of tritium that has not burned up in each fuel cycle. Outflows (to the gas purification unit and through leakages and radioactive decay) are expressed by the term $\lambda_4 Y_4$.

5-Gas Purification Unit (Y_5)

The Gas Purification Unit (GPU) receives the tritium gases from the exhaust system. This flow is controlled by the tritium inventory in the exhaust system and is described with the term $r_4 Y_4$. Tritium gases and tritiated water vapor leave the GPU through the conventional pathways discussed above, namely gas leakages, leakage to the solid body of the reactor (hydrogen permeation mechanisms) and radioactive decay. Again, a lumped expression describing all three mechanisms is given by the term $\lambda_5 Y_5$.

6-Isotope Separation System (Y_6)

The ISS is one of the major concentration nodes of tritium in the whole fuel cycle together with the WPU. Flows from the breeder processing ($r_2 Y_2$), the coolant processing ($r_3 Y_3$), the GPU ($r_5 Y_5$) and the WPU $[r_7(1 - g)Y_7]$ are concentrated to the ISS. The coefficient g expresses the fraction of tritium wastes that is released to the environment from the WPU. The rest of the tritium wastes, after having been processed, are fed back to the ISS.

7-Waste Processing Unit (Y_7)

Tritium inflows to the WPU come from tritium losses from each other component of the system (besides plasma). Outflows include radioactive decay as well as liquid and solid wastes and losses to the atmosphere are contained in the term $\lambda_7 Y_7$.

8-Fueling Chamber (Y_8)

Tritium flows into the fueling chamber from the storage unit at a rate of $r_0 Y_0$ (donor-controlled process) and flows out of it through minor leakages and radioactive decay as well as through the fueling channel to the plasma. The tritium feed rate to the plasma (v) poses a physical constraint to the outflow of tritium from the fueling chamber. It is required that it either remain constant or follow a particular operational scheme to ensure the undisrupted operation of the power plant (possibly including regular fill-ups of the storage unit with tritium fuel).

Although the above described model corresponds to a tritium system that is characteristic of the tokamaks discussed in the ESECOM Report[3.9] and the NET design, the distinct compartments can be modularized, thus allowing for a fast and user-friendly input of the basic concepts of the fuel cycle design. Interactive sub-routines containing the corresponding differential equations can be used to facilitate the incorporation of major changes in the reactor design (e.g. restructuring of the tritium process system). The

computational system could even be equipped with advanced-graphics techniques that could translate a graphical on-screen representation of the tritium cycle into the corresponding set of differential equations.

3.1.3. Numerical Method

The numerical method adopted for the solution of the above system of ordinary differential equations is a third-order variable-step-size Runge-Kutta. The local error is estimated by comparing the third order results of the integration with second-order terms. The development of the numerical method for the specific application involved the Taylor series expansion of the differential equations (in the neighborhood of time t) according to the following general case :

$$y_{t+1} = y_t + (\delta t/1!)y' + [(\delta t)^2/2!]y'' + [(\delta t)^3/3!]y''' \qquad (3.13)$$

where y', y'', y''' are the first, second and third derivatives of the function y(t) (the state variables of the model), respectively. The accuracy of the simulation is checked on-line by comparing the above third-order solution with a second-order one (one that incorporates only the 3 first terms of the left-hand side of Eq. (3.13)). Depending on the result, it accepts or rejects the calculation and selects the size of the next or repeated step. Runge-Kutta methods have the advantage of being able to change step-size practically at will. Consequently, the computer code can increase δt when appropriate, reducing the number of computations, thereby reducing both inaccuracy due to computer round-off error and the cost (in computer time) of the simulation. The approximation of the corresponding integral over the interval from t to t+δt is done according to the following 6 steps :

1. Computation of the derivative at t :

$$k_1 = y_1'(y(t),t) \qquad (3.14)$$

2. Estimation of the integral at the middle of the interval by Euler's method :

$$y_1 = y_t + \delta t k_1 /2 \qquad (3.15)$$

3. Computation of the derivative based on y, $t=t_0 + \delta t/2$, and

$$k = y'(y , t_0 + \delta t/2) \qquad (3.16)$$

4. Estimation of the integral at $t + 3\delta t/4$ based again on y(t) and k just computed by Euler's method

$$y_2 = y_t + 3\delta t k_2 /4 \qquad (3.17)$$

5. Computation of the derivative based on this y_2 and $t = t_0 + 2\delta t/3$

$$k_3 = y'(y_2, t_0 + 2\delta t/3) \qquad (3.18)$$

6. Calculation of a third-order estimate of y(t) at t + δt based on y and the three k's just computed

$$y_{t+1} = y_t + \delta t(2k_1 + 3k_2 + 4k)/9 \qquad (3.19)$$

The coefficients used above have been chosen to give a third-order result. The same k's can be recombined with different weights to form a second-order result :

$$y_{2,t+\delta t} = y_t + \delta t(k_1 + 3k_2 + 2k_3) \qquad (3.20)$$

By subtracting the two estimates, an upper bound on the local truncation error is obtained :

$$y_{t+\delta t} - y_{2,t+\delta t} = \varepsilon = \delta t(k_1 - 3k_2 + 2k_3)/18 \qquad (3.21)$$

If this error is unacceptable, the cycle must be repeated (starting at step 2) with a smaller δt. If the error is acceptable, the next cycle can be started with a δt adjusted according to a comparison of the estimated error ε and a user-defined acceptable error.

3.1.4. Stiffness of the Model

A "stiff" model is one that -- like the one presented above -- contains both long and short time constants. In system dynamics terms, the short time constants generate only transient effects compared to the long time constants. However, the short time constants permanently force the integration method to choose δt according to their values. Because δt must remain small even though the transients have died out, considerable computer resources may be required and round-off error may become significant.

The integration method may become "unstable" when applied to a stiff system. The dynamic properties that result from the combination of the dynamics of the system being integrated and the integration method cannot be accounted for independently.

One way to detect stiffness is to compare the sign of the largest error term in one step with the sign of the error for the same integral in the succeeding step. If the model is unstable, these signs will alternate. In non-stiff systems, these signs are generally the same. The error term is proportional to the highest derivative sensed by the method. If the system being modeled is continuous, no derivatives should change drastically between one step and another. On the other hand, the stiffness-induced instability produces alternating results which would lead to alternating signs in the error term (this is true for methods that involve an odd number of derivative calculations, like the one chosen in this work). Our computer code can keep a running average of sign reversals and infer instability from that indicator. [3.10]

The system described in Section 3.1.2 has a significantly stiff dynamic behavior. Using the Runge-Kutta method of third-order, we obtained unstable behavior from the very first time steps. In such a case, the simpler (but less sensitive to alternating shifts of derivative signs) Euler's method is better, except when the system is so stiff that the round-off error is intolerable. This method was monitored by a Runge-Kutta second-order method to insure accuracy. Using this combination of numerical methods, the model provided a

stable and reproducible simulation of the reactor fuel system behavior. If Euler's method was not satisfactory, we would be forced either to reformulate the model replacing the stiff portion with its steady-state equivalent, or to resort to one of the methods specifically designed for stiff systems.[3.11]

3.2. SIMULATION RESULTS AND CONCLUSIONS

The model simulations confirmed the theoretically expected behavior of the system, while revealing some unexpected features related to the most "vulnerable" components of the system, i.e. the exhaust processing, purification, and isotope separation systems. In more detail, the most interesting finding so far has been the identification of the three above mentioned units to be of critical importance with respect to safety considerations in the fusion power plant, both in terms of the relative tritium inventories (in steady-state operation) and of the dynamic behavior of the tritium processing system. The findings of the simulation are:

(a) the steady-state inventories in each of the above mentioned subsystems amount to about 0.8 - 1.5 kg of tritium (corresponding to start-up inventories of 5 kg of tritium in storage) while each of the other subsystem inventories hardly exceed 0.8 kg of tritium;

(b) from days 2 to 4 from the reactor start-up, a transition period characterized by excessive tritium inventories in the three vulnerable subsystems that have been mentioned above could cause possible disruptions to the fuel cycle with hazardous consequences (see Fig. 3.2).

This behavior of the tritium fuel cycle has not been identified in the case of the few similar models found in the literature.[3.7-8] The reason for this might have been the fact that those models focused mainly on the long-term behavior of the system (time scales of 100 to 10000 days of reactor operation), thus losing sight of the short-term effects such as phenomena occuring during the first 1-10 days of reactor operation. On the other hand, the replication by our model of the long-term behavior described in both relevant publications from our model provides "empirical" confirmation of its validity.[3.7-8]

Sensitivity analysis with respect to the average tritium residence times in the vulnerable subsystems (10-fold variations were imposed to the residence times) showed that although the system was driven to different steady-state tritium levels, the operational pattern that we noted above was characteristic of its behavior (Fig. 3.3-6).

The parameter set that was used as the reference case for the simulations is given in Table 3.1. The chosen values, in the absence of experimental or designer's data, represent values found in the literature[3.7-8] providing thus both a point-of-departure parameter set and a set of results that can easily be compared with results of other relevant models.

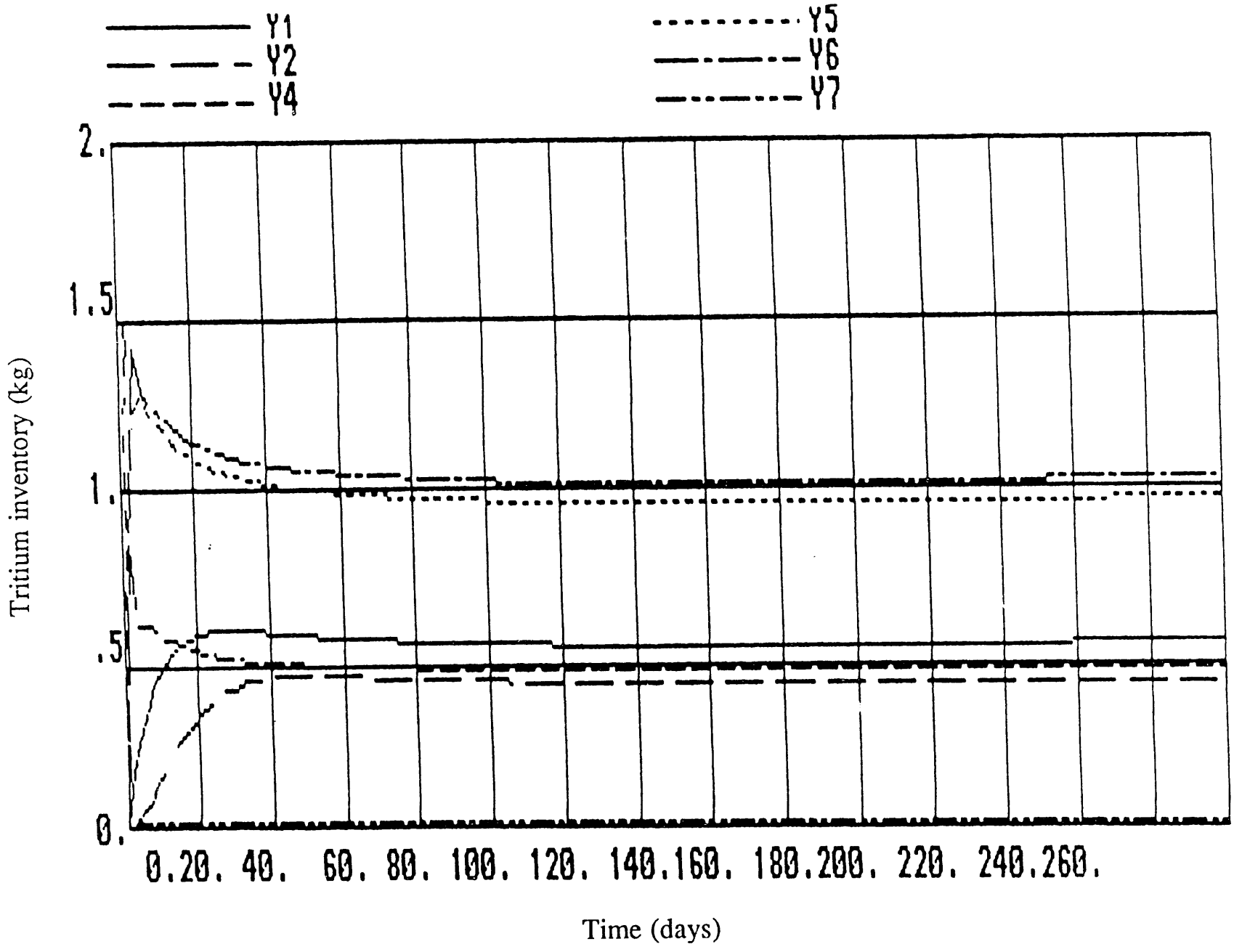

Figure 3.2. Unstable behavior of the tritium system in a typical simulation run.

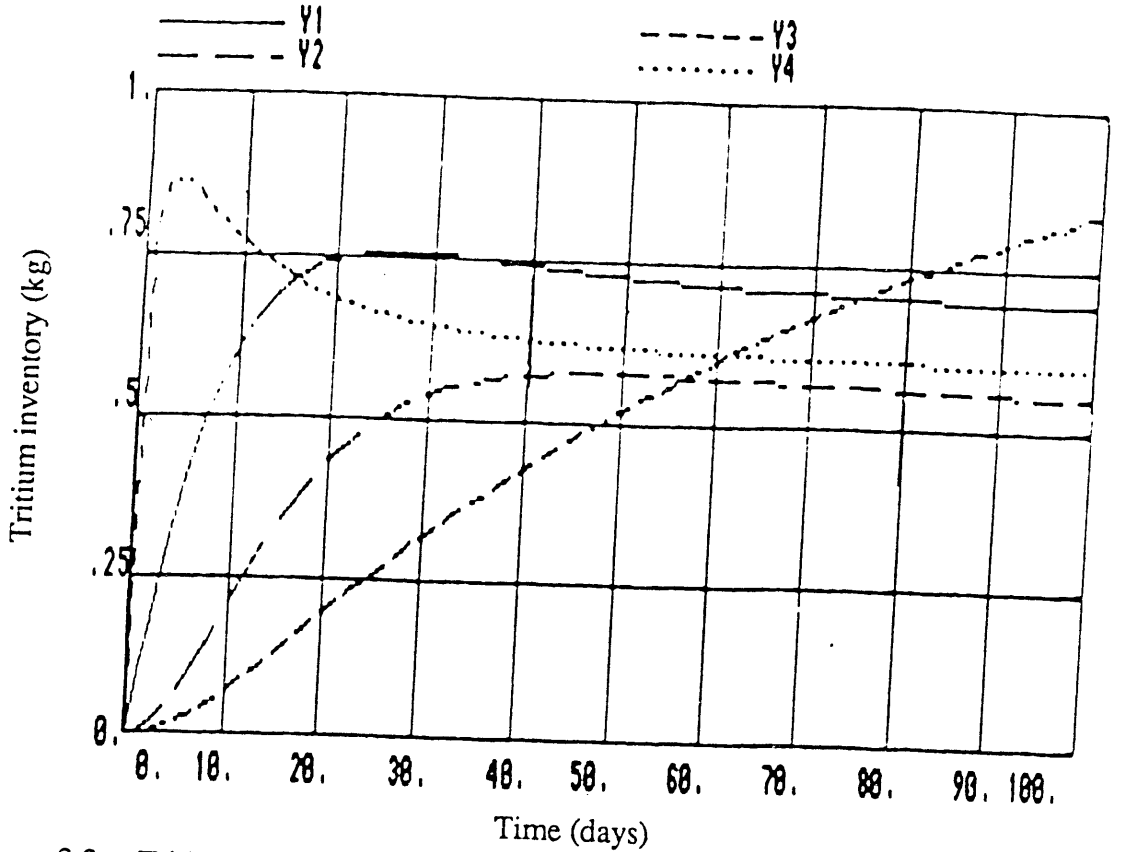

Figure 3.3a. Tritium inventory dynamics in the blanket, breeder processing, coolant processing, and exhaust processing units (T_5 = 0.1 days).

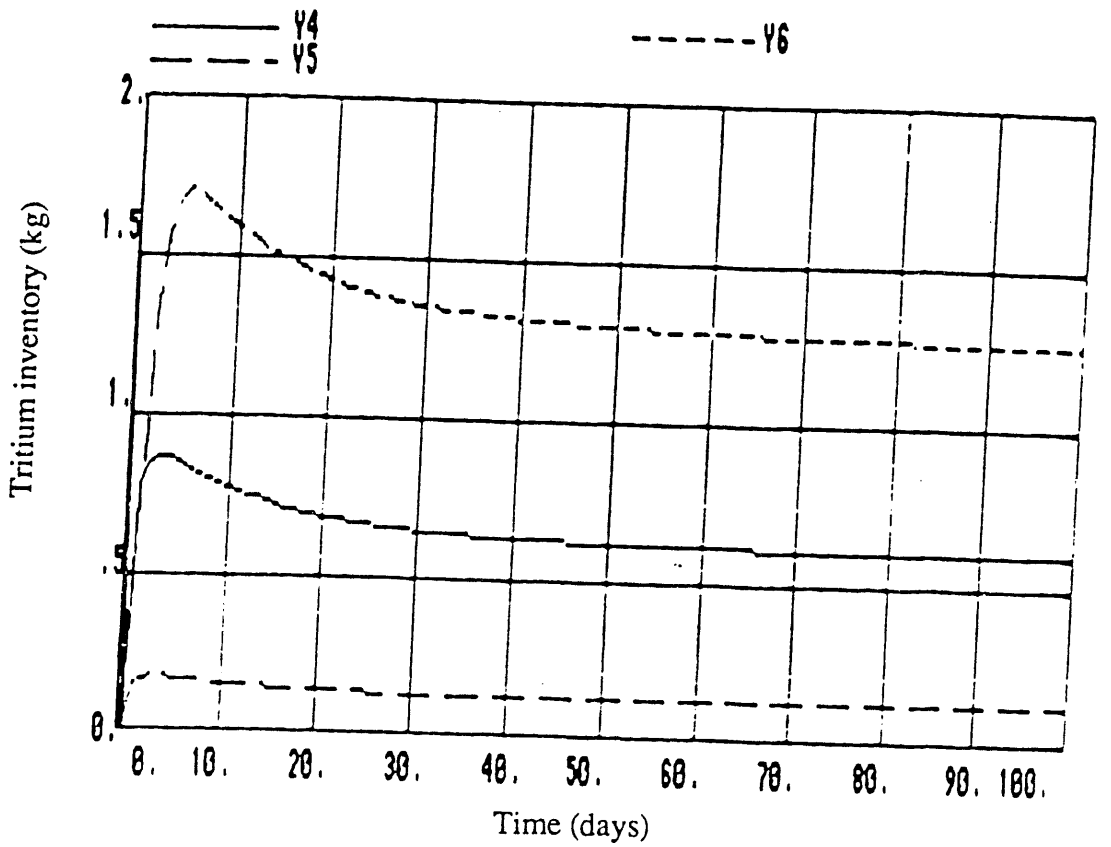

Figure 3.3b. Tritium inventory dynamics in the exhaust processing, gas purification, and isotope separation subsystems (T_5 = 0.1 days).

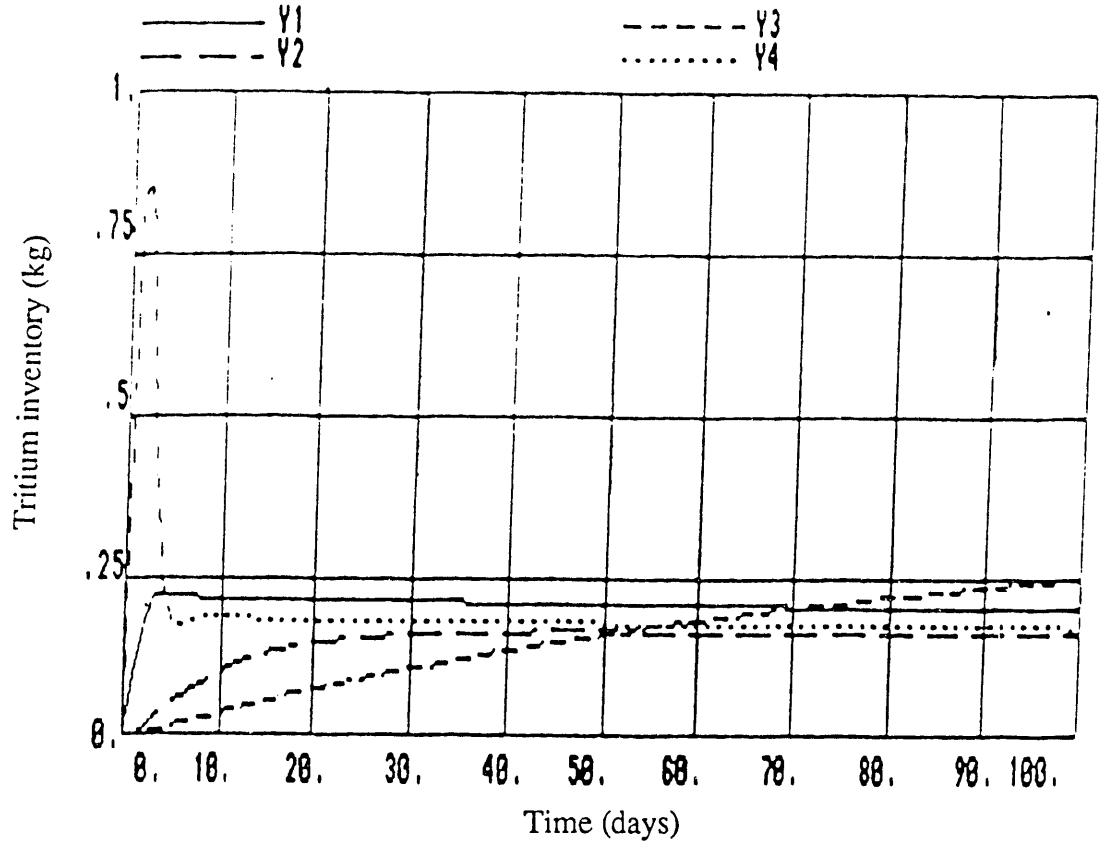

Figure 3.4a. Tritium inventory dynamics in the blanket, breeder, coolant, and exhaust processing units (T_5 = 10 days).

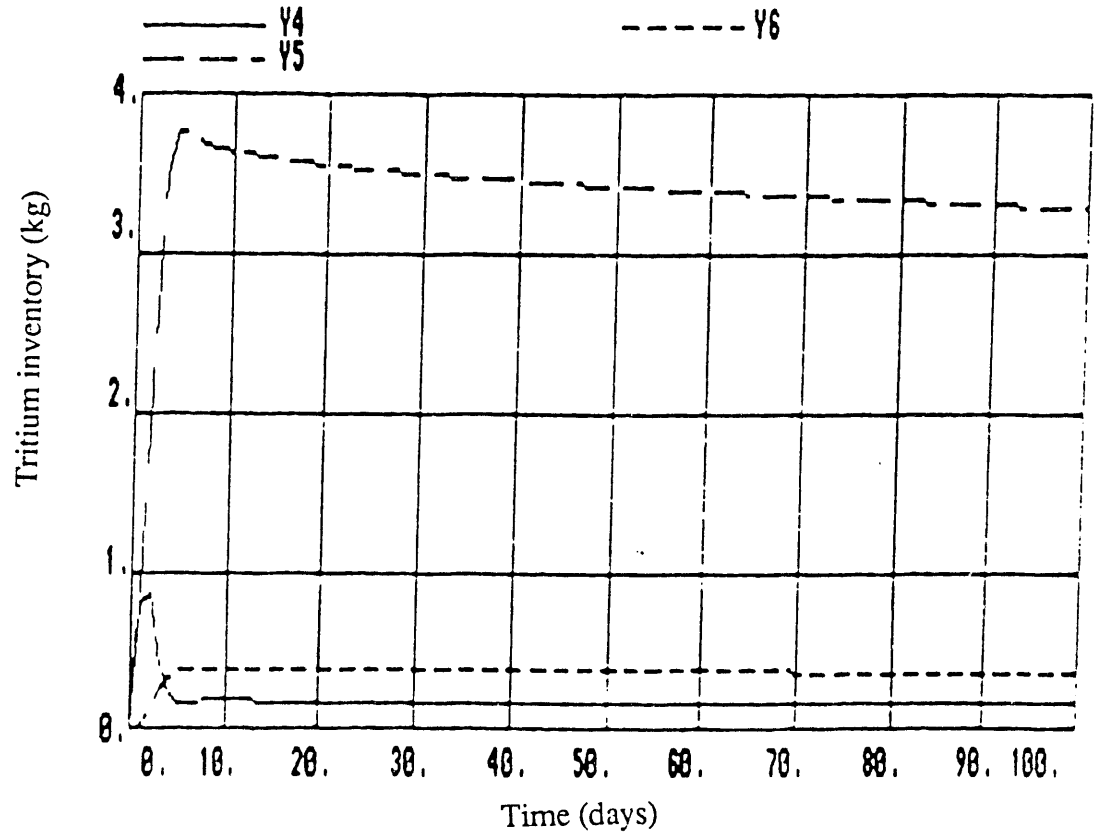

Figure 3.4b. Tritium inventory dynamics in the exhaust processing, gas purification, and isotope separation subsystems (T_5 = 10 days).

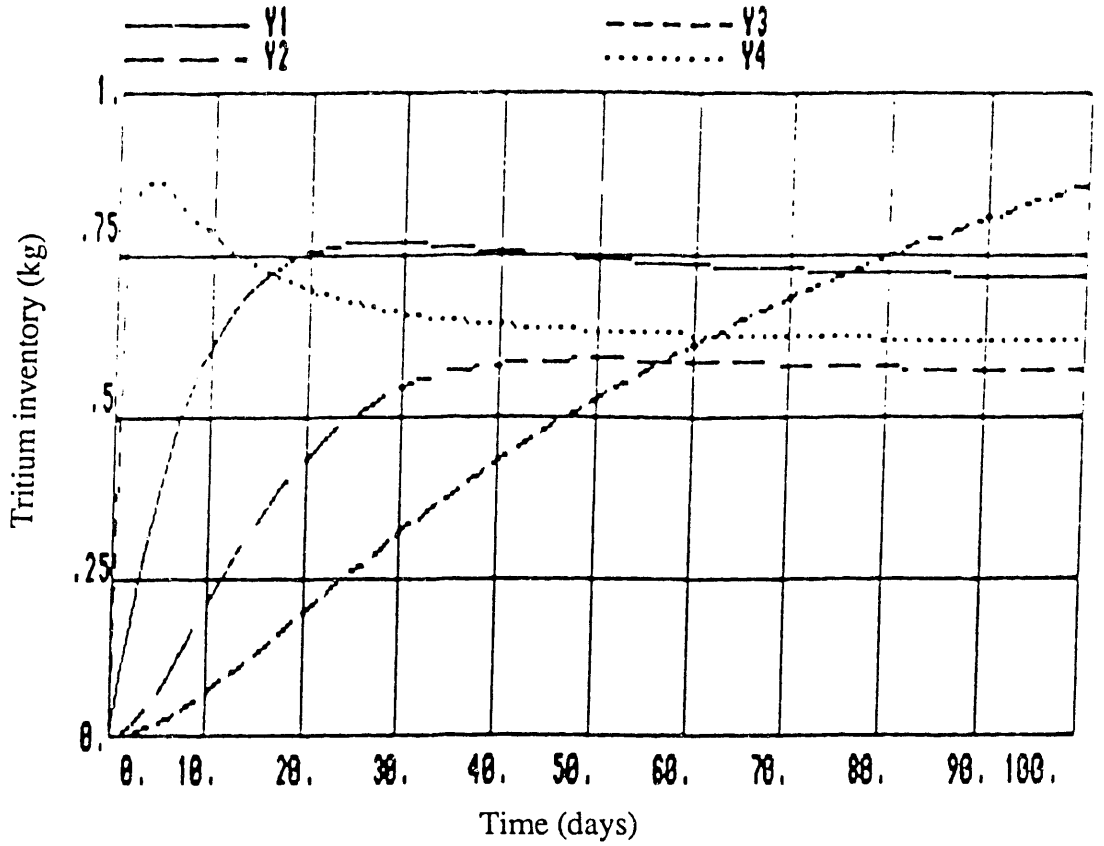

Figure 3.5a. Tritium inventory dynamics in the blanket, breeder processing, coolant processing, and exhaust processing units (T_6 = 0.1 days).

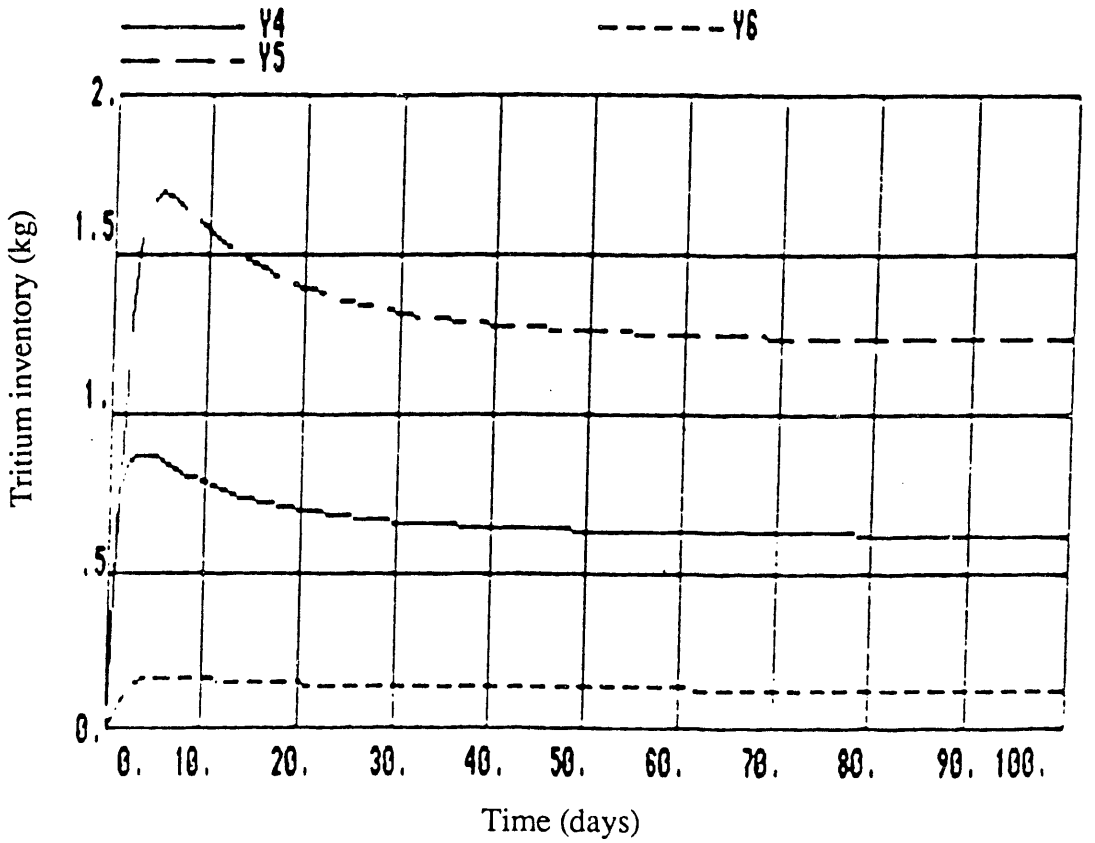

Figure 3.5b. Tritium inventory dynamics in the exhaust processing, gas purification, and isotope separation subsystems (T_6 = 0.1 days).

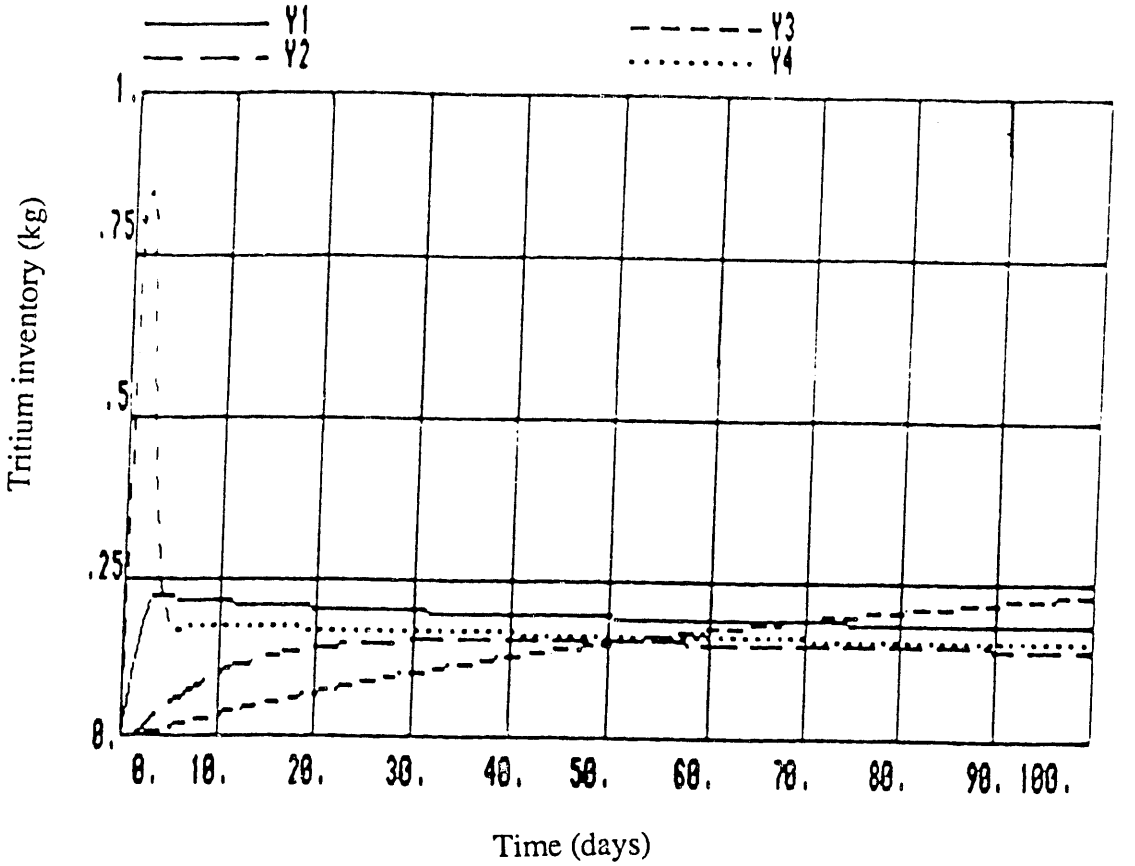

Figure 3.6a. Tritium inventory dynamics in the blanket, breeder, coolant, and exhaust processing units (T_6 = 10 days).

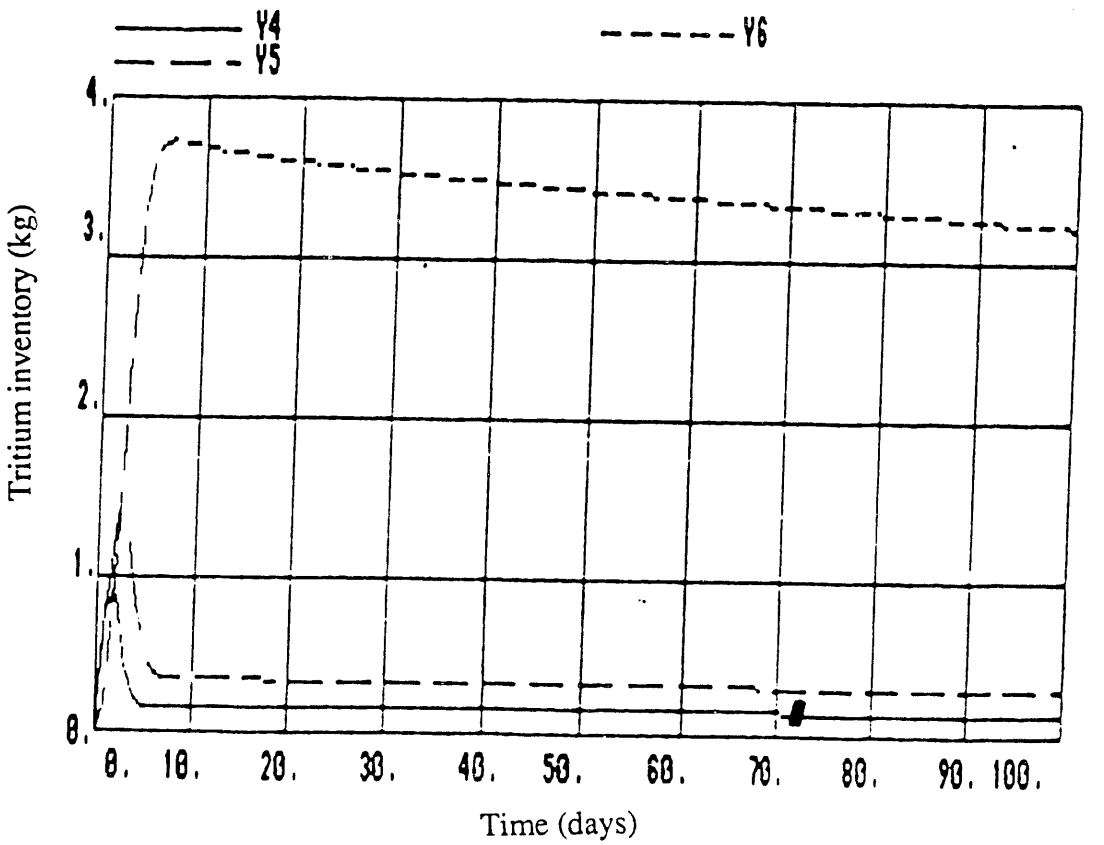

Figure 3.6b. Tritium inventory dynamics in the exhaust processing, gas purification, and isotope separation subsystems (T_6 = 10 days).

Table 3.1. Dynamic simulation parameters.

Subsystem (S)	Tritium mean residence time, T (day)
Storage	1
Blanket	10
Breeder processing	10
Coolant processing	100-600
Plasma exhaust unit	0.5
Purification	1
Isotope separation	1
Waste processing	1
Fueling	0 (effectively)

An attempt will now be made to explain the "unexpected" behavior of the system at this early stage from both the purely mathematical and the physical perspective. To start with the mathematical features of the system, it should be pointed out that the subsystems that have been identified to be the most vulnerable ones are characterized by rather small tritium residence times (in the range of 0.5 - 1 day) compared with the tritium residence times of 10 - 100 days that correspond to the rest of the power-cycle subsystems. This means that although in steady-state operation they should be expected to have rather low tritium inventories, in the early transition period they should tend to rapidly process and locally accumulate tritium, before the rest of the system has the time to respond. This would eventually lead to the observed peak in the tritium inventory, which, in turn, should rapidly --practically exponentially-- fall back into the normal operation mode as the rest of the system starts to effectively respond to the startup of the fuel cycle. The excessive accumulation of tritium in that case would be characteristic of systems consisting of compartments with different response (transit) times. It is the reflection in the tritium system of the *"pipeline effect"*, well-known in systems' theory. This transient phenomenon occurs only through approximately 2-3 days which is within the order of magnitude of the tritium residence time in the corresponding compartments. This shows that before tritium starts dissipating towards the rest of the system, it should be expected to accumulate in those subsystems driven by the constant inflow due to the fueling requirements of the plasma. After this period, tritium flows to the next subsystem and the transient period expands overall to 2-3 days until tritium reaches the ISS for recycling.

From the physical explanation point of view, it can be argued that since all three related subsystems include essentially conventional process-engineering technologies (cryogenic pumps, valves, distillation columns, separators, heat exchangers and a lot of piping), the response time of the specific systems to the initial perturbation of the tritium inventory would be sufficiently large to allow for excessive accumulation of tritium before the distribution system drives it to the rest of the reactor. The relatively conventional technology used in these parts of the system makes them much more vulnerable to accidental release in the case of excessive tritium inventories than most of the other subsystems. The above considerations combined with the steady-state inventories of approximately 1 kg could constitute a real risk from the operation of the fusion power plants that should be taken into consideration even in the case of experimental model-reactors (e.g. the ITER design).

An analysis was carried out of the effect of the time grid that was used in the simulations. Specifically, the time step δt of the integration method was varied from 10 minutes to 1 hour (for simulations of 1-3 years of reactor operation). The results showed that although the numerical method, as discussed in Section 3.1.4, was sensitive to the magnitude of the time step, the general pattern of the system behavior remained the same as above. This last check of the validity of the numerical result proved the reproducibility and accuracy of the simulation.

The traditional consideration concerning the startup inventory[3.7] assumes self-sufficiency operation of fusion reactors. Fusion reactors will, in theory, be able to satisfy their fuel requirements through tritium breeding in the reactor blanket. The reactors will only need an initial tritium inventory to start the fuel cycle and reach sustainable operation conditions; after that breeding should provide enough tritium to sustain the plasma burnup. But for $\Lambda < 1$ and even for some values of $\Lambda > 1$, the operational strategy of plasma burning during the total time of operation cannot be implemented in practice by the initial supply of tritium. Rather small tritium supplies fed into the reactor over the entire period of operation seem to be a more realistic assumption.[3.8] For the mathematical model of tritium inventory, this means that the initial conditions of the system need to be changed. The exact solution would look different in that case. This operational behavior would include reactor operation characterized by long scheduled shutdown periods. It should be pointed out that this more realistic strategy of operation implies simultaneous interruptions in tritium consumption and breeding, but not necessarily in tritium processing.[3.8] The computer code that has been developed has the ability to be interrupted --either programmed or on-line-- at any point of simulation time; the results of the simulation to that point will be saved on the computer memory, and the system can restart using the previously saved values of tritium as initial conditions to the new simulation. This kind of simulation has not been tried so far in this project, because the prevailing assumption has been continuous operation of the reactor which pushes the system to its operational limits. It can, however, provide useful and perhaps more realistic information on the actual tritium burden of the reactor system.

In conclusion, a computer code simulating the tritium processing system in a typical magnetic fusion reactor was developed, after an extended literature survey on tritium systems. The simulation of the tritium system for a parameter set typical of the current design options for magnetic confinement fusion reactors provided useful information on the tritium inventory in the power plant as a function of time. Transient phenomena resulting in excessive tritium inventories in vulnerable parts of the reactor were observed during the first few days after the reactor startup. The results have been checked for their accuracy and reproducibility through sensitivity analysis with respect to the tritium residence times in the corresponding subsystems. The usefulness of the dynamic simulation of the tritium systems is proven by the results described above. The simulation showed that the safety features of the exhaust processing, purification and isotope separation systems have to allow for excessive tritium stocks for short periods of time -- similar behavior is expected to occur each time that the reactor is refueled and restarted-up. This type of behavior could not be identified through a conventional steady-state analysis of the fuel cycle. Dynamic modeling allows for a fast, concise overview of the impact any reactor design alteration would have on the tritium inventory of the fusion power plant both in short- and long-term operation. The dynamic tritium model will be the core of an integrated code that will encompass the design parameters and the interactive and user-friendly parts. In this way, the use of the dynamic model will permit adequate simulation strategies of operation based on actual availabilities of the fuel cycle. The fast computational capacity of the computer code that has been developed will, thus, provide fusion reactor designers with a tool that would allow them to "experiment" with the design features keeping reactor safety in mind.

The future steps that are required to integrate the above model to the work produced by our group include :

-- verification of the validity of the basic assumptions underlying the above described model
-- investigation of the behavior of the model under interrupted operation of the reactor for refueling purposes (in a programmed or stochastic time distribution)
-- simultaneous investigation of the best ways to modularize the part of the code acting as an intermediate between the design and the model parameters (including a closer study of the critical factors affecting the tritium inventory)
-- connection of the two major parts of the code and investigation of the most informative ways to present the results of the simulation
-- linkage of the tritium modeling code for the SUPERCODE that is being developed specifically for the needs of the ITER project.

Subsequently the behavior of the model in critical operating conditions needs to be studied, including incorporation of accident occurrence and stochastic operation mode.

References

3.1. T.J. Dolan, "Fusion Research, Vol. III--Technology", Pergamon Press, New York, (1982).

3.2. "STARFIRE - A Commercial Tokamak Fusion Power Plant Study", Argonne National Laboratory, ANL-FPP-80-1, Argonne, IL (1980).

3.3. M. Kinoshita, H. Yoshida, and H. Takeshita, "A Simulation Study for Hydrogen Isotope Distillation Columns in the Tritium Breeding Blanket System of a Fusion Reactor," Fusion Technol. **10**, 462 (1986).

3.4. W.J. Holtslander, R.E. Johnson, F.B. Gravelle, and C.M. Schultz, "An Experimental Evaluation of a Small Fusion Fuel Cleanup System," Fusion Technol. **10**, 1340 (1986).

3.5. R. Baratti, A.M. Polcaro, P.F. Ricci, A. Viola, and G. Pierini, "Mathematical Model Applied to Permeation Problems of Process Designs for Tritium Recovery from Liquid Blankets," Fusion Technol. **10**, 266 (1986).

3.6. A.Nicolai and P. Boerner, "Minimization of the Tritium Content within the First Wall of a Tokamak Reactor," Fusion Technol. **12**, 119 (1987).

3.7. M.A. Abdou, E.L. Vold, C.Y. Gung, M.Z., Youssef, and K. Shin, "Deuterium-Tritium Fuel Self-sufficiency in Fusion Reactors," Fusion Technol. **9**, 250 (1986).

3.8. E.Gabowitch and G. Spannagel, "Computer Simulation of Tritium Systems for Fusion Technology," Fusion Technol. **16**, 143 (1989).

3.9. J.P. Holdren (Chair), D.H. Berwald, R.J. Budnitz, J.G. Crocker, J.G. Delene, R.D. Endicott, M.S. Kazimi, R.A. Krakowski, B.G. Logan, and K.R. Schultz, "Report of the Senior Committee on Environmental, Safety, and Economic Aspects

of Magnetic Fusion Energy," Lawrence Livermore National Laboratory, UCRL-53766 (1989).

3.10. "Professional DYNAMO+ Reference Manual," Pugh-Roberts Associates, Inc., Cambridge, MA (1986).

3.11. "A User's View of Solving Stiff Ordinary Differential Equations," SIAM Review (1989).

4. ENVIRONMENTAL AND SAFETY INDICES AND THEIR GRAPHICAL REPRESENTATION

This work took as its starting point the indices of environmental and safety (ES) characteristics employed by the Committee on Environmental, Safety, and Economic Aspects of Magnetic Fusion Energy (ESECOM) in its 1985-89 study comparing an array of fusion-reactor and fission-reactor concepts.[4.1] The ES indices used in the ESECOM study covered three classes of hazards, as follows:

(i) ACCIDENT RISKS were portrayed in terms of threshold-dose release fractions (TDRFs) and maximum plausible release fractions (MPRFs) for radioactive materials in different mobility classes and different reactor components. The TDRFs are release-fraction values that must not be exceeded if the resulting doses to members of the public are not to exceed specified threshold values. ESECOM used two such thresholds: a "critical dose threshold" of 200 rem delivered to an individual 1 km downwind of the reactor at the time of the release (below which dose no early fatalities from acute radiation syndrome would be expected); and a "chronic dose threshold" of 25 rem over a period of 50 years from ground contamination at a distance of 10 km from the reactor (above which extraordinary decontamination and/or evacuation measures would be required). The MPRFs were based on time-temperature profiles for accident scenarios judged to be the most severe plausible for the specified reactor designs, coupled with experimental and theoretical results for the mobility of activated materials under the hypothesized conditions. No credit was taken for the effects of a containment building or active release-suppression measures.

(ii) RADIOACTIVE-WASTE MANAGEMENT BURDENS were portrayed in terms of: intruder doses, calculated according to scenarios devised by the U.S. Nuclear Regulatory Commission (NRC) for the circumstance of inadvertent intrusion into shallow waste-burial sites after 100, 500 and 1,000 years; annualized waste volumes; annualized intruder hazard potentials (combining intruder doses with volumes); and deep-disposal indices (reflecting the quantity and intensity of wastes failing to qualify for shallow burial under existing NRC guidelines).

(iii) POTENTIAL RADIATION HAZARDS TO WORKERS were represented by remote maintenance ratings based on contact radiation doses from semi-infinite surfaces having the activation composition of various plant components (first wall, inner blanket, manifold, shield) at various times after shutdown (0, 1 hour, 1 day, 1 week, 1 month, 1 year, 30 years).

In the ESECOM study, these indices were calculated on a VAX computer using the FUSEDOSE code,[4.2] given results of neutron-activation calculations for a specified reactor design as input and given certain conclusions—from a safety-assessment team—about release fractions for the most severe physically plausible accident sequences. All of the ES indices computed in the ESECOM study were presented simply as tables of numbers; none were in graphical form.

From this starting point, the part of the UCB ESE Code Development project dealing with ES indices and their graphical representation had the following specific aims:

(a) extend, refine, and update the ESECOM array of ES indices to improve their accuracy, comprehensiveness, and comparability with other studies, in the process making use of ongoing work elsewhere on the releasability and dosimetry of fusion isotopes;

(b) develop graphical representations of the ES indices in order to improve ease of interpretation and comparison (e.g., between different fusion-reactor designs and between fusion and fission cases);

(c) streamline, modularize, and automate the calculation of the indices and the preparation of their graphical representations, so that these steps can be carried out on desktop computers (or, at least, workstations) and so that they can be embedded eventually in modular form into fusion-reactor design codes;

(d) apply these improved tools to the ES characterization of the ESECOM reference cases, of fusion-reactor designs based on the ESECOM cases but with materials changes intended to facilitate comparison with other work (e.g., designs with stainless steel structure), and of emerging fusion-reactor designs.

The ultimate aim of these efforts is to increase the attention given to ES aspects of fusion-reactor design by making available a generally accepted, easily used, and easily interpreted set of calculational tools that will make it simple—indeed, almost automatic—for fusion-reactor designers to see and understand the ES implications of their design choices.

Progress on aims (a)-(d) during the first three years of the project is summarized in the subsections that follow.

4.1 EXTENSION, REFINEMENT, AND UPDATING OF ESECOM ES INDICES

The relationships among a variety of ES indices and the calculations that generate them are shown in flow-diagram form in Fig. 4.1, and the characteristics of the indices are described further in Table 4.1. Because of the liabilities indicated in the table for inventory versus time and biological hazard potential (BHP), these indices were not used in the ESECOM study; dose potentials requiring somewhat more calculation, but in exchange offering more insight, were used instead.

Since, however, many other fusion and fission ES studies in the past have used radioactivity and BHP as hazard indices, and some contemporary studies continue to do so, we modified the FUSEDOSE code in the current project to calculate and plot radioactivity inventory and BHP as a function of time, as well as time-integrated biological hazard potential (IBHP), in addition to the more illuminating dose-based indices. Figure 4.2 provides samples of the radioactivity-inventory and BHP outputs. The Recommended Concentration Guidelines (RCGs) used in the BHP calculations for fusion isotopes not yet included in the RCG tables of the Code of Federal Regulations were obtained from the recent work of Fetter.[4.3]

The findings from this recent work of Fetter were also used to update the dosimetry for fusion isotopes (and to include some isotopes previously omitted for lack of data) in the parts of the FUSEDOSE code that calculate potentials and threshold dose release fractions. At the same time, all the dose equations in FUSEDOSE were rechecked, some minor errors in the calculation of ground doses were found and corrected, and some approximations were improved.

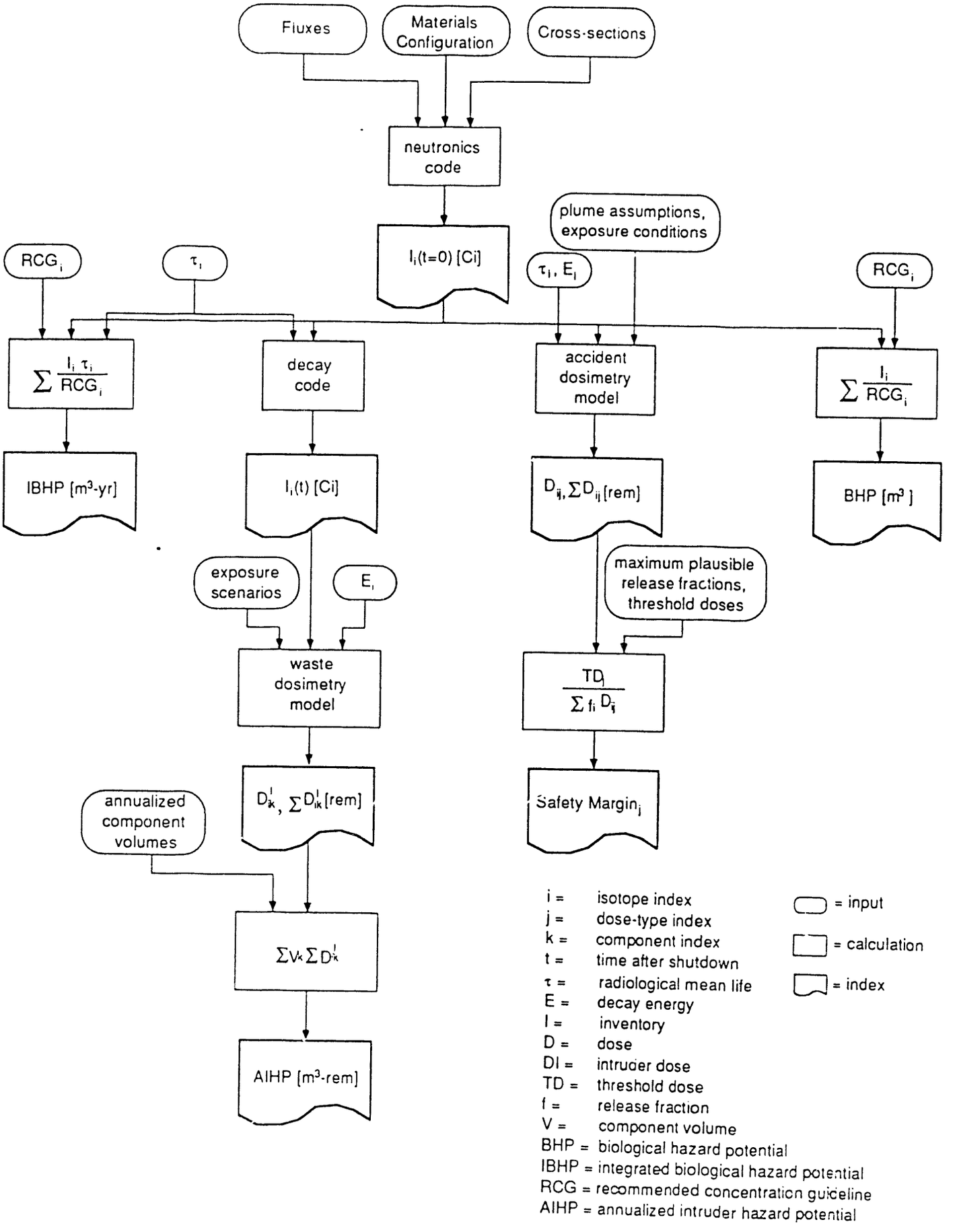

Figure 4.1. Some consequence-oriented hazard indices.

Table 4.1. Some hazard indices and their characteristics.

Symbol	Description	Units	Meaning	Derivation	Attractions as an Index	Liabilities as an Index
I (t=0)	inventory at shutdown	Ci	instantaneous rate of radiation producing nuclear transformations	neutronics calculation requiring materials, configuration, fluxes, and cross-sections as inputs	easiest radioactivity-related measure to calculate	no information about duration of hazard, or dose potential per transformation
I(t)	inventory as a function of time	Ci	time-varying rate of radiation-producing nuclear transformations	obtained from $I_i(t=0)$ using decay/buildup code	adds temporal dimension to initial inventory	still no information about dose potential per transformation
BHP	biological hazard potential (or dilution volume)	m^3	volume of air or water required to dilute a given inventory to the allowable concentration	BHP=I/RCG, where RCG is the Recommended Concentration Guideline in Ci/m^3. BHP may be summed over isotopes, and as functions of time.	incorporates information about fate of particular isotopes in body, energy deposited per transformation, and effectiveness of this energy in causing harm	RCGs are based on continuous exposure (not transient exposure as in accidents) and do not incorporate info about actual pathways of released material.
IBHP	integrated biological hazard potential	m^3yr	initial dilution volume times radiological mean life	IBHP = BHP x tau. IBHPs may be summed over isotopes	weights BHPs by longevity of hazard, incorporating time more simply than showing time trajectory of BHPs	other defects of BHP remain
CRDP	complete-release dose potential	rem	dose that would be delivered to a person by release of 100% of inventory under unfavorable conditions	transport and dosimetry calculations requiring distances, weather conditions, and aspects of behavior of victim as inputs	dose is what we really care about, since it can be directly correlated with effects we seek to avoid	doses depend strongly on assumption that can be the subject of dispute. Full release is usually not plausible.
MPD	maximum plausible dose	rem	dose that would be delivered to a person by worst physically plausible release	in addition to requirements for CRDP, requires knowing maximum plausible release fractions and worst plausible weather	avoids unrealistic implications that 100% release is possible	calculations of maximum plausible release fractions re-quire detailed and difficult accident analysis, easily subject to dispute
SM	safety margin	dimensionless	ratio of threshold dose to MPD	SM = TD/MPD, where the threshold dose, TD, is what one wishes to avoid	it is useful to express distance from threshold as a dimensionless number.	liabilities same as for MPD, plus difficulty of agreeing on threshold.
EPD	expected population dose	person-rem/reactor-yr	expectation value of sum of individual doses from reactor accidents	probabilistic risk assessment, entailing product of probability and population-dose consequences summed over all possible accidents	weights potential consequences by their probabilities, giving best overall measure of hazard	probability calculations for complex systems are notoriously difficult.

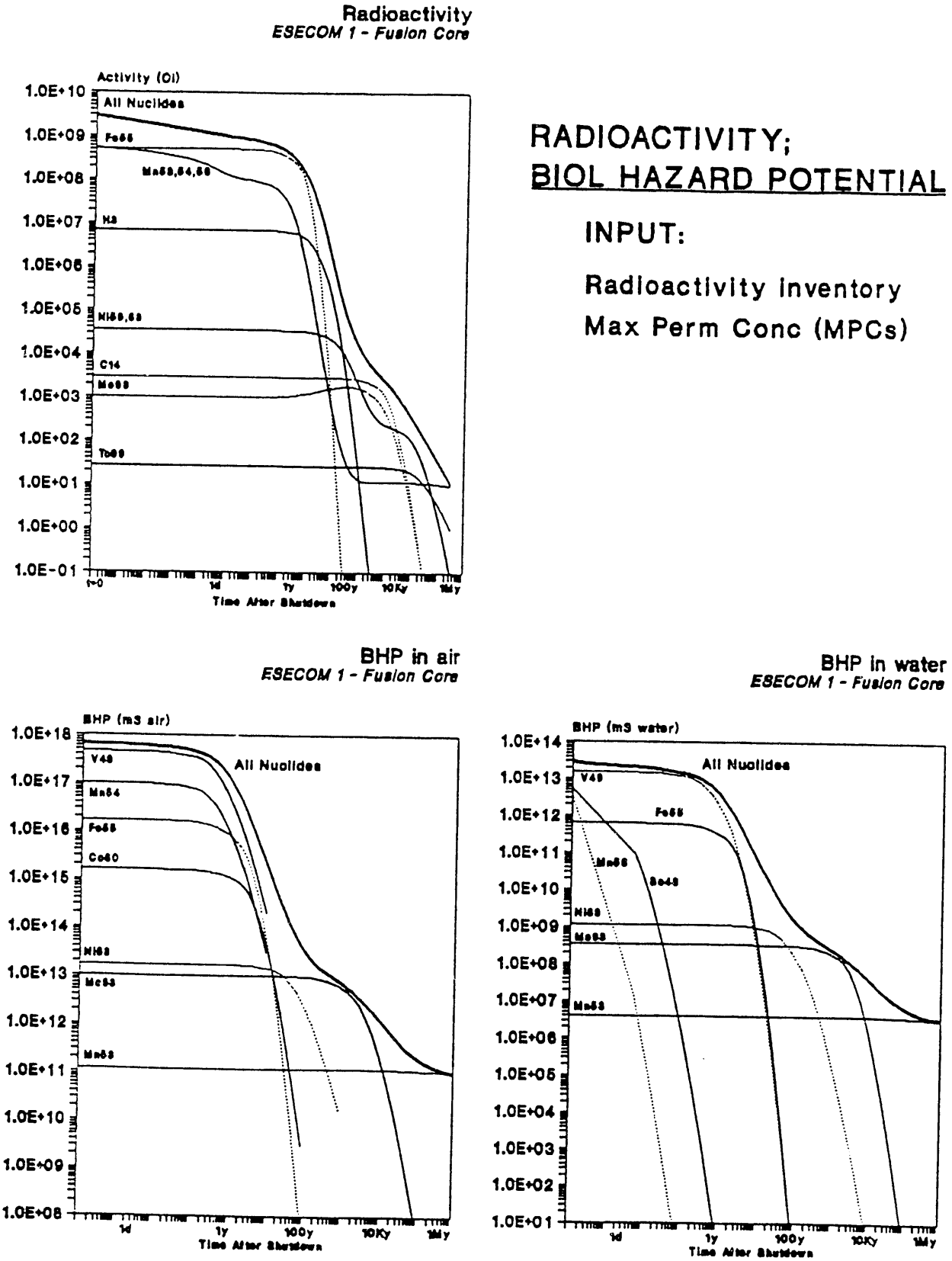

Figure 4.2. Radioactivity inventories and Biological Hazard Potentials (BHPs) in air and water, based on Recommended Concentration Guidelines for public exposure, are shown for times between shutdown and 1 million years for the ESECOM study's Case 1, a tokamak with vanadium-alloy structure and liquid lithium coolant/breeder.

In the ESECOM study, a part of the safety analysis not easily amenable to encoding was the estimation of plausible release fractions in severe accidents. This work—which required development of accident scenarios, estimation of the associated magnitudes and durations of elevated temperatures, and integration of these estimates with data and theories about the mobilization of structural materials under extreme conditions—involved diverse models, substantial iteration, and much committee discussion. It is a major aim of the second three-year period of the current project to devise algorithms that will provide a satisfactory encodable version of this process of relating reactor-design characteristics to plausible release fractions; given the difficulty of the problem and the press of other priorities in the project, only limited progress was made on this issue in the first three years (incorporation into FUSEDOSE of the capacity to calculate afterheat generation rates versus time in different reactor components, and the beginning of development of a scheme combining this information with surface to volume ratios and materials properties to characterize vulnerability to release).

To permit an automated approach in the meantime, we incorporated into FUSEDOSE a user-controlled option to select one of a limited number of standardized "envelopes" of severe-accident release fractions of isotopes in the five mobility classes. (These categories, as developed in the ESECOM study, range from Class I—material highly mobile even at normal operating temperatures, such as noble gases and tritium—to Class 5—material highly resistant to mobilization even at the highest temperatures attainable in an accident, such as uranium and titanium.) Examples of such "envelopes" are as follows:

Severe-accident release fraction under:

	Conservative Envelope	Optimistic Envelope
Class I	1.0	1.0
Class II	0.3	0.1
Class III	0.1	0.01
Class IV	0.03	0.001
Class V	0.01	0.0001

The "optimistic" envelope resembles the one deduced in the ESECOM study for a vanadium/titanium-structure fusion reactor subjected to a lithium fire; the "conservative" envelope resembles the ones obtained in the NRC's 1975 Reactor Safety Study[4.4] for the most severe accidents in fission light-water reactors, and arguably can serve as an upper limit as well for fusion cases with substantial amounts of stored energy and enhanced mobilizability of refractory materials because of erosion, corrosion, and effects of neutron bombardment. In any case, use of the "conservative" envelope for both fission and fusion cases when comparing the two energy sources avoids the criticism that fusion is being made to look superior simply through an insufficiently substantiated assumption of lower release fractions.

4.2 GRAPHICAL REPRESENTATION OF ES INDICES

Providing ES indices in graphical form can make the associated information easier to assimilate—compared to tables of numbers—especially in cases of comparisons between different reactor components, different reactor types, and different time frames. Particularly for individuals who are not specialists in ES issues, good graphics can be the key to communicating the ES consequences of specific choices in the process of reactor design.

Results of the work of the current project in graphical representation of ES indices are shown in Fig. 4.3 through 4.6. These figures were produced using Harvard Graphics software on a 286-class PC, starting from the numerical output produced by our updated version of the FUSEDOSE code. (We have also developed a version of the ES-graphics code for the Macintosh.)

Figure 4.3 displays the complete release dose potential and the maximum plausible dose (measured as "critical' doses—the 7-day dose plus half of the 8th-through-30th-day dose to an individual 1 kilometer from the reactor during plume passage) for ESECOM's "point of departure" vanadium-structure/lithium-cooled tokamak, disaggregated by reactor component and by the mobility categories of the contributing isotopes. The dark horizontal lines denote the 200-rem threshold dose corresponding to the possibility of early fatalities from acute radiation syndrome. Vertical bars extending above this horizontal line indicate dose potentials exceeding the threshold. The stacked (diversely shaded) bars alone contain all of the information, but the solid black bars for the separate mobility categories facilitate comparisons between these mobility categories. The release envelope used for the maximum plausible dose (bottom half of the figure) is the "conservative" one described above. This maximum plausible dose figure reveals at once that the principal critical-dose problem in this reactor design is the Category III isotopes in the iron part of the manifold; shifting to an all-vanadium manifold would solve this problem.

Figure 4.4 shows aggregated critical dose potentials—full release and maximum plausible release with the "conservative envelope"—and safety margins for nine ESECOM cases, seven fusion and two fission. The upper part of the figure conveys a great deal of information at a glance: where the shaded bars denoting the maximum plausible release do not reach the horizontal 200-rem line, there is no chance of early fatalities off-site from even the worst accident. (Additional information could easily be provided in this graphic, at the expense of a bit more visual clutter, by stacking the mobility-category contributions within the bars.) Essentially the same information is presented in the bottom half of the figure; the "safety margin" is just the ratio of threshold dose divided by the complete release dose potential or the maximum plausible dose, so that where this figure is less than unity it is actually a "hazard margin".

Figure 4.5 uses the stacked-bar format in horizontal orientation to show the contact dose rates for different components at different times after shutdown. The dark vertical line is drawn at 1 rem/hour—a level corresponding to the possibility of limited "hands-on" maintenance using protective clothing. The graphic makes strikingly apparent the differences between reactors in the contact-dose profiles across components at different times after shutdown. It also shows iron and steel components do not fall to the 1 rem/hour level until 30 years or more after shutdown, even if they are as far removed from the most intense neutron fluxes as is the shield.

Figure 4.6 shows radioactive-waste indices for seven ESECOM fusion cases plus a fission LMFBR. Part "a" combines information about life-cycle volume of wastes (LCV), annualized intruder hazard potential (AIHP), and deep disposal index (DDI), and Part "b"

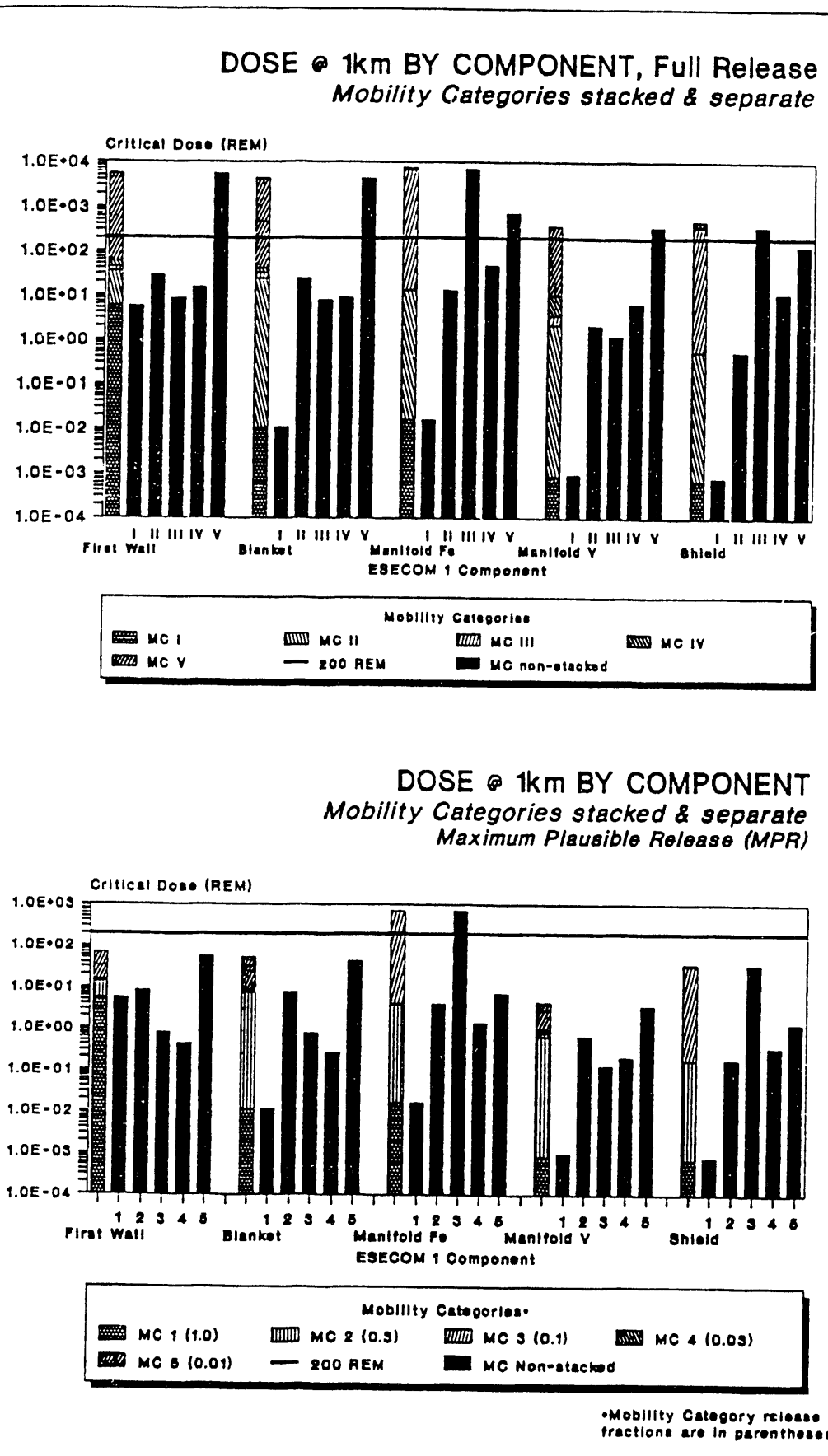

Figure 4.3. Complete release and maximum plausible release critical-dose potentials for ESECOM Case 1.

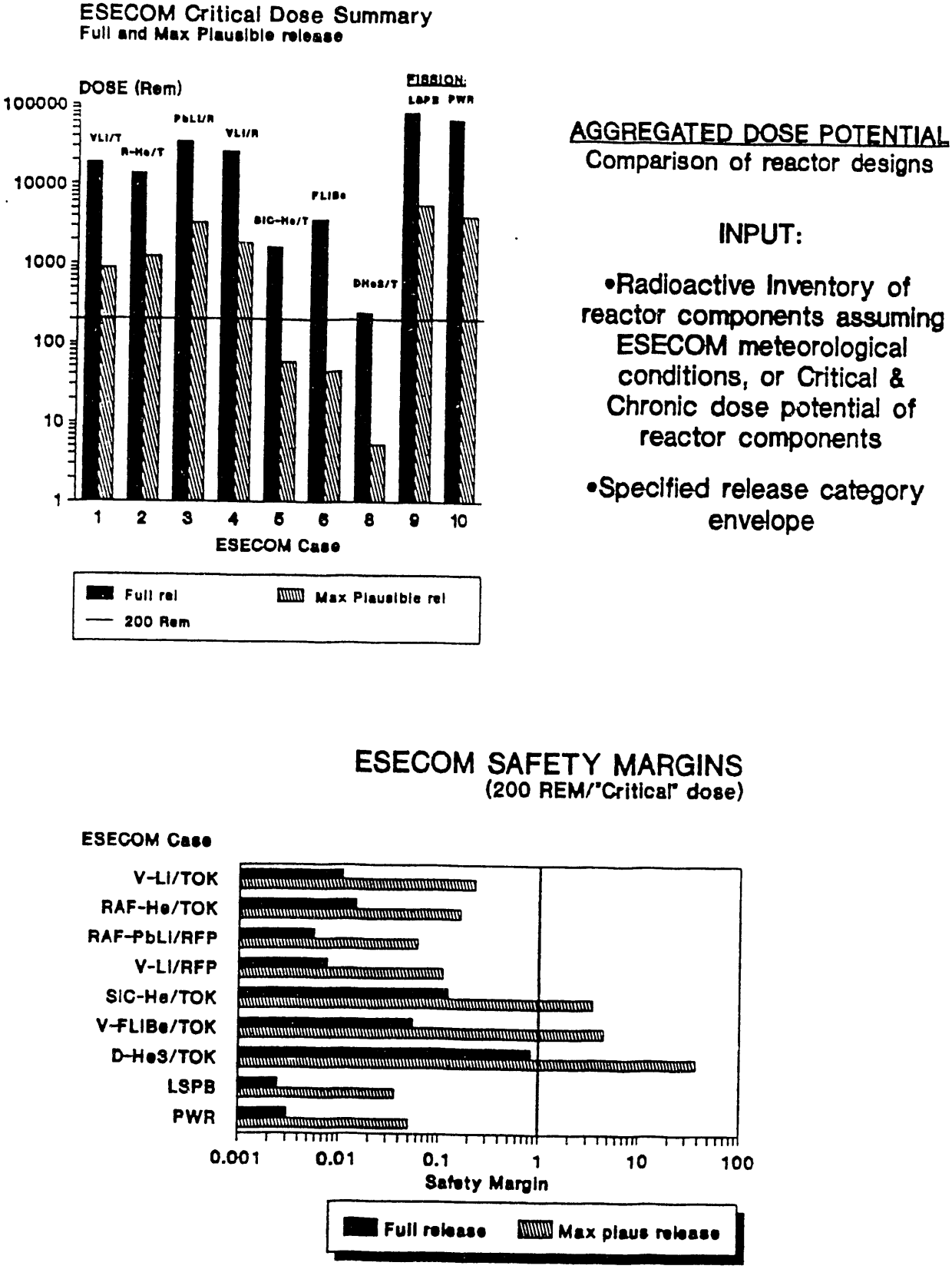

Figure 4.4. Comparison of critical-dose potentials and safety margins for seven fusion and two fission cases from the ESECOM study.

MAINTENANCE, OCCUPATIONAL HAZARD

INPUT: Contact Dose Rate of reactor components

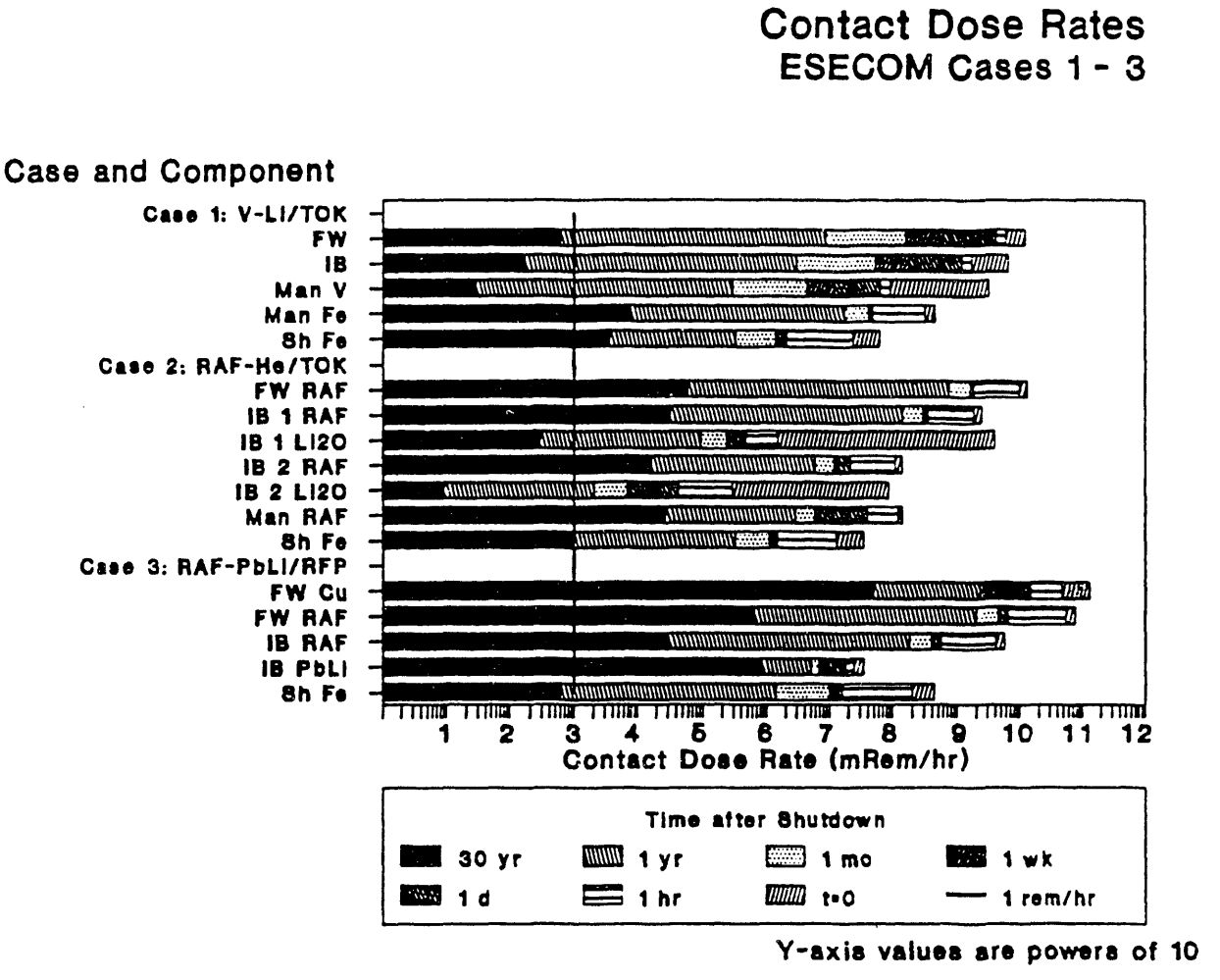

Figure 4.5. Contact dose rates versus time after shutdown for three ESECOM cases.

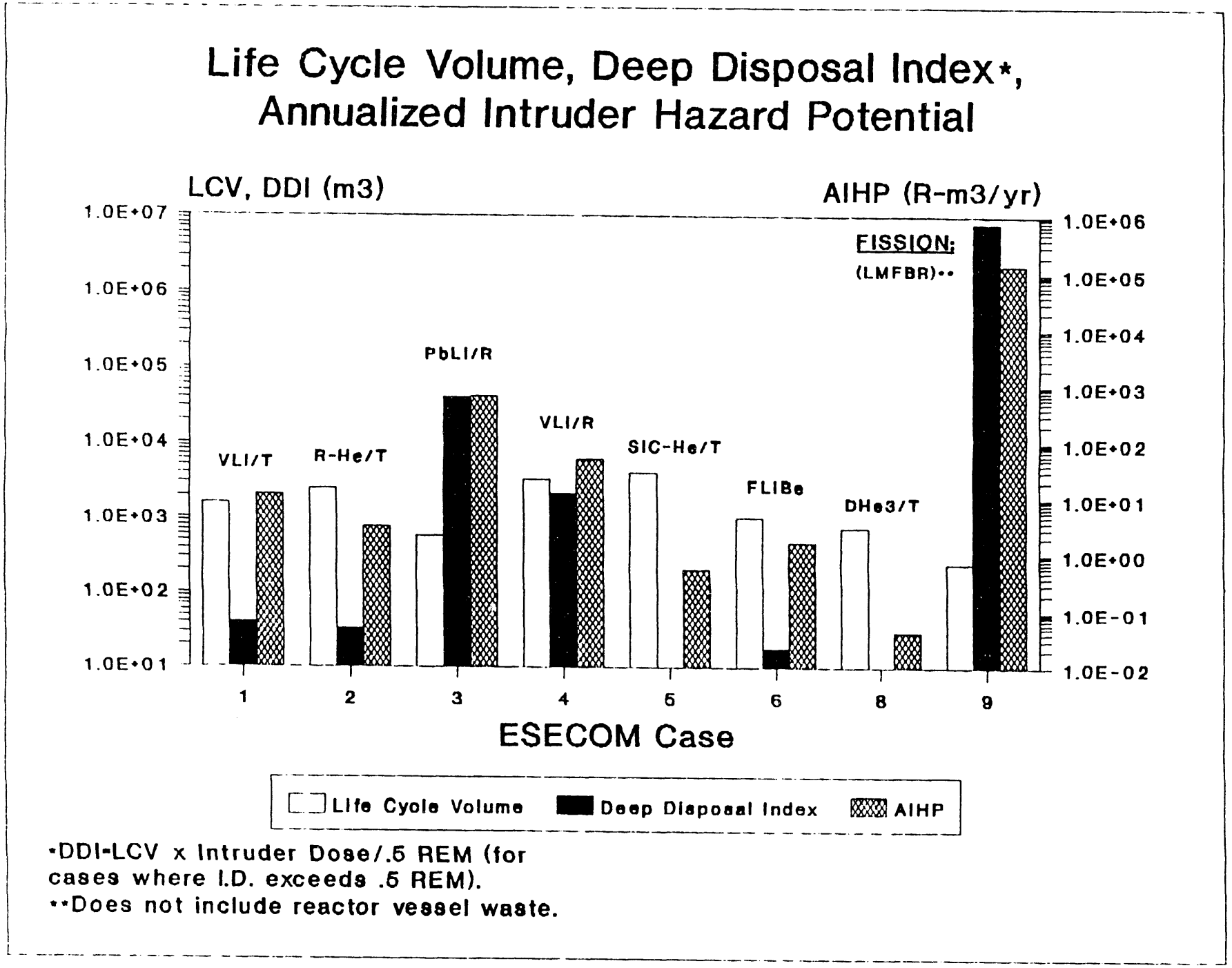

Figure 4.6a. Three indices of radioactive waste hazard for seven fusion and two fission cases from ESECOM study.

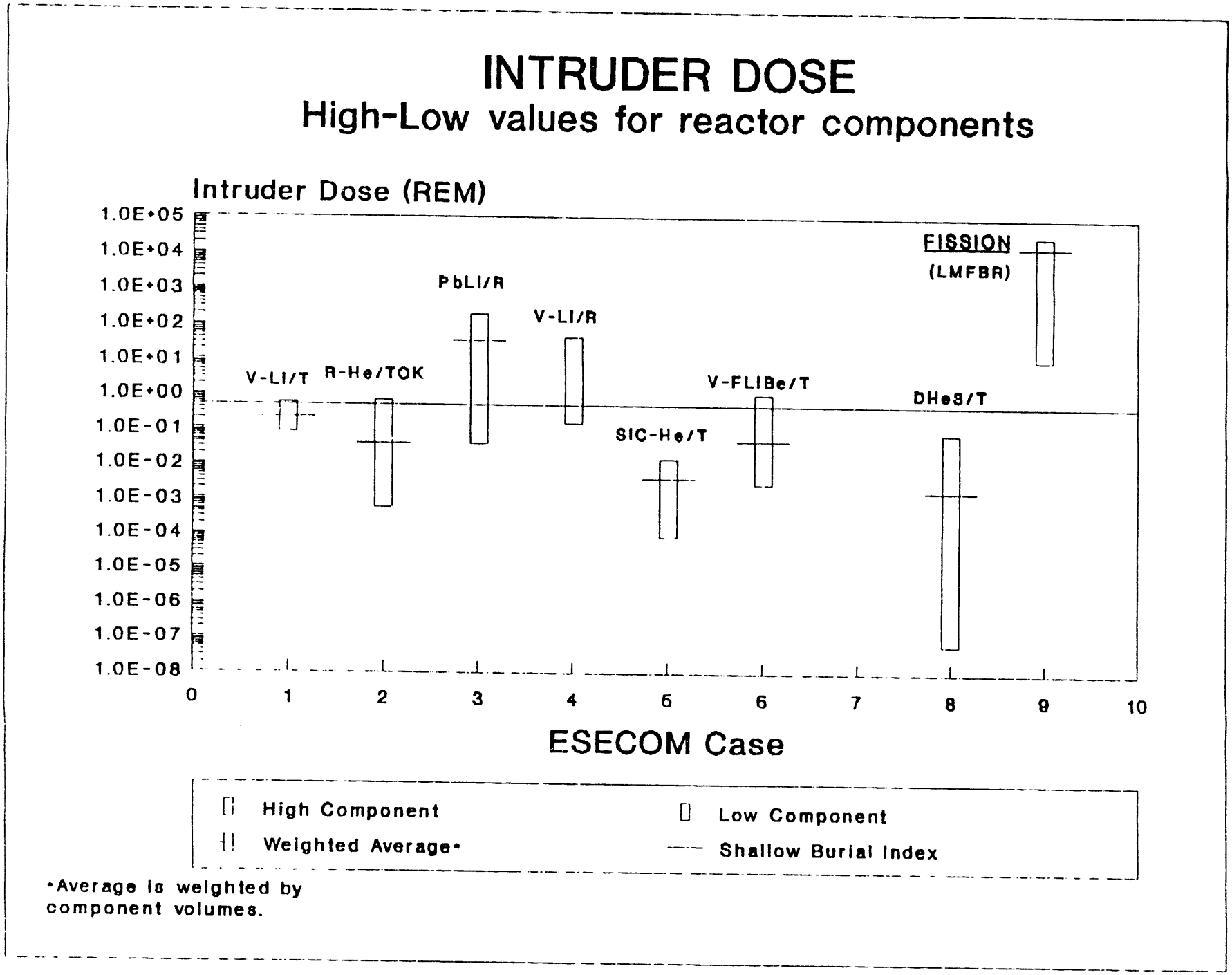

Figure 4.6b. Intruder dose potential associated with shallow burial of wastes from seven fusion and one fission case from the ESECOM study.

shows the variation in intruder dose among reactor components in relation to the volume-weighted average. The horizontal line in the bottom graphic is at 0.5 rem/year, which is the threshold for shallow burial under current U.S. regulations. If any part of the vertical bar extends above the 0.5 rem/year line, it means that at least some reactor components would not qualify for shallow burial; if, however, the volume-weighted average is below the line, then in principle mixing of the activated material from different components would qualify the wastes for shallow burial. We note, as did the ESECOM study, that our use of indices based on current U.S. shallow-burial criteria does not imply any conclusion on our part that shallow burial will necessarily prove to be the best approach for managing fusion waste; rather, the use of such criteria is simply a convenient way to characterize relative waste-management burdens in a manner that accounts systematically for mobility and dose potentials based on an internally consistent model of release pathways. We are continuing to work to improve our approach to characterizing waste hazards, recognizing that our indices in this category are less transparent and potentially more controversial than those we have developed for reactor accident potential and worker hazard potential.

Much of the work summarized here is described in much greater detail in the M.S. thesis of Paul Hibbard.[4.5] Additional work is underway to select a graphical format for portraying in summary form, on the screen of a reactor designer's workstation, a maximally informative subset of the ES indices presented here. The designer would then be able to call up more detailed presentations as needed.

4.3 STREAMLINING, MODULARIZATION, AND AUTOMATION

The Fetter FUSEDOSE computer codes have been rewritten to speed up the calculations and modularized to facilitate integration with fusion-reactor design codes in a way that offers the user an array of choices about how much and what kinds of ES information will be calculated and presented. Development of automated interfaces between neutronics codes and the FUSEDOSE modules is largely complete. The graphical user interface with which the user would interact at a workstation in order to direct the ES calculations and inspect their output is also well along; sample screens from the Macintosh version are shown in Fig. 4.7 through 4.10.

References

4.1. J. P. Holdren, D.H. Berwald, R.J. Budnitz, J.G. Crocker, J.G. Delene, R.D. Endicott, M.S. Kazimi, R.A. Krakowski, B.G. Logan, K.R. Schultz, "Exploring the competitive potential of magnetic fusion energy: the interaction of economics with safety and environmental characteristics," Fusion Technol. **13**, 7 (1988). See also J. P. Holdren, D.H. Berwald, R.J. Budnitz, J.G. Crocker, J.G. Delene, R.D. Endicott, M.S. Kazimi, R.A. Krakowski, B.G. Logan, K.R. Schultz, "Report of the Senior Committee on Environmental, Safety, and Economic Aspects of Magnetic Fusion Energy," UCRL-53766, Lawrence Livermore Natl. Lab., (1989).

4.2. S. Fetter, "A calculational methodology for comparing the accident, occupational, and waste-disposal hazards of fusion reactor designs," Fusion Technol. **8**, 1359 (1985).

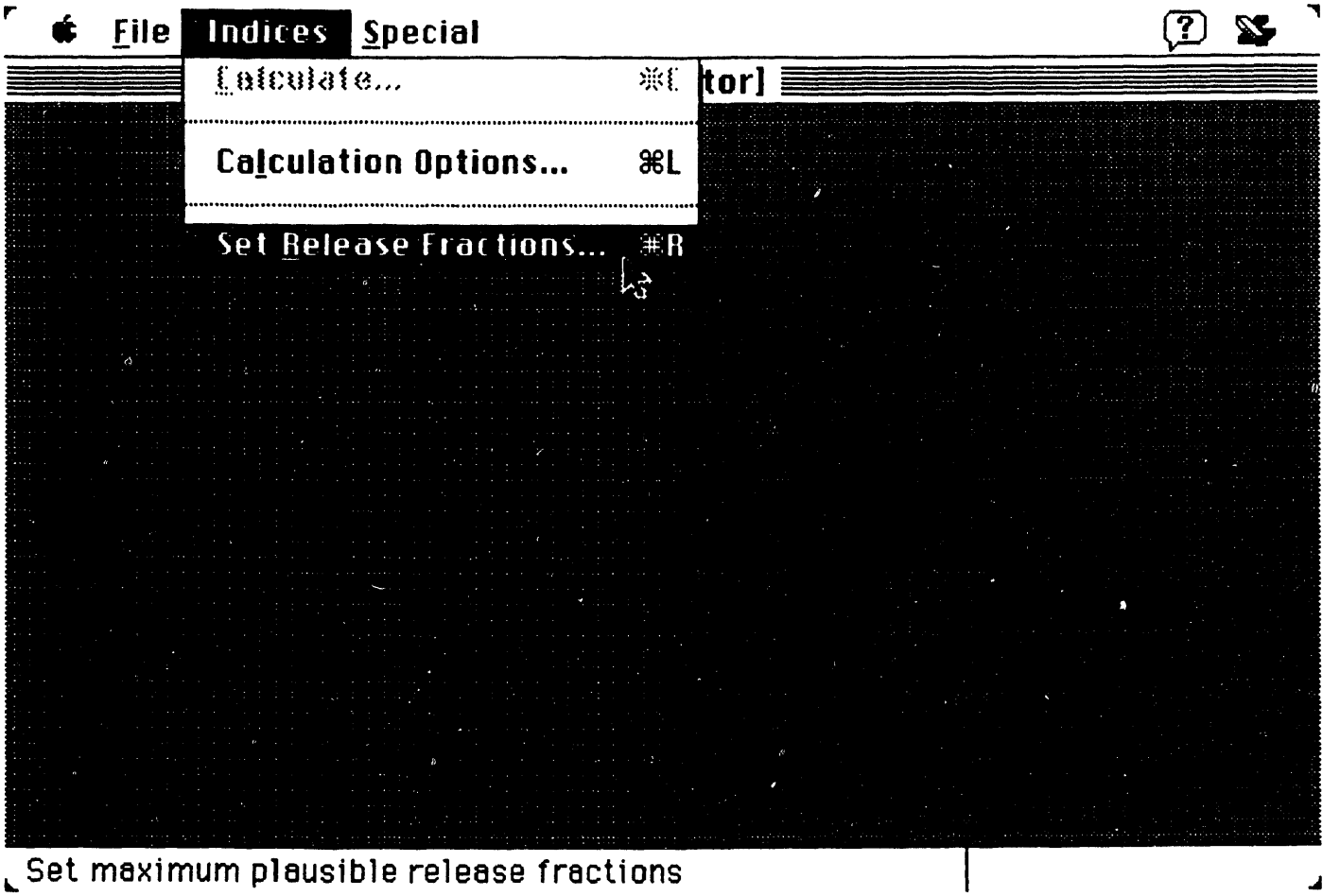

Figure 4.7. Pulldown menu in the Macintosh version of the ES code's new graphical user interface. Menus can be navigated by mouse or by keyboard.

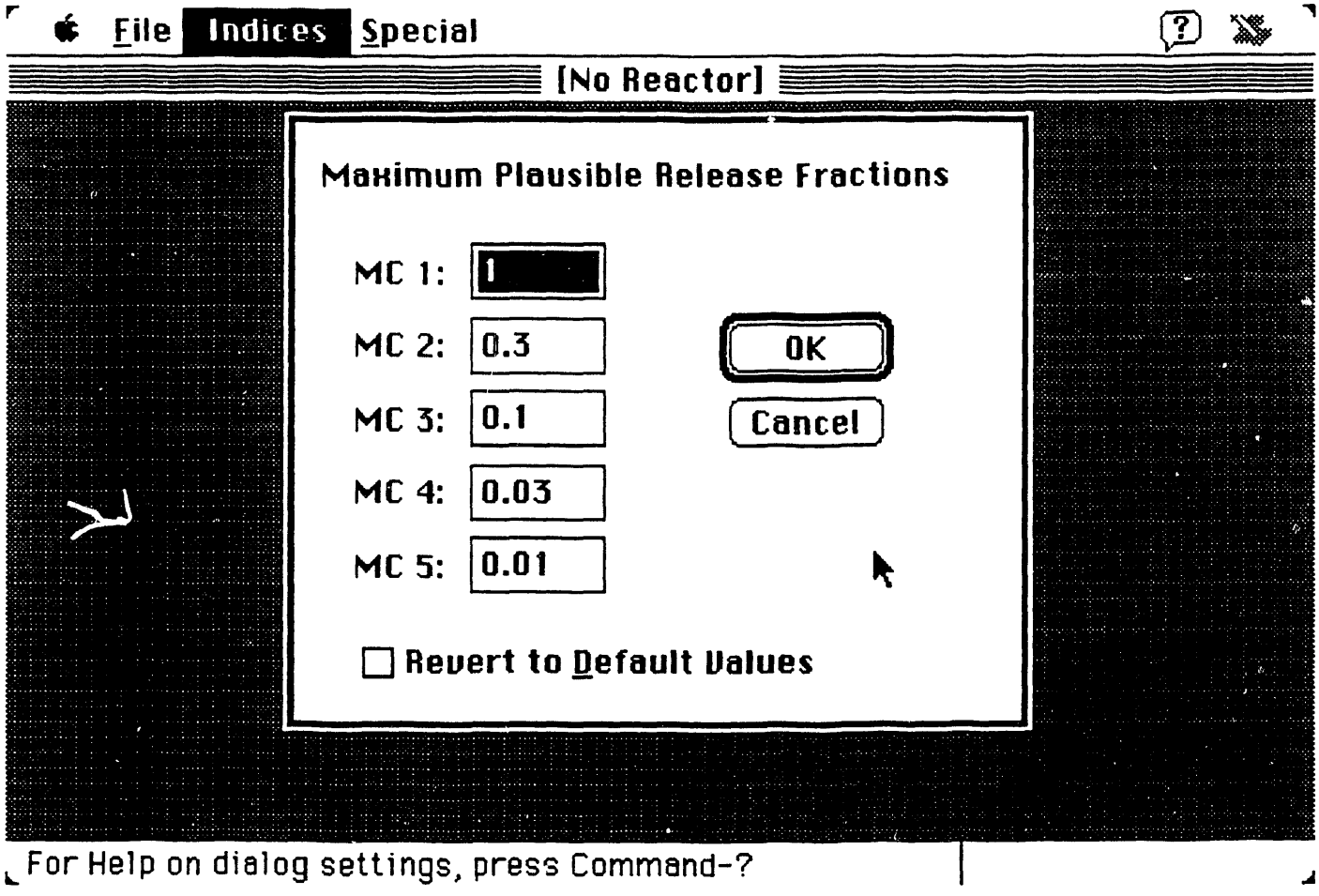

Figure 4.8. Dialog box in the Macintosh version of the ES code's new graphical user interface. In this dialog box, the user sets Maximum Plausible Release Fractions.

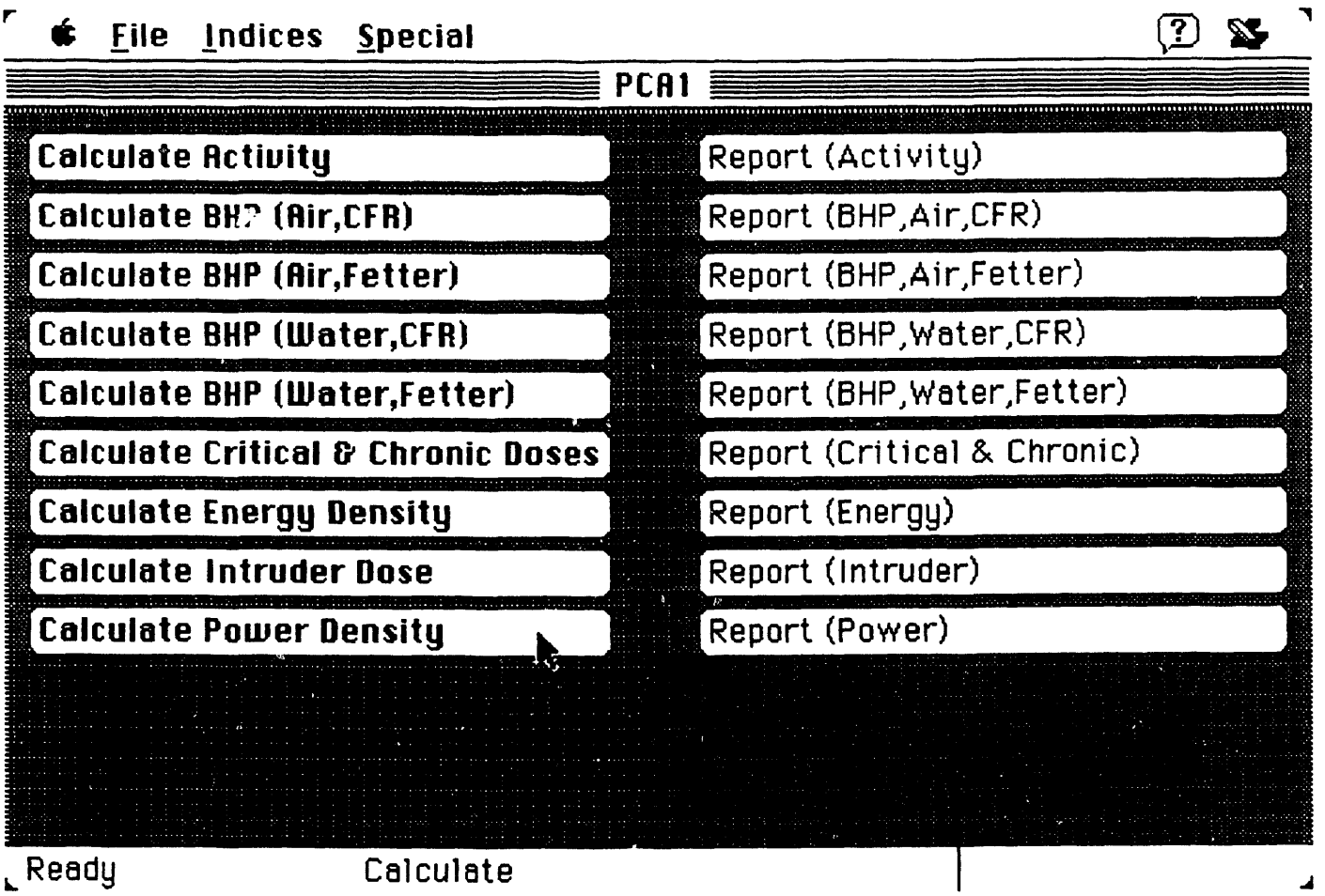

Figure 4.9. Push buttons in the Macintosh version of the ES code's new graphical user interface. Push buttons start calculations or display results on-screen.

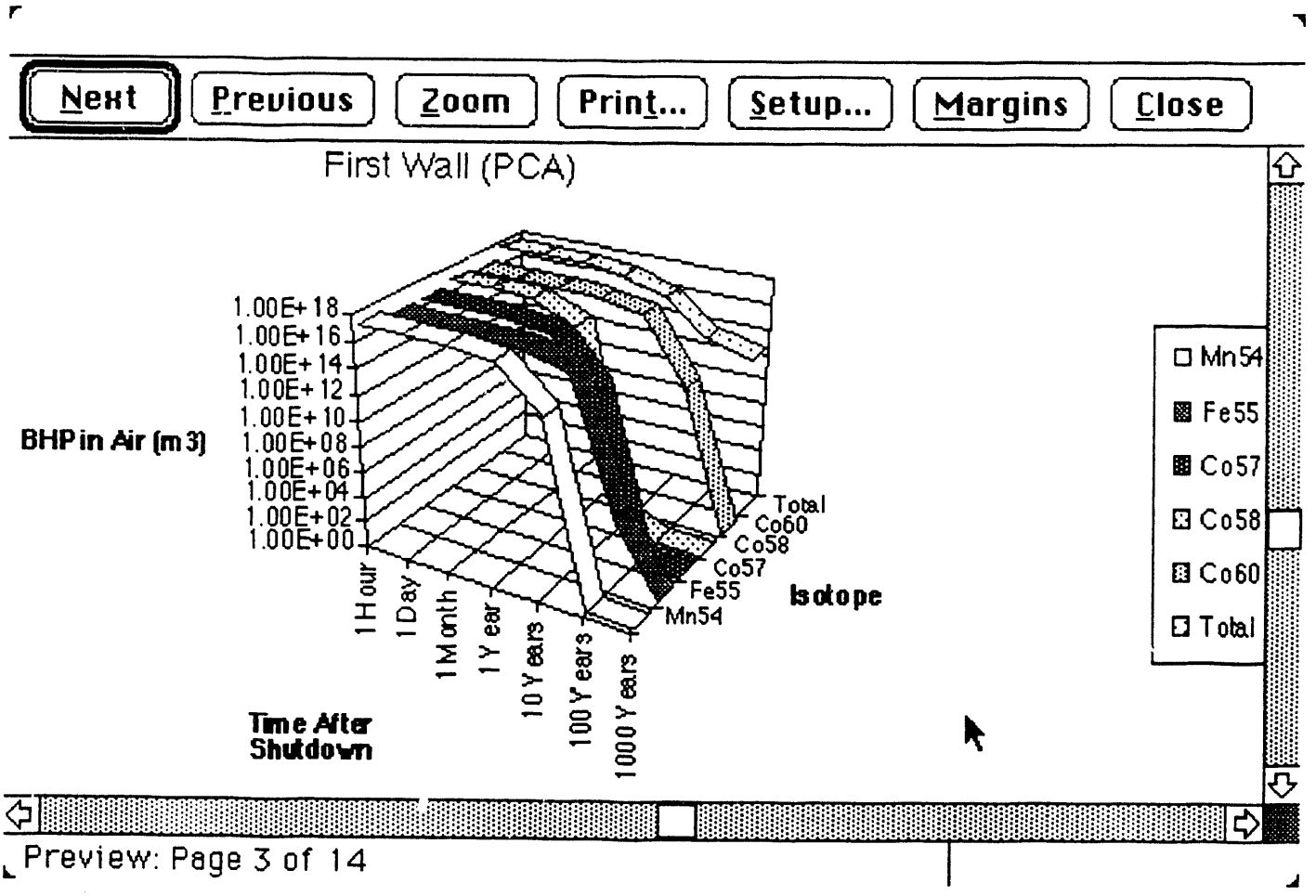

Figure 4.10. Graph displayed on-screen in the Macintosh version of the ES code's new graphical user interface. All results can be viewed on-screen.

4.3. S. Fetter, "Internal dose conversion factors for 19 target organs and 9 irradiation times and external dose-rate conversion factors for 21 target organs for 259 radionuclides produced in potential fusion reactor materials," EGG-FSP-8036, Idaho Natl. Engineering Lab., (1988).

4.4. US Nuclear Regul. Comm., "Reactor Safety Study," WASH-1400 (NUREG-75/014). Springfield, VA: Natl. Tech. Inf. Serv. (1975).

4.5. P.J. Hibbard, "The Display of Fusion-Reactor Radiological Hazards," M.S. Thesis, Energy and Resources Group, University of California, Berkeley, December, (1990).

5. PROBABILISTIC RISK ASSESSMENT (PRA) AND DECISION ANALYSIS

Consistent with our long-term goals, we have initiated an evaluation of applications of PRA and decision analysis to reactor fusion design. Thus far we are carrying out this work in parallel with other approaches to provide information to the designers and decision makers. Section 5.1 explores the merits and points out the difficulties of PRA for a fusion reactor at this early stage of design, while section 5.2 undertakes a probabilistic analysis of tritium release accidents based on a simple model. In section 5.3, the application of multi-objective decision-under-uncertainty analysis to reactor design selection is considered, specific theoretical tools and their potential extension are presented, and an analysis of a sample problem is demonstrated.

5.1 APPLICATION OF PRA TO FUSION REACTOR DESIGN

5.1.1 Introduction

In its comparative analysis, the ESECOM study[5.1-2] focused mainly, and for good reasons, on fission as fusion's potential competitors. However, the methods used for the analysis are not those prevalent in the fission industry since the publication of the "Reactor Safety Study"[5.3], namely probabilistic risk (or safety) analysis. ESECOM explains its avoidance of the probabilistic approach arguing that "trying to carry out such an exercise (PRA) for fusion reactors, for which neither operating experience nor even highly detailed designs are available, would be premature at best."

The foregoing explores in general the potential application of PRA methods from the very early stages of design of fusion facilities and suggests a possible framework within which this can be accomplished. Accident risks are discussed, but the arguments would be much the same for radioactive-waste aspects and occupational hazards.

5.1.2 Advantages of PRA Application to Fusion

The major advantages of probabilistic (as opposed to deterministic) risk analysis of MFE facilities are explained briefly below. Although PRA strengths (or corresponding shortcomings of the deterministic approach) specific to fusion and fission devices are emphasized, some are generic, albeit not less important. A few examples are given.

(A) Probabilistic models most adequately describe the *inherent stochastic nature* of major safety and environment related factors. Among these are:

(1) Accident progression (escalation) from initiating events, through possible failure of safety sub-systems, to potential release of radioactivity to the environment.
(2) Meteorologic conditions determining the atmospheric dispersion of released radionuclides.
(3) Location, shielding, and response of potentially exposed population during a major accident.
(4) Effects of radiation (especially low-dose, latent and genetic).

(B) Deterministic point-value risks and safety criteria are unsatisfactory.

Figure 5.1 depicts an instant of comparing the risks of two hypothetical designs, using both deterministic and probabilistic approaches. The risks of the designs (with respect to some specific consequence) are represented by *risk curves* (see Addendum and Ref. 5.4 for the definitions of risk used here*) "A" and "B", where, the point (deterministic) estimate shows design "B" to be preferred to design "A" (since $E(X_A) > E(X_B)$, where E(X) denotes the expected consequence in a unit time, say, one year**). Also, let x_0 denote the deterministic safety criteria (meaning the maximum permissible consequence magnitude). Clearly, design "B" is unacceptable by this criterion while design "A" is! A properly constructed probabilistic safety curve (connecting points each of which allows a consequence of magnitude x_n or higher to occur at a maximum rate R_n), like the one shown in dashed line, could not lead to such inconsistencies when applied to the risk curves.

(C) PRA allows for consideration and evaluation of many risk acceptance factors. Two of these are (1) high-consequence-low-probability versus low-consequence-high-probability risks; and (2) the level of certainty with which risks are known.

Figure 5.2 illustrates these factors. Again, risk curves of two hypothetical designs are compared, but this time the point estimates of the risk are the same: $E(X_A) = E(X_B)$. A probabilistic approach will immediately reveal, however, that design B is associated with higher consequences at lower rate of events than design "A" and is possibly, therefore, less acceptable by public or individuals. If, in addition, the certainty with which risks are known in both cases is represented by the confidence level curves shown, design "B" might be preferred after all since it is much less uncertain in the high consequence range.

(D) Probability distributions of system parameters (e.g., failure rates of components) are explicitly considered in the analysis. They can be updated, using observable data from operating history and conducted experiments, and propagated through the analysis into significant uncertainties of results. (In contrast, deterministic analysis does not end up with confidence margins of results.)

(E) During the PRA process (especially the system analysis stage) "weak links" of the system (materials, components, sub-systems ties) are identified; the impact of changes in design on the risk can be quantitatively evaluated and compared to alternative designs. The vast experience in constructing fault trees, analyzing event trees and, lately, using influence diagrams, allows, for example, to quickly determine the change in a risk curve affected by the addition of a specific safety feature, given its (conditional) probability distributions of failure in various postulated scenarios.

(F) Use of vague or qualitative notions in the deterministic approach such as "worst case", "maximum plausible/credible accident", etc., is eliminated by assigning explicit probabilities to all thinkable mishaps of the facility.

---

* This is the conventional definition (model) for risk used by the U.S. Nuclear Regulatory Commission. An alternative and more natural definition is also given in the appendix.

** Strictly speaking, the integral of the risk curve is equal to E(X) for the second definition of risk only (see appendix). It can be shown, however, that for consequences not too small in magnitude, the integral is a good approximation for E(X) with the conventional definition as well.

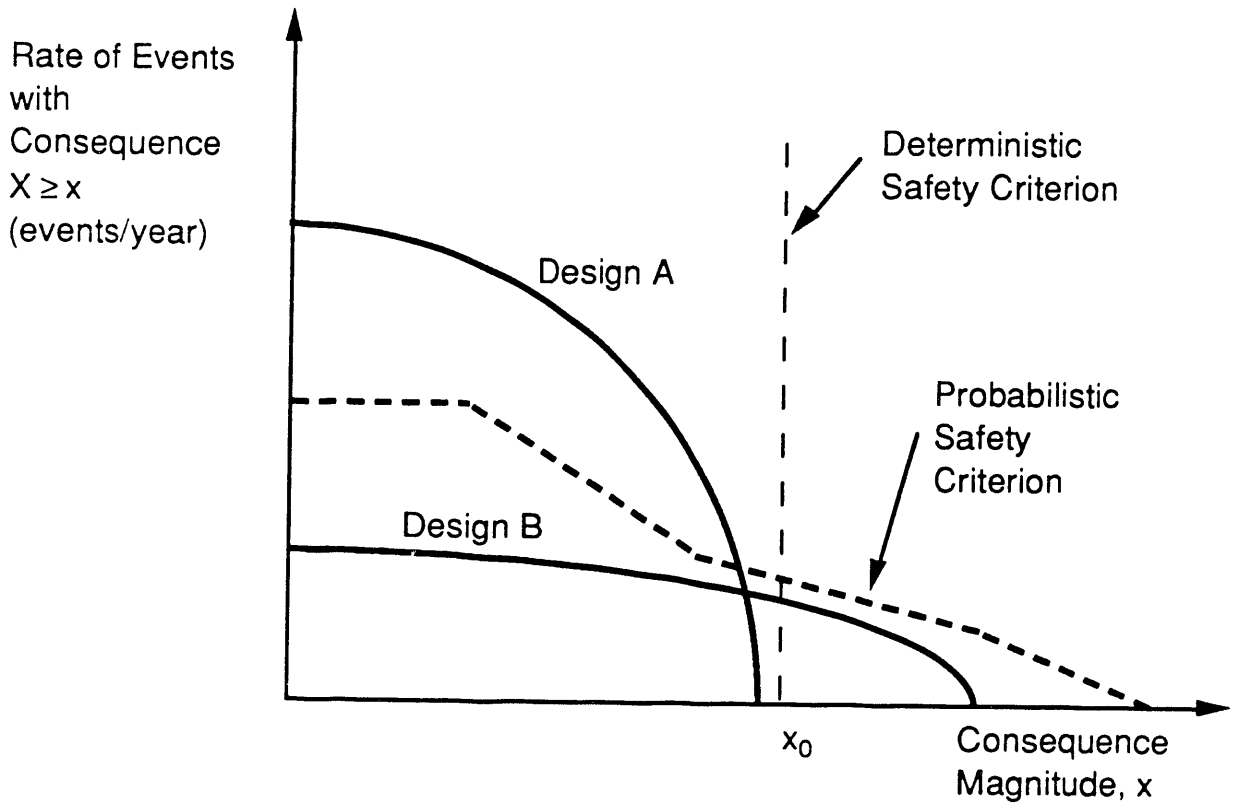

Figure 5.1. Inadequacy of deterministic safety criteria.

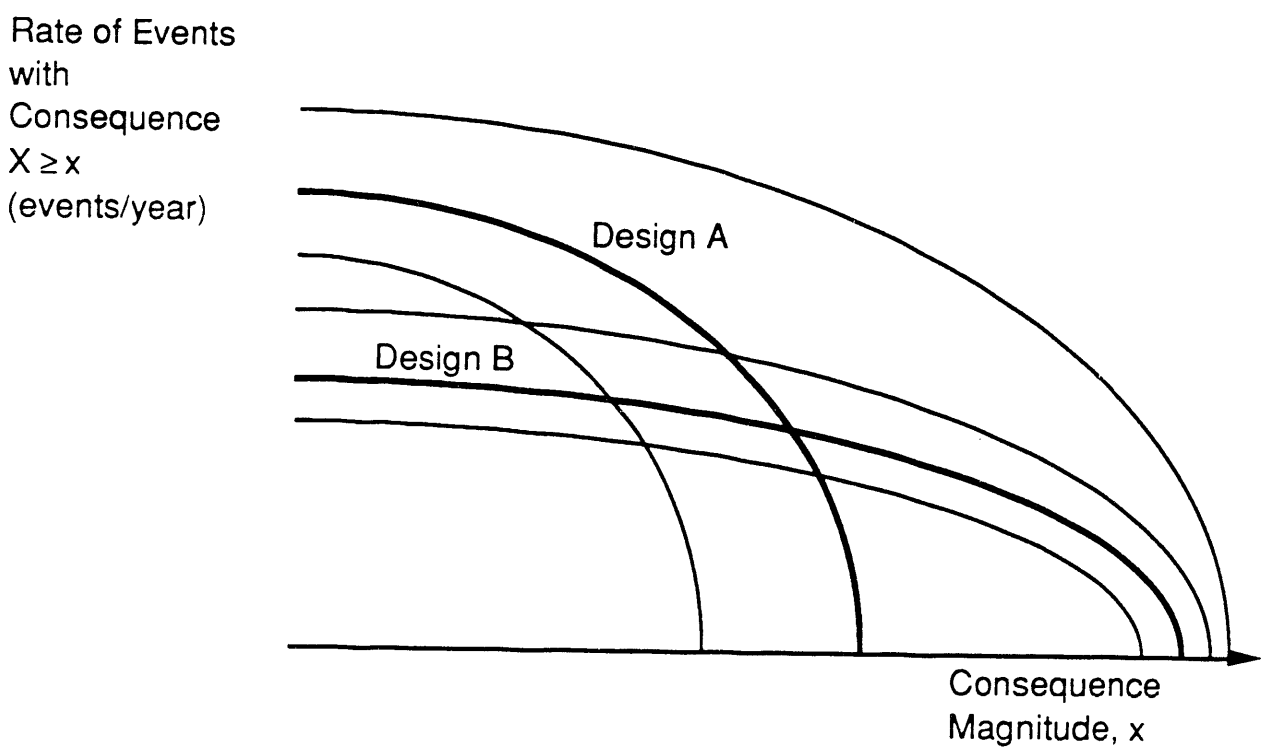

Figure 5.2. Explicit consideration of risk acceptance factors.

With thousands of reactor-years of operating experience in the fission reactor industry, the above advantages have been demonstrated again and again. PRA techniques have also become increasingly significant in the nuclear regulatory process.[5.5] Indeed, a lesson ought to be learnt from the fission case and conclusions can be applied to the MFE:

(1) The earlier in the design process PRA is applied, the more profound its impact on the system safety will be.
(2) With clearly set safety goals, PRA can be used to optimize design, in the sense of minimizing cost of safety-related systems and better protection of capital investment in the plant.
(3) Operational experience data existing from the fission industry on some "conventional" components and sub-systems (e.g., stand-by generators, motor-operated valves, etc.) could be directly used in the analysis of MFE systems.

It should be noted that difficulties in conducting a PRA analysis for an MFE facility are hard to estimate; not only as mentioned in Section 5.1.1, operating experience and highly detailed designs are practically unavailable, but also the range of design variations (associated with different materials, power densities, and conversion schemes) is wide. Additionally, no data on human operator errors (which proved critical to safety of fission plants[5.6])specific to an MFE plant is available.

Notwithstanding these difficulties, it should be recognized that the lack of operational history, and therefore wide prior distributions for system parameters, "merely" gives rise to increased uncertainties of the results. However, these can be be substantially reduced by using many-expert estimates for system parameters, or better, conducting tests for the new materials and components. Undetailed designs will also result in higher uncertainties, but PRAs should go along with the design process from early stages and grow in complexity (and certainty of results) with it.

5.1.3 Suggested Use of PRA in the Design of a Magnetic Fusion Plant

Figure 5.3 summarizes the main constituents of PRA to be applied during the design of an MFE machine. The general framework emphasizes the iterative use of PRA: with clear safety goals and a specific design in hand, risks can be calculated and critical links identified; an alternative design, eliminating or improving the latter, will be examined in a similar manner, and repeatedly so until safety criteria are satisfied or design is optimized in some sense.

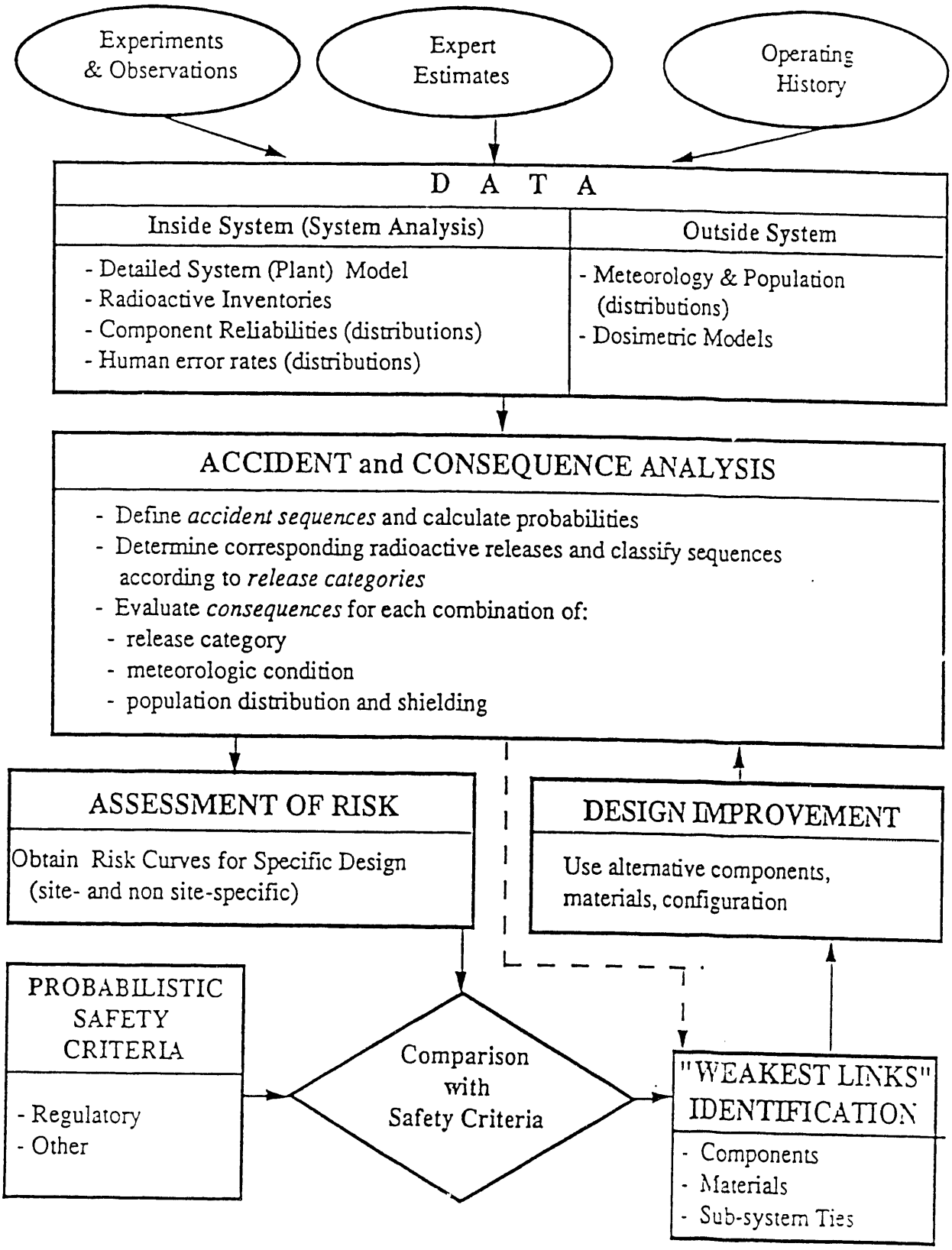

Figure 5.3. Iterative use of PRA in the design of a nuclear fusion plant.

Addendum: Some Definitions of Risk and their Interrelation

The first definition of risk and the following three derived upon are conventionally used in the U.S. Nuclear Regulatory Commission reports.

Risk Density, $R_i(x_j, t)$ [events/time unit/consequence unit]

Expected rate of events of type i at time t producing an ultimate consequence of type j with magnitude in the range (x_j, x_j+dx_j), per unit of consequence.

Risk, $R_i(X_j \geq x_j, t)$ [events/time unit]

Expected rate of events of type i at time t to produce an ultimate consequence of type j with magnitude x_j or greater:

$$R_i(X_j \geq x_j, t) = \int_{x_j}^{\infty} R_i(x,t)dx$$

Composite Risk, $R(X_j \geq x_j, t)$ [events/time unit]

Expected rate of all possible events at time t to produce an ultimate consequence of type j with magnitude x_j or greater:

$$R(X_j \geq x_j, t) = \sum_i R_i(X_j \geq x_j, t)$$

Time Integrated Composite Risk, $R(X_j \geq x_j, T)$ [events]

Expected number of all possible events in a future period [0, T] to produce an ultimate consequence of type j with magnitude x_j or greater:

$$R(X_j \geq x_j, T) = \int_0^T R(X_j \geq x_j, t)dt$$

An alternative and different definition for risk ($R_i(X_j \geq x_j, t)$, second above) is the probability of one or more events of type i in the interval (t, t + 1), each producing an ultimate consequence of type j with magnitude x_j or greater.

If N(t) represents the number of such events in the interval (t, t + 1), then the first definition is E[N(t)], while the second is P[N(t) > 0], where P stands for the probability. Note, however, that:

$$E[N(t)] = \sum_{j=0}^{\infty} P[N(t) > j] = P[N(t) > 0] + \sum_{j=1}^{\infty} P[N(t) > j]$$

and for not too low consequence X_j, it is generally true that the probability of 2 or more events per year, say, is much smaller than the probability of 1 or more events. Hence, the two definitions comply with this restriction. See also appendix in Ref. 5.7.

5.2 A SIMPLE-MODEL PRA OF TRITIUM RELEASE ACCIDENTS

5.2.1 Introduction

Fuel cycle activities and handling of tritium-contaminated materials can result in release of tritium to the environment. Tritium may be released either as routine leaks from imperfect fluid system connections, valves and pumps, permeation through pipes and vessel walls, or in accidents. Only the accidental releases will be examined here. The process of the safety analysis adopted in this paper is depicted in Fig. 5.4.

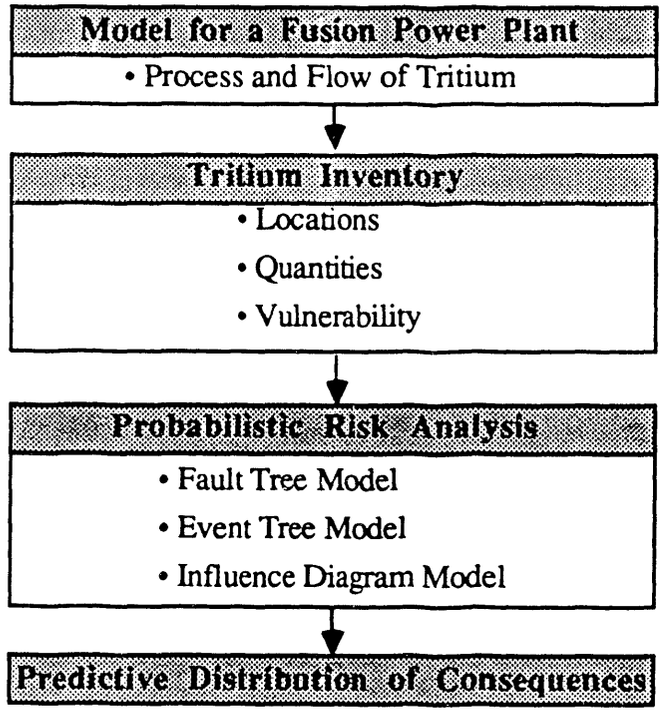

Figure 5.4. Process of safety analysis of tritium release accidents.

We first describe the fusion plant with a simple model that concentrates on the flow of tritium. The potential consequences from a tritium release are directly related to the tritium inventory and tritium flow rates through the plant. So, the next step is the assessment of the tritium inventory and vulnerability at various locations. Then we construct an event tree to model tritium release from abnormal initiating events. Branch parameters on the event tree are assessed from fault tree analysis (not carried out here). An influence diagram, equivalent to the event tree model, which is more useful for the parameter updating and analysis, is then constructed. We briefly discuss how a predictive distribution of consequences can be obtained and how the branch parameters can be updated.

5.2.2 A Model for Tritium Flow

A simple model for the tritium process and flow in a typical power plant design has been adopted. It consists of the plasma chamber, the vacuum system (VAC), the coolant system, the fuel cycle system, the blanket tritium recovery (BTR) system, and the emergency tritium cleanup (ETC) system. The fuel cycle system includes the fuel cleanup (FCU) system, the isotope separation system (ISS), the fuel storage, the fuel injection (FIJ) system, and the tritium waste treatment (TWT) system. Figure 5.5 shows the flow of tritium through these systems.

The tritium inventory and vulnerability in each of the systems was then estimated. For simplicity, inventories were classified as either vulnerable or non-vulnerable, depending on their probability of release (if it was estimated to be higher than 10^{-6} per year, we say the tritium is *vulnerable*).

The quantity of tritium found in the plasma chamber during operation of the reactor is the product of the average tritium density and the plasma volume. The amount of tritium contained in the torus at a given time is not large. But this inventory is classified as vulnerable, since breach of containment would allow for the immediate release of the tritium inventory.

The tritium inventory in the cryopumps depends on the tritium exhaust rate from the torus and the regeneration period. The tritium in vacuum pumps can be affected by accidents and failures of other components because these pumps are close to the torus. The ingress of air into torus, and hence into the vacuum system, or loss of liquid-helium cooling to the pumps would cause tritium release. Thus the tritium inventory in the cryopumps is also considered as vulnerable.

The tritium inventory in the breeding blanket is established from neutron interactions with lithium. The inventory in the blanket is considered as vulnerable because of the possibility for the liquid metal to drain from the reactor and release its tritium inventory in certain accident scenarios.

The blanket structure contains tritium inventory because of tritium implantation and permeation. Tritium implantation is dependent upon the tritium flux impinging on the first wall and the first wall condition. Tritium permeation is a function of the permeability and thickness of the metal involved. The diffusion rates of tritium in metals are fairly high, thus possible thermal transients could "bake-out" the tritium in a short period of time. Tritium contained in the structure is designated as vulnerable.

The coolant system presents another potential source for tritium release. Tritium can permeate or leak from the plasma through the first wall or from the blanket into the coolant system. This inventory is also classified as vulnerable.

The tritium inventories in the fuel cleanup system, the isotope separation system, the tritium waste treatment system, and the fuel storage are classified as *non-vulnerable* because of multiple containment used and/or high reliability of components. These inventories are disregarded from further analysis. Table 5.1 summarizes typical vulnerable tritium inventories at the various locations.

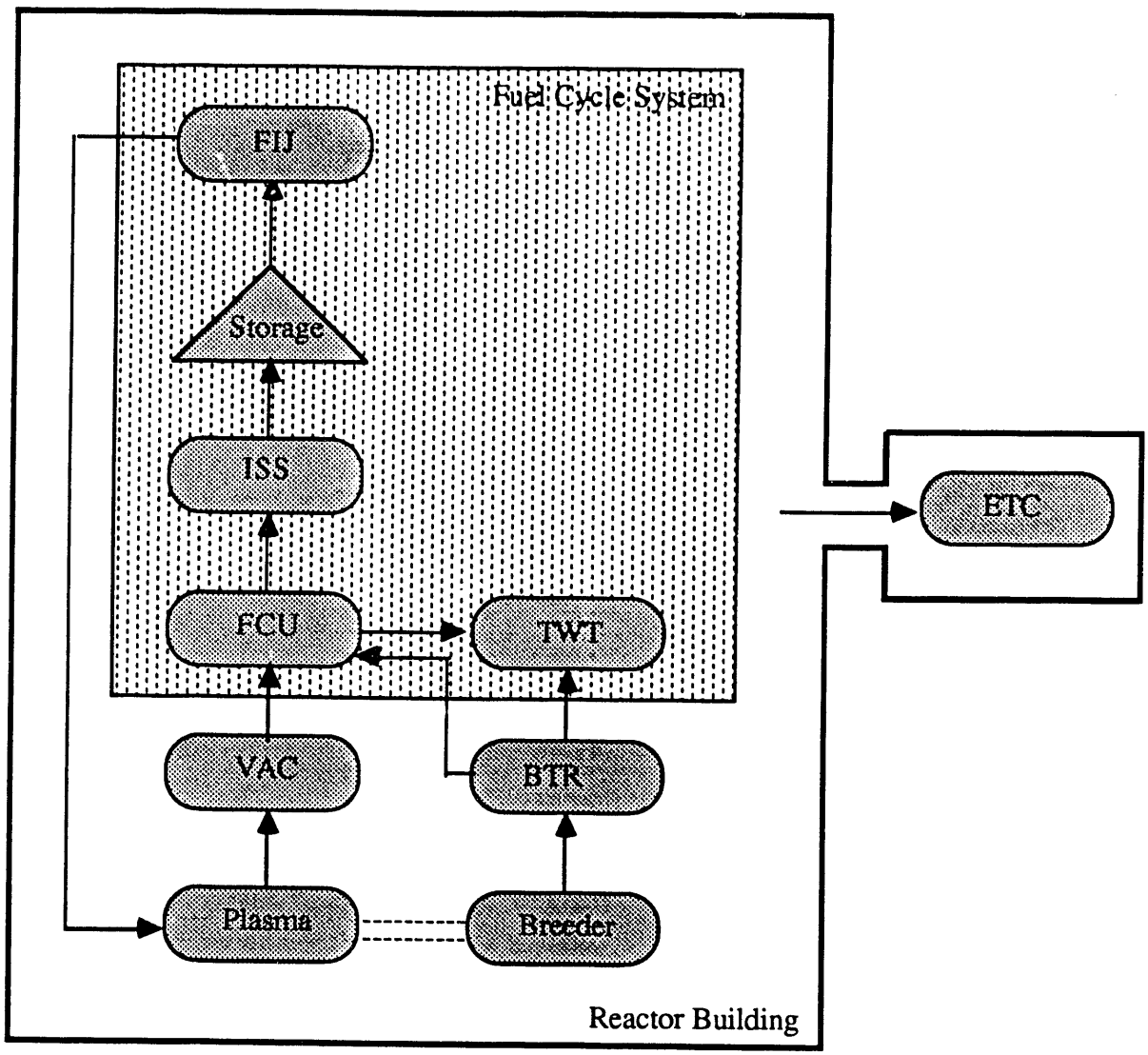

Figure 5.5. Tritium flow.

Table 5.1. The Vulnerable Tritium Inventory.

Locations	Amount(g)
Plasma Chamber	0.55
Vacuum System	133
Breeder/ BTR	310
Blanket structure/ Coolant	14
Fuel Injection	90
Total Vulnerable Inventory = 547g = 5.25MCi	

5.2.3 An Event Tree Model

Three major safety systems were considered in the release accident analysis: system shut down or isolation, secondary enclosure, and activation of the emergency tritium cleanup (ETC) system. The reactor building itself can be considered as the final defensive system from the public safety point of view, but even with the failure of "only" the three major safety systems mentioned above, the potential hazard to the workers is high.

Initially, the tritium accident escalation was modelled by a simple event tree whose branch parameters, π_1, π_2, π_3, are the probabilities of failure of each of the above safety systems and λ is the rate of an initiating event. In Fig. 5.6, m_i is the count of accidents of category i in a given period of time, say (0,T), where i=1 is the most hazardous category and i=4 is the least hazardous category.

Another classification of the accidents, into four *levels*, is convenient for a model using an influence diagram (ID). Level 1 accidents consist of category 1 accidents; level j accidents consist of level j-1 accidents and category j accidents, j=2,3,4. Thus level j accidents is a subset of level i accidents for i>j. We use n_j to denote the count of level j accidents in the time interval (0,T). Thus we have:

$$n_j = \sum_{k=1}^{j} m_k$$

5.2.4 An Influence Diagram Model

The ID in Fig. 5.7 is statistically equivalent to the event tree in Fig. 5.4 but it has the usual advantages peculiar to ID analysis, primarily allowing the explicit representation of conditional independence among the parameters. In the IDs that follow nodes denote random variables and directed arcs denote probabilistic dependence of the node at the arrow head on the node at the arrow tail. Nodes containing Greek letters denote unobservable (branch) parameters that influence the observable counts of events, the observability of which is denoted by shaded nodes. (For further discussion of the structure of influence diagrams refer to Howard and Matheson[5.8], and Shachter[5.9]) From the influence diagram

model in Fig. 5.7, it is clear how an initiating event escalates to more severe accidents. The initiating event occurs with the rate λ. This accident escalates to a more severe one if we fail to shutdown system with probability π_3. Similar escalation process is repeated. One important point to note is that the number of level 4 accidents is influenced by λ only, and the number of level j accidents is influenced by the number of level j+1 accidents and π_j only, j=1,2,3. In other words, the number of level j accidents conditional on level j+1 accidents and the corresponding branch parameter are independent of all other parameters and counts. The information on conditional dependency from the structure of the ID simplifies further analysis pretty much, especially in the parameter updating scheme.

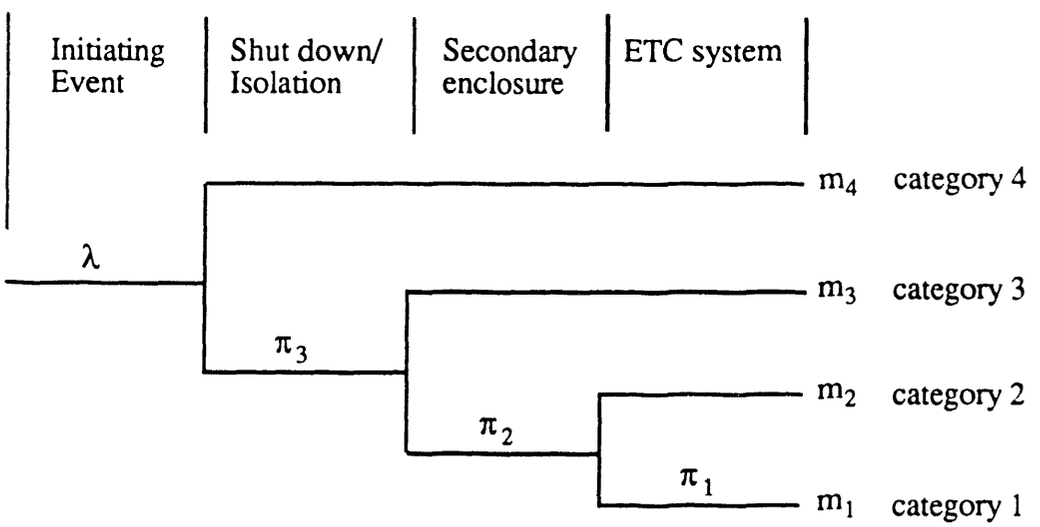

Figure 5.6 Event-tree model for tritium release accidents.

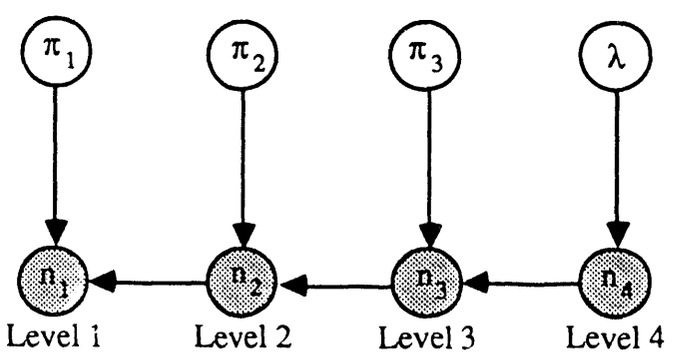

Figure 5.7. An influence diagram equivalent to the event tree in Fig. 5.4.

5.2.5 Prediction of Consequences

We can expand the model in Fig. 5.7 in order to include the hazard to the public. Figure 5.8 shows a possible expanded model, where we assume that the amount of tritium released, R, is determined by n_1 to n_4. The assessment of the amount of tritium released by each accident category needs more analysis. In addition, random factors, such as weather conditions, population distribution and protection during accidents, etc., are involved in determining the consequences resulting from the release of tritium to the environment in the time period (0, T), that is C = C(0, T). In principle, if we denote those by the random vector **W**, the parameters vector by $\Phi = (\lambda, \pi_1, \pi_2, \pi_3)$, the testing and operating data available for their estimation by time T by **D**, then, assuming that the joint conditional distribution $f(\phi, \mathbf{w} \mid \mathbf{D})$ is known, we can express the predictive distribution of the consequences in a future time interval (T, T+ΔT) by:

$$p(C \mid \mathbf{D}) = \int\cdots\int g(C \mid \mathbf{w}, \phi)\, f(\phi, \mathbf{w} \mid \mathbf{D})\, d\phi\, d\mathbf{W} \qquad (5.1)$$

where $g(C \mid \mathbf{w}, \phi)$ is the conditional distribution of some consequence C given **w** and ϕ.

Note that the distribution of ΔC is based on the *observable* counts only. Also note that we did not make any distributional assumptions on branch parameters and likelihoods. The influence diagram model and the predictive distribution in Eq. (5.1) apply to any type of prior distribution assumptions.

Using expert opinion and engineering knowledge, the parameters are usually estimated from fault trees whose top events yield the desired probabilities. A positive-skewed distribution that has a long tail is usually assumed for the rate of initiating events, because a safety system provided with many redundancies tends to bunch up towards the low probability of failure. Log-normal or Gamma distributions with appropriate parameters can be good candidates. For the distributions of π's we may assume beta distributions, which are quite flexible covering almost all forms of distributions on [0,1]. The likelihood of count of level 4 accident, n_4, given λ is assumed Poisson with parameter λ. The likelihood of n_j given n_{j+1} and π_j is assumed to be Binomial with parameters n_{j+1} and π_j.

5.2.6 Updating Branch Parameters

From Eq. (5.1), we can see that lower uncertainties in branch parameters result in lower uncertainties in the consequences. We cannot have operating data at the design stage of a fusion reactor, but the data from testing is helpful to sharpen the distributions of branch parameters. The results from testing can be used to update parameters in the same way as we utilize the information obtained from operating experience. Figure 5.9 is an example of a model that incorporates the results of testing when we perform testing on the efficiency of secondary enclosure.

U denotes the total number of testings and V denotes the number of failures in those testings. Figure 5.10 is the influence diagram that updates the parameter π_2 with the information available (it is equivalent to that part of the ID in Fig. 5.9 that influences π_2). For details on the parameter updating scheme, see Ref. 5.10.

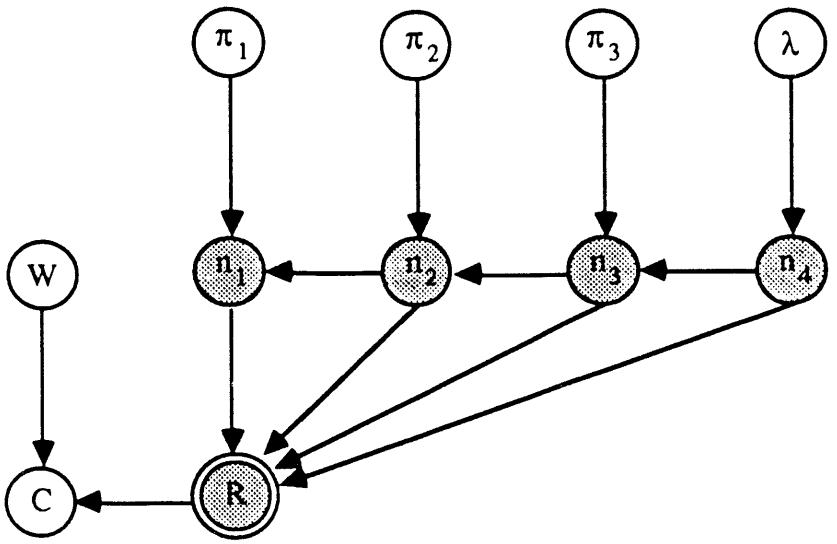

Figure 5.8. An expanded model for consequences of tritium release.

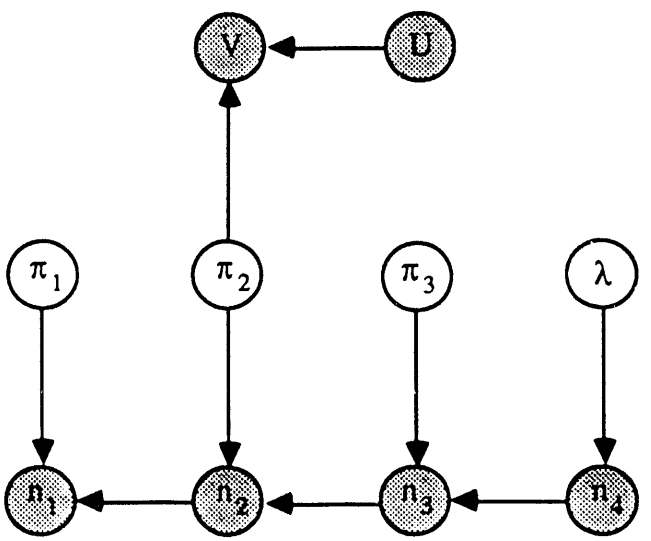

Figure 5.9. A model incorporating the testing results of secondary enclosure.

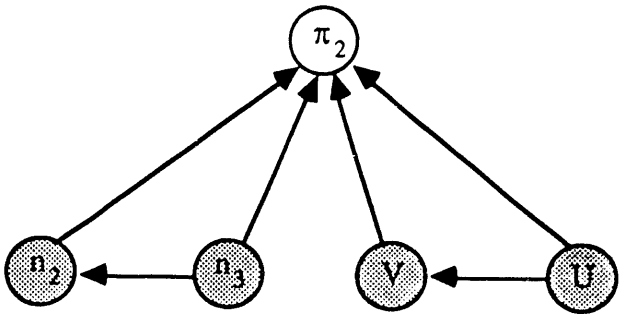

Figure 5.10. Updating π_2.

The prior distribution of π_2 can be assumed as Be(1, 1) if we do not have any information about the failure probability of secondary enclosure. Suppose that we had no failures on secondary enclosure during 10 testings under the simulated condition of an initiating event *and* failure of system shutdown; then the resulting posterior distribution is Be(1, 11). Thus we have a very much sharper distribution of π_2 and we can estimate a tritium release accident with somewhat less uncertainty. Figure 5.11 demonstrates how such a testing result influences the degree of uncertainty on a branch parameter. One lesson we can learn from Fig. 5.11 is that separate testing of each safety system provides us with valuable information that reduces the uncertainties on the overall system.

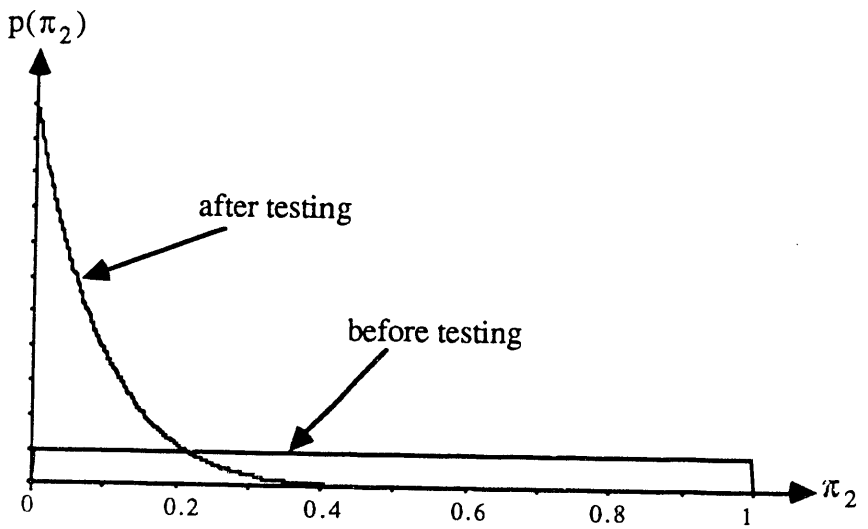

Figure 5.11. Sharpened branch parameter distribution due to testing.

5.3 APPLICATION OF MULTI-OBJECTIVE DECISION ANALYSIS TO FUSION REACTOR DESIGN

5.3.1 Introduction

Magnetic Fusion Energy (MFE) systems have the potential to achieve electricity with cost comparable to those of fission systems and better environmental and safety (ES) characteristics. However, the potentially significant advantage of fusion in ES is not guaranteed to materialize automatically. The better fusion ES performance relative to coal, oil, gas, and fission depends in large measure on the choice of structural materials, blanket, fuel cycles, power densities, and other design parameters out of a large variety of available and envisioned options.[5.11]

Associated with many of these design alternatives are large uncertainties, arising from new, untested materials, components, and schemes. These uncertainties propagate from the design stage into many properties of the resulting reactors, such as potential occupational and accidental radiological hazards, radiological waste impacts on the environment, implied monetary costs, the viability of, and the time until, commercialization, etc.

Facing a wide range of alternatives coupled with budget constraints that allow only a small fraction of the alternatives to be studied, tested or developed, fusion programs in the US and abroad find themselves confronted with complex decision-making problems under uncertainty (in addition to the physics and engineering ones). Under such circumstances, decisions tend sometimes to be made using qualitative reasoning, intuition, and subjective beliefs. A quantitative, rationalized analysis of some of the alternatives, using modern methodologies of decision analysis, seems to be desirable and may be of great value in making the "right" choices.

It is our intention to explore the application of existing tools of multi-objective decision analysis, and extensions thereof, to specific fusion reactor design selection problems. The purpose of the rest of this section is to give the reader an idea of the nature of the problems that could be addressed, and examples thereof, and of the main methodology to be used and its desirable extensions. The multi-attribute decision-tree analysis method (MADAM) is briefly presented, and other tools and specific decision analysis issues to be addressed are mentioned. Finally, to demonstrate the MADAM method, a very simple example of a multi-objective decision problem is given and some sensitivity analysis presented.

5.3.2 The Nature of the Problems to be Addressed

In the general type of problems stated above, the decision analysis is complicated not only by the intricacy of the new technology and the large uncertainties inherent particularly to the first stages of R&D, but also by the following factors:

- *Attributes* are multiple, non-commensurate, and occasionally conflicting. They include costs (e.g., construction, operation, and maintenance); revenues; some that can indirectly be valuated in monetary terms (e.g., the power of the evolving plant, its reliability and availability); and others that cannot (e.g., the expected time to first commercial operation, or the risks of loss of life and adverse health effects from accidental

or routine exposure to radiation). The value to be gained by experimentation has also to be measured by multiple attributes.

- *Multiple parties* are involved in the decision making (e.g., government, public, and utilities), which seldom share the same preferences.

- The *preference structures* of the decision makers and their attitudes towards risk have to be properly represented. In particular, for a risk-averse public, the possibility of low-probability high-consequence (catastrophic) events renders the only quantification of risks by their expected values inappropriate because this scalar representation commensurates events of all levels of losses and their corresponding probabilities.[5.12]

- The analysis should consider a *multi-stage* problem to allow at least for the transition from an experimental reactor (at the end of the engineering-feasibility demonstration stage) to a first commercial reactor. As experimental and other data become observable during early stages, analysis of a Bayesian-updated model is repeated for later stages.

- A complete analysis should, in principle, consider the alternative existing and time-extrapolated technologies for power generation with their associated attributes.

To keep the decision making problem amenable, some major reductions and simplifying assumptions must be made. We will limit our attention to MFE only (though, occasionally, partial comparisons to other technologies may be valuable) and with one decision maker, and will generally avoid the difficulties of utility theory by resorting to non-inferior frontiers and employing multiple measures of risk.

5.3.3 Possible Decision Problems to be Addressed

Following are some examples of typical questions (yet to be precisely defined) that could be addressed and answered quantitatively using multi-objective decision analysis techniques.

1) Should the design of an experimental tokamak reactor, intended to demonstrate "engineering feasibility" be based on well-known, conventional, but relatively high-activation materials (such as 316SS), or on advanced, low-activation, but untested materials (such as SiC or V alloys), for structure, blanket, first wall, and diverter? To what extent would the second choice promote or hinder the successful implementation of commercial fusion in the future at hand?

2) Given a fixed MFE program budget, how should it be allocated between two conflicting R&D strategies: (a) design and eventually build a reactor employing currently known physics and engineering, at the risk that the product will not be perceived as a viable alternative to future competition (mainly advanced, modular, passively-safe fission); and (b) with economical and ES goals in mind, develop and test promising advanced materials, that could eventually be employed in an advanced reactor design, at the risk of postponing demonstrability and commercialization to a farther future?

3) Which of two reactor designs, both employing advanced but different materials and conversion schemes, and having mutually non-dominating ES performance and cost attributes (with comparable large uncertainties), is to be preferred?

5.3.4 Multi-attribute Decision-Tree Analysis

When faced with multi-objective decision problems, several approaches have been used by analysts to represent the best procedure to be followed by the decision maker in arriving at an optimal choice. In one of those (the parametric approach, Ref. 5.13), the decision maker puts weights on the different objectives and the problem is transformed into a single-objective optimization. In another approach (the k-th objective ε-constrained problem[5.14]), one objective is extremized, while others are constrained to some "satisfactory" range. The more general approach, that searches for non-inferior, or Pareto optimal solutions, widely used in microeconomic models, preserves the essentials of the original problem throughout the solution process, to finally present the decision maker with a set of non-inferior alternatives known as the non-inferior frontier. This last, general approach seems the most appropriate to be implemented in decision problems where safety (implying a direct risk to human lives) is one of the objectives, that is not to be amalgamated with other objectives in the solution process.

Decision-tree analysis has emerged over the years as an effective and useful tool in decision making under uncertainty. Most applications, however, have involved the use of a single objective. Single-objective models, in relation to decision trees or other methodologies, are today considered by many to be too unrealistic and totally inadequate for some of the real world problems. The use of decision trees can be naturally extended to multiple objectives. We will describe in short after Haimes[5.15] the MADAM method, that incorporates the concepts of vector optimization and non-inferior optimality.

The conventional procedure of averaging-out and folding-back for a single-objective decision tree will not be reviewed here. With multiple objectives, a vector-valued objective function is defined at each of the leaves, i.e. for each feasible combination of actions and chance outcomes (in general, both the decision space and the states of nature could be continuous, in which case the objective function would have continuous arguments, but we will focus attention here on the somewhat simpler discrete case).

Multi-objective optimization problems are often formulated as either vector minimization or vector maximization without loss of generality. However, it is possible to minimize some objective functions while maximizing others, as the example in the last section illustrates. In a vector minimization problem a point $\mathbf{r} = (r_1, r_2, ..., r_n)$ is said to be *non-inferior* (or Pareto-optimal) if there does not exist another feasible point $\mathbf{r}' = (r'_1, r'_2, ..., r'_n)$ such that:

$r'_i \leq r_i$ for i = 1, 2, ..., n, with at least one *strict* inequality holding.

The MADAM solution procedure is as follows. The procedure starts at each leave fold-back on the tree. At each branch k, emerging to the right of each *decision* node D_j, we proceed to find the set $R_j(k)$ of objective-function vector values corresponding to taking action k at decision node D_j. Then, the noninferior solutions at D_j for the set R_j are determined by solving,

$$R_j = \min U_k R_i(k),$$

where U_k is the union operator on sets $R_j(k)$. Subsequently, the noninferior actions k are identified. Note that in contrast to single-attribute decision-tree analysis, more than one (noninferior) action exists in general at a decision node, each leading to some noninferior points in the attribute space. At each branch m, emerging to the right of each *chance* node

C_l, the set $S_l(m)$ of objective-function vector values corresponding to the outcome m at chance node C_l is found. Then we calculate the expectation over m of the objective function for each combination of the elements in the sets $S_l(m)$. If set $S_l(m)$ has $d_l(m)$ elements, then there exist $\prod_m d_l(m)$ combinations to be averaged-out. When decision nodes follow node $S_l(m)$, which is usually the case, these combinations correspond to all strategies the decision maker can follow beyond chance node $S_l(m)$. Subsequently, identify the inferior combinations and discard from further consideration the corresponding strategies. In contrast to single-attribute decision-tree analysis, where there is no choice process at chance nodes, usually there exists more than one (noninferior) strategy (or in general combinations as above) at a chance node. The procedure ends when the root of the tree (usually a decision node) is reached. The surviving noninferior solutions form the noninferior frontier.

5.3.5 Extensions and Theoretical Issues to be Addressed

Although the above promising methodology to analyze multi-objective decision problems has been established, several theoretical and computational issues have to be addressed before the usefulness of it can be fully realized. Here are some that can be envisioned right away:

1) Develop an efficient algorithm to eliminate inferior solutions at the early stages of the decision-tree analysis.
2) Devise a method to allow computational tractability when using conditional expected values as measures of risk without resorting to major simplifications (see Ref. 5.15).
3) Use influence diagrams to identify situations where conditional independence among random variables plays a major role in simplifying the analysis of the problem. Research the potential benefits of extending influence diagrams to incorporate multiple objectives. (On the usefulness of influence diagrams, especially when the objective function is separable, see Ref. 5.16)
4) Devise a method to effectively represent graphically non-inferior frontiers when 3 or more objectives are involved.

5.3.6 Application of MADAM to a Simple Sample Problem

The MADAM method is illustrated with a very simple example and followed by a graphical representation of the analysis results.

Consider the decision problem of choosing among three alternatives: (1) constructing a conventional fusion reactor (D = "C"), (2) constructing an advanced, promising but relatively untested reactor (D = "A"), and (3) testing modules of the advanced design (D = "T") to subsequently decide on construction of "C" or "A". Each of the designs, if implemented, will either fail or succeed in a given period of operation for simplicity. Failure can be interpreted as a major accident occurring during this period that involves loss of the reactor, damage to additional property, and loss of human lives from released radioactivity to the environment. The first two losses can be expressed in monetary terms while the last cannot. Success can be interpreted as favorably generating power for a given period, which we assume can be associated with a specific monetary value. The various costs and payoffs are summarized as below.

Reactor Design	Cost of construction	Loss of Property in accident	Loss of Lives in accident	Value of successful operation
C	2	2	4	10
A	4	6	1	12

Note that an accident in "A" involves a higher monetary loss (10=4+6 vs. 4=2+2), but a lower loss of life (1 vs. 4), when compared to "C". Design "A's" value of operation is higher (12 vs. 10) because of higher efficiency. The numbers are arbitrary, and monetary values may be thought of as billions of dollars.

Suppose the success probability of the conventional reactor is known to be $p_C = 3/4$ while the apriori success probability of "A", p_A, is not well known. Testing modules of "A" could, for simplicity, be either successful or not. It will improve the knowledge of p_A in the following sense. If "T" = s(uccess) then "A" will succeed with probability 8/9, while if "T" = f(ailure), "A" may only succeed with probability 2/9 (and fail with probability 7/9). Let $p_1 \equiv P(A=s|T=s) = 8/9$ and $p_0 \equiv P(A=s|T=f) = 2/9$. For,

$$p_A = p_T p_1 + (1-p_T)p_0, \tag{5.2}$$

where p_T is the marginal probability of success of the testing, hence,

$$\frac{2}{9} \le p_A \le \frac{8}{9} \tag{5.3}$$

Figure 5.12 depicts the decision tree. The results of the various outcomes with the corresponding decisions are shown as two-element vectors at the tree leaves in the form of (monetary value, loss of lives). Obviously, the decision maker wants to maximize the expected monetary value and minimize the expected loss of lives assuming that the decision maker is risk neutral. The exact cost of the test, c_T, is unknown at the time the analysis is performed. Note that if "C" is chosen after the test result is known (at D_2 or D_3) the probability of success of "C" is still $p_C = 3/4$. The independence of "C" and "T" is clearer in the influence diagram that depicts the simple structure of the problem in Fig. 5.13.

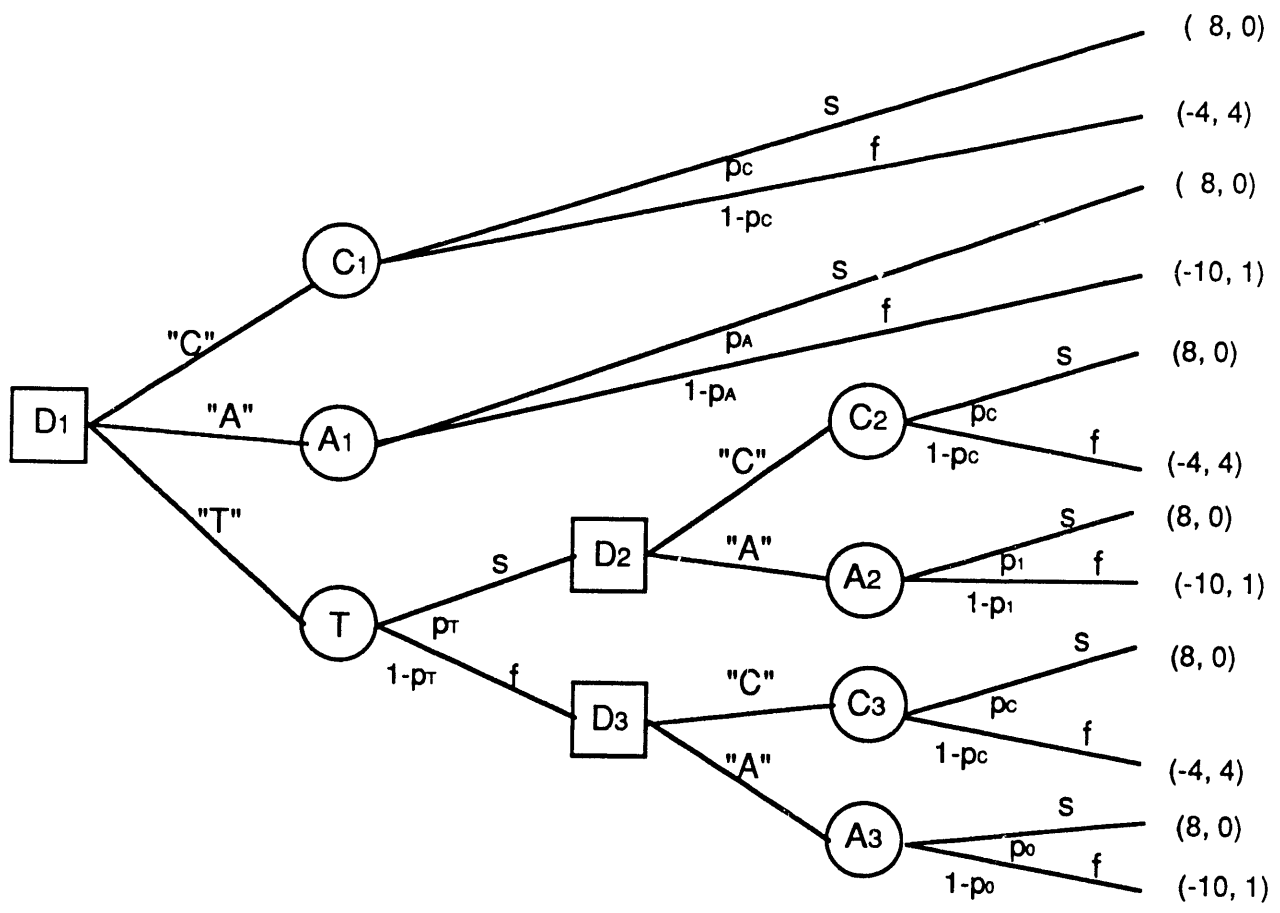

Figure 5.12. The decision tree with 2 attributes.

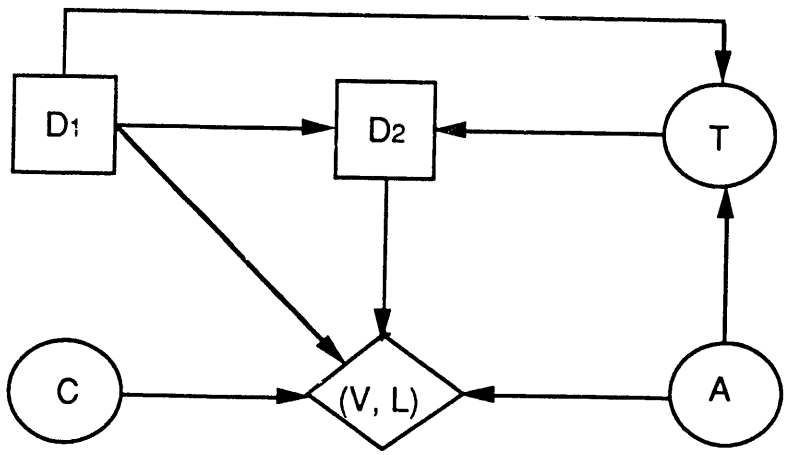

Figure 5.13. The corresponding influence diagram.

The Solution

Starting at the tree leaves and averaging out, we get the following expected value vectors:

$$\begin{aligned}
&\text{at } C_1: && (8p_C - 4(1-p_C),\ 4(1-p_C)) = (5,\ 1),\\
&\text{at } A_1: && (8p_A - 10(1-p_A),\ 1 - p_A) = (18p_A - 10,\ 1 - p_A),\\
&\text{at } C_2 \text{ and } C_3: && (8p_C - 4(1-p_C),\ 4(1-p_C)) = (5,\ 1),\\
&\text{at } A_2: && (8p_1 - 10(1-p_1),\ 1 - p_1) = (18p_1 - 10,\ 1 - p_1) = (6,\ 1/9),\\
&\text{at } A_3: && (8p_0 - 10(1-p_0),\ 1 - p_0) = (18p_0 - 10,\ 1 - p_0) = (-6,\ 7/9).
\end{aligned} \tag{5.4}$$

If D_1 = "T" the four possible strategies (i.e., here, combinations of actions in the second stage, contingent on the outcome of the test) at D_2, D_3 are "CC", "CA", "AC", and "AA", where the first is the decision (at D_2) if "T" = s and the second is the decision (at D_3) if "T" = f. The expected-value vectors for these strategies are:

$$\begin{aligned}
&\text{"CC":} && p_T(5,\ 1) + (1-p_T)(5,\ 1) = (5,\ 1),\\
&\text{"CA":} && p_T(5,\ 1) + (1-p_T)(-6,\ 7/9) = (11p_T - 6,\ 2/9p_T + 7/9),\\
&\text{"AC":} && p_T(6,\ 1/9) + (1-p_T)(5,\ 1) = (5 + p_T,\ 1 - 7/9p_T),\\
&\text{"AA":} && p_T(6,\ 1/9) + (1-p_T)(-6,\ 7/9) = (12p_T - 6,\ -2/3p_T + 7/9).
\end{aligned} \tag{5.5}$$

Comparing the above under the assumption $0 < p_T < 1$ it can be seen that "CC" is inferior to "AC" (the latter has a larger expected monetary value and a smaller expected loss of lives), and that "CA" is inferior to "AA". Therefore, "AC" and "AA" are the only noninferior strategies to be carried back to the T node. Therefore, at D_1 the only relevant strategies to be considered are "C", "A", "TAC", and "TAA", where the last two mean "T" has to be chosen at D_1 and then "AC" or "AA", according to the test result. From Eq. (5.2) we can express p_T in terms of p_A, $p_T = 3/2p_A - 1/3$, and substituting in Eq. (5.5) to get the expected-value vectors of the above yet-to-be-considered strategies:

$$
\begin{array}{ll}
\text{"C":} & (5,\ 1), \\
\text{"A":} & (18p_A - 10,\ 1 - p_A), \\
\text{"TAC":} & (-c_T + 14/3 + 3/2p_A,\ 34/27 - 7/6p_A), \\
\text{"TAA":} & (-c_T + 18p_A - 10,\ 1 - p_A).
\end{array} \tag{5.6}
$$

Assuming testing is not free, $c_T > 0$, "TAA" is inferior to "A" and the only Pareto-optimal strategies are "C", "A", and "TAC". This gives the trivial result that, without knowing anything more about p_A or the cost of testing, it is never optimal to test and then make the same choice regardless of the test result ("TCC" or "TAA"), or to test and decide contrary to the test indication ("TCA"). These results of the basic analysis are trivial in this simple example and are derived above explicitly for demonstration purposes only.

Comparing "TAC" with "A", we get from Eq. (5.6) that "A" is preferred whenever $18p_A - 10 \geq -c_T + 14/3 + 3/2p_A$ and $1 - p_A \leq 34/27 - 7/6p_A$, and at least one inequality being strict, i.e. $p_A \geq 8/9 - 2/33c_T$ and $p_A < 42/27$, where the latter is always strictly true. Similarly, comparing "TAC" with "C" we get that the former is preferred whenever $p_A \geq 2/9 + 2/3c_T$. Finally, comparing "C" with "A", we find "C" is inferior whenever $p_A \geq 5/6$.

Figure 5.14 depicts in the c_T-p_A space the feasible and various noninferior zones. When more than one strategy shows in one zone, they form a set of noninferior strategies. Some insights from the figure follow. When the testing costs more than 11, it's never optimal to test. When p_A is believed to be larger than 5/6 the "C" option should never be considered, in that case, the testing cost is large enough ($c_T \geq 11/12$), "A" should be implemented without testing. For lower probabilities of success of the advanced design (than 5/6), the decision maker has to be presented with a choice of three possible sets of noninferior strategies, depending on the cost of testing--for low testing cost, "A" and "TAC" form the noninferior set; for medium cost, "C" joins them; for large cost, "TAC" becomes inferior and only "A" and "C" have to be considered. The threshold values of c_T, where the transitions among the sets occur depend on what the value of p_A. When p_A is higher, "C" becomes noninferior at a relatively higher cost and testing becomes inferior at a relatively lower cost.

The noninferior alternatives to be presented to the decision maker obviously depend on both p_A and c_T. Figure 5.15 depicts their p_A dependence in the V-L space for a specific value of cost at $c_T = 3$. The figure can be best understood when compared with Fig. 5.14. The decision maker prefers points closest to the lower right. The solid line represents the change with p_A in E[(V, L) | "TAC"], while the dashed-dotted-solid line represents similar changes in E[(V, L) | "A"]. Different points on the lines correspond to different values of p_A. The extreme values of p_A are shown at the ends of the lines, and small circles denote the points corresponding to $p_A = 2/3$. E[(V, L) | "C"], being independent of p_A, shows just as a point. The "A" and "TAC" lines cross at $p_A = 70/99$. For lower values of p_A, the noninferior frontier consists of the dashed part of the "A"-line, the "C" dot, and the "TAC" line. For $70/99 \leq p_A \leq 5/6$, it consists of the "C" dot and the dotted part of the "A" line. Finally, for $p_A > 5/6$ the solid part of the "A"-line is the only optimal solution.

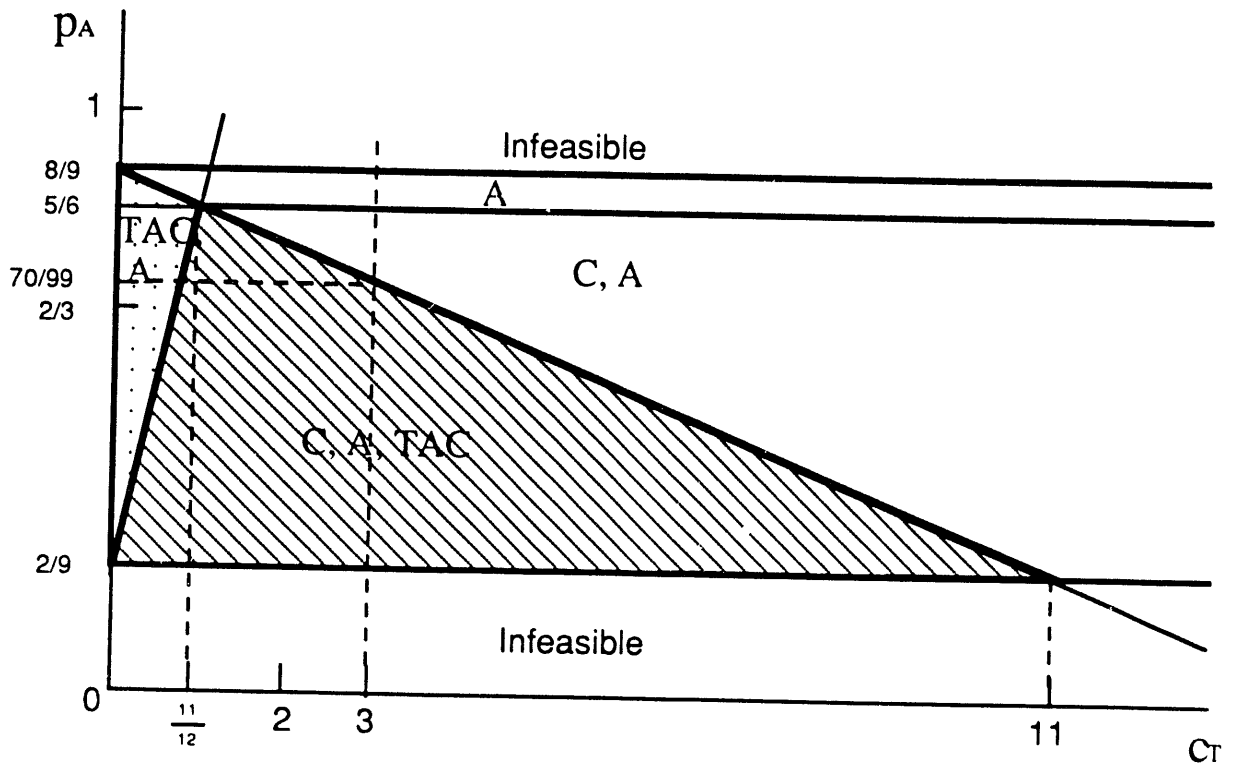

Figure 5.14. Feasible and noninferior decisions in the c_T-p_A space.

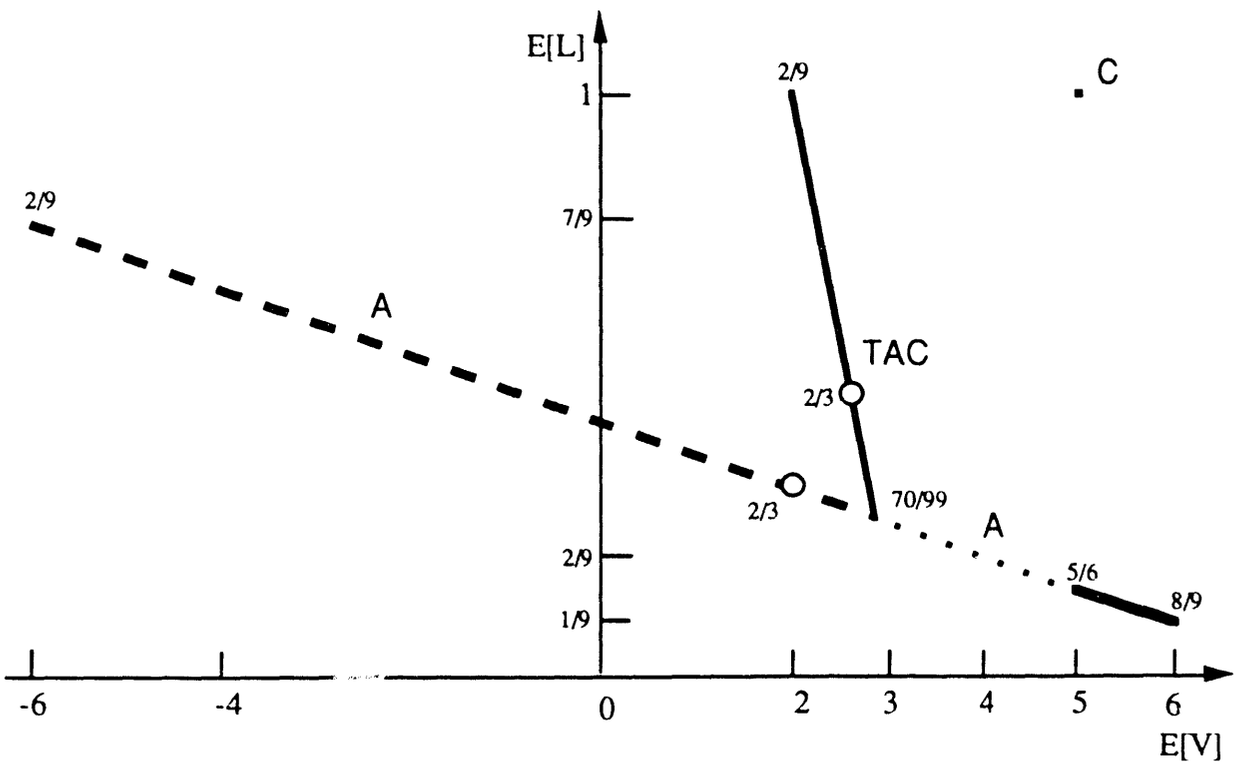

Figure 5.15. Noninferior frontiers as a function of p_A in the (Value, Life loss) space, for c_T=3.

References

5.1. J.P. Holdren, D.H. Berwald, R.J. Budnitz, J.G. Crocker, J.G. Delene, R.D. Endicott, M.S. Kazimi, R.A. Krakowski, B.G. Logan, and K.R. Schultz, "Exploring the Competitive Potential of Magnetic Fusion Energy: The Interaction of Economics with Safety and Environmental Characteristics," Fusion Technol. **13**, 7 (1988).

5.2. J.P. Holdren (chair), D.H. Berwald, R.J. Budnitz, J.G. Crocker, J.G. Delene, R.D. Endicott, M.S. Kazimi, R.A. Krakowski, B.G. Logan, and K.R. Schultz, "Report of the Senior Committee on Environmental, Safety, and Economic Aspects of Magnetic Fusion Energy," UCRL-53766, Lawrence Livermore National Laboratory, Sept. 1989.

5.3. U.S. Nuclear Regulatory Commission, "Reactor Safety Study: An Assessment of Accident Risks in U.S. Commercial Nuclear Power Plants," WASH-1400, NUREG 75/014 (1975).

5.4. N.J. McCormick, "Reliability and Risk Analysis: Methods and Nuclear Power Applications," Academic Press, (1981).

5.5. S. Levine, "The Role of Risk Assessment in the Nuclear Regulatory Process," Annals of Nuclear Energy **6**, 281 (1979).

5.6. U.S. Nuclear Regulatory Commission, "Human Factors Evaluation of Control Room Design and Operator Performance at Three Mile Island-2," NUREG/CR-1270, Jan. 1980.

5.7. T-C Chow, R.M. Oliver, and G.A. Vignaux, "A Bayesian Escalation Model to Predict Nuclear Accidents and Risk," Operations Research **38**, 2 (1990).

5.8. R.A. Howard and J.E. Matheson, in "The Principles and Applications of Decision Analysis," Vol. II (R.A. Howard and J.E. Matheson, eds.), Menlo Park, California, (1984).

5.9. R.D. Shachter, "Evaluating Influence Diagrams," Operations Research **34**, 6 (1986).

5.10. R.M. Oliver and H.J. Yang, "Updating Event Tree Parameters to Predict High Risk Incidents," Conference on Influence Diagrams for Decision Analysis, Inference and Prediction, U.C. Berkeley, California, (1988).

5.11. J.P. Holdren, "Safety and Environmental Aspects of Fusion Energy," Annual Review of Energy **16** (1991).

5.12. E.L. Asbeck, and Y.Y. Haimes, "The Partitioned Multiobjective Risk Method (PMRM)," Large Scale Systems **6**, 13 (1984).

5.13. S. Gass, and T. Saaty, "The Computational Algorithm for the Parametric Objective Function," Naval Research Logistic Quarterly **2**, 39 (1955).

5.14. V. Chankong and Y.Y. Haimes, "Optimization-based Methods for Multiobjective decision-making: An Overview," Large Scale Systems **5**, (1983).

5.15. Y.Y. Haimes, D. Li, and V. Tulsiani, "Multiobjective Decision-Tree Analysis," Risk Analysis **10**, 1 (1990).

5.16. J.A. Tatman and R.D. Shachter, "Dynamic Programming and Influence Diagrams," IEEE Trans. on Sys., Man and Cybernetics **20**, 2 (1990).

6. PLASMA BURN CONTROL -- APPLICATION TO ITER

Our interactions with the fusion community continue, in particular with the ITER and ARIES reactor design teams. The interactions have been mutually beneficial. These efforts facilitate our code development in obtaining updated information on fusion reactor design, utilizing existing computer codes, and developing new models. We will discuss our contributions to the ITER design in this section. Work related with the ARIES design efforts will be discussed in the next section.

The group was involved in the ITER planning and review process: Prof. Fowler as a member of the ITER Scientific and Technical Advisory Committee, and Prof. Holdren as a member of the U.S. National ITER Conceptual Review Committee in February-March, 1991.

We contributed a talk on "Plasma Operating Point Control" in the ITER Plasma Burn Control Workshop at Garching, FRG in July, 1990. A paper on "Emergency Plasma Shutdown for ITER" was presented at the Ninth Topical Meeting on the Technology of Fusion Energy at Oak Brook, Illinois in October, 1990.

6.1 OPERATING POINT CONTROL

6.1.1 Introduction

A brief account of the plasma operating point control work is described as follows. The selection and control of an operating point for ITER are very important for meeting the reactor performance requirements and assuring operational safety. The ITER design candidate should meet the reactor performance of operating at various desired fusion power levels, with the highest possible Q (fusion power/input power), within the operational constraints. The plasma burn should be controllable without major disruptions or thermal runaways.

The operational constraints include required fusion powers and wall loadings, plasma beta limit, density limit, MHD safety factor (q), divertor heat load, required burn time, installed heating power, and plasma burn controllability. Any acceptable operating points should satisfy all these requirements and constraints simultaneously. These conditions are not independent of each other. And often times, adjusting some design parameters to accommodate a particular constraint may result in pushing the operating point to exceed some other limits. Hence, we may have to trade-off between the various constraint margins in selecting an operating point.

These operating point selection and control procedures are complicated by the fact that there are much uncertainties in current tokamak database. The major physics uncertainties include formulation of energy confinement time (τ_E), H-mode confinement enhancement factor (H), thermal alpha fraction (C_α), impurity content (as manifested in the plasma effective charge Z_{eff}), density and temperature profiles (α_n , α_T), and fast alpha loss (f_{loss}). There are also different assumptions and models in treating some critical physics issues which greatly affect the outcomes of the design.

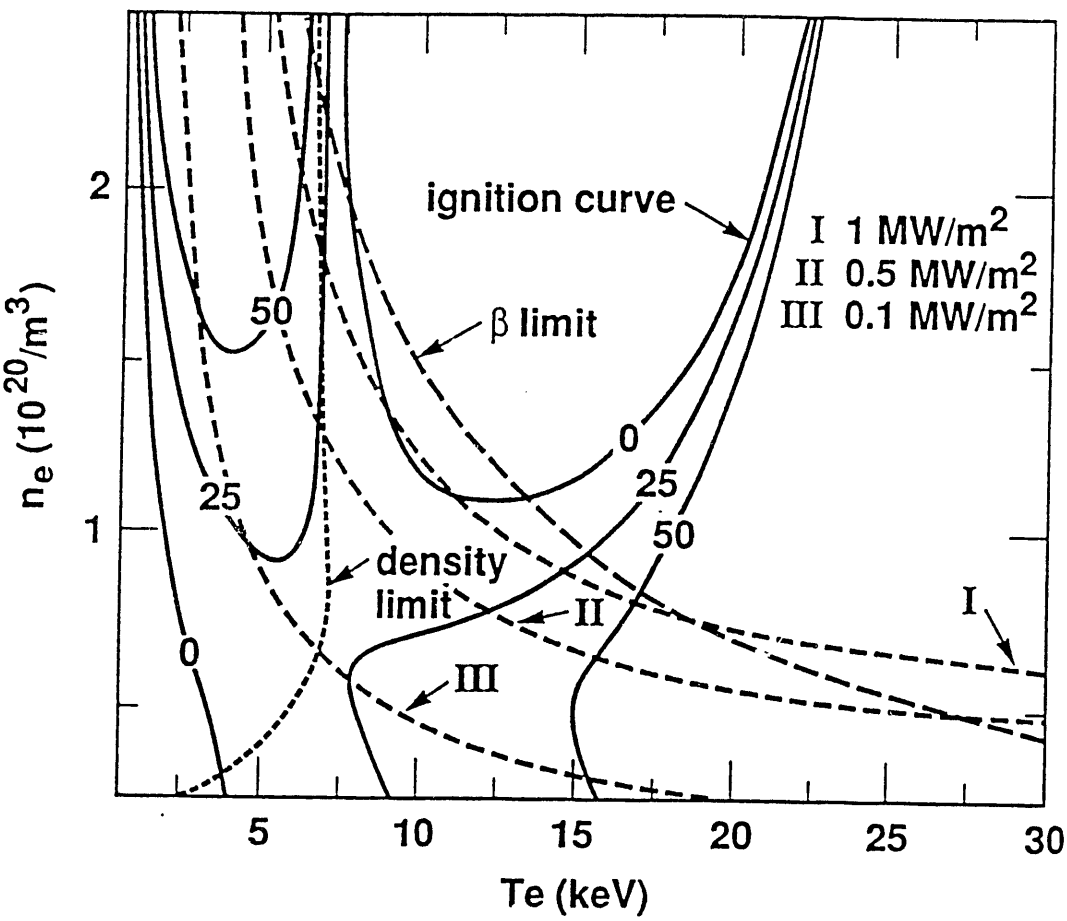

Figure 6.1. Contours of heating power required and various operational constraints in (n,T) space. The ITER-power energy confinement scaling is used.

The code also runs in a time-dependent mode to simulate the plasma burn history. The variations of the density and temperature of the fuel ions, alphas, and electrons in time are solved in a set of coupled first order differential equations. This mode enables us to examine the thermal stability property and evaluate the required installed heating power for burn control purpose.

6.1.3 Selection of Operating Points

The rationales for selecting feasible operating points are examined. The selection of operating points will require some sort of trade-off between the various constraint margins and the reactor performance.

The procedure of operating points selection in the density-temperature space is illustrated in Fig. 6.1 for fixed machine and operational parameters. We first examine the constraints explicitly shown in the figure. The plasma must be operated below the plasma beta limit in order to satisfy the MHD requirements. Any higher density or temperature above the beta limit curve is not allowed. The other constraint is a plasma edge radiation induced density-limit disruption.[6.4] This constraint restricts the operation at low temperature except at very low density, otherwise the heat flux at the edge cannot support the radiation and causes a collapse of the plasma. For the plasma in thermal equilibrium, it has to be at ignition or sub-ignited with auxiliary heating power. Moreover, for burn control of thermal stability, the plasma must be sub-ignited and has a margin away from the ignition curve. This allows for response time of the auxiliary power modulation burn control system before the plasma goes super-ignited and runs away thermally. This constraints then define an acceptable operating regime bounded by their limits for various fusion power.

Along a fixed desired fusion contour of, say, 1081 MW which corresponds to a neutron wall loading of 1 MW/m^2, there exists two possible operating regions below the beta limit, density limit, and ignition curve, namely a high-n, low-T region and a low-n, high-T region. We now look at some constraints not shown explicitly in Fig. 6.1. The low-n, high-T region is thermally stable but produces a very large amount of heat load to the divertor. The other region has less constraints in the divertor heat load, but requires active burn control with some reserve heating power and restricts the maximum achievable Q. Also the burn time is relatively shorter for a fixed PF system because more volt-seconds are consumed in a lower-temperature, higher-resistivity regime.

The severity of these constraints and the trade-offs in the two regions described are examined. The divertor heat load at the high-n, low-T region is about 9 MW/m^2, which is approaching the credible maximum value. Operating at the other region will increase the heat load by about 30%. On the other hand, time dependent simulations at the high-n, low-T region indicate a range of maximum Q values of 30-90 for the various energy scaling laws, with the ITER-power scaling being the most optimum. The required installed power is about 50 MW for burn control. A burn time of 250 seconds is obtained. These results still achieve acceptable operating performance.

From this comparison, we conclude to select an ITER-baseline operating point in the high-n, low-T region. To be more specific, the baseline operating point is at 22 MA plasma current, 4.85 T magnetic field on axis, plasma density and temperature of 1.8 x 10^{20} m^{-3} and 7.2 keV, respectively, based on the ITER-power energy confinement scaling law. As we will discuss later in fractional power operation, this selection process depends

on the particular conditions of the plasma and the results may be different for other scenarios.

6.1.4 Uncertainties in Confinement Assumptions

We first look at the uncertainty in the energy confinement time of the plasma. Because of the lack of comprehensive theoretical understanding of the transport loss process, many empirical experimental data fitting formulae have been proposed for the energy confinement time. It is observed experimentally that the energy confinement time degrades with the increase in auxiliary heating power. Most empirical energy confinement time formulations include a power degradation contribution for this effect. There are basically two types of power degradation, $\tau_E \sim P^{-y}$ or $\tau_E \sim f_1 + f_2 / P$, where P is the generalized net input power, $P = P_\alpha + P_{aux} - P_{rad}$, y is a coefficient evaluated from data regression (in the range of 0.3- 0.6), f_1 and f_2 are empirical fitting functions. For the energy confinement time scalings that we have studied, the ITER-power, Goldston, and T-10 are of the former type power form, while ITER-offset-linear, JAREI, and Rebut are of the latter type offset-linear form.

Figure 6.2 shows a POPCON similar to Fig. 6.1, using the ITER-offset-linear confinement scaling instead of the ITER-power form. The two figures agree qualitatively at low temperature (below 7 keV), but differ very much at higher temperature. The ignition window does not close at higher temperature for the ITER-offset-linear (all offset-linear in general) confinement scaling. There is no thermal stable ignition point even if the beta limit is not considered. This effect is due to no further reduction in the confinement from higher fusion power in the f_1 term in the offset-linear formulation.

Table 6.1 shows the maximum controllable Q value for various confinement scalings of the ITER baseline design. The availability of operating points at the high-density, low-temperature regime is also indicated. In general, the power degradation forms have a slightly higher Q. These scaling forms have a larger reduction in confinement as the alpha power increases, thus slowing down the thermal runaway. As a result, they can be operated closer to the ignition curve and still have enough time for the burn control system to respond. For the scaling laws considered, the ITER-power, Goldston, T-10, and ITER-offset-linear have acceptable operating points at the high-density, low-temperature regime. The confinement of JAREI and Rebut scalings are too large for this ITER reference design that the 1 MW/m^2 fusion contour is either above ignition (hence no controllability), or it is over the density limit.

Another major uncertainty in the plasma is the thermal alpha fraction. The thermal alphas tend to dilute the fuel ions at a given beta and increase the overall radiation power loss. Since there is no existing alpha-producing tokamak experiment, much of the alpha information is from various physical modelings and projections. ITER physics guideline suggests using a fixed thermal alpha to electron density ratio of 10%.

There are two approaches to treat the thermal alpha concentration. We can either fixed an assumed value of alpha fraction and calculate the thermal alpha particle confinement consistently, or we can choose a reasonable alpha particle confinement time and evaluate the alpha fraction accordingly. The effect of alpha fraction or alpha particle confinement has been investigated.[6.5] The alpha fraction as a function of both the ratios of alpha particle confinement and ion particle confinement to the energy confinement is studied. A large alpha fraction essentially closes the ignition window and greatly reduces the fusion power. However, there may exist an optimum alpha fraction that degrades the

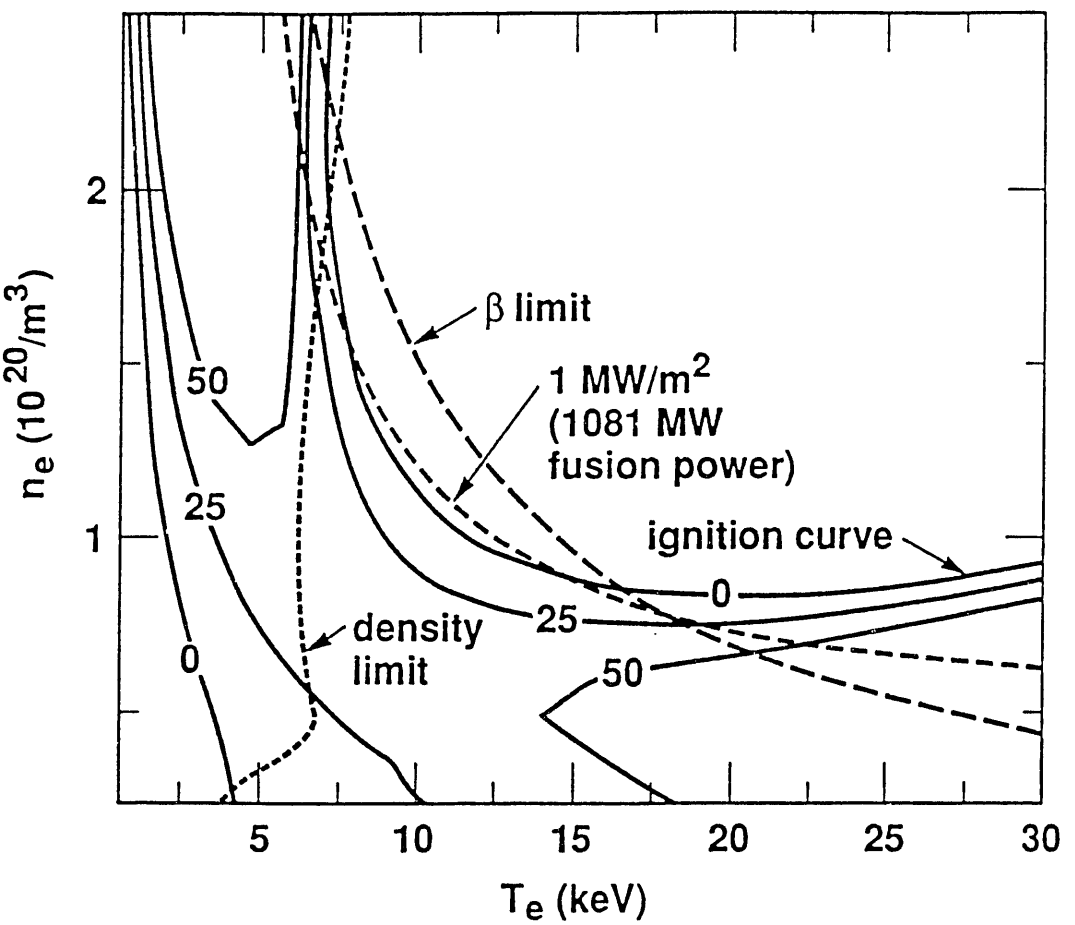

Figure 6.2. Contours of heating power required and various operational constraints in (n,T) space. The ITER-offset-linear energy confinement scaling is used.

fusion power and closes the ignition curve mildly that a thermally stable ignition point is obtained below the beta limit.

Table 6.1. Maximum controllable Q for various confinement scaling forms.

τ_E	Paux(MW)	Q	$n_e(10^{20}m^{-3})$	T(keV)
ITER-Power	12	90	1.47	8.48
ITER-Offset	23	47	1.86	6.95
JAREI	19	57	2.12(a)	6.27
REBUT	26	42	2.44(b)	5.68
GOLDSTON	14	77	1.78	7.20
T-10	16	68	1.36	9.18

(a) density limit exceeded, very narrow operation window in high-T and low-n region.
(b) density limit exceeded, no operation window.

To illustrate the ambiguity of the alpha fraction assumption, we look at the ITER specification of 10% alpha fraction in all the density-temperature space. At high temperature, this results in a ratio of alpha particle to plasma energy confinement of about 1-10. The ratio would have to be orders of magnitude larger at low temperature to compensate for the lack of fusion-born alphas. This incredibly large difference in the confinement time ratio is clearly non-physical. Also, if we normalize this confinement ratio at the ITER operating point to 10% alpha fraction to determine an appropriate value for our analysis, we find the confinement ratio to be 13 and 8 at the high-density, low-temperature and low-density, high-temperature regimes, respectively. A subsequent analysis shows that a confinement ratio of 8 can achieve a modified acceptable operating point while a ratio of 13 fails to do so.

In Table 6.2, we show the possibility without adjusting the design or operational parameters to obtain acceptable operating points with Q greater than 40, at 1 MW/m^2 neutron wall loading, for the ITER baseline design under various physics assumptions. The values of variables from projected ranges of the uncertainties are listed in parentheses. We see that a 25% deviation in the energy confinement enhancement factor H, alpha fraction of 15%, effective charge increment to 2.3, or 10% fast alpha loss will prevent the availability of a satisfactory operating point.

6.1.5 Adjustments to Confinement Uncertainties

We proceed to investigate the feasibility of a present day tokamak physics directed ITER machine after its construction, i.e. fixing the machine design parameters such as

major radius, aspect ratio, etc. Our objective is to examine the operating flexibility of the baseline design whether it can tolerate and adjust to a certain range of tokamak database uncertainties without undermining the performance goals.

Table 6.2. Possibility of ITER baseline design operating points with Q > 40 at 1081 MW fusion power under various physics assumptions.

H-Factor (1.5, 2.5)	No	No
Thermal Alpha Fraction (0.05, 0.15)	yes[a]	No
Density Profile Exponent (0.25, 1.0)	Yes	Yes
Temperature Profile Exponent (0.5, 1.5)	Yes	Yes[a]
Zeff (1.3, 2.3)	Yes	No
Fast Alpha Loss (0.05, 0.10)	Yes	No

(a). high-T, low-n regions

The control parameters to compensate for these uncertainties are mainly the magnetic field on axis (B) and plasma current (I_p). We may also increase Z_{eff}, however, this scheme is somewhat questionable because it may cause some undesirable effects. We can only adjust B and I_p in such a way that B and beta limit (Troyon coefficient) do not exceed their allowable values and q is above the required MHD minimum simultaneously. Figure 6.3 shows a control knob window in B-I_p space bounded by these constraints. The adjustable range of I_p will be larger if B is also increases. The ITER baseline reference B and I_p values are also shown. We do not consider profiles control as a knob to adjust for the physics uncertainties because the profiles themselves are very uncertain and their controllability is still doubtful.

Following the discussion in the previous section, we use as examples for operating point control when H is either 1.5 or 2.5 instead of the baseline value of 2.0. For the case of inadequate confinement of H=1.5, the transport power loss is so large that it requires an excessively large amount of external heating to maintain power equilibrium. As a result, there does not exist any operating point that can produce the desired fusion power with a Q of 40 or more. We have to reply on changing the operational parameters. In this case, we can increase both B and I_p towards the corner at the B and q limits as shown in Fig. 6.4. Increment in I_p will increase the confinement time according to the functional dependence of τ_E in I_p. The magnetic field has a lesser effect in τ_E but it is necessary to raise B in order to extend the range of I_p within the q limit. In this manner, we can recover legitimate operating points with this modified operational parameters satisfying all constraints, except

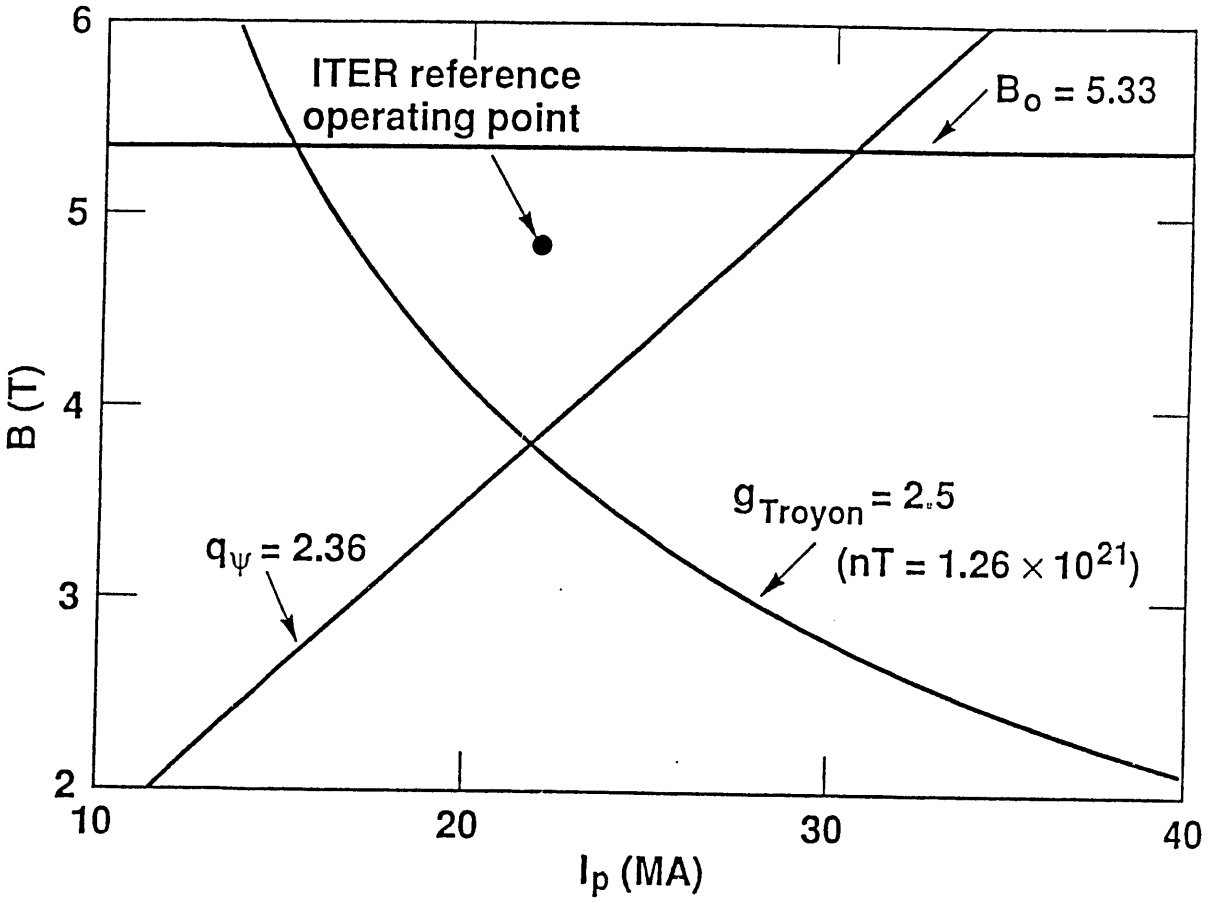

Figure 6.3. Control knob window in B-I_p space bounded by operational and technological constraints.

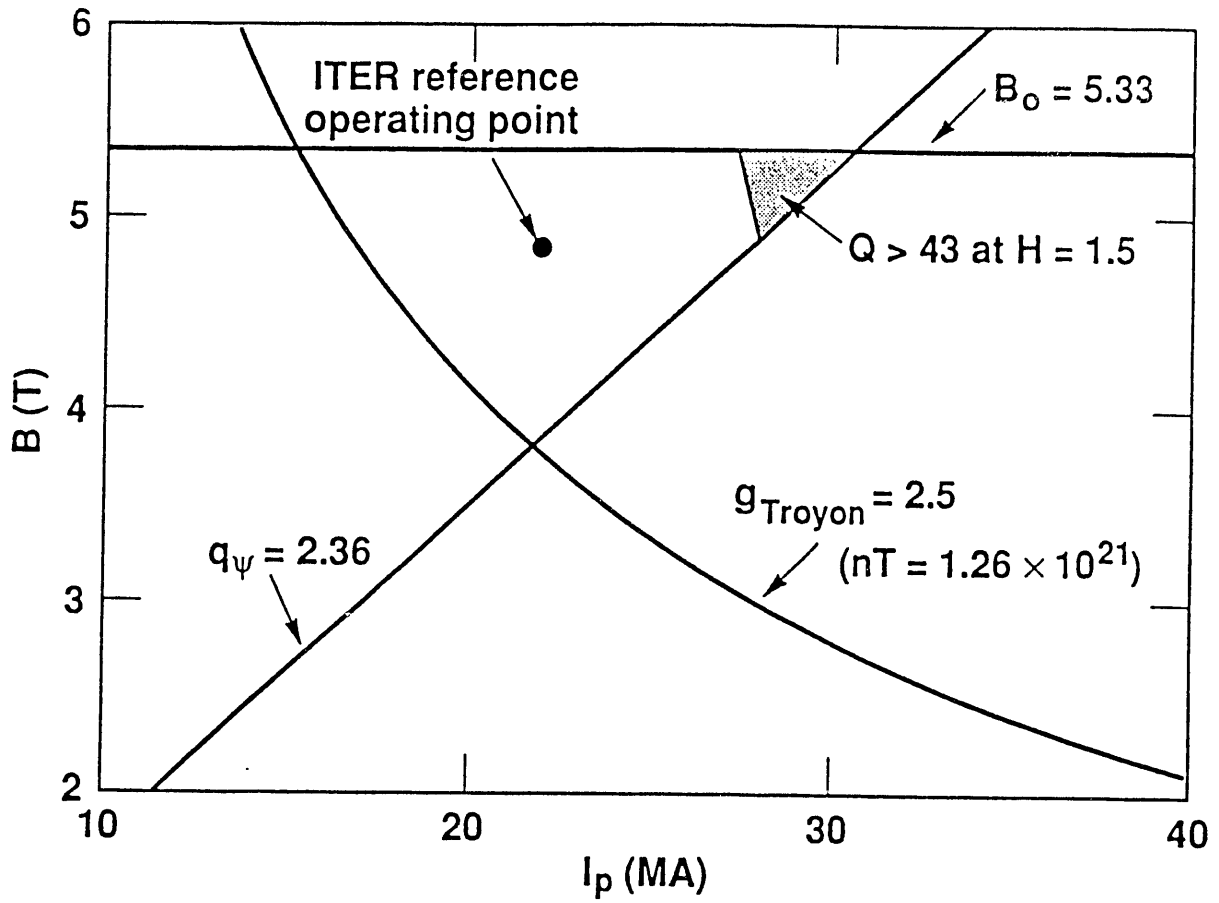

Figure 6.4. Operating point control window in (B,I_p) space and adjustments to compensate for H = 1.5

the burn time requirement. The higher I_p consumes much more volt-seconds than a lower one with the same plasma conditions. Additional volt-seconds are needed from the PF system to offset the consumption from the higher I_p.

For over-confinement if H = 2.5, the transport heat loss is smaller, and the ignition curve is extended to low-temperature and density regions that the desired fusion power curve is well inside the ignition regime. We repeat the procedure in scoping the allowable control window in B-I_p. In this case, the B-I_p control window can only generate operating points within a narrow high-n, low-T region very close to the density limit if I_p is reduced, or in the low-n, high-T region if B and I_p are increased. The adjustment in B-I_p space is shown in Fig. 6.5. The first region is not acceptable because a slight perturbation in the plasma temperature can cause a density-limit induced disruption. The second region still has the problem of excessive divertor heat load. Hence, there is no satisfactory operating point by simply adjusting B and I_p. An alternative scheme is to inject impurity into the plasma or reduce the edge recycling and impurity pumping in order to dilute the plasma with impurity and raise the radiation loss. Under this scheme, we can then locate feasible operating points by increasing the effective charge from 1.6 to 4. Also the divertor heat load condition is better due to the elevated radiation loss. We should be cautious in this scheme as mentioned before and additional study is needed to assess the operation at higher impurity content. The control in B-I_p space is preferred if it can result in acceptable operating points.

The operating conditions for the baseline, H = 1.5, and H = 2.5 cases are listed in Table 6.3. The operational constraints are also shown to indicate the constraint margins. In each case, we show a scenario of Q equal to 43, which is the value for the ITER baseline burn control case. We also evaluate a highest Q scenario that can be controlled with heating power modulation. For H = 1.5, the best case without operating point control is also listed for comparison.

6.1.6 Conclusions

The plasma operating point selection is performed with zero-dimensional POPCON analysis and plasma burn dynamics simulation. The trade-off in various operational constraint margins is required to determine an optimum operating point. The sensitivity of the plasma performance and operation window with respect to tokamak database uncertainties are studied. The maximum controllable Q and availability of operating points for various energy confinement scalings are investigated. The ITER baseline design can accommodate "some" range of the tokamak database uncertainties and achieve design performance goals by operating point control. The operating control knob in B-I_p space and impurity injection may be adjusted to compensate for the uncertainties and provide flexibility of the design. Further work is required in both better uncertainty analysis modeling with multi-variables[6.6] and improved physics models deriving from experimental results.

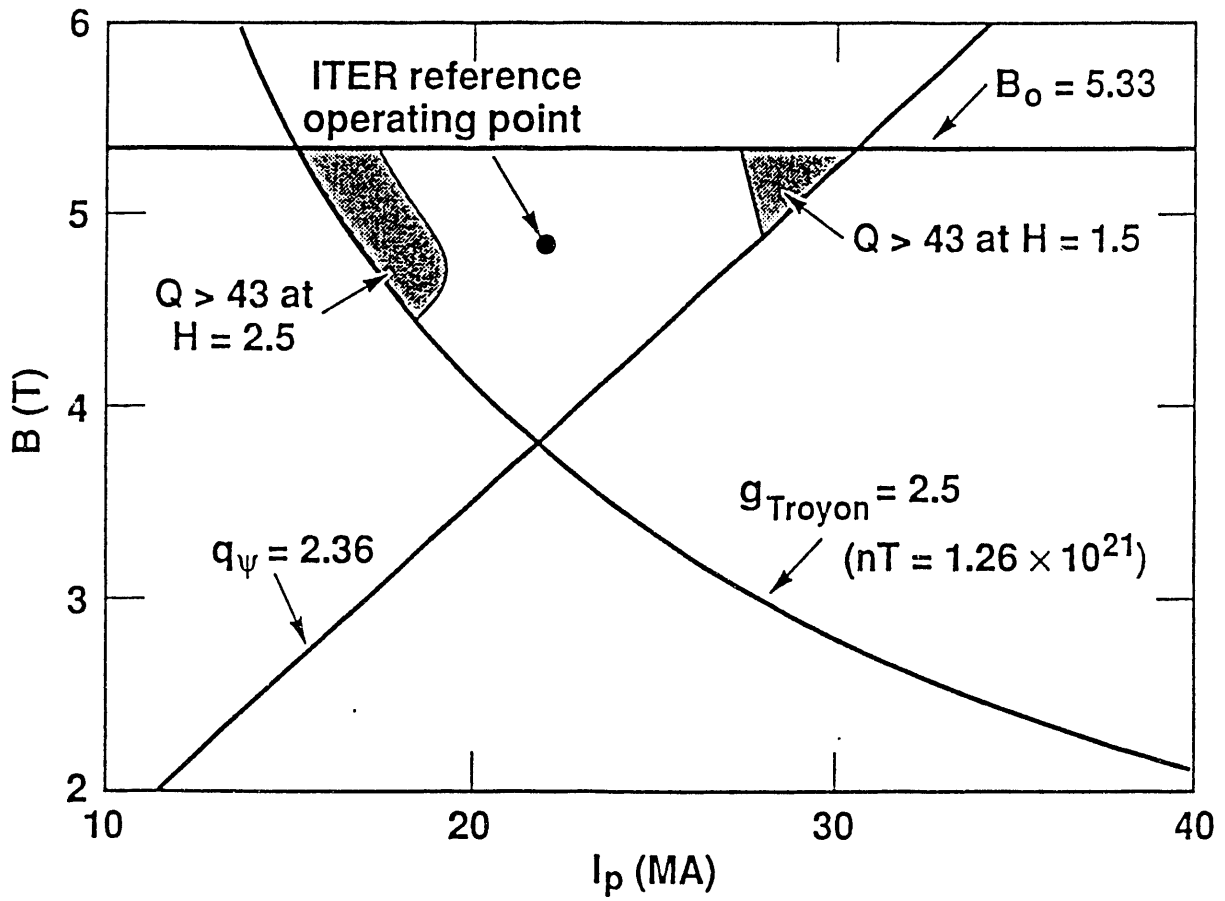

Figure 6.5. Operating point control window in (B,I_p) space and adjustments to compensate for H = 2.5.

Table 6.3. The operating conditions for the baseline, H=1.5, and H=2.5 cases.

	H=2.0		H=1.5			H=2.5	
B (T)	4.85	4.85	4.85	4.85	5.33	4.85	4.85
I_p (MA)	22.0	22.0	22.0	28.0	30.8	22.0	22.0
P_{aux} (MW)	25	12	110	25	10	25	9
Q	43	90	10	43	108	43	120
n (10^{20} m^{-3})	1.80	1.62	1.25	1.32	1.67	1.30	1.17
T (keV)	7.2	7.8	10.5	9.5	7.6	9.8	10.9
Z_{eff}	1.58	1.59	1.65	1.64	1.59	4.10	4.07
P_{nbmax} (MW)	53.0	39.7	110.0	49.8	37.8	53.9	37.6
g_{Troyon}	2.0	2.0	2.0	1.6	1.3	2.0	2.1
n/n_{crit}	0.94	0.84	0.43	0.55	0.82	0.89	0.72
q_φ	3.0	3.0	3.0	2.4	2.4	3.0	3.0
H_{div} (MW/m^2)	8.4	8.6	25.1	12.8	8.3	5.3	5.9
τ_{burn} (s)	257	285	427	<0	<0	388	451

6.2 EMERGENCY PLASMA SHUTDOWN

6.2.1 Introduction

Under normal operational procedures, a fusion plasma with all its thermal stored energy is generally shut down on a timescale of 50-100 seconds.There are two situations where we will require a fast shutdown of the plasma: (1) when the plasma is operating at the required equilibrium point but an external accident event occurs, and (2) when the burn control system fails to stabilize a thermal excursion.

The possible accident scenarios, as mentioned in the ITER Concept Definition[6.7] are, in the order of risk (defined as potential dose times occurrence probability): major rupture of divertor or first wall cooling pipes; major failure of vacuum vessel elements, vacuum ducts and pumps, heating and fueling devices; total LOCA (loss-of-coolant accident) in major cooling system failure outside the vacuum vessel; major plasma disruption; major tritium system failure; major rupture of blanket cooling pipes; magnet current lead break or quench; and total LOFA (loss-of-flow accident) of the entire device.

The ignited operation phase of ITER may operate in a regime subject to thermonuclear burn instabilities.[6.8] In this regime, the plasma temperature runs away and the fusion power output can increase to levels in excess of 3000 MW, depending on the point at which the discharge is terminated by a violation of a beta limit. This undesirable excessive amount of power can severely damage the reactor and possibly induce accidents.

In this section, we will first look at the timescale requirement for plasma shutdown in these emergency scenarios. We then examine the various candidate shutdown schemes and their applicability and limitations. Implications from this analysis in fusion reactor design will be discussed. Overall assessment of the emergency plasma shutdown issue will also be presented. We emphasize that licensing of ITER for full power operation will probably only be granted when we have demonstrated reliable operation of such emergency shutdown systems.

6.2.2 Emergency Shutdown Timescale

The importance and necessity of viable emergency plasma shutdown schemes for fusion reactors can be illustrated by the analysis of Piet and Watson[6.9] in evaluating the melting time of various divertor materials and composites. Figure 6.6 shows the maximum allowed tile thickness at a surface heat load of 15 MW/m^2, which is the nominal value for the ITER baseline design. The tile thickness ranges from about 20 mm for CAPG/copper to about 0.5 mm for aerolor CFC/niobium. This thickness is determined by optimizing the heat transfer efficiency and the life time material erosion. For the same amount of surface heat load, the melting time for these materials is shown in Fig. 6.7 under a LOCA condition. We see that the time to melt depends on the material type and the thickness. The longest time allowed before melting is about 13 seconds for CAPG/molybdenum. However, for aerolor CFC/copper tile, the melting point is less than 1 second. This table clearly indicates that we have to shut down a plasma in about 1 to 10 seconds in order to avoid the melt down of the heat sink and the subsequent accident events. The actual available time for the shutdown depends on the choice of materials. Hence we must be able to shutdown the plasma in 10 seconds; and preferably have capability to do so in about 1

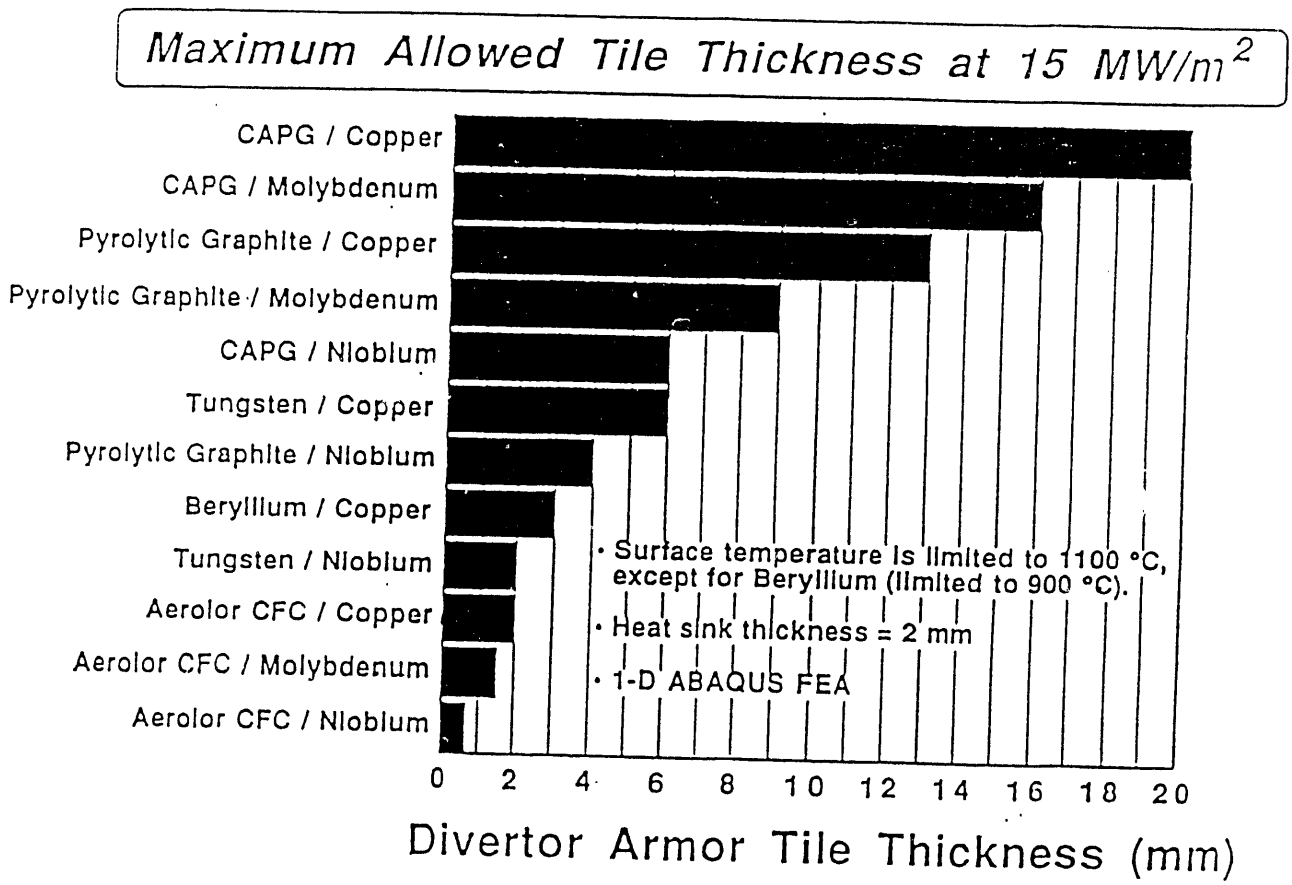

Figure 6.6. Optimized maximum divertor armor tile thickness for various candidate materials at a surface heat load of 15 MW/m^2.

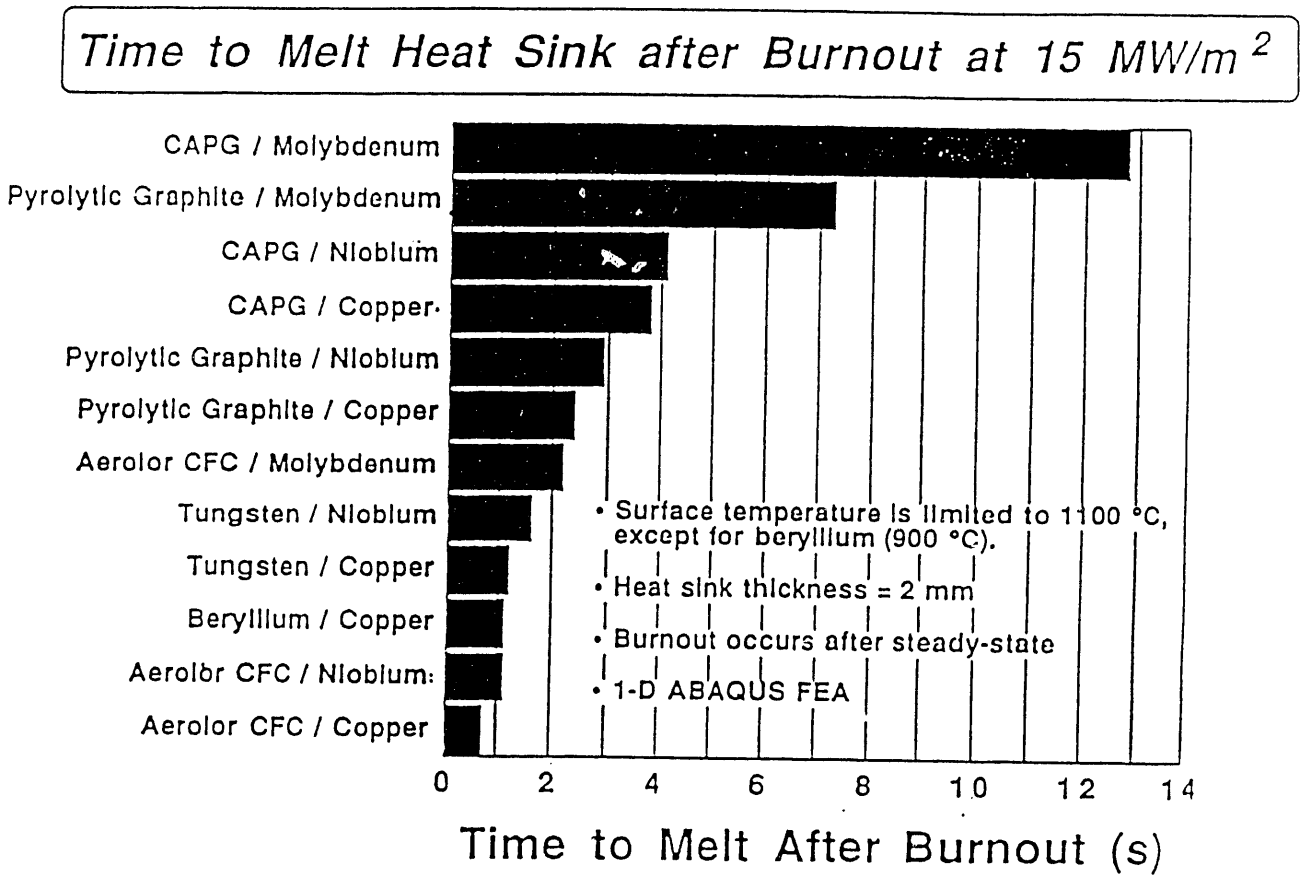

Figure 6.7. The time duration to melt the heat sink in the divertor armor for the various candidate materials after a burnout with a surface heat load of 15 MW/m^2.

second. A successful emergency shutdown scheme will enhance the flexibility in the choice of design materials and reliability in safety features.

6.2.3 Plasma Burn Simulation Model

Our analysis is performed with the zero-dimensional code DYNASTY.[6.2] The code calculates the particle and power balance for fuel ion species, fusion product alpha particles, and electrons. It uses parabolic density and temperature profiles of the form $(1-x^{\alpha})$ where x is the normalized radial location (radial position / plasma minor radius) and α is the ITER-specified exponent coefficient. The values of α for density and temperature profiles are 0.5 and 1.0, respectively. The zero-dimensional particle and power balance is computed by the various global quantities averaged over their respective profiles. The power balance terms include alpha heating P_{α}, conduction (confinement) loss P_{con}, radiation (bremsstrahlung and synchrotron) loss P_{rad}, ohmic heating P_{oh}, and auxiliary (external) heating P_{aux}. The conduction loss is calculated by using an empirical scaling formulation of the plasma energy global confinement time. The ITER-offset-linear scaling law is used in this work. The particle balance is calculated by charge neutrality and specified impurity deduced plasma effective charge Z_{eff}. External fueling is provided to sustain the convection loss and plasma burn up of the fuel ions. We treat the thermal alpha particles by either fixing the concentration fraction or the ratio of alpha particle to plasma energy confinement times.The code runs in a time-dependent mode to simulate the plasma burn history. The variations of the density and temperature of the fuel ions, alphas, and electrons in time are solved in a set of coupled first order differential equations. This mode enables us to examine the thermal stability properties, required installed heating power for burn control, and the burn history of the plasma.

6.2.4 Shutdown Scheme Candidates

There are basically two approaches of shutting down a burning plasma: (1) trigger an abrupt, uncontrolled, fast (of the order of 100 milliseconds) disruption of the plasma, and (2) adjust the system for a controlled decay in the stored thermal energy governed by the global plasma power balance equation:

$$\frac{d}{dt}\, 3\,nT = P_{\alpha} + P_{aux} + P_{oh} - P_{con} - P_{rad}. \qquad (6.1)$$

The first approach can effectively shut down a plasma in a relatively short time. However, it is not so desirable because it puts a very large amount of heat load and mechanical force on the reactor vacuum vessel in a short pulse. Repeated disruptions can severely damage the reactor system. If the second approach is used to shutdown a plasma, we can adjust the system to reduce P_{α} and P_{aux} , or increase P_{con} and P_{rad}. Listed below are several candidate schemes for emergency plasma shutdown.

(a) Beam and Fuel Shutoff

In this scheme, the auxiliary heating and the fueling are shutoff instantaneously at time equal to zero. The shutoff of the heating sets P_{aux} to zero and causes a negative thermal excursion through the power balance. The absence of fuel supply also enhances the reduction of fusion power. The fusion power decays from 1100 MW to about 300 MW in 10 seconds and a total shutoff at about 20 seconds as shown in Fig. 6.8. Both the energy

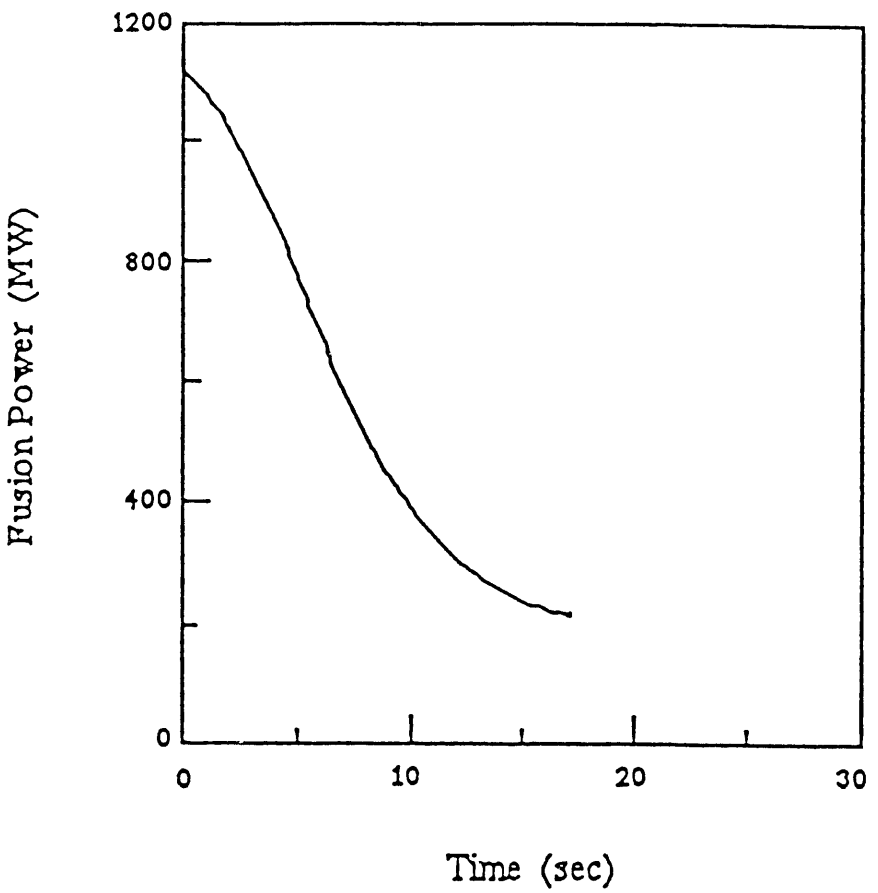

Figure 6.8. Time history of the fusion power during a rapid shutoff of the heating and fueling for an ITER-type plasma.

and particle confinement times have a degradation term proportional to $P_d = P_\alpha + P_{aux} - P_{rad}$, which reduces the confinements at high P_d. Hence, as the fusion power diminishes, the energy and particle confinements are longer than their equilibrium values at the start of the shutoff. This characteristic of the confinement scaling law prolongs the plasma shutdown time.

In Fig. 6.9, we see that the actual plasma density exceeds its limiting value for a density induced disruption at time zero. This density limit disruption model[6.4] is based on the notion that the plasma radiative and parallel energy transport losses in the scrapeoff region and near the divertor plates are maintained by power flow from the core plasma. If the stability of the edge power balance is disturbed, edge temperature collapses, the current channel shrinks, and a disruption ensues. The quantitative aspects of this model are still under development and at present the model is uncertain to about a factor of two. The equilibrium n_e/n_{crit} value is about 0.95. This value exceeds unity at the shutoff because P_{aux} can be turned off instantaneously, but the density has to decay through the particle balance even after fueling is stopped. The reduced heat flow to the scrape-off region is insufficient to supply the radiative power loss and results in a disruption.

The controlled shutdown scheme as shown in Fig. 6.8 is only possible if the density limit disruption has not occured. This may be amended by the plasma at a different operating initial equilibrium point well below the disruption density limit. However, the n_e/n_{crit} ratio increases during the shutdown process as indicated in Fig. 6.9, and this may prevent a controlled shutdown without a disruption.

(b) Impurity Injection

There are two choices of impurity injection into a plasma for shutdown purposes, namely, the type of impurity and the deposition profile. We can inject low, medium, or high Z materials to enhance the radiation loss, or hydrogen to dilute the fuel density. The impurity is deposited at the edge unless it is launched from a high velocity pellet injector. The medium and high Z impurity materials require less injection velocity for penetration than that of hydrogen and low Z materials. Deposition at the center of the plasma is essential because most of the fusion power is generated at this peaking temperature and density region. Also, it is very likely for a plasma to disrupt if the impurity is deposited at the edge due to the sudden increase in edge radiation power.

We have looked at an example of injecting tungsten into a candidate ITER design. The fusion power initially has a slight increment due to better plasma confinement as a result of reduction in P_d. The n_e/n_{crit} ratio is slightly exceeded at the beginning, then decreases afterward. It then gradually decays to 600 MW in 10 seconds and vanishes in about 20 seconds. The density limit is reached at about the time the plasma is almost shutdown.

The merits of various impurity injection schemes will be listed at the end of this subsection where an overview of all the emergency shutdown schemes is discussed.

(c) H to L Modes Transition

Biasing the divertor plates to modify the radial electric fields may allow the control of the transition from a H-mode to a L-mode plasma operation. This scheme reduces the decay times of the stored energy, alpha and transport powers by approximately the L-mode enhancement factor H. The fusion power decays from full power to 100 MW in about 5 seconds. The initial total heat load increases due to a higher transport loss, but the peak heat

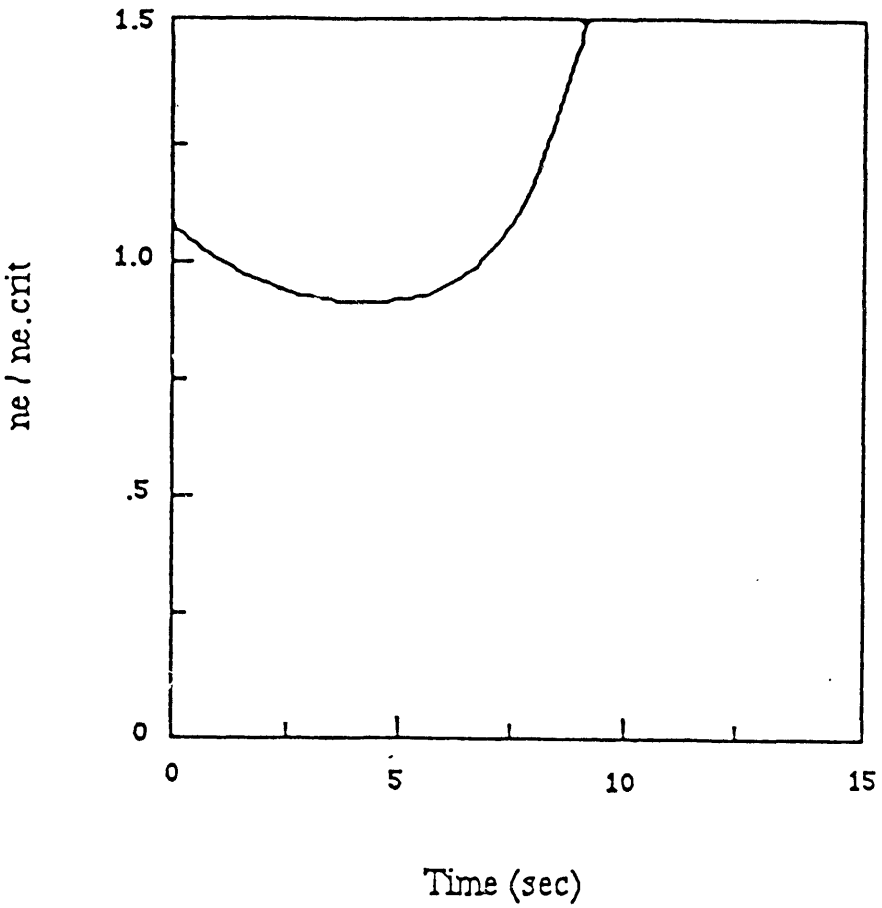

Figure 6.9. The ratio of the plasma density to the critical disruptive density as a function of time during the shutoff.

load does not have the same increment because the scrape-off layer is enlarged and partially offsets this effect. The initial density limit margin increases due to the enhanced transport loss. However, the rapid loss of alpha power reduces the available heat flow to the edge plasma that pushes the plasma over the disruption density limit in about 2.5 seconds.

(d) Vertical Field System Shutoff

In this scheme the poloidal field coils used for the feedback stabilization of MHD vertical instabilities are turned off by some kind of sensor actuated switch. The plasma will then move vertically on the timescale of the L/R time of the passive vertical control structure (which is on the order 10-100 milliseconds) at which point the plasma deposits both its thermal and poloidal field energy onto the structure in roughly the same manner as a hard disruption. This scenario should only be employed as a last resort if all other methods fail.

The effectiveness of the above mentioned plasma shutdown schemes is listed in Table 6.4 in terms of the shutdown timescale. The probability of disruption and potential for system passivity are ranked as assessed from Refs. 6.10 and 6.11. The timescales are relative to critical thermal transient timescales in reactor components or time for significant fusion power transients in thermal runaway regime. The potential for passivity is relative to the techniques utilizing thermal expansion, melting, and gas pressure buildup. Schemes which rely on switches to turn off electrical systems are less desirable than those that can be directly actuated by local thermal effects.

The results are of a preliminary nature because there are many uncertainties in the physics models of a tokamak reactor. The theory of tokamak plasma transport and its energy and particle confinement losses are not very well understood. The shutdown time depends on the choice of the various empirical scaling laws for the energy confinement time and the plasma (fuel ions, thermal alphas, and electrons) particle confinement assumptions. Our zero-dimensional computational modeling lacks the information of the profile evolutions, which can be important because the majority of the fusion power comes from the center region. The edge profiles should also be examined independent of the core profiles during shutdown by a profile dependent transport code to study the possibility of an edge density initiated disruption.

6.2.5 Implications For Reactor Design

From the above analysis, we see that the capability for fast shutdown of a plasma is indeed a very difficult problem. Because of the importance to accomplish this task, we should utilize all available resources to do so. Here we suggest to take emergency shutdown into consideration in reactor design studies.

The design operating point should be adjusted so that it is far away from the density limit, even if we have to trade-off in plasma performance. This enables the plasma to stay below the density disruption limit when an emergency shutdown scheme is initiated. The choice of plasma facing components should be weighted favorably for those materials that allow for a relatively longer shutdown time. Finally, the various machine components and integrated design should be able to absorb a certain number of disruption to handle emergency shutdown scenarios.

Table 6.4. Candidate ITER emergency plasma shutdown schemes.

Method	Time-Scale	Probability of Disruption	Potential for Passivity
1. Controlled Reduction of Auxiliary Heating & Fueling	slow	low	poor
2. H-L Mode Transition	medium	low	poor
3. Controlled Impurity Injection			
hydrogen	medium	low	poor
medium to high Z	medium	moderate	poor
4. Rapid Shutoff of Heating & Fueling	medium	moderate-high	moderate
5. Vaporization of Divertor Substrate	medium	moderate-high	very good
6. Uncontrolled Central Impurity Injection	fast	moderate-high	good
7. Uncontrolled Edge Impurity Injection (pressurized burst diaphragm)	fast	high	good
8. Interruption of Vertical Control	fast	100 %	moderate

6.2.6 Conclusions

In this paper we have studied several candidate emergency shutdown schemes. We have found that it is difficult to apply the concept of passive inherent safety in fission directly to fusion, primarily because the power producing element (plasma) is not in direct communication with the media (coolant and blanket material) undergoing the accident condition.

Work by Piet and Watson[6.9] indicates that plasma emergency shutdown schemes are required to reduce the fusion power production in 1-10 seconds, and preferably in less than 1 second. The schemes considered include shutting off the heating and fueling systems, triggering an H-mode to L-mode transition, injecting various impurities, and shutting off the vertical stability control systems. Most controlled shutdown schemes not relying on a disruption do not meet or are at best marginally satisfying the timescale requirement. A plasma can be shut off fast enough via a disruption, but other undesirable effects also are produced.

Because of performance considerations, ITER operates near the density limit derived from a power balance in the scrapeoff layer. As soon as the fusion power decays away, the edge energy balance is upset and the plasma may tend to disrupt. This effect appears in all the shutdown schemes we have investigated so far.

We have to take into account the capability of emergency plasma shutdown in a reactor design. This implies modifications may be needed in operating point selection, choice of reactor materials, and disruption force tolerance margin.

Further work is required to implement acceptable emergency shutdown schemes. Better understanding of tokamak confinement physics and radial profiles dependent modeling are warranted.

References

6.1. L.J. Perkins, et al., IAEA Technical Report, ITER-IL-SA-1-0-9, March 18, 1990.

6.2. S.W. Haney, L.J. Perkins, J. Mandrekas, and W.M. Stacey, "Active Control of Thermonuclear Burn Conditions for the International Thermonuclear Experimental Reactor," to be published in Fusion Technol.

6.3. W.A. Houlberg, S.E. Attenberger, and L.M. Hively, Nucl. Fusion **22**, 935 (1982).

6.4. K. Borrass, "Disruptive Tokamak Density Limit as Scrape-Off Layer/Divertor Phenomenon," Euratom Report EUR-FU/80/89-95, The NET Team, November, 1989.

6.5. S.K. Ho and M.E. Fenstermacher, Fusion Technol. **16**, 85 (1989).

6.6. S.K. Ho and L.J. Perkins, Nucl. Fusion **29**, 81 (1989).

6.7. "ITER Concept Definition." IAEA/ITER/DS/3, International Atomic Energy Agency, 1988.

6.8. L.J. Perkins, S.H. Haney, S.K. Ho, and J. Mandrekas, et al., "US Burn Control Studies for the International Thermonuclear Experimental Reactor," Lawrence Livermore National Laboratory, UCRL-ID-105546 (1991).

6.9. S.J. Piet and R. Watson, "Need for Emergency Shutdown and Burn Control," presented at ITER Plasma Operational Control Workshop, Garching, FRG, July 1990.

6.10. L.J. Perkins, R.B. Campbell, S.H. Haney, and S.K. Ho, "ITER Emergency Shutdown," presented at ITER Plasma Operational Control Workshop, Garching, FRG, July 1990.

6.11. S.K. Ho, R.B. Campbell, L.J. Perkins, and S.W.Haney, "Assessment of Emergency Plasma Shutdown Schemes for ITER," Fusion Technol. **19**, 1322 (1981).

7. OTHER APPLICATIONS

7.1 APPLICATION TO ARIES

We have regularly attended the ARIES Project Meetings in order to obtain updated information on the current fusion reactor design work. We have performed comprehensive calculations of radioactive inventories and radiological hazard indices for an ARIES-I-type reactor design candidate in 1989. This work[7.1] was reported to the 13th Symposium on Fusion Engineering at Knoxville, in October, 1989. We have also examined the radiological hazards of an ARIES-III-type reactor utilizing the advanced fuel cycle of D-^{3}He.

7.1.1 Radiological Hazards of An ARIES-I-Type Reactor Design

The ARIES-I[7.2] design is a 1000-MWe D-T fusion reactor design based on modest extrapolation of current physics database and advanced technology. The design utilizes low activation silicon carbide (SiC) composite as the structural material. The silicon carbide is also used as the first wall. The blanket consists of a breeder with lithium zirconate (Li_2ZrO_3), a beryllium neutron multiplier/reflector, and a silicon carbide reflector.

Assumptions and modeling in the activation and dose conversion analyses are as follows:

1. the irradiation lifetime of the components is 7.2 years so that the total electrical power output and wall loading are compatible with the ESECOM[7.3] cases;
2. no divertor is included in the first wall region;
3. the tritium inventory is assumed to be 1 kg, which is placed in the first wall and fully released during an accident;
4. the critical, chronic, and intruder doses are as defined in the ESECOM studies;
5. class F weather conditions are used for accident analyses;
6. ESECOM listed plausible fusion release categories are used;
7. ESECOM computational methodology are employed--activation radioactivity is evaluated by a set of neutronics codes TART,[7.4] ORLIB,[7.5] and FORIG;[7.6] various doses are computed by a dose-conversion code FUSEDOSE.[7.7]

The critical and chronic doses from the total release of the radioactivity inventories in each zone are calculated as shown in Table 7.1. The doses are reduced if the release of radioactivities is according to the plausible release fractions.

The numerical results in Table 7.1 are based on calculations excluding any specific divertor designs. If carbon divertors are used, the results remain the same. However, if tungsten divertors are used, the radioactivity will be increased appreciably.

The critical dose from the plausible release due to an accident is well below the threshold limit of 200 rem, implying no early fatalities. However, the chronic dose exceeds the threshold limit of 25 rem, and it imposes some potential long term (e.g. 50 years) radiological hazards. The intruder dose is considerably low that it does not have any waste disposal problem. The components are acceptable for shallow burial under 10CFR61. Maintenance requires remote handling due to the relatively high contact dose rate.

Table 7.1. Total and plausible releases of radiological doses in each zone of an ARIES-I-Type Reactor.

	first wall	breeder	Be-reflector	SiC-reflector
Total Release:				
critical	13	5500	100	46
chronic	37	12000	6000	3100
contact (1 day)	5.5e6	1.9e9	7.0e7	3.0e5
(1 year)	3.5e5	2.9e7	3.3e7	2.6e5
intruder	0.015	0.11	0.089	4e-4
Plausible Release:				
critical	8	71	9	4
chronic	3	650	210	92

The breeder produces a relatively high dose from the natural lithium zirconate. If breeding materials such as lithium oxide (Li_2O) and lithium silicate (Li_4SiO_4) are used instead of lithium ziconate, the induced radioactivity will be reduced accordingly. Also, it has been suggested[7.2] to tailor the composition of the lithium zirconate by advanced isotopic separation techniques in order to reduce the activation level. If we reduce the "bad" isotope of Zr-90 from the natural 51% to 5% while increasing the composition of Zr-91 and Zr-92, we find the doses in the breeder zone to be reduced as shown in Table 7.2.

Table 7.2. Radiological doses for selective isotopic tailored breeder.

	full release	plausible release
critical	930	28
chronic	12000	360
contact (1 day)	2.6e8	2.6e8
(1 year)	1.3e7	1.3e7
intruder	0.062	0.062

Both the critical and chronic doses are reduced by about a factor of two. The isotopic tailoring of materials (with several natural isotopes, some have greater radiological hazard potential than the others) is an alternative for reducing the radiological hazards. This provides a trade-off between the safety features and the additional cost of the reactor in the isotopic tailoring.

In summary, the ARIES-I-type fusion reactor design utilizing the low-activation silicon carbide has accident doses two orders of magnitude less than the PWR fission reactor as studied in the ESECOM report. The critical dose is below the threshold for early fatalities. The 50-year chronic dose exceeds the threshold for land denial after an accident. It does not impose any waste-disposal restrictions for shallow burial. The design presents favorable environmental and safety features, even though further research and development are warranted to examine the applicability of silicon carbide as fusion structural material.

7.1.2 Radiological Hazards of An ARIES-III-Type Reactor Design

Preliminary assessment of the radiological hazards of burning deuterium and helium-3 (D-^{3}He) as fuels for a fusion reactor is presented here. The motivations of this analysis are to examine the impacts of utilizing neutron-lean fusion reactions and to supplement a current reactor design study by the ARIES team.

Neutron activation is a major source of radioactivity for fusion reactors. The conventional deuterium-tritium (D-T) reactions produce 14-MeV neutrons which may induce severe radiological hazards. If the fusion reactor is constructed of currently manufactured materials like stainless steel, the induced activation doses may even be comparable with that of fission reactors. However, if low-activation materials like silicon carbide are used for the reactor, the doses may be greatly reduced to a level of avoiding early fatalities in accidents.

Applications of alternative fusion fuels may remove the restriction of using low-activation materials. The idea is to suppress the D-T reactions, thereby reducing the population of the 14-MeV neutrons. For the D-^{3}He reactions, no neutrons will be generated. However, the fusing of the deuterons in a D-D reaction has two equal-probable reactions, one of which produces 2.5-MeV neutrons. Moreover, the small amount of tritons generated from the other branch of the D-D reaction can also burn in the D-T reaction. As a result, both 14-MeV and 2.5-MeV neutrons will be produced in a D-^{3}He cycle. However, the flux levels will be much smaller than that of a comparable D-T cycle. Hence, the burning of D-^{3}He fuels in a fusion reactor can reduce the fast neutron flux substantially, which makes this scheme more attractive from an environmental and safety perspective. Nevertheless, the smaller levels of fusion neutrons produced can still induce undesirable activation radioactivity. The evaluation of this effect will be discussed later.

The D-T fuel cycle has the highest fusion reactivity and hence has the least stringent physics requirements for net power generation. If other fuels (so-called advanced fuels) are employed, various areas of physics improvements are required. For example, the plasma has to be operated in a higher temperature and density regime, the plasma beta is higher, and a larger energy confinement time is also needed. The advantage of using advanced fuels in order to reduce 14-MeV neutrons for environmental and safety benefits has to be traded-off with more stringent physics requirements.

We adopt the ESECOM computational methodology in calculating the neutron activation radioactivity. A set of computer codes TART, ORLIB, and FORIG, and their associated databases are used similar to Section 7.1.1. The tokamak configuration is approximated as a set of concentric cylinders consisting of the plasma, first wall, blanket, and shield regions. The length of the cylinder is determined such that the volumes of the cylindrical layers are approximately equal to that in the real toroidal design configuration.

We studied, as an example, an ARIES-III-type D-^{3}He reactor using HT-9 steel as the structural material. This is a 1000-MWe fusion power reactor using current technology structural material. There is no need for a tritium-breeding blanket as in the D-T reactors. The irradiation time is assumed to be the lifetime of the components at 30 years. The critical and intruder doses, as defined in the ESECOM studies, are used to characterize the accident and waste disposal hazards, respectively. Class F weather conditions and ESECOM listed plausible fusion release fractions are used for accident analyses.

Major HT-9 steel activation products contributing to the critical dose are found as indicated in Table 7.3. The critical dose in the first wall and shield modules, and the contributions of various activation products of HT-9 steel to the critical dose from both 14-MeV and 2.5-MeV neutrons are listed in Table 7.4.

Table 7.3. Major radionuclides from activation of HT-9 steel.

Major Radionuclides	Release Fractions	Half-lives
Fe54 (n,p) Mn54	0.10	312.5 days
Fe56 (n,p) Mn56	0.10	2.5 hr
W186 (n,g) W187	0.03	23.8 hr
Re185 (n,g) Re186	0.30	3.7 days
Re187 (n,g) Re188	0.30	16.9 hr

The activation radioactivity inventories are mainly from iron (Fe) and the 5% by weight of tungsten (W) in the HT-9 steel. Both Mn54 and Mn56 are produced from the activation of Fe, while W187, Re186, and Re188 are generated from W. Applying the plausible release fractions from the ESECOM studies, we find that the total critical dose is almost twice the fatality threshold of 200 rem. It should be pointed out that this activation level in the HT-9 steel is almost an order of magnitude less than that from a similar reactor using D-T fuel cycle.

The intruder dose from HT-9 steel is mainly due to impurities within the steel. The intruder dose is found to be less than 0.1 rem if we calculate the intruder dose only from the activation products of the main constituents of HT-9 steel (Fe, Cr, W, V, and C). It is far below the 0.5 rem limit specified in 10CFR61 and therefore acceptable for Class C shallow burial. On the other hand, if Nb and Mo are included at an impurity level of 0.001% by weight, the resulting intruder dose will exceed 1 rem and the requirement for shallow burial will not be satisfied.

The results imply that utilizing the D-^{3}He alone while using the conventional structural materials may not be able to solve all our environmental and safety concerns. Further work is needed to investigate improvements in this area.

Table 7.4. Critical dose from HT-9 steel structure of an ARIES-III-type D-^{3}He fusion reactor.

First Wall:

	14 MeV-neutron	2.5MeV-neutron
Mn54	19 rem	5.0 rem
Mn56	31	0.3
W187	6.9	11
Re186	2.9	5.6
Re188	8.1	27

Shield:

	14 MeV-neutron	2.5MeV-neutron
Mn54	37 rem	6.5 rem
Mn56	48	0.2
W187	49	89
Re186	3.3	9.2
Re188	12	41

First Wall	117 rem
Shield	300 rem
Total	417 rem

As a comparison, we checked the radiological doses for an ARIES-I-type D-T-fuel 1000-MWe reactor utilizing low-activation materials as presented in Section 7.1.1. It should be cautioned that the tritium breeding module in a D-T reactor may have a larger activation hazard potential depending on the choice of breeding materials. The low-activation silicon carbide apparently can withstand a high neutron flux, producing a relatively benign level of activation. The resulting critical dose for a low-activation D-T reactor is below the fatality threshold and the waste is acceptable for shallow burial.

From the above analyses, we observe that utilizing both low-activation structural materials and advanced-fuel cycles can significantly reduce the neutron activation radioactivity. Obviously, the environmental and safety prospects will be even better if low-activation materials are used in advanced-fuel cycles. In this particular example, the low-activation materials approach seems to have a relatively better environmental and safety performance. There are uncertainties in the applicability of low-activation materials in a fusion reactor and the possibility of physics enhancements in advanced-fuel fusion. Strong research and development efforts in these areas are required to capitalize on the potential environmental and safety advantages of fusion reactors.

7.2 PCA CASE IN ESECOM SCHEME

Our improved tools for calculation and presentation of ES indices, as described above, were first applied to ESECOM reactor designs to benchmark the new codes and confirm that the streamlining and updates produced no unexpected changes. We then turned to applications to additional cases: applications to designs emerging from the ITER and ARIES projects are described in Sections 6 and 7.1 of this report; we turn here to the application to modifications of ESECOM fusion-reactor designs exploring the consequences of using stainless steel structural material in place of vanadium/titanium alloy and ferritic steel.

The ESECOM study did not investigate any stainless-steel cases because the committee believed previous work had already demonstrated such severe environmental and safety (ES) liabilities for stainless-steel structure that this material was unlikely to be chosen for commercial reactor applications. In the meantime, however, slowness to demonstrate the usability of alternative materials in fusion environments (along with, perhaps, insufficient attention to ES issues by reactor designers) has helped generate continuing interest in the possible use of stainless steel. This interest motivated us to investigate, as an early application of the improved ES assessment tools we had developed, the consequences of use of stainless steel in ESECOM reactor designs.

We constructed our stainless-steel cases by modifying Cases 1 and 2 from the ESECOM study. In Case 1, which in ESECOM was a vanadium/titanium alloy, lithium-cooled tokamak, we substituted the stainless-steel alloy used in the STARFIRE study ("Primary Candidate Alloy" = PCA) on a one-to-one volumetric basis for the vanadium/titanium alloy wherever it occurred (the first wall, inner blanket, and manifold); we denote this modified case PCA1. In Case 2, which in ESECOM was helium-cooled tokamak with Li2O breeder and reduced-activation ferritic-steel structure, we substituted PCA on a one-to-one volumetric basis for the ferritic steel in the first wall, inner blanket, and manifold; we denote this modified case PCA2. Of course, it would have been more rigorous to develop new designs reoptimized for the stainless steel structural material, but the much easier procedure described here permitted a rapid first-order estimate of ES consequences of using stainless steel in place of lower-activation alloys.

Figures 7.1 through 7.9 show the results for PCA1, with comparisons to the unmodified ESECOM Cases 1 and 2 and fission reactors. With respect to BHPs (Figs. 7.2 and 7.3), the stainless steel case is 3-100 times worse than the vanadium/titanium and ferritic-steel cases, but still 50 to 100,000 times better than the LMFBR. With respect to maximum plausible dose potentials, however, the stainless steel case loses most of the advantage over fission enjoyed by the vanadium/titanium and ferritic-steel cases (Figs. 7.4-7.6): if the "conservative" release envelope is used for all cases, PCA1 is only better than the LMFBR by a factor of about 2 in critical dose at 1 km, compared to the factor of 6 advantage for the vanadium/titanium and ferritic-steel cases; and in terms of the chronic dose potential from ground contamination at 10 km, PCA1 is worse than the fission cases by about a factor of 2, in contrast to vanadium/titanium being 2 times better than fission and ferritic steel being better by 40 percent. In terms of contact dose rates after 30 years of cooling, the PCA1 first wall is worse than the vanadium/titanium case by 5 orders of magnitude and worse than the ferritic-steel case by 3 orders of magnitude. With respect to qualification for shallow burial (Fig. 7.9, top), the volume averaged intruder dose for the PCA1 case is too high by about a factor of 20, although still 2000-fold lower than the LMFBR,whereas by this measure the vanadium/titanium and ferritic-steel cases qualify for shallow burial with margins of 3-fold and 20-fold, respectively; the annualized intruder hazard potential for PCA1 wastes is 60 times bigger than for the vanadium/titanium case

Comparison with ESECOM cases

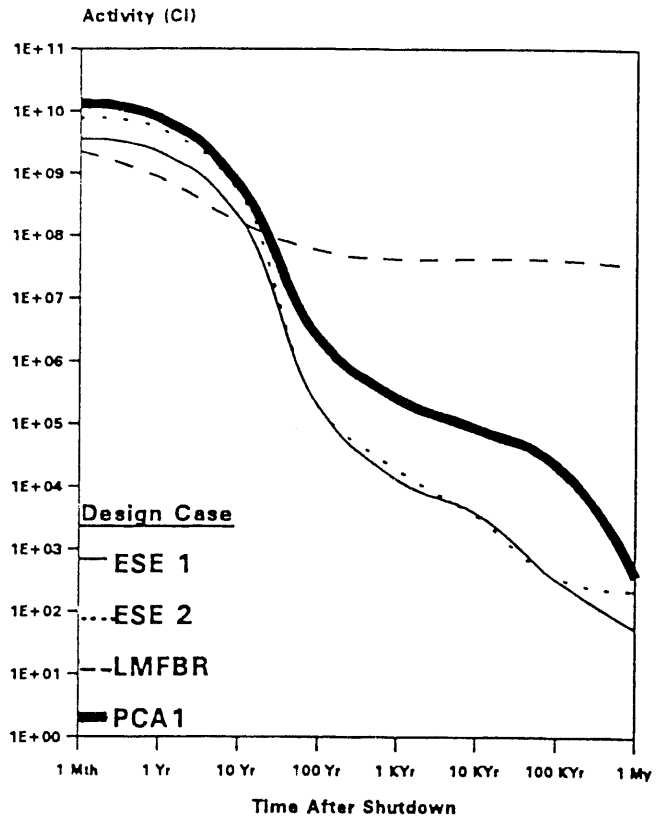

RADIOACTIVITY DECAY

*initial inventory represents life-cycle radioactive waste

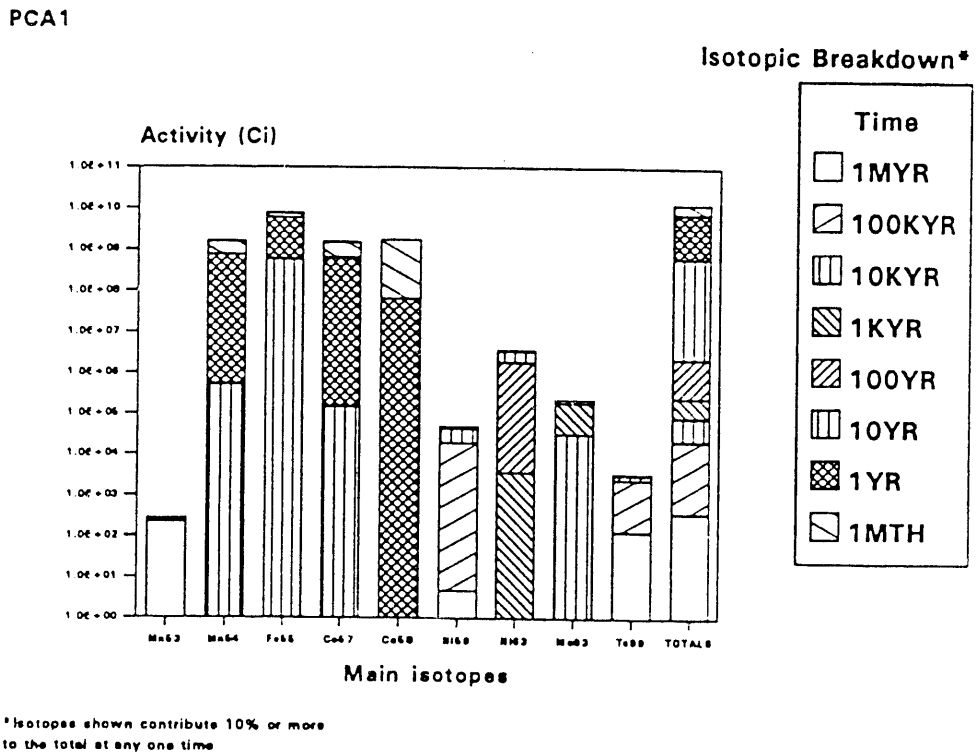

Figure 7.1. Comparison of radioactivity decay for stainless-steel variant of ESECOM Case 1 (PCA1), ESECOM Cases 1 and 2 (ESE1 and ESE2), and LMFBR. Main contributing isotopes to PCA1 case are shown at bottom.

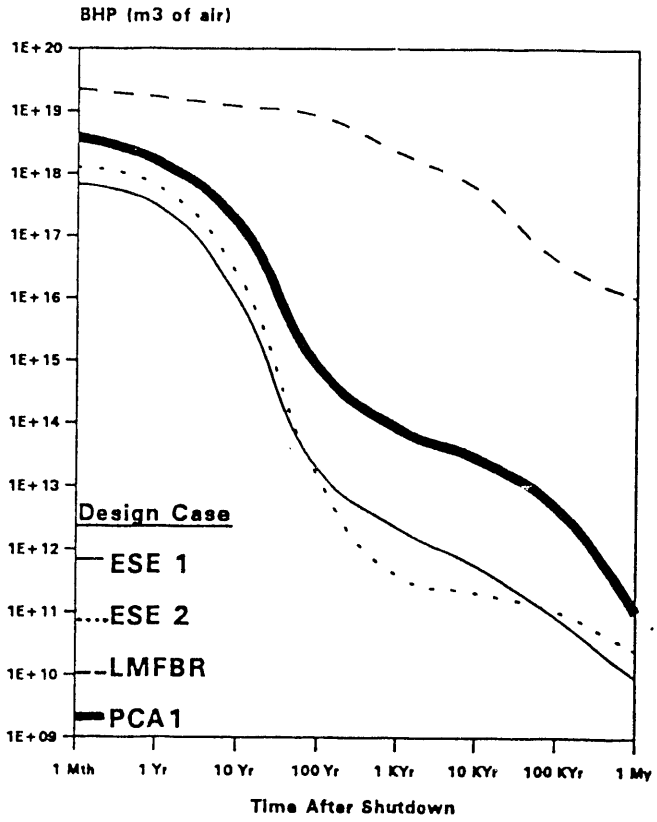

BIOLOGICAL HAZARD POTENTIAL IN AIR

*initial inventory represents life-cycle radioactive waste

*MPCs are from Fetter

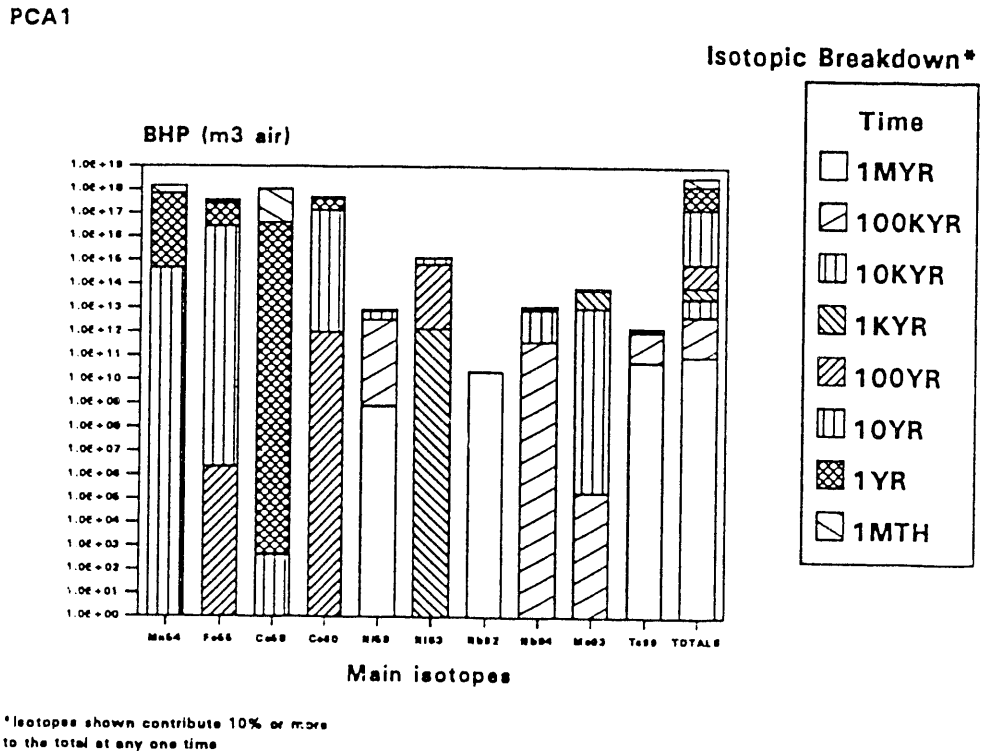

Figure 7.2. Comparison of Biological Hazard Potential in air for stainless-steel variant of ESECOM Case 1 (PCA1), ESECOM Cases 1 and 2 (ESE1 and ESE2), and LMFBR. Main contributing isotopes to PCA1 case are shown at bottom.

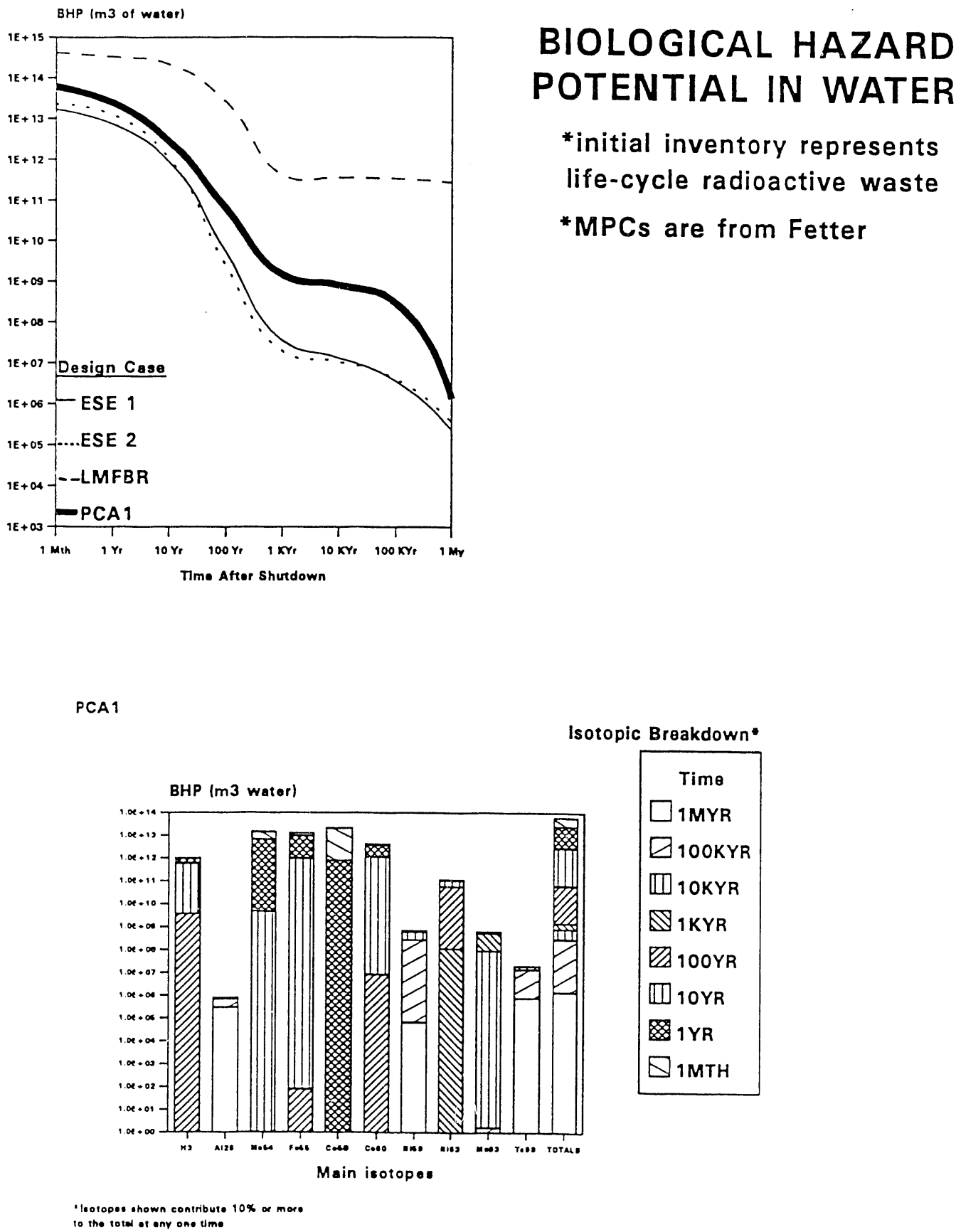

Figure 7.3. Comparison of Biological Hazard Potential in water for stainless-steel variant of ESECOM Case 1 (PCA1), ESECOM Cases 1 and 2 (ESE1 and ESE2), and LMFBR. Main contributing isotopes to PCA1 case are shown at bottom.

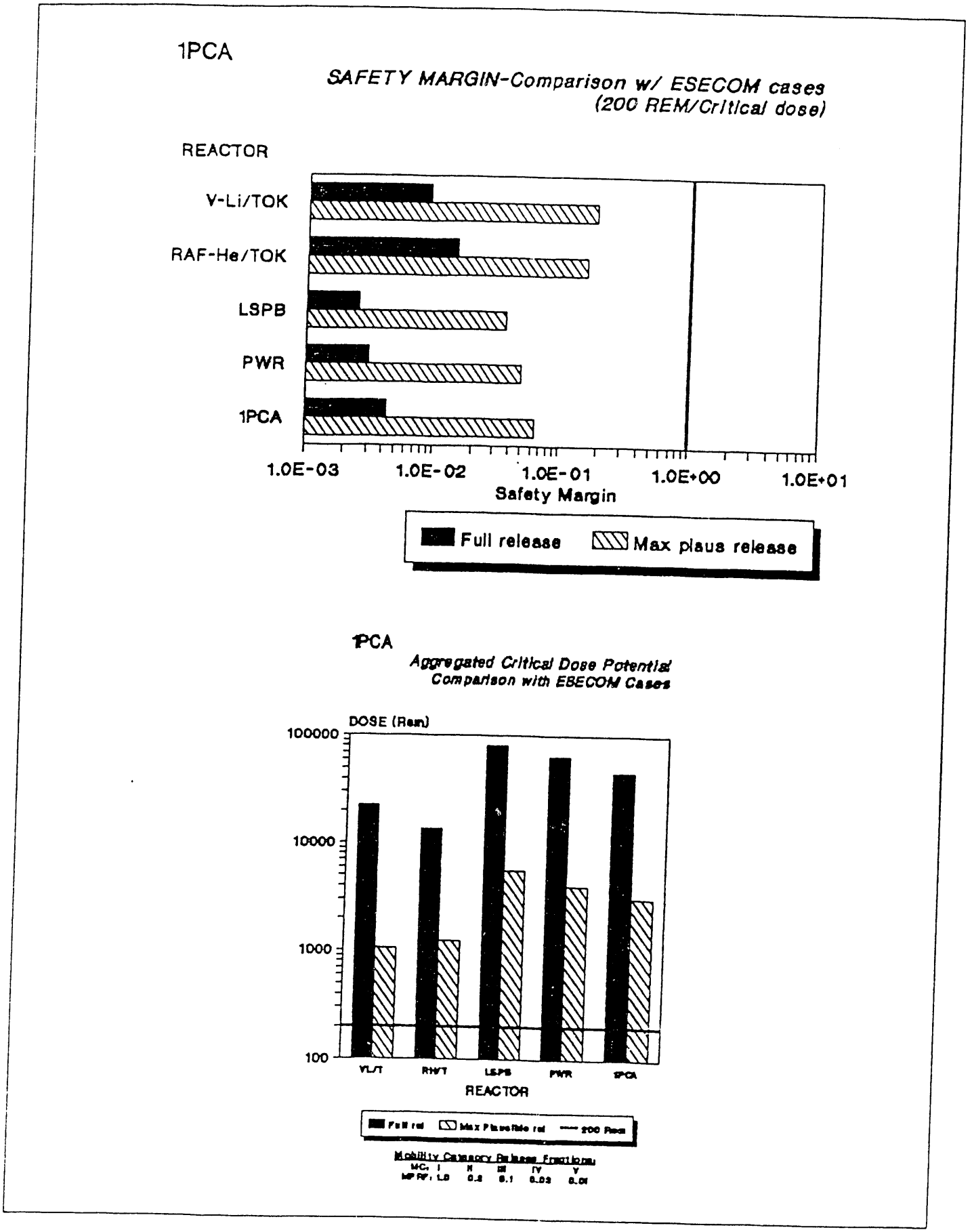

Figure 7.4. Comparison of critical-dose safety margin and aggregated critical dose for stainless-steel variant of ESECOM Case 1 (PCA1) with ESECOM fusion Cases 1 and 2 and two fission cases.

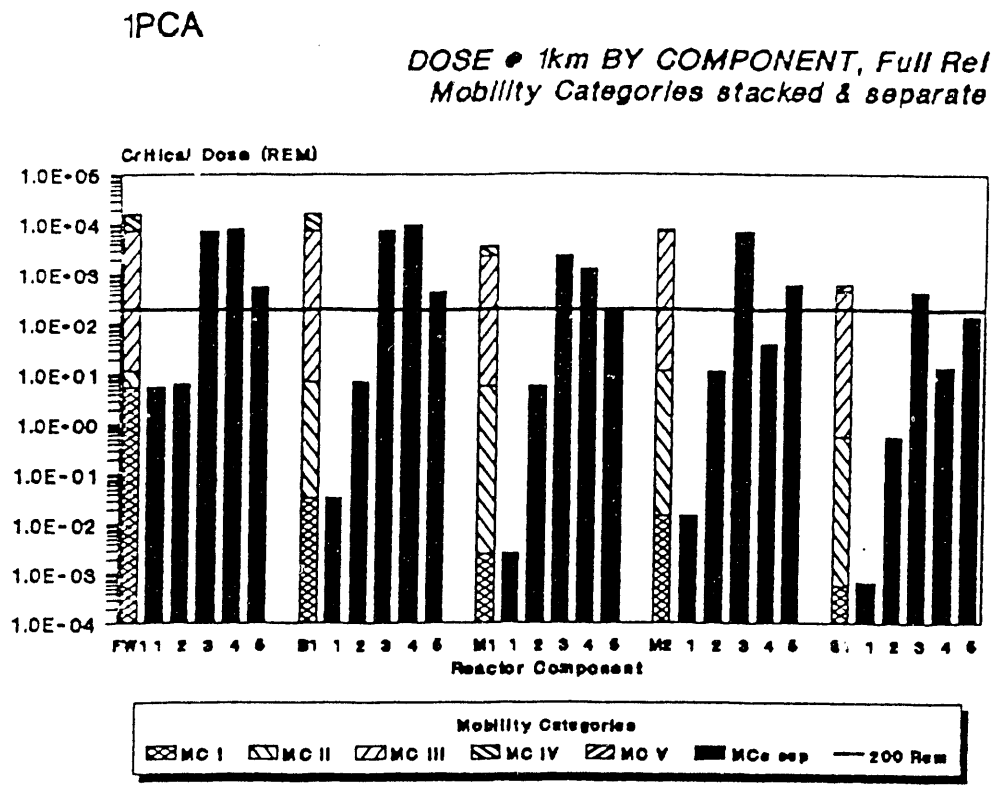

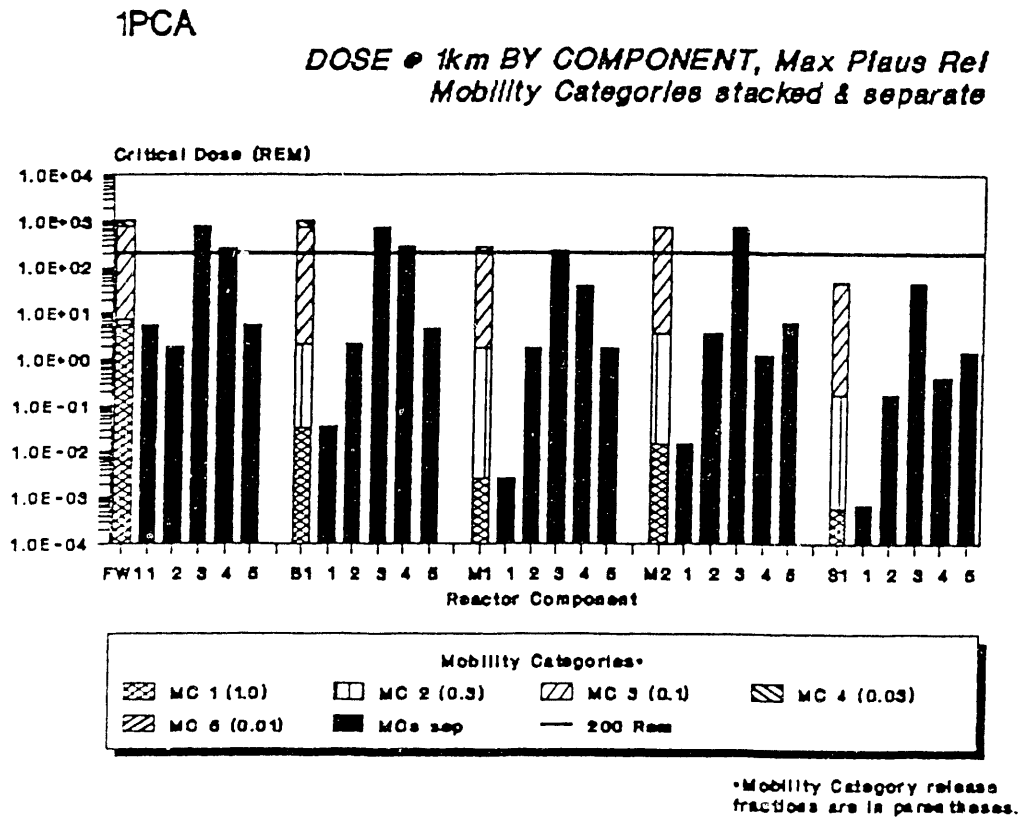

Figure 7.5. Complete release and maximum plausible release critical-dose for stainless-steel variant of ESECOM Case 1, by component and mobility category. FW1 = first wall, B1 = inner blanket, M1 = inner manifold, M2 = outer manifold, S1 = shield.

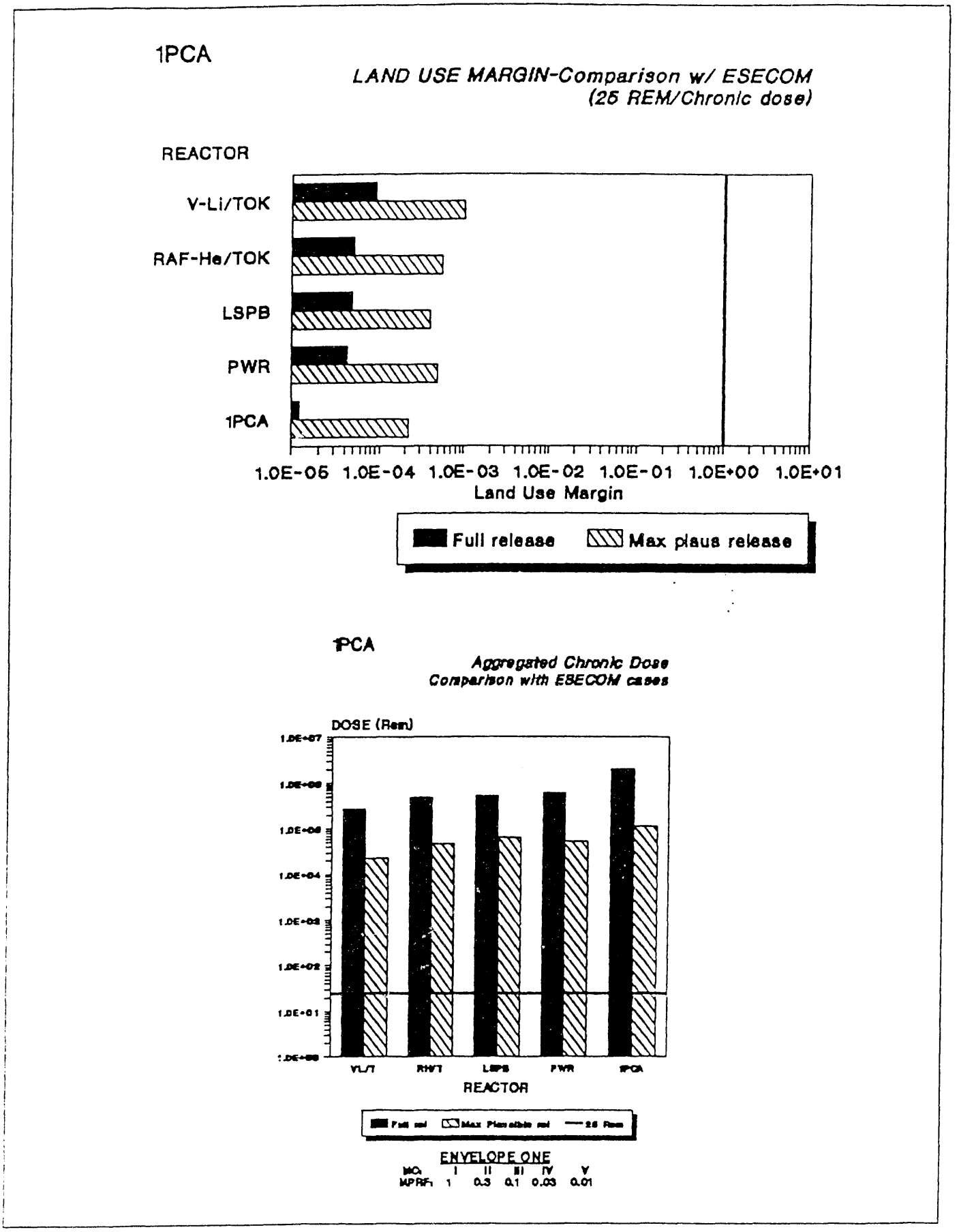

Figure 7.6. Comparison of chronic-dose safety margin and aggregated chronic dose for stainless-steel variant of ESECOM Case 1 (PCA1) with ESECOM fusion Cases 1 and 2 and two fission cases.

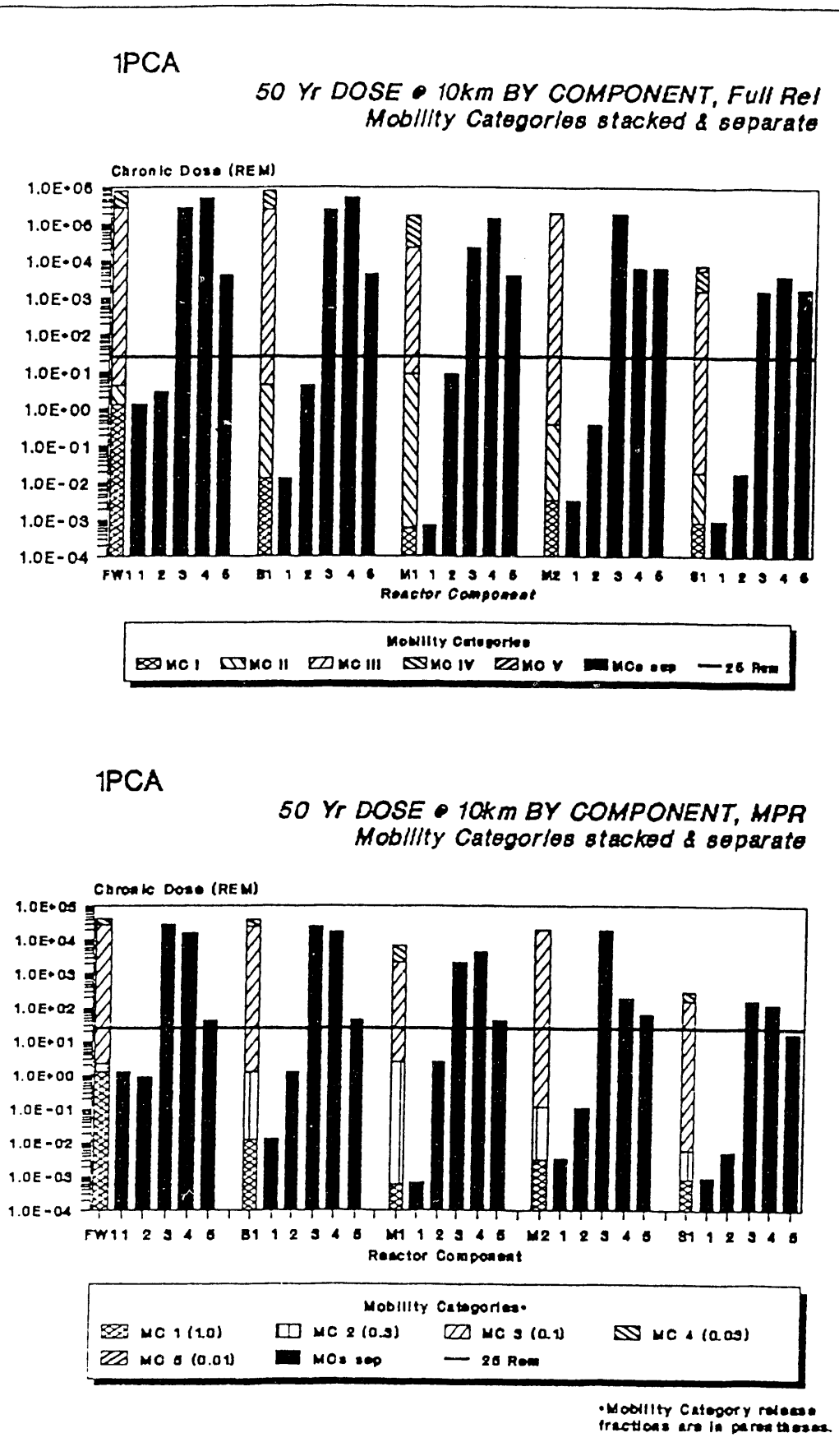

Figure 7.7. Complete release and maximum plausible release chronic-dose for stainless-steel variant of ESECOM Case 1, by component and mobility category. FW1 = first wall, B1 = inner blanket, M1 = inner manifold, M2 = outer manifold, S1 = shield.

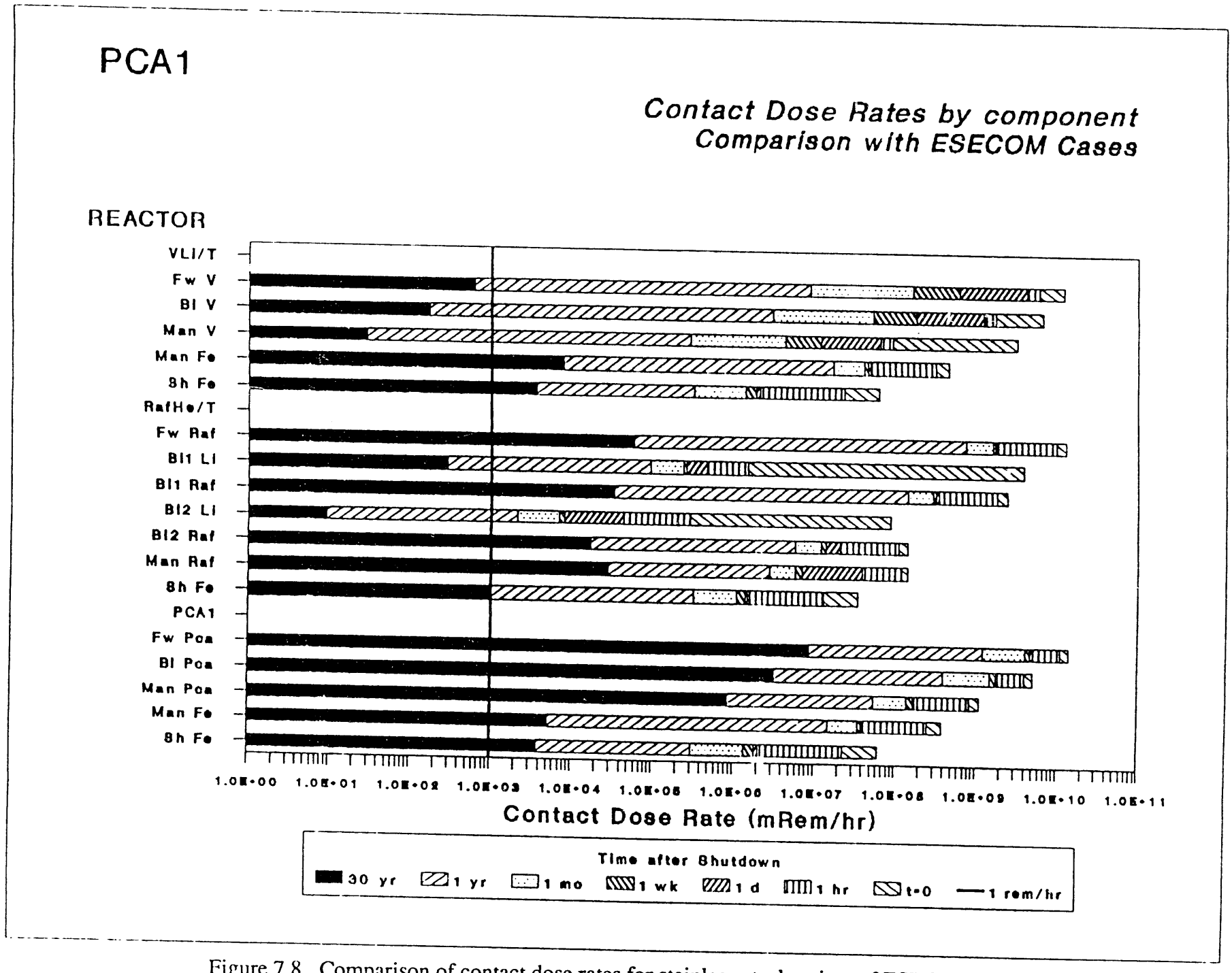

Figure 7.8. Comparison of contact dose rates for stainless-steel variant of ESECOM Case 1 and ESECOM Cases 1 and 2.

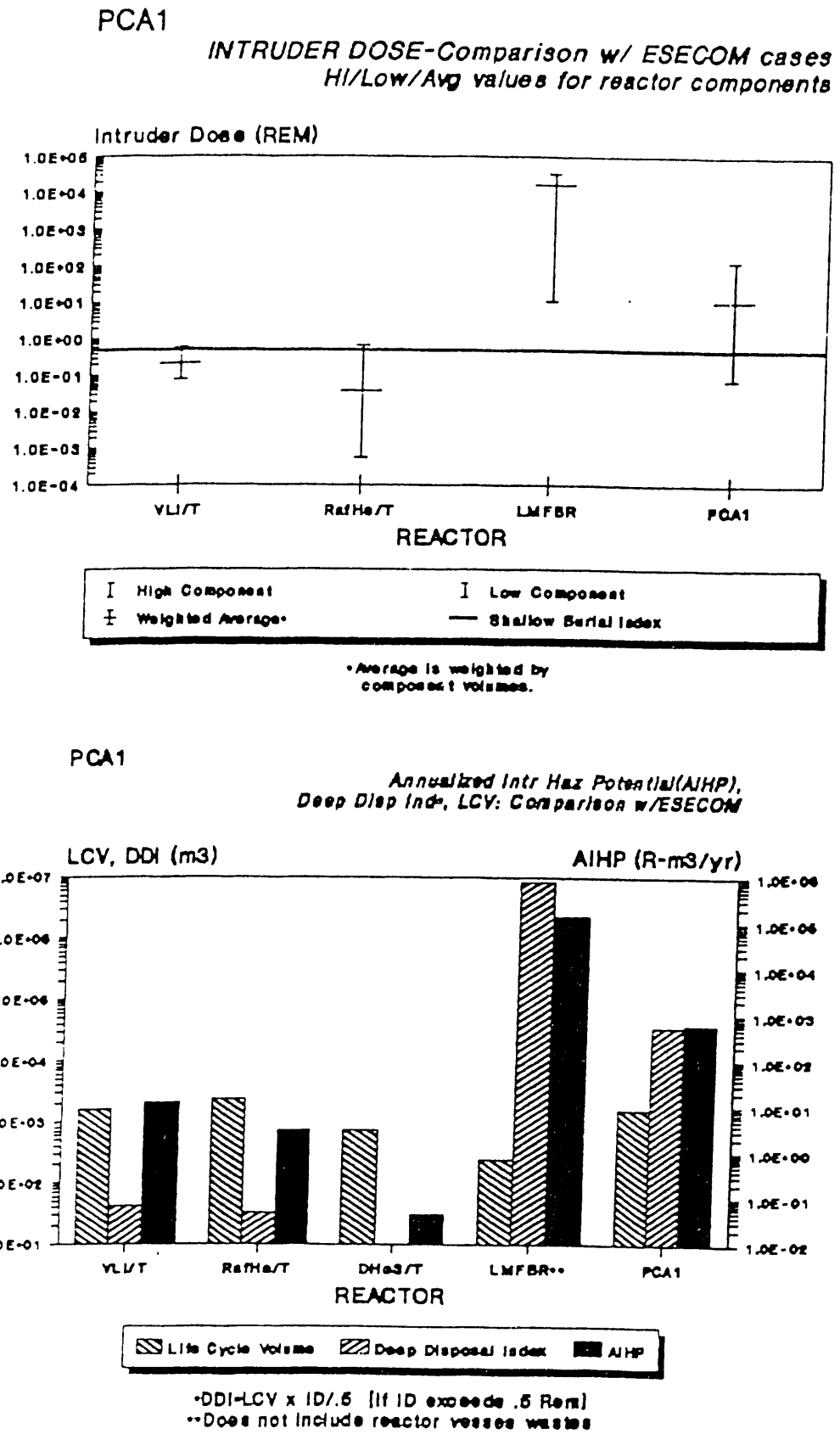

Figure 7.9. Comparison of radioactive waste indices for stainless-steel variant of ESECOM Case 1, three ESECOM fusion cases, and LMFBR.

and 200 times bigger than for reduced-activation ferritic steel, albeit still 150 times smaller than for LMFBR wastes.

The numerical comparisons for the PCA2 case were quite similar to those just described for PCA1. The bottom line is that use of stainless-steel structural materials surrenders much of the potential advantage of DT fusion over fission with respect to dose potential from severe reactor accidents, unless it can be shown either that the probability of such accidents is substantially lower in the fusion case than for fission or that the maximum plausible release fractions are substantially lower in the fusion case than for fission. With respect to the magnitude of radioactive-waste burdens, use of stainless steel makes it impossible for fusion wastes to qualify for shallow burial under current US regulations (whereas wastes from fusion reactors based on reduced-activation ferritic steel or vanadium/titanium alloy can qualify), but stainless-steel-based fusion still retains a substantial numerical advantage in waste-hazard potential compared to fission.

7.3 UPDATE OF ESECOM COMPARISON OF FUSION AND FISSION: SOME PRELIMINARY CONSIDERATIONS

The core of the findings of the ESECOM study[7.3] consisted of numerical indices intended to illuminate some of the key environmental, safety, and economic characteristics of a range of fusion-reactor designs. The indices for the fusion designs were presented side by side with analogously calculated indices for a set of four fission-reactor types -- one representative of currently operating reactors and three others representative of more advanced fission-reactor types still on the drawing boards. The purpose of including comparisons with an existing fission reactor type was to provide a familiar reference point -- that is, to help readers interpret in the context of a known technology what the values of the indices mean. The purpose of including comparisons with more advanced fission-reactor types was to provide a fairer basis for judgment about the relative advantages and disadvantages of fusion compared to fission reactors more closely resembling those with which future fusion reactors will be competing for a share of the central-station electricity generation role.

The four fission designs used for these comparisons in the ESECOM study were: (1) a "best present experience" Westinghouse pressurized water reactor (PWR), where best present experience refers to a reactor for which construction was completed in 6 years and which operates over its lifetime at an average capacity factor of 75 percent; (2) a loop-type, sodium-cooled breeder reactor design under development by the Department of Energy and Electric Power Research Institute (known as the Large-Scale Prototype Breeder or LSPB); (3) the General Electric modular sodium-cooled breeder design known as PRISM (initially standing for Power Reactor Inherently Safe Module, renamed as the Power Reactor Innovative Small Module following some controversy over whether the label "inherently safe" ought to be applied to any fission reactor); and (4) a modular, high-temperature gas reactor (MHTGR) by General Electric.

The fusion and fission reactor designs studied by ESECOM were "frozen" for the purposes of the study in 1986. In the current project we have been applying ESECOM-type assessment techniques and indices -- and extensions of them -- to newer fusion-reactor designs than those studied in ESECOM, some more advanced (such as ARIES) and others closer to attainment (such as ITER). The question naturally arises whether, in light of ongoing work on advanced fission reactors, the fission side of fusion-fission comparisons of the sort presented by ESECOM might also need to be updated. To what extent, in other

words, do prospective improvements in the environmental, safety, and economic characteristics of fission represent, for fusion-reactor designers, a "moving target"?

In the work reported here we have made only a modest beginning toward answering that question. We have confined ourselves, so far, to the reactor-safety side of this issue, having looked neither at routine emissions and exposures, nor at radioactive-waste characteristics, nor at the economics of evolving fission-reactor designs. Neither have we yet studied the two particular kinds of fission-reactor innovations -- on-line reprocessing and enhanced in-reactor actinide burnup -- that could really substantially influence the reactor-building radioactivity inventories on which nearly all of the ESECOM-type indices are based.

It is helpful to recall here that the indices of accident hazard employed in the ESECOM study -- and up until now in the current work -- depend, first, on the dose potentials represented by the total radioactivity inventory in the reactor and, second, on the fractions of these dose potentials that could be realized in physically plausible accidents, based on the fractions of the inventories of different classes of elements that could be volatilized at the temperatures such accidents could generate. No credit is taken in the ESECOM approach for the possible effectiveness of containment buildings (which means that the ESECOM-type safety indices cannot be affected by changes in containment-building design or other active release-suppression mechanisms); and no consideration is given to the probabilities of initiating events (except insofar as judgment is applied to the question of whether events capable of producing particular temperatures are possible at all, given the materials and stored energies present and the pathways available for transforming those energies into elevated temperatures).

The part of the ESECOM-type safety analysis that has so far been modularized and automated, moreover, omits even the sorts of judgments just mentioned. One calculates "maximum plausible dose potentials" by applying a pre-selected envelope of worst-case release fractions (e.g., 1.0, 0.3, 1.0, 0.03, and 0.01 for the five "mobility categories" into which all the elements present are divided). Automating a process for determining how this release envelope should vary -- depending on details of materials choices, stored energies, and configurations -- remains a major challenge for the next phase of the work. In the meantime, the automatically calculated accident-hazard indices will vary only with those aspects of reactor design that alter the inventories of the main dose-producing isotopes in each mobility category. And changes in fission-reactor design, except those that involve on-line reprocessing or enhanced actinide burnup, cannot change these inventories very much (per unit of thermal power) because they are dominated by fission products whose production rates depend only very weakly on design (through the influence of design on neutron spectrum).

Thus the influence of changing fission-reactor designs on fusion-fission reactor-safety comparisons based on the automatically computed ESECOM-type hazard indices will be small except in those cases where a major modification to the fission fuel cycle substantially alters the radioactivity inventory in the fission plant. (For the same reason, the effect of fission-reactor design changes on numerical indices of radioactive-waste hazard also will be small unless the design change includes a major change in the fuel cycle.) On the the other hand, to the extent that reactor-safety comparisons also include -- as they should -- such influences on accident hazard as the effects of reactor design on the maximum plausible release fractions and, eventually, effects on the probabilities of initiating events (factors not yet automated in our code-development work and, in the second instance, still far from even the possibility of automation), the evolution of fission-reactor designs toward greater safety can of course be important for the outcome.

In the remainder of this section, therefore, we survey the trends in fission-reactor design that may bear on these latter (non-automated) dimensions of reactor safety, and we give some preliminary consideration to the implications of these dimensions for the fusion-fission comparison.

7.3.1 Trends in Fission-Reactor Design

The main directions in fission-reactor design that are sufficiently well developed to warrant attention here are advanced light-water reactors (ALWR), advanced liquid-metal-cooled reactors (ALMR), and the modular high-temperature gas reactor (MHTGR). In what follows, these are treated in turn.

7.3.1.1 The Advanced Light-Water Reactor Program

The ALWR program has two main branches of development: (1) evolutionary plant designs of gigawatt electric power for both PWR and BWR, and (2) "small" (600 MWe) simplified PWR and BWR plants incorporating passive safety systems.

Typical utility sponsor requirements for the general ALWR programs are:

(1) core damage frequency < 10^{-5} events/reactor year,
(2) severe accident events (probability > 10^{-6}/reactor year) not to cause doses > 25 rems within half a mile,
(3) occupational exposure < 100 man rem/reactor-year averaged over plant lifetime,
(4) construction schedule < 54 months,
(5) availability 87% averaged over plant lifetime, with less than one inadvertent trip per year,
(6) solid radioactive waste volume < 2500 ft^3/year in shippable form,
(7) design life of 60 years without outage,
(8) economically competitive with coal.

Evolutionary ALWRs

These are direct descendants of existing light-water designs in the 900-1300 MWe size with improvements in the areas of simplicity in design and operation, economics, and safety, intended to meet the ALWR utility requirements above. They may satisfy the new NRC regulatory approach to standard plant licensing.

Three U.S. reactor vendors are developing evolutionary ALWRs for sale to, and in collaboration with, Asian countries:

(1) General Electric is working jointly with Hitachi, Toshiba, and Tokyo Electric Power Co. (TEPCO) in the design of the 1350-MWe Advanced Boiling Reactor (ABWR).[7.8] Two such units have been ordered by TEPCO for commercial operation in 1996 and 1997. In the U.S., the ABWR design effort is coordinated with the EPRI/ALWR program, and is being reviewed by the NRC for possible certification as a pre-approved US standard BWR.

(2) Combustion Engineering is developing its "System 80+" (1300 MWe) for sale to South Korea and designing a simpler version with lower core power density and larger safety margins for the EPRI/ALWR program for certification by DOE.

(3) Westinghouse is working with the Japanese companies Mitsubishi and Kansai Electric Power in the design of a 1350-MWe Advanced Pressurized Water Reactor (APWR), the "Standard Plant - 90" (SP/90), with an advanced fuel cycle, improved control and wider safety margins.

These evolutionary designs are intended to have improved capacity factors, reduced costs, improved operability, and some passive safety features for severe accident mitigation. They reflect extensive international experience in LWR technology. On paper, they meet the utility requirements document, and they are probably close to licensing in the decade of the 1990s. On the other hand, they offer no dramatically different environmental and safety features and are not likely to affect public perceptions of fission nuclear power. In one respect -- that of economics -- these reactors are, however, quite relevant to comparisons with fusion reactors. Reflecting design improvements over many years of LWR technology and advantages in fuel cycle, availability, operability, reduced construction time, and the prospect of generic licensing, these reactors may (at last) reflect "economies of scale" and become truly competitive in cost with coal-based electricity generation in the U.S.

The ABWR is typical of the ALWR category. It has been selected as the next generation BWR in Japan, and it is the lead plant under review by the NRC under its new standard licensing approach. The reactor description and characteristics are as follows. The 3926-MWt, 1356-MWe reactor has a core of 872 fuel bundles operating at a power density of 50 kW/liter with inlet/outlet temperatures 216/290°C and a pressure of 7.3 MPa (1060 psi). The reactor pressure vessel (Fig. 7.10), 7 m in diameter and 21 m tall, has 10 internal recirculation pumps of the wet-motor glandless type and electric-hydraulic control rod drives for fine motion rod control. The RPV is of standard GE design except that the annular space between the shroud and wall is larger, and the support skirt is conical, to accommodate the internal pumps. This reactor design eliminates external recirculation piping and large nozzles on the reactor vessel below the core. The latter feature permits the design of an ECCS system with no core uncovery during a loss-of-coolant-accident (LOCA) and a 50% reduction in total ECCS pump capacity. The control and instrumentation system features digital/solid state equipment and a multiplexing system for signal transmission. The containment design (Fig. 7.11) is of the pressure suppression type with a covered suppression pool

Small Passively Safe Light Water Reactors—Passive ALWRs

A second path being pursued in parallel in the ALWR development program is that of smaller reactors containing less radioactivity that are easier to build and easier to cool in case of malfunction. These reactors employ principally passive means (gravity, natural convection, stored energy, etc.) to provide emergency cooling, remove decay heat, and contain fission product activity in potential accident situations, and to provide core protection without operator action for about three days. In principle, the issues of passive means for accident prevention and mitigation and plant size are separate, and one can imagine some passive features in a gigawatt-scale reactor. In practical terms, however, the smaller simplified designs are more readily adapted to passive safety design, largely because core power densities are low compared to heat removal capability. The smaller passive reactors have the following attractive features.

(1) By reducing reliance on active engineered safeguards and on human intervention, these designs offer greater safety over a wide range of upset conditions.

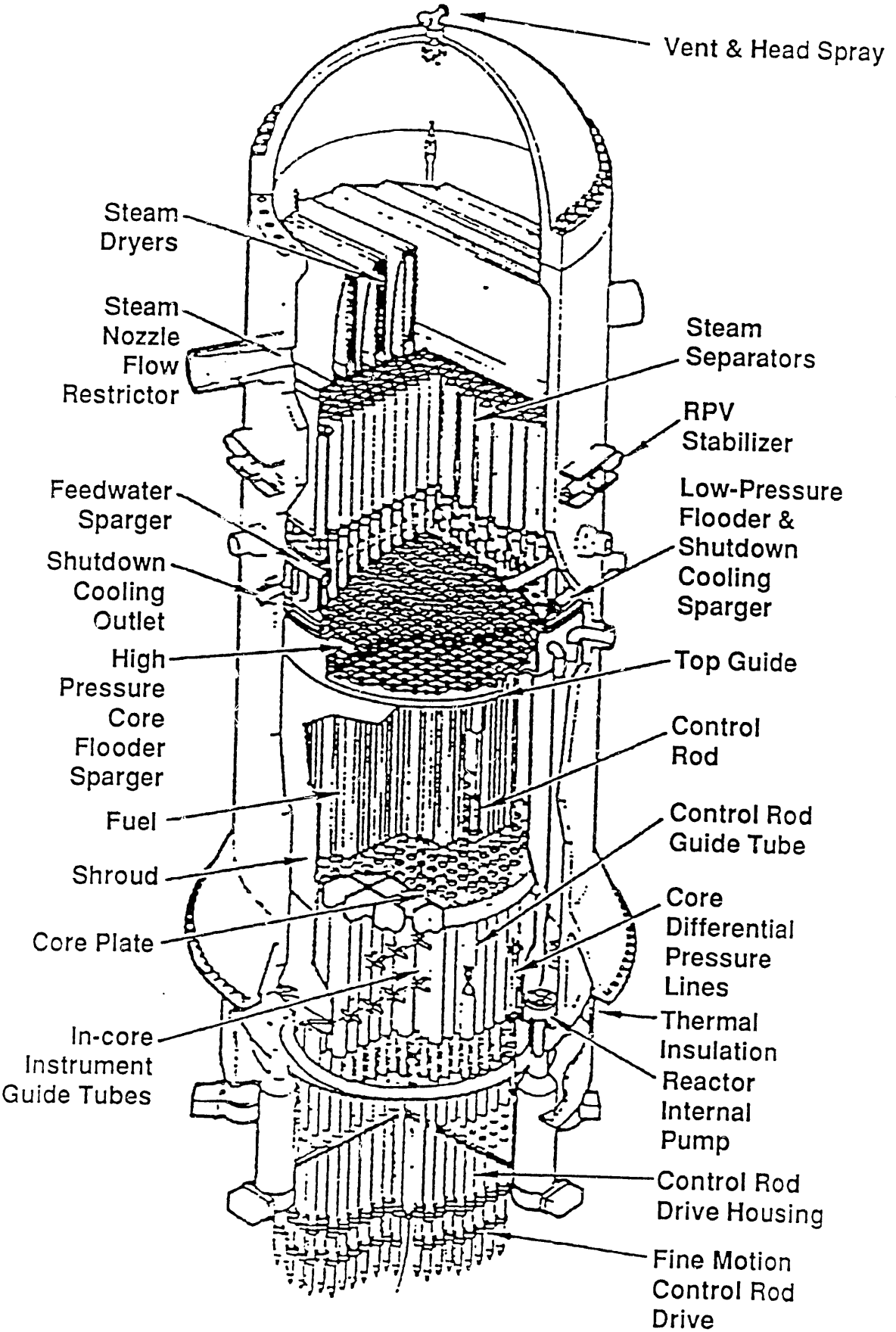

Figure 7.10. ABWR pressure vessel and core.

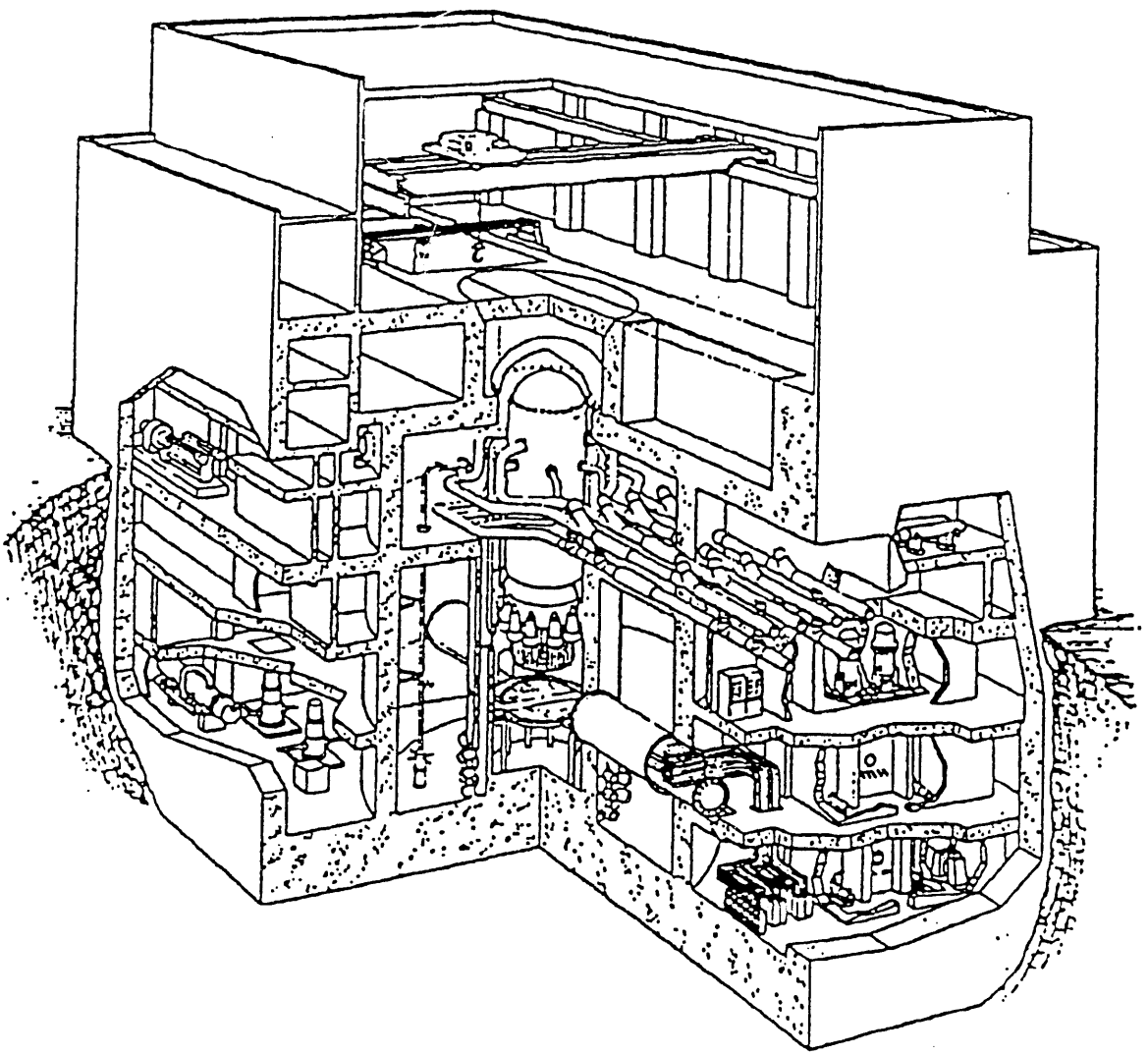

Figure 7.11. ABWR containment.

(2) Simplification over conventional plants means that they are easier to construct, operate, and maintain. Reduction in complexity of plant is itself a safety feature.

(3) Although their economics is uncertain, they may be competitive with larger units which enjoy economy of scale because they are a better match to utility needs in a period of uncertain demand growth, and because the cost advantages associated with simplicity are substantial.

(4) The "walk-away" safety of some passive designs, if demonstrated, could renew public confidence in nuclear power. A reactor which requires no core-protective actions by operators for a three-day period following a loss of coolant or other disturbance would represent a dramatic improvement in safety in light of the influence of incorrect operator actions in the history of reactor accidents.

There are two small (600 MWe) passive LWRs in the ALWR program. One is a PWR plant called AP-600, developed by Westinghouse and Burns & Roe. The other is a BWR called SBWR (Simplified-Boiling Water Reactor), being developed by General Electric and Bechtel. The basic reactor, coolant systems, and passive safety features of these reactors are described below.

The Advanced Westinghouse 600-MWe Passive PWR (AP-600)[7.9] has a low power density (14 kW/liter) core of 145 assemblies (17x17 type) with an active fuel length of 12 feet (Fig. 7.12). The fuel cycle is designed for 18 months with a three-region core to improve plant availability, and the stainless steel and water radial reflector improves neutron economy and thus reduces neutron enrichment and fuel cycle cost.

The reactor coolant system uses hermetically-sealed canned motor pumps. The two-loop steam generators are attached directly to the pumps, eliminating the need for separate supports and greatly improving access to the steam generators and pumps for inspection and maintenance. The instrumentation and control equipment is microprocessor-based, with advanced ergonomic features to decrease the probability of operator error and expert systems for helping operators in normal and emergency situations. The passive safety features of the AP-600 are as follows.

(1) A passive residual heat removal heat exchanger (PRHR HX) to remove core decay heat if the normal or startup feed-water systems are not available, located above the RCS loop piping forming a closed natural circulation loop within the containment and in the refuelling water storage tank which acts as a heat sink.

(2) Two core makeup tanks (CMT's) filled with borated water using only gravity feed and located above the RCS, to provide passive reactor-coolant makeup for small leaks.

(3) Two accumulators in addition to the CMT's, to provide safety injection for larger leakage rates including LOCA's up to the guillotine break of a main loop pipe; one CMT and one accumulator utilize a common injection line to the reactor vessel downcomer.

(4) An in-containment refuelling water storage tank as an additional longer-term source of water.

(5) A passive containment accumulator type spray system to reduce the concentration of iodine and cesium which consists of two tanks containing borated water and tanks

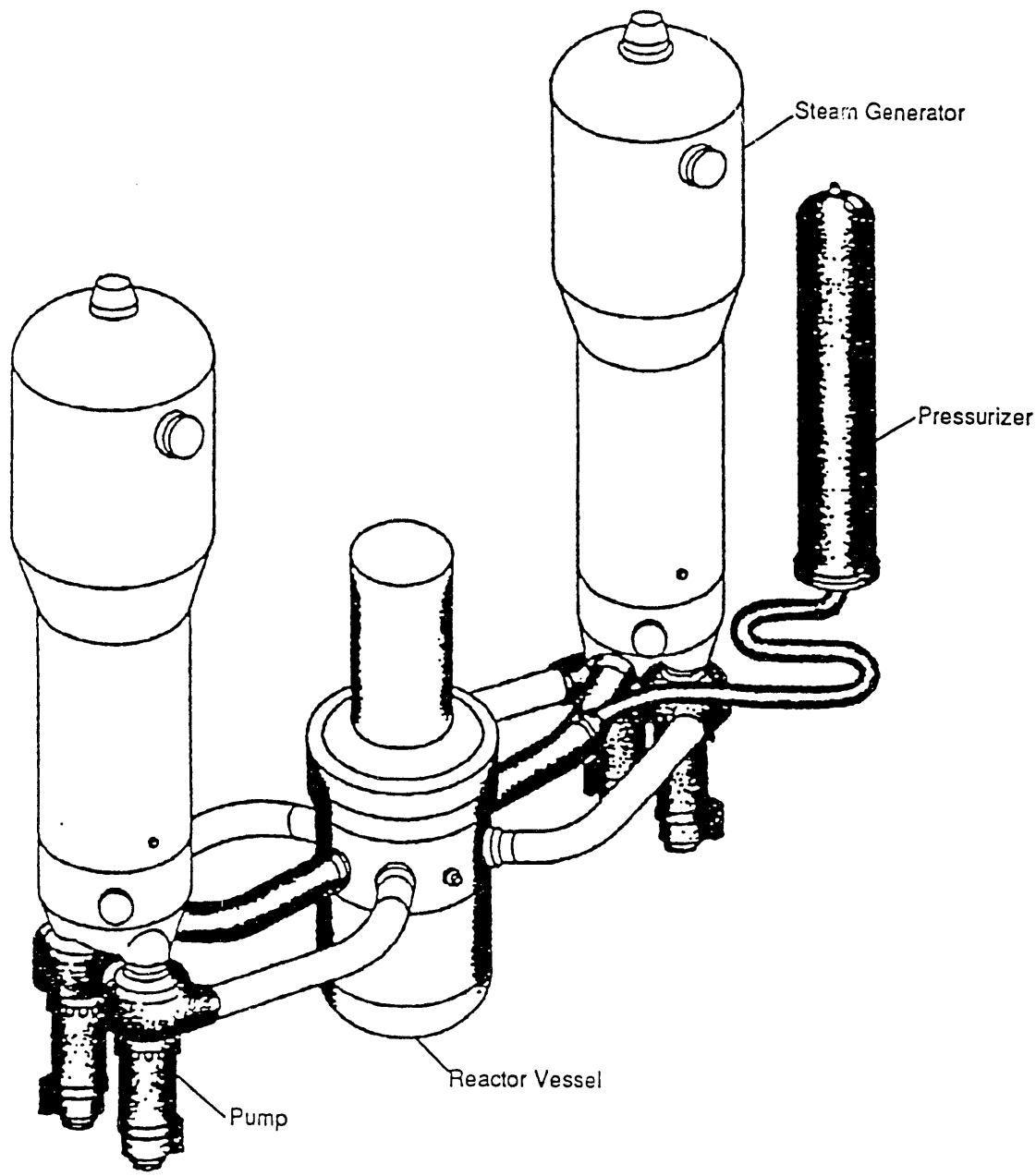

Figure 7.12. AP600 NSSS configuration.

containing compressed nitrogen all located outside the containment. The passive spray system is turned on by a high activity signal, and it can supply an 1100 gpm spray for at least thirty minutes.

(6) A passive containment cooling system (PCCS) using the natural circulation of air between the reactor containment structure and the surrounding shield building (Fig. 7.13) to provide a heat sink to the environment, preventing the containment from exceeding its design pressure in the case of accident.

The passive safety features allow a significant reduction in pumps and valves and a side benefit of reduced occupational exposure in service tests, inspection, and maintenance. Accident analyses on the AP-600 with canned coolant pump, passive safety injection systems, and passive containment cooling systems show that the core damage frequency is a factor of 10 lower than the best current US PWRs (10^{-5}/yr vs. 10^{-4}/yr) while estimated containment failure has been shown to be 100 times less likely (10^{-7}/yr vs. 10^{-5}/yr). The lower power density core and plant simplifications in coolant system and containment improve capital costs, public safety, and plant availability and reduce occupational exposure over standard gigawatt-scale PWR's.

Since the early 1980s, General Electric has been developing a smaller (600 MWe), simpler boiling water reactor known as the Small Passive Boiling Water Reactor (SBWR).[7.8, 7.10] The relation of this so-called SBWR to other BWR designs is illustrated in Fig. 7.14.

The basic features of the SBWR are as follows (Fig. 7.15 and 7.16):

(1) A low power density (42 kW/liter) core using natural circulation for coolant flow through the core. The elimination of recirculation loops, pumps and controls simplifies the design while the low power density provides lower fuel costs and increased thermal margin for transients.

(2) A gravity-driven cooling system from water in an elevated suppression pool for emergency core cooling without pumps and diesels, which assures full core coverage for all design-basis events.

(3) An isolation condenser located in the elevated suppression pool, which isolates the RV from the turbine condenser -- thus controlling reactor pressure automatically without the need to remove fluid from the pressure vessel by safety relief valves.

(4) A passive containment cooling system, using natural convection, in which heat is rejected to the isolation condenser pool (elevated suppression pool) whose wall is cooled by natural circulation water flow. This provides a three-day passive cooling for the containment (without venting) which can be extended by operator-initiated water make-up.

(5) A high pressure coolant injection system which uses reactor steam to pump water into the RV from the condensate or fuel pool and which starts automatically on a low water level signal.

The SBWR conceptual design was completed in the 1985-89 period, and testing of components (e.g., depressurization valve and steam injector) is now underway. In 1989 the SBWR was selected by EPRI and DOE for a design development and certification program to be carried out by a U.S., Italian, Dutch, and Japanese international team.

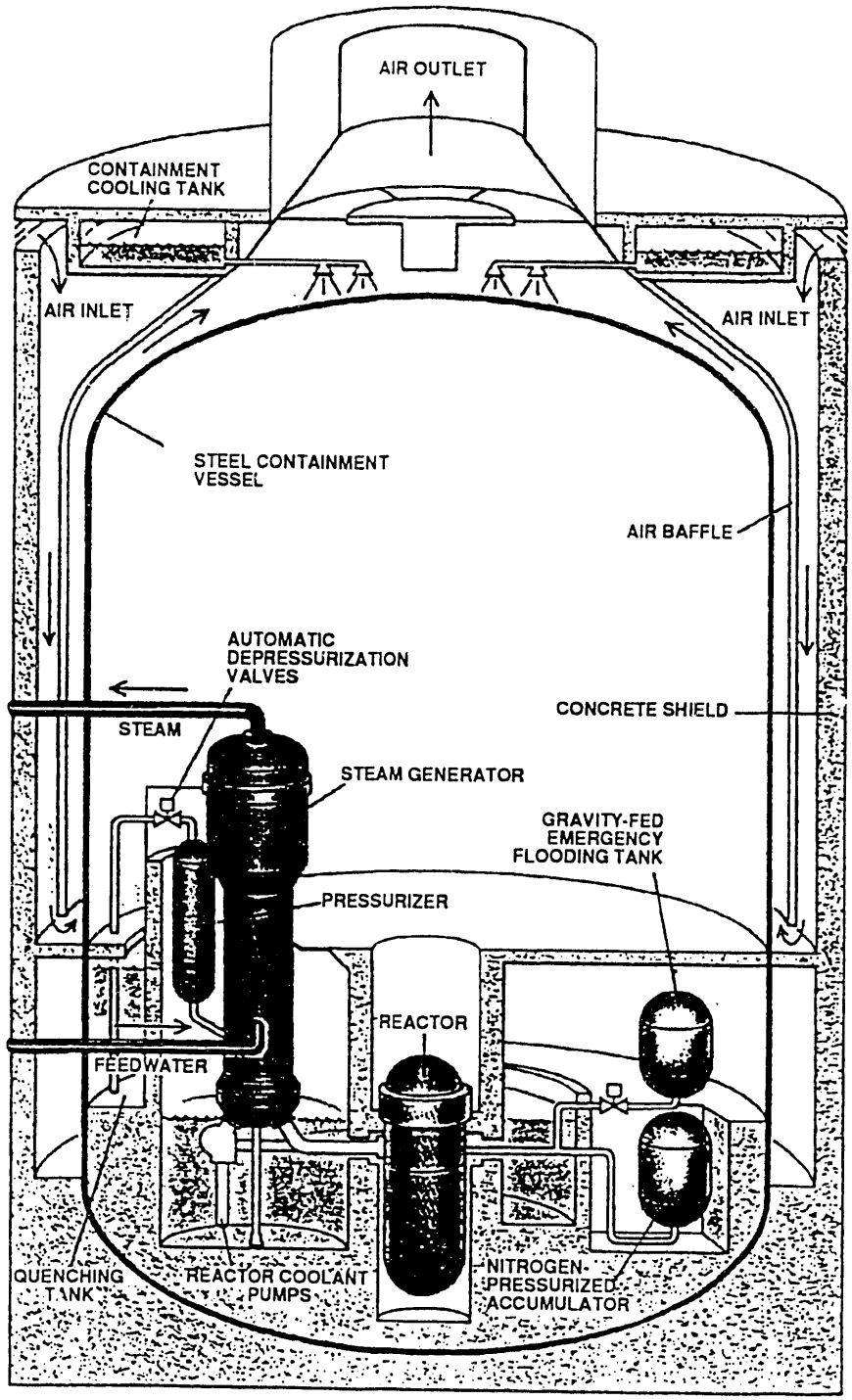

Figure 7.13. AP600 containment.

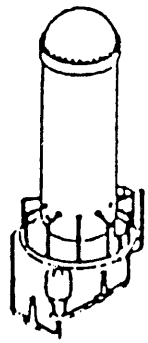

CURRENT BWR

- 900-1200 MWe
- External Forced Circulation
- Many Plants Operating Worldwide
- Nonstandard
  - utility requirements
  - architect-engineers
  - regulatory backfits

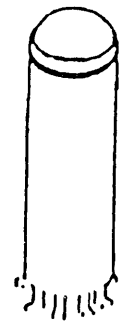

ADVANCED BWR (ABWR)

- 900-1300 MWe
- Internal Forced Circulation
- World-class Design bu International Team
  - Best Proven Features
- Development Complete
- Lead Project Underway
  - Tokyo Electric Power Co.
  - GE NSSS, Turbine
- Next-generation Standard BWR in Japan
- US Certification Underway
  - first US standard plant
  - DOE/EPRI/GE cooperation
  - demonstrate standard plant licensing process
  - complete 1991

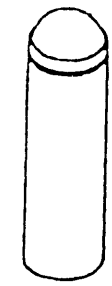

SIMPLIFIED BWR (SBWR)

- 600-900 MWe
- Natural Circulation
- Focus on Simplification and Passive Safety
- Builds on ABWR
- Development Underway
  - DOE/EPRI/GE/international cooperation
  - new features tested
- Certification by 1994?

Figure 7.14. Relation of SBWR to other BWRs.

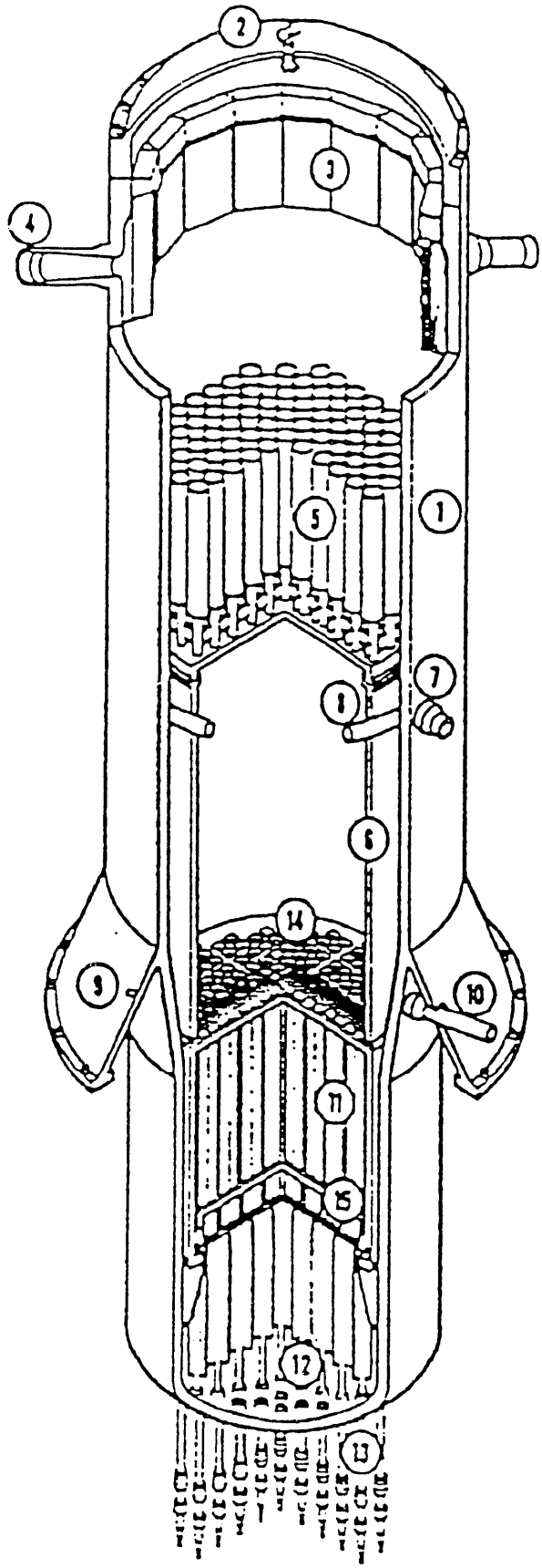

Simplified
Boiling Water
Reactor Assembly

1 Reactor Pressure Vessel
2 RPV Top Head
3 Steam Dryer Assembly
4 Main Steam Line Nozzle
5 Steam Separators
6 Chimney
7 Feedwater Inlet Nozzle
8 Feedwater Sparger
9 RPV Support Skirt
10 Gravity-driven Cooling System Inlet Nozzle
11 Fuel Assemblies
12 Control Rod Guide Tubes
13 Fine-Motion Control Rod Drives
14 Core Top Guide Plate
15 Core Plate

Figure 7.15. SBWR core features.

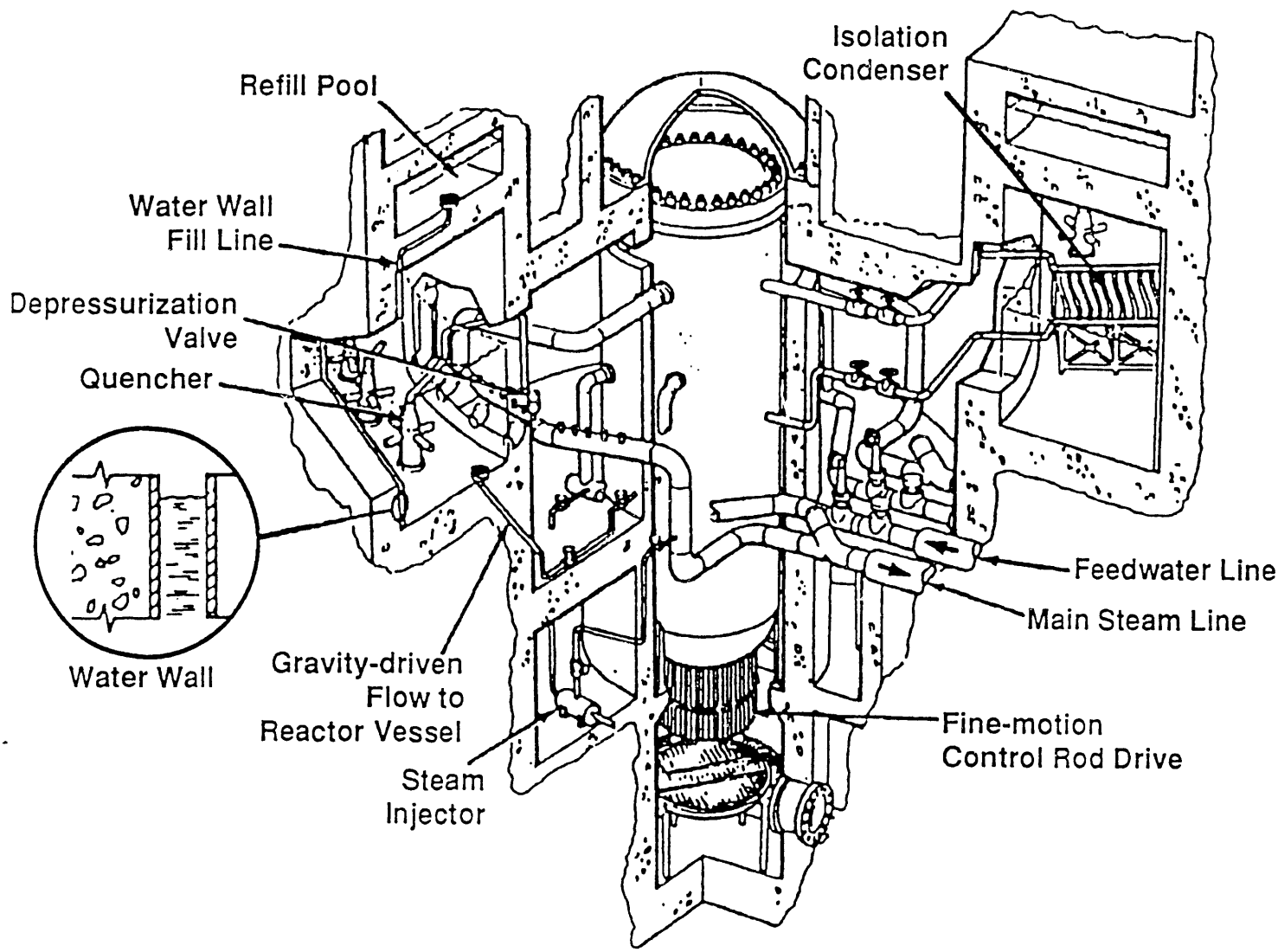

Figure 7.16. SBWR safety features.

7.3.1.2 The Advanced Liquid-Metal-Cooled Reactor Program -- PRISM

The U.S. program for the development of an ALMR is being carried out by an industrial team led by General Electric, with the collaboration of national laboratories (ANL, INEL, ORNL) and EPRI. The reactor is based on the Power Reactor Innovative Small Module (PRISM) design originated by General Electric, with a fuel cycle based on the integral metal fuel concept under development by ANL in its EBR-II program. The basic elements of the design comprise:

(1) liquid sodium cooling at atmospheric pressure with margin to boiling > 400K,
(2) metallic fuel with high breeding potential and large negative reactivity feedback,
(3) modular pool-type reactors with factory fabrication,
(4) integral fuel cycle based on pyrometallurgical processing,
(5) seismic isolation of reactor module.

The objectives of the program are to produce a standard commercial ALMR with NRC certification around the year 2000, demonstrating passively safe shutdown under loss of cooling and even for scram failure, breeding, a secure fuel cycle, and the possibility of actinide recycle.

A brief plant description of PRISM follows; more detailed descriptions can be found in Refs. 7.11 and 7.12.

The PRISM design uses a low pressure pool-type LMR system with standardized reactor modules fabricated in a factory and shipped by rail or barge to the site. The projected plant utilizes nine such reactor modules arranged in three identical 465-MWe power blocks, for an overall plant net electrical rating of 1395 MWe. Each of the three reactor modules has its own steam generator, heated by secondary sodium from an intermediate heat exchanger (IHX). The three steam generators supply 616 MPa saturated steam to a single 465-MWe turbine associated with a power block (Fig. 7.17).

The reactor module is about 6 m in diameter and about 18 m high. The reactor module, the two IHXs, and the four EM pumps are located below grade in the reactor silo (Fig. 7.18). There is a 12.7 cm gap between the reactor vessel and the containment vessel, filled with argon gas, so that sodium would be retained in the containment in the case of a sodium leak.

The reference fuel for PRISM is a metallic U-Pu-Zr alloy of the type under development by ANL in its IFR program. A heterogeneous arrangement of blankets and fuel is used, with six control rod locations. MOX (mixed oxide UO_2/PuO_2) fuel is being retained as an option. Reactivity is controlled by a system of six control rods, but inherent negative reactivity feedbacks can reduce power to near decay-heat levels for anticipated transients without scram. The most important of these feedbacks are the thermal expansion of the core and a small Doppler feedback. PRISM has a positive sodium density/void feedback coefficient, and concern over this issue was expressed in the course of initial safety evaluations by NRC and ACRS.

Normal decay heat removal from a shut-down reactor is accomplished by turbine bypass of steam from the steam generator to the condenser. Two passive backup heat removal systems are: (1) natural air circulation in a shroud around the steam generator, or (2) a reactor vessel auxiliary cooling system (RVACS) consisting of atmospheric air always in natural circulation around the containment vessel in the underground silo. The RVACS

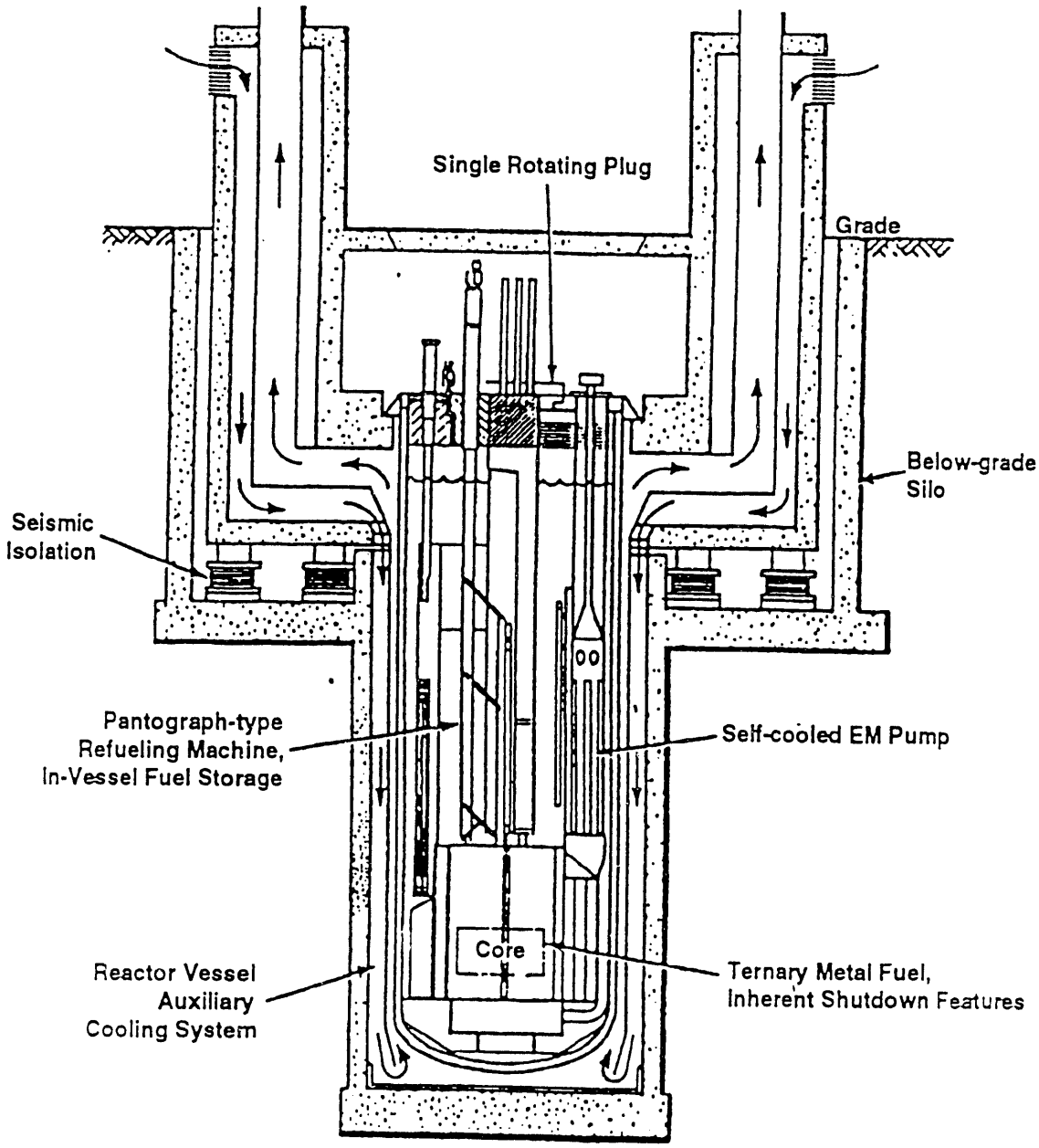

Figure 7.17. PRISM reactor-overall view.

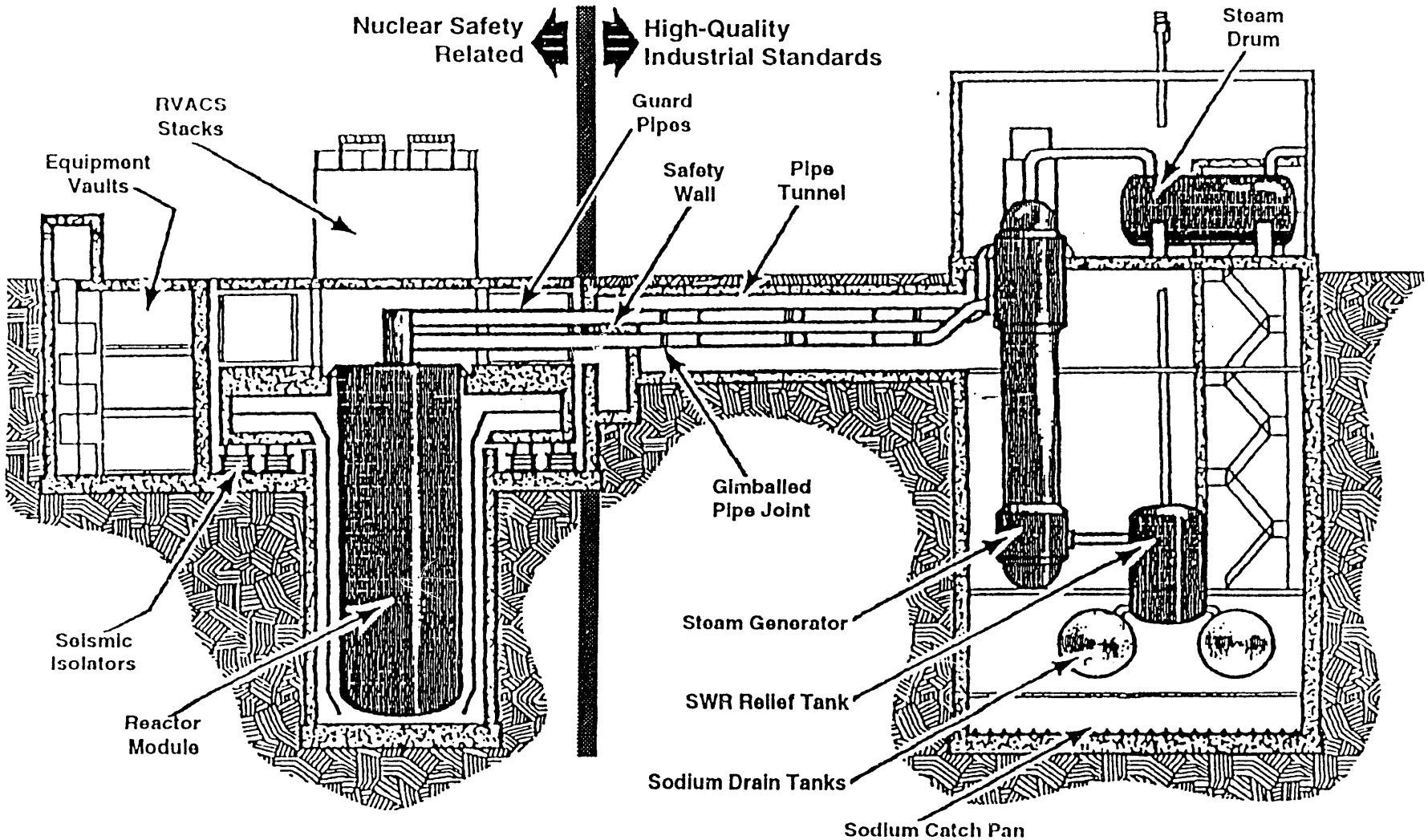

Figure 7.18. PRISM Reactor-Below Grade.

performance increases as temperature rises because of radiant heat transfer and free convection. The primary closure consists of the reactor vessel head closure and the IHXs. The containment (more correctly designated a confinement) is a second leaktight pressure boundary comprising a lower containment vessel, an upper containment dome, and IHTS piping isolation valves for the IHXs.

7.3.1.3 The Modular High-Temperature Gas Reactor -- MHTGR

The MHTGR[7.13-15] is an advanced reactor concept based on design and operating experience with the HTGR in this country and in the FRG, using HTGR's basic features, namely: refractory-coated fuel particles retaining radionuclides at high temperatures; a graphite moderator with high heat capacity and structural stability at high temperatures; and a helium coolant which is inert, non-corrosive, and a single-phase gas under all operating and potential accident conditions.

The reference MHTGR plant consists of four 350-MWt (140-MWe) reactor modules cross-headered to feed superheated steam to two turbine generators operating in parallel in the energy conversion area (Fig. 7.19). Within the nuclear island each reactor module is housed in adjacent but separate reinforced concrete structures located below grade to reduce seismic amplification and to provide (a type of) containment. A reactor module consists of a reactor and a steam generator in separate cavities connected by a cross-duct. The reactor vessel is 21.9 m high and 6.8 m in diameter -- the size of a typical boiling water reactor vessel -- while the steam generator vessel is 4.2 m in diameter and 25.9 m high.

The core uses UCO fuel in 0.7-mm diameter fuel particles surrounded by three ceramic layers. The coated particles are mixed with a binder and formed into fuel rods that are placed in high-purity, high-density graphite fuel elements, with the graphite acting as moderator. The 60 fuel columns, comprising 660 prismatic fuel elements (hexagonal blocks 335 mm across flats and 787 cm long), which form the active core are in an annular region surrounded by inner and outer graphite reflectors and top and bottom reflectors. Six control rods are inserted in the inner reflector and 24 rods in the outer reflector. The average core power density is 5.9 MW/m^3; the equilibrium fuel burnup is 92,200 MWd/Mg. The heat transport system circulates 6.4 MPa helium through the primary loop with inlet and outlet temperatures of 295°C and 687°C, respectively. Helium flows through the hot duct in the cross duct through the helical bundle steam generator up the annulus between the steam generator vessel and the shroud to the main circulator (a single-stage axial compressor on top of the steam generator vessel) and back through the annulus in the connecting vessel and up the reactor vessel to the top plenum (Fig. 7.20).

The shutdown cooling system with its own circulator and heat exchanger is located at the bottom of the reactor vessel. Hot helium enters the shutdown heat exchanger through a shutoff valve. The shutdown circulator discharges the gas into a plenum at the bottom of the RV, and the gas returns to the core inlet plenum by way of the outer flow passage in the RV.

If neither the heat transport system nor the shutdown cooling system operates, the ultimate safety-grade decay heat removal system is the completely passive reactor cavity cooling system (RCCS). Heat is conducted from the active core, through the radial reflector blocks and reactor vessel walls by conduction and radiation to the RCCS. The latter consists of air cooling panels located on the inside surface of the reactor enclosure, rejecting heat to the atmosphere by natural circulation of outside air within the panels. There

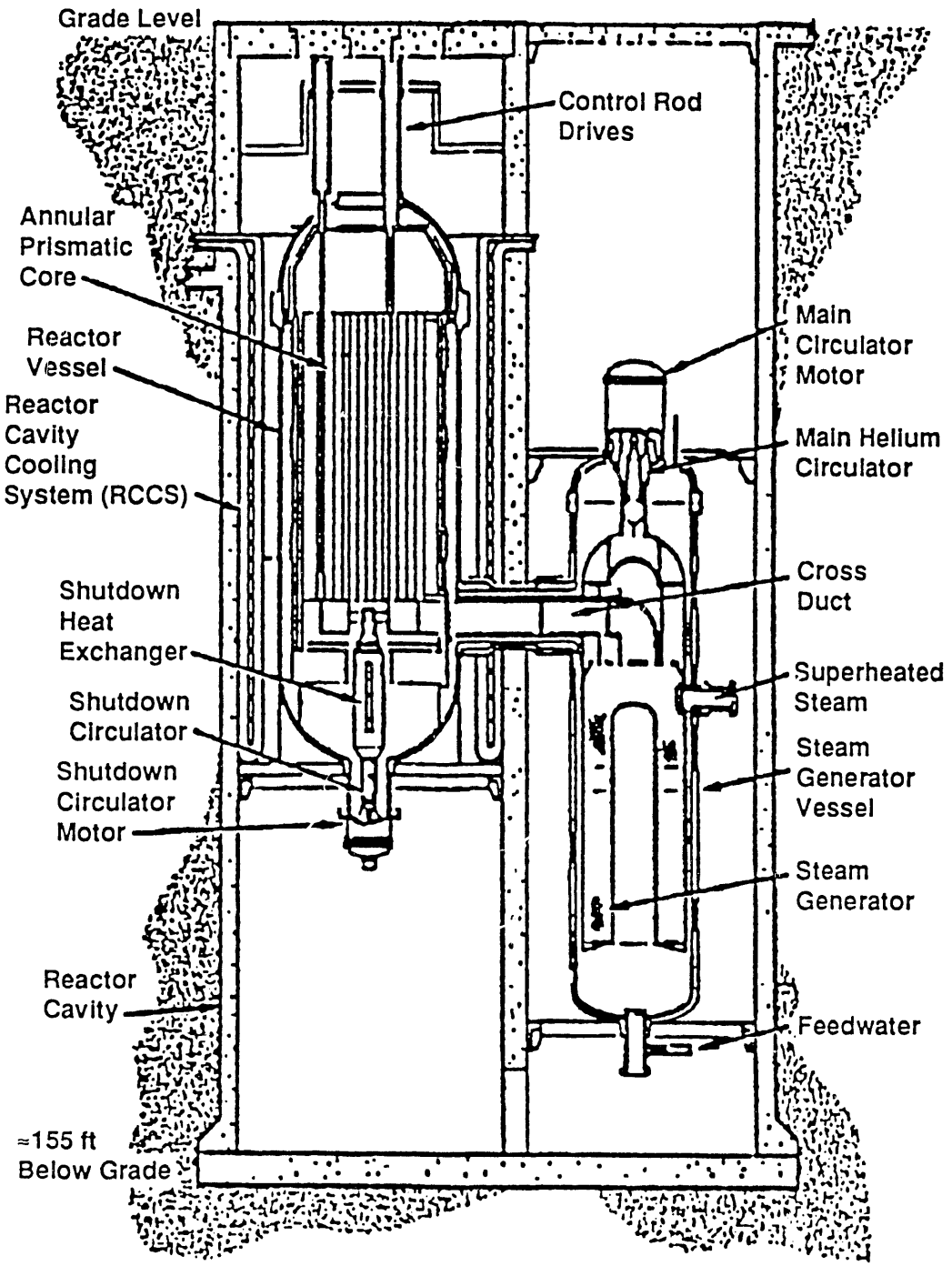

Figure 7.19. MHTGR reactor configuration.

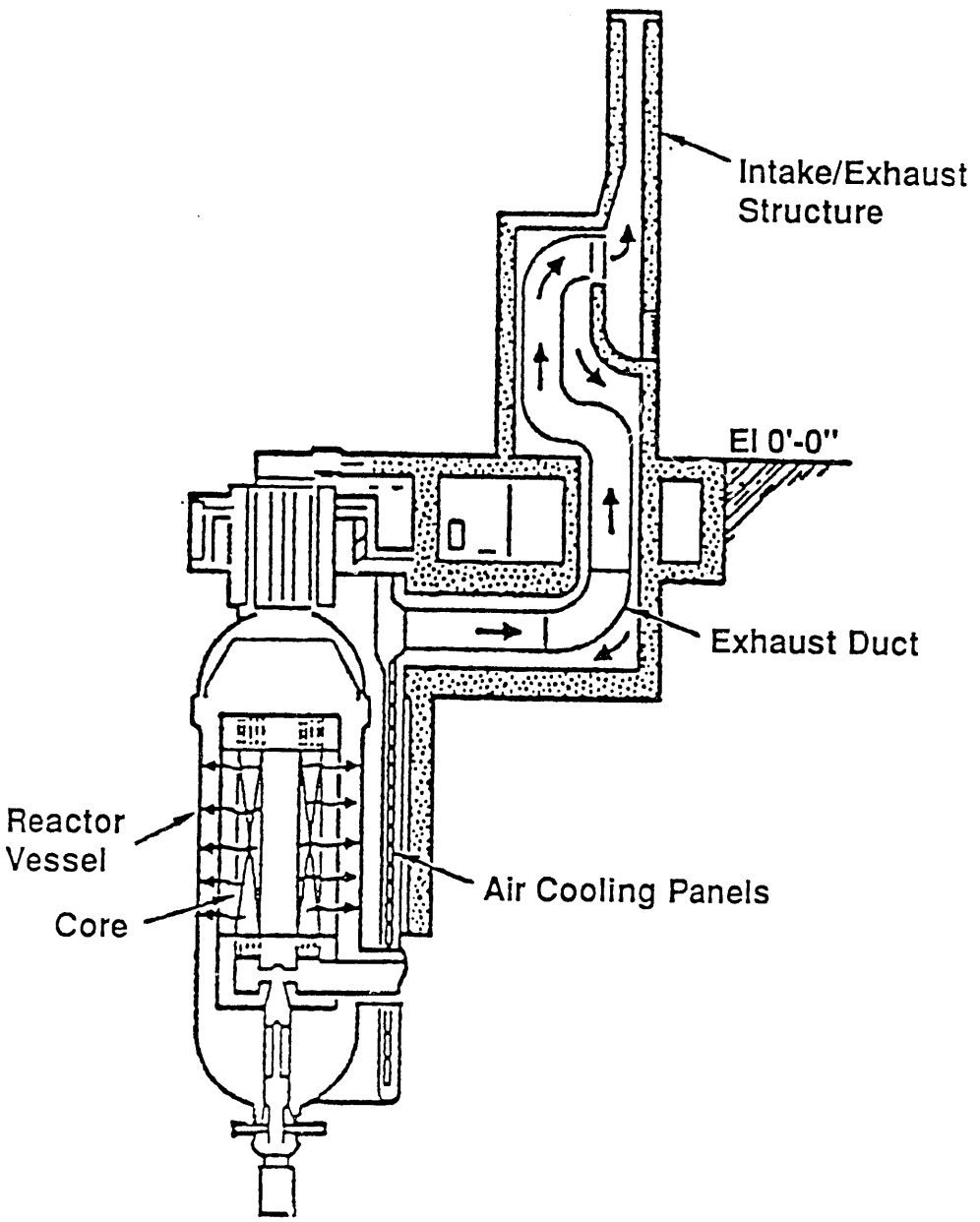

Figure 7.20. MHTGR coolant passages.

are no motors, valves, dampers or any other moving parts in the RCCS; it is self-activated whenever there is heat flow from the reactor vessel.

The safety characteristics of the MHTGR can be summarized as follows:

(1) Operational experience with the HTGR and experimental evidence show that refractory coated fuel particles of the MHTGR type can contain all significant fission products at temperatures as high as 1700°C.

(2) The core has an inherent negative temperature coefficient due to the strongly negative Doppler feedback coefficient.

(3) The graphite fuel elements and reactor structure have a high heat capacity and maintain their strength at temperatures beyond 2760°C. Temperature rises in the core following reactivity-insertion accidents or loss-of-core-cooling accidents occur very slowly (hours and days) and without damage to the core structure.

(4) Design core power levels and core power density are set at levels such that afterheat production cannot cause high fuel temperatures even if only passive cooling systems are in use. Estimates of the peak fuel temperature following a LOCA (depressurization without forced convection flow of the coolant) are well below 1600°C. The peak fuel temperature is about 1400°C when only the RCCS is operational. Even if the RCCS were to fail, heat transfer to structures surrounding the RV yields a peak temperature of around 1400°C (but for longer times).

(5) The high-temperature stability and slow heat up characteristics of the low power-density graphite reactor core yield a relatively forgiving reactor design, allowing many hours, even days, for operator corrective action.

7.3.2 General Safety Issues in the Case of Advanced Fission Reactors

As has been mentioned, the advanced fission reactor program in the U.S. comprises evolutionary LWR designs in the 1300 MWe range, and advanced designs in the 600 MWe range for light water, high-temperature gas-cooled, and liquid-metal reactors. The advanced reactors have lower power density and fuel rating, simplicity, and passive rather than engineered heat removal systems. Table 7.5 summarizes the reactor designs currently under review by the NRC.

There can be some question on how "advanced" some of the smaller reactor designs really are. For example the MHTGR can trace its lineage to very early gas-cooled reactors in Britain and France, and its designers emphasize that it uses well proven materials, fuel technology, and heat-removal solutions. Nevertheless, the evolutionary reactors represent much smaller variations on designs with a very large experience base and with well-developed analysis tools (transient codes and Probabilistic Risk Assessment, among others), so that safety issues for them are more traditional. Their improvements in engineered safeguards and in some few passive systems leading to claims of reduced core-damage frequency need to be reviewed in detail, but they raise no generic safety issues.

The situation with respect to the "new generation" of small, passively safe reactors is quite different. These are conceptual designs which, while rooted in the knowledge base of their reactor type, represent significant design innovations and departures from existing LWR, HTGR, and LMR types. They offer a challenge to reviewing bodies, as well as to public understanding, for two interrelated reasons.

Table 7.5. Future reactor designs.

	Designer	Size (MWe)
Evolutionary LWRs		
* Advanced Boiling Water Reactor (ABWR) (a)	General Electric	1356
* System 80+ (a)	Combustion Engineering	1270
* Standard Plant - 90 (SP / 90) (a)	Westinghouse	1350
Advanced LWRs		
* Advanced Passive - 600 (AP-600) (a)	Westinghouse	600
* Simplified Boiling Water Reactor (SBWR)	General Electric	600
* Safe Integral Reactor (SIR)	Combustion Engineering	320
* Process Inherent Ultimate Safety (PIUS)	ASEA Brown Boveri	600
Advanced Non-LWRs		
* Modular High-Temperature Gas-Cooled Reactor (MHTGR) (a)	General Atomics	137 per module
* Power Reactor Inherently Safe Module (PRISM) (a)	General Electric	138 per module
* CANDU-3	Atomic Energy of Canada Limited	450

(a) Currently under NRC review.

On the one hand, there has been confusion over the terms inherent safety and passive safety, although gradually the term inherent is being dropped in favor of "passive features that enhance the safety level of a component or system." There are inherent physical features affecting safety, such as Doppler-broadened resonances, but one could also argue that a nuclear reactor is "inherently" dangerous since it is a concentrated energy source with a high radioactive content. A passive safety feature is one that depends on natural phenomena such as convection, radiation, or gravity, without the intervention of mechanical or electrical components or operator action. The designers of advanced reactors seem, at present, to be emphasizing accident-prevention capabilities above accident-mitigation capabilities, in a departure from the traditional "defense in depth" policy which includes elements of both. Thus the PRISM and MHTGR designers propose to reduce the number of licensed operators in the multi-reactor power stations, to eliminate conventional containment, and to reduce significantly the number of "safety-related" plant systems -- i.e. those that require a full quality assurance program (as set out in 10CFR Part 50 Appendix B). In addition, several advanced designs have proposed the elimination of offsite emergency planning based on a calculated low probability of release of radioactive material. Since the NRC is requiring that future plants achieve a level of safety at least equivalent to present generation LWRs, the challenges posed by advanced designs to the "defense-in-depth" concept are of serious concern to regulatory agencies.

Any fission reactor, whatever its design, must be provided with reactivity control and shutdown provision, heat removal under operating and post-shutdown conditions, and barriers to the release of fission products. These requirements are met differently in the ALWR, the LMR, and the MHTGR, and some features of the inherent or passive systems for these reactors have been described previously.

Reactivity control is perhaps the most complex issue because various core components have different reactivity significance and temperature coefficients, and these change with the degree of burnup. Reactivity control over the full range of operational and transient upset conditions -- transient overpower (TOP), loss of flow (LOF), loss of heat sink (LOHS), reactor start up -- cannot be supplied by inherent reactivity feedbacks alone. In LMRs, moreover, core geometry changes are significant. While the reactivity feedbacks in metal fuel will bring the reactor safely to a lower power level, it is not certain that a configuration change would decrease reactivity both locally and globally. Each of the advanced designs has some capacity for passive reactor shutdown in the event of failure to scram, but the effectiveness of these mechanisms under a range of anticipated transients without scram (ATWS) is not fully demonstrated.

The advanced reactors discussed above, with low power densities in the core, have safety-grade shutdown (decay heat) removal systems which depend upon free convection heat transfer. This dependence on natural-circulation flows as a major heat transfer mechanism raises significant safety questions. On the one hand, predicted performance assumes integrity of the core and support structure, as well as flow passages, in a variety of possible accident scenarios. In addition, the thermo-hydrodynamic phenomena in natural convective flows in complex geometries with multiple flow paths are very difficult to model, calculate, or scale. The passive ultimate shutdown heat removal systems will require some demonstration, as the designs mature, before a final determination on licensing can be made.

The potential safety issues associated with advanced reactors are under continuing review by the NRC. The major safety issues of evolutionary reactor designs are those involving the treatment of severe accidents. In the case of the advanced LWR, LMR and MHTGR, specific safety questions have been raised by NRC staff and the ACRS -- for

example, the potential for large reactivity insertions in PRISM from sodium boiling and in the MHTGR from steam generator tube ruptures and control rod ejection; the vulnerability of the AP-600 to LOCA's; and the risk of fire in both graphite and sodium systems. Generic issues for advanced reactors such as the range of events/accidents to be considered, the satisfaction of "defense-in-depth" criteria, and the determination of appropriate emergency planning are currently being considered by the NRC. The interaction of regulators with the advanced reactor vendors will undoubtedly lead to design changes in the coming years as detailed technical safety issues are addressed. It is quite possible that the goal of eliminating all engineered safety features (ESFs), relying wholly on inherent or passive features to control neutronics and temperatures, eventually will be deemed unwise, and that the provision of redundancy, diversity, and independence in reactivity and heat removal control systems may lead to plants combining ESFs and passive systems. It would be unfortunate if a "rush to judgement" on small advanced reactors would prevent gaining the benefits that these potentially attractive energy systems might eventually provide.

7.3.3 Fusion Characteristics Relevant to Safety Comparisons With Fission

In recent years there has been increased attention to environmental and safety (ES) questions of MFE plants, since one of the main incentives for investing in the development of fusion energy is the prospect that the ES characteristics of fusion reactors will be more benign in fact, and in public perception, than those of fission and fossil fuels. Indeed, there are many in the energy field who feel that the only way that fusion can compete with a moving fission target, i.e. the advanced and passively safe reactors discussed above, is to realize to the full the potential ES advantages of fusion, namely:

- reduced radiological inventories,
- absence of supercriticality,
- reduced severe accident consequences,
- easier waste management,
- increased opportunities for passive safety (energies driving releases are low compared to fission and volumes and areas are large),
- easier licensing requirements,

All of these prospective advantages arguably need the adjective "possibly" before them. Assuring that fusion technology develops in ways that exploit its potential advantages is a major challenge and a difficult task for at least three reasons:

(1) A fusion power reactor is a complex nuclear, thermal, and chemical engineering system, important elements of which are not yet fixed in design.

(2) The data base for safety analyses is inadequate, and in some respects totally lacking.

(3) Physics and engineering problems for testing, demonstration, or commercialization of fusion reactors are so daunting that it is hard to focus the attention of designers and researchers on ES issues. This is changing as the technology matures, but it is still mainly true.

The earliest fusion ES assessments concentrated largely on tritium release in normal operation and accidents, and on the amount and nature of neutron activation products. These are still dominant issues, but, as MFE design and technology have evolved, the scope of attention has broadened to consider such topics as pathway and mobility estimates for radioactive material release, dose estimates, accident scenarios and phenomena, refined

hazard indices, studies on low-activation materials, and increased attention to passive safety schemes.

In a broad and general sense, the safety issues for fission and fusion reactors are the same. One needs to control the reaction (reactivity in the fission case, burn control in fusion) and the system temperatures for equilibrium heat removal, and to provide barriers to the release of radioactivity in normal operating and accident situations. The "source term", that is the nature, inventories, release fractions, and paths to the environment of radioactivity, is a central issue in both types of system.

There are, of course, significant differences in the nature and importance of these issues in fission and fusion which are directly related to the comparison of safety and environmental features of both. These will be apparent in the discussion to follow, but it is useful at this point to point up some major ES characteristics of fusion facilities, as compared to fission. These are:

(1) Tritium, distributed throughout a complex system, requires containment over a range of physical states from cryogenic fuel pellets to ions in the plasma.

(2) Plasma disruptions may cause large localized deposits of thermal and mechanical energy on major radioactivity barriers.

(3) Radioactivity is not caused mainly by the fusion process itself, in contrast to fission, but is produced by fast neutron interactions with various reactor materials and hence is controllable by careful selection of reactor materials.

(4) Some reactor designs entail a rather large inventory of chemical energy in breeder and/or neutron-multiplying materials, including the possibility of liquid-metal reactions differing in kind, contact modes, and environment from those studied in LMR fission reactors.

(5) Large amounts of energy will be stored in superconducting magnets, under high stress, located close to large inventories of radioactive material.

In what follows, we elaborate on some of the relevant issues, with particular reference to fusion reactor designs -- ITER and ARIES -- that have evolved since the time of the ESECOM study. (The ITER and ARIES designs were described above in Sections 6 and 7.1.)

7.3.3.1 Burn-Control and Emergency Shutdown

The projected design for ITER is such that its operating points are in temperature regions where the reaction is subject to thermal runaway because of the temperature dependence of the D-T cross-section. This thermal instability has the potential to cause violation of the beta limit and the limit on the neutron wall loading. Although it is possible in principle to operate in stable high-temperature, low-density regimes for most confinement scalings, and thus avoiding active burn control, these operating points are undesirable from the point of view of divertor conditions as well as proximity to plasma beta limit.

Among the methods suggested for controlling thermal instability are injection of high-Z impurities, controlling injected fuel, and modulating the external heating power in feedback response to measured ion or electron temperatures.

The modeling of burn control in fusion plasmas is a very difficult non-linear, spatially-dependent problem (e.g. edge transport phenomena are important), but progress on zero-dimensional dynamical particle and power balance ODEs has been made,[7.16] and some beginning treatment of spatially dependent stability[7.17] can be found in the literature.

If the burn-control system fails to stabilize a thermal excursion, or if there should be a failure in plasma-facing components, there may be need for an emergency plasma shutdown scheme. In a recent paper,[7.18] S.K. Ho et al. have examined candidate emergency shutdown schemes and the time scale requirements for them in reference to ITER. A fast shutdown by an induced disruption can place a large thermal and mechanical load on the wall and divertor in a short pulse. If one uses the methods mentioned above for control, without triggering a disruption, it is difficult to achieve passive safety because of the weak linkage between the plasma power and coolant and blanket failure modes. It is clear that more work needs to be done on desirable operating points and/or fast reactivity feedback mechanisms in possible accident situations for fusion reactors

7.3.3.2 Tritium

Tritium, either as HT gas or as HTO liquid and vapor is a highly mobile radioactive material, and it can be released in normal operation and certainly in many accident scenarios. Tritium exists in fusion reactors in a large interlinked system (about 15 subsystems in ITER, see Fig. 7.21) and numerous chemical engineering processes. Equipment consists of pumps and pipework, chemical reactors, cold traps, pellet injectors, and gas and liquid detritiation systems. As has been mentioned, considerable attention has been devoted to the tritium problem from the earliest fusion reactor designs, and a fairly large data and technology base exists from the Tritium Systems Test Assembly (TSTA) at LANL and the tritium processing laboratories at the JAERI in Japan and the DTRF in Canada. Safety system design is based on multiple barrier containment and redundancy of key components.

The tritium in a fusion reactor using the D-T reaction is in an "active" inventory in the systems mentioned above, and in a part kept in storage well confined and protected which is not usually considered in safety discussions. The amount of tritium in a fusion facility is very dependent on the design, and varies greatly from several hundred grams to several kilograms depending on the fractional burnup in the "core", the breeding multiplication in the blanket, and special features of the tritium processing and recovery systems.

The active tritium inventory estimated for ITER is shown in Table 7.6. The total of 4.3 kg-T shown there corresponds (at tritium specific activity of 9700 Ci/gm) to an activity of 42 MCi; (an average LWR contains about 10,000 MCi of total radioactivity). The 50-year effective dose equivalent (EDE) to the maximum exposed individual at a distance of 1 km assuming T as HTO is calculated to be 0.50 mSv/gm-T. Thus, even if 85% of the ITER active tritium inventory were to be released in an accident (an extremely unlikely scenario), the 2 Sv critical-dose threshold for fatalities from acute radiation syndrome would not be exceeded.

Tritium can escape in normal operation from diffusion through high temperature structures and under accident situations in losses from various subsystems. There are several existent codes for time-dependent, multiple-compartment tritium inventory

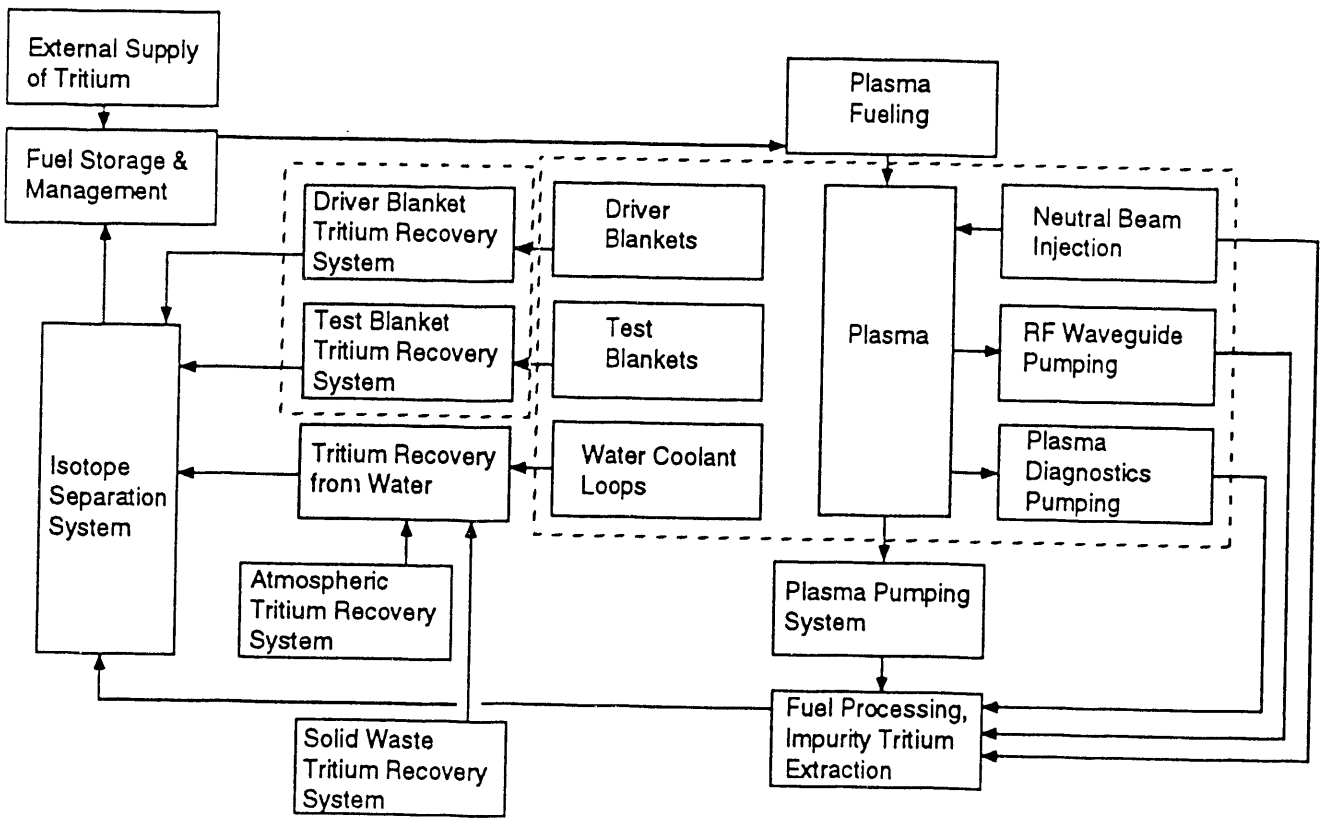

Figure 7.21. ITER fuel cycle diagram.

Table 7.6 Safety assessment for technology-phase tritium.

Pathway and System	Inventory (g)	Maximum Mobility Fraction	Confinement Release Fraction	Dose (mSv)	Uncertainty Factors (a)
GROUP 1 - Tritium Inventories in Tritium Processing Systems					
Backing pumps	487	100%	2%	4.87	2/30
Fuel processing	210	1%	2%	0.02	50/2
Isotope separation	430	100%	2%	4.30	2/3
Atmosphere process	30	1%	2%	0.00	2/20
Water detritiation	40	10%	2%	0.04	2/8
* Pellet injector	160	100%	2%	1.60	2/7
* Gas puffing	100	100%	2%	1.00	2/8
* NBI lines	10	100%	2%	0.10	2/2
* Breeder H3 recovery	160	100%	2%	1.60	2/20
PROCESS INVENTORIES	1627			13.5	2/5
GROUP 2 - Tritium Conponents inContact with the Torus					
PFC - W surface	220	10%	2%	0.22	200/200
Cold PFC dust	100	100%	2%	1.00	20/20
Primary vacuum pumps	150	100%	2%	1.50	2/300
DIV water coolant	35	30%	2%	0.11	2/2
* FW water coolant	35	30%	2%	0.11	2/2
* Pellet injector	160	100%	2%	1.60	2/7
* Gas puffing	100	100%	2%	1.00	2/8
* NBI lines	10	100%	2%	0.10	2/2
TORUS INVENTORIES	810			5.60	10/10
GROUP 3 - Tritium Inventories Associated with Blanket Systems					
Solid Breeder	14	10%	2%	0.01	2/5
Beryllium mulitplier	1200	1%	2%	0.12	200/20
Blanket water coolant	1	30%	2%	0.00	2/2
* Breeder H3 recovery	160	100%	2%	1.60	2/20
* FW water coolant	35	30%	2%	0.11	2/2
BLANKET INVENTORIES	1409			1.8	10/10
GROUP 4 - Isolated Inventories (not to be added together)					
Solid waste recovery	180	10%	2%	0.18	2/4
Carbon processing	100	10%	2%	0.10	2/20
Long-term fuel storage	600	1%	2%	0.06	2/4

TOTAL TRITIUM INVENTORY (no scenario would release all of this): 4.3 kg-T

(a) The uncertainty factors are for the maximum dose estimate where the first is upward and the second is downward. For example, the reference dose from primary vacuum pump is 1.5 mSv whereas the actual dose might be two times higher or 300 times lower.

calculations which are useful in analyzing breeding ratios and burnup fractions. Much remains to be done, however, in modeling failure modes in various parts of the overall system and in predicting their effects on tritium releases in accident situations. The complexity of the tritium processing and delivery system and its physical spread-out over the total fusion system renders analysis difficult even in normal operating modes, but especially with component failures.

7.3.3.3 Thermal Transients and Accident Scenarios

As with fission reactors, the control of system temperatures by maintaining the balance:

power = cooling = heat sink

is a central issue in fusion reactor safety. The cooling portion of this thermal balance can be disturbed by two major mechanisms. Loss of cooling transients can arise due to LOFA or LOCA. In a LOFA, the coolant for heat removal from the blanket or divertor by forced convection stops flowing either because of failure of coolant pumps or because of flow blockage possible due to structural failure. A LOCA can arise if there is a rupture in the coolant piping allowing the coolant to leak out of the system.

The local definition of power in the above balance is not simple. On the one hand there is the plasma power and associated heat flux on the divertor and first wall and the power density from neutron and gamma interactions within the plasma-facing components. On the other, there is the decay heat of radioactive isotopes formed in the structure and especially in the blanket by neutron activation.

Clearly the system temperature will rise if the plasma power increases without a corresponding increase in cooling rate or if the plasma continues to burn after cooling is lost. The decay heat source is relatively small compared to the plasma heat flux on the surface of the first wall, but it needs to be considered (at least for short times after shutdown) in certain accidents.

The accident scenarios that are currently considered in ARIES or ITER design studies are:

(1) a major rupture of the divertor or first wall cooling pipes, causing a LOCA inside the vacuum vessel;
(2) a LOCA in the cooling system outside the vacuum vessel, due, for example, to rupture of blanket cooling pipes;
(3) a LOFA in the first wall cooling system inside and outside the vacuum vessel and/or in the blanket piping;
(4) a major failure of vacuum vessel elements (e.g. heating and fueling devices) leading to a loss-of-vacuum accident (LOVA).

It is generally conceded today that, although the entire blanket is important, the plasma-facing components play an especially key role in fusion reactor designs because they have large radioactive inventories, large mobilizable fractions, and important accident initiators. These components include the first wall, divertor, RF antennae, the microwave launchers, and the diagnostic equipment. They are exposed during routine operation to the most intense neutron fluxes and heat loads in the reactor; under accident conditions they are especially vulnerable to the effects of plasma disruption, severe temperature transients, pressurization of the vacuum vessel, and chemical reactions (such as water-metal and carbon-steam), with possible release of tritium and activation products.

Although most major safety issues are associated with the plasma-facing components and potential loss of integrity of the vacuum vessel, quantitative studies of thermal transients have until now[7.19] mainly focussed on the blanket, perhaps because thermal-hydraulic phenomena there lend themselves more easily to traditional heat transfer analyses.

In any case, the study of possible accident scenarios, and the ranking of accidents in terms of frequency and consequences, is still in early stages in fusion reactor design. Probabilistic risk assessment (PRA), so important in fission reactor safety considerations, is still of only limited usefulness in the present fluid state of fusion reactor design (see Section 5) and it may be assumed that some potentially important accident scenarios have not been identified, not to mention thoroughly analyzed.

7.3.3.4 Radioactivation Inventory

An important first step in the estimation of the "source term" for fusion reactors is the calculation of the inventory of radioactivity induced by neutron activation which is added to the tritium burden.

A fundamental difference between fission and fusion is that, in the latter case, the radioactivity is not caused mainly by the fusion reaction itself (except for tritium produced by D-D reactions) but is produced by fast neutron interactions with various reactor materials. This means that the induced radioactivity can in principle be controlled by careful selection of these materials, and the realization that materials tailoring could lead to significant benefits has led to numerous studies of low-activation materials.[7.20-22]

Materials selection to reduce radioactivation can reap benefits in reactor maintenance, normal effluent and accident releases, decay heat generation, decommissioning, and waste disposal.

For a given design, calculation of the induced radioactivities is straightforward in principle, involving neutron transport calculations and isotope balance equations. But it is difficult in practice, because the many possible reactions for high-energy neutrons require large nuclear data libraries with significant data-handling problems.

There are several examples of codes that calculate radioactivity inventories but a recent comparative study of these with the same inputs of spectra and initial compositions has revealed considerable discrepancies in calculated results from international groups using their own codes and data libraries.[7.23] It is not yet clear which differences are due to differences in activation libraries and which ones arise from differences in methods of solution of the neutron and isotope equations.

7.3.3.5 Magnet System Safety

The magnet system (TF coils, PF coils, power supplies and the cryogenic system) is generally considered of lesser importance to safety, since it does not contain significant radioactive inventories compared to other elements of the fusion system. On the other hand, the large energy inventory of the magnets is a potential accident initiator, and the proximity of the magnet coils to the vacuum vessel needs to be considered.

The fault conditions for the TF and PF magnets are coil quench, loss of coolant, loss of power, and loss of cryostat vacuum. The toroidal field coils have the highest stored magnetic energy and also the greatest possibility of interaction with the vacuum vessel. There are very large forces on the TF magnet, and its structural integrity is related to detailed features of the central vault design.

Although the fault analysis of fusion magnet systems is only in its beginning stages, magnet experts in both the ARIES and the ITER projects seem confident of their ability to design magnet systems resistant to failure under normal and transient conditions.

7.3.4 Influence of Advanced Fission Designs on Fission-Fusion Comparison

We turn now to the question raised in the introduction to this section, namely whether the development of "next generation" "passively safe" fission reactors significantly affects the comparisons on ES issues in the ESECOM report. We discuss this under several headings.

7.3.4.1 Radioactive Inventory

The actinides and fission product production in fission reactors are inherent in the fission reaction and are not strongly affected by neutron spectrum or the details of core design. They have nothing to do directly with passive safety features. The production of fission product radioactivity is proportional to reactor power, but it is intended to site modular low-power advanced reactors together.

The induced radioactivity in coolant and structure does depend on the design details of fission reactors, and while this issue is significant for occupational exposures it is not important in major accident releases.

We conclude that the results of the comparison of fission and fusion with respect to the advantage of fusion in critical threshold-dose release fractions remain valid whether one opens up the comparison to advanced fission reactors or not.

7.3.4.2 Barriers to a Major Release of Radioactivity

The actinide and fission product radioactivity in fission reactors is physically concentrated in the fuel elements, with multiple barriers to the environment. The smaller induced radioactivity in the coolant is, of course, more dispersed. The passive safety features and lower power density of advanced fission reactors will contribute significantly to protecting the integrity of fission reactor radioactivity barriers in the core and throughout the plant.

The activation radioactivity in fusion reactors, although physically more dispersed than the fission products and actinide inventory in fission reactors, is still fairly concentrated close to the plasma-facing component. The integrity of plasma-facing components in accident scenarios involving initiators driven by plasma, chemical, and/or magnetic energy, however, is still being investigated in major design efforts such as ITER and ARIES.

The barriers to the release of tritium are multiple and widely dispersed. The physical spread of tritium leakage sources has been mentioned previously. It is a major design

problem, especially in terms of routine releases and the radioactive burden to which plant workers may be exposed.

7.3.4.3 Thermal Safety Issues

Advanced fission reactors can claim greater safety over existing designs largely because of passive safety features concerning heat removal from the core, at power and for decay heat removal. These heat removal processes have a greater margin of safety for cores with low power density. This is true because the time before mitigating action must be taken is extended, and because the reactor can remove decay heat by natural convection rather than by forced cooling. The calculational techniques for thermal reactors are well developed, with large codes for PWR, BWR, and LMR thermal transients. These are being applied in the advanced reactor designs with submissions to regulatory bodies such as the NRC.

Thermal analysis of fusion reactor designs is naturally less advanced, because details of divertor design and first wall and blanket are still being developed. LOFA and LOCA analyses were carried out by Kazimi et al.[7.19] for ESECOM fusion blanket variants with some consideration of the contribution to temperature rise from lithium fires.

The divertor plate design for ITER as now proposed consists of carbon fiber composite with copper or molybdenum tubes brazed to the composite. Tests are underway to assess the heat removal and burn-out limits of this design. The performance of the first wall and divertor has been analyzed for ITER under steady conditions using the FLIP code showing burnout heat fluxes for the divertor of 15 MW/m^2 and a limit for fatigue cracking of about 11 MW/m^2. Heat deposition on the first wall is a maximum of 0.6 MW/m^2 with, in the case of localized disruptions, energy disposition of about 2 MJ/m^2 in 0.1-0.3 milliseconds. Runaway electrons with energies up to 300 MeV may impinge locally on the walls. Study of the divertor heat load under transient conditions is still in the beginning stages. It is generally conceded that the divertor presents very difficult design compromises in thermal, strength and plasma physics issues.

The LOCA and LOFA analyses that have been done on ITER blanket designs have not shown significant differences over the previous results. There is a current tendency to reduce performance requirements on the ITER blanket for safety, lowering the coolant temperature and reducing the breeding ratio to less than unity. The blanket, however, is of secondary importance to plasma-facing components, whose thermal analysis especially under transients (accident or cycling) is still rudimentary.

7.3.4.4 Levels of Safety Assurance

Lawrence Lidsky of MIT originally proposed the concept of levels of safety[7.24] for fission reactors based on a four-level qualitative scale, and this has been taken up by S.J. Piet[7.25] and by J. Holdren et al. in the ESECOM report. The levels in broad terms are:

1 = Fatal release precluded under all conceivable conditions by radioactive inventories, energy sources and materials properties (inherent safety).

2 = Safety assured by passive mechanisms of release limitation which are immune to major structural failure and operator error; system coolant and material boundaries remain intact under all conditions (complete passive safety).

3 = Not immune to major structural failure or operator error, but no need for active systems in the event of subsystem failure; safety assured by passive mechanisms of release limitation as long as coolant boundaries are substantially intact (qualified passive safety).

4 = Not immune to major structural failure; active safety systems required in response to subsystem malfunction, boundary violations or reconfigurations (engineered safety).

The authors of the ESECOM report assigned LSA values to the fourteen cases examined in that study -- eight fusion, four fission, and two fusion-fission hybrid -- based on consideration of the dose potentials represented by the reactor inventories of radioactivity, the inherent and engineered barriers to release these inventories, and the combinations of stored energies and pathways for their release through which these barriers plausibly could be breached. "Nominal," "optimistic," and "conservative" LSA evaluations were made for each design, although in some cases two or all three of these ended up with the same value. The "nominal" estimates ranged from 1 to 4 for the fusion cases; they were 4 for the fusion-fission hybrids and the PWR and LSPB fission reactors, and 3 for the two advanced fission designs -- the PRISM breeder and the MHTGR.

Such LSA assignments are necessarily judgmental and therefore arguable at the margins -- that is, between 1 and 2, between 2 and 3, and between 3 and 4 -- and the uncertainties about them are all the greater in the case of fusion reactor designs that, because of their preliminary and incomplete character, cannot be as well understood in terms of either strengths or weaknesses as are fission designs that have been built or are closely related to designs that have. It seems likely to us that application of the ESECOM mode of analysis to today's advanced fission reactor designs would, as before, yield "nominal" LSA evaluations of 3 and "conservative" evaluations of 4; application of this mode of analysis to the ARIES-I advanced fusion reactor design might yield a "nominal" value of 2 and a "conservative" one of 3; but we have not done enough work of our own with any of these designs to put much weight on these values.

The extensive safety analysis by the ITER team on the conceptual design for that experimental fusion reactor did not specify an LSA value, but our reading of the ITER safety assessments suggests that the ESECOM mode of LSA analysis probably would produce a 3 for the "nominal" evaluation and a 4 for the "conservative" one. It is widely agreed that the current ITER design does not fully exploit the potential of fusion for reducing radiological accident hazards.

Comparing accident-hazard characteristics of fusion and fission reactors with more confidence will require better data on the behavior of fusion-reactor materials and components under accident conditions (above all, more data on the mobility of fusion radioisotopes under these conditions), more systematic study and characterization of the mechanisms by which accidents could occur in fusion reactors, and continuing study of accident mechanisms in evolving fission reactor designs, as well. Whether characterization of reactor designs in terms of LSAs can be made sufficiently systematic and unambiguous to be very useful in this effort (perhaps through refinement in the LSA concept itself as well as in the data and analysis underlying assignment of values) is still, in our view, an open question -- to which we hope to be able to give some attention in the next phase of this work.

Reference

7.1. S.K. Ho, "An Estimation of Radiological Hazards of Current Tokamak Reactor Concepts," Proc. 13th Symp. Fusion Engineering, Knoxville, Tennessee, (1989).

7.2. F. Najmabadi and R.W. Conn, et al., "The ARIES Tokamak Reactor Study," Proc. 13th Symp. Fusion Engineering, Knoxville, Tennessee, (1989).

7.3. J.P. Holdren, D.H. Berwald, R.J. Budnitz, J.G. Crocker, J.G. Delene, R.D. Endicott, M.S. Kazimi, R.A. Krakowski, B.G. Logan, and K.R. Schultz, "Exploring the Competitive Potential of Magnetic Fusion Energy: The Interaction of Economics with Safety and Environmental Characteristics," Fusion Technol. **13**, 7 (1988).

7.4. E.F. Plechaty and J.R. Kimlinger, "TARTNP: A Coupled Neutron-Photon Monte Carlo Transport Code," Lawrence Livermore National Laboratory, Report UCRL-50400 (1976).

7.5. J.A. Blink, R.E. Dye, and J.R. Kimlinger, "ORLIB: A Computer Code that Produces One-Energy-Group, Time- and Spatially Averaged Neutron Cross Sections," Lawrence Livermore National Laboratory, UCRL-53262 (1981).

7.6. J.A. Blink, "ORLIB: A Computer Code for Calculating Radionuclides Generation and Depletion in Fusion and Fission Reactors," Lawrence Livermore National Laboratory, UCRL-53633 (1981).

7.7. S.A. Fetter, "Radiological Hazards of Fusion Reactors: Models and Comparisons," PhD Thesis, University of California, Berkeley (1985).

7.8. D.R. Wilkins, "G.E. Advanced Boiling Water Reactors," Proc. American Power Conference, Chicago, April 23-25 1990.

7.9. S.N. Tower, T.L Schultz, and R.P. Vijuk, "Passive and Simplified System Features for the Advanced Westinghouse 600 MWe PWR," Nuclear Engineering and Design **109**, 147 (1988).

7.10. J.D. Duncan, "SBWR, A Simplified Boiling Water Reactor," Nuclear Engineering and Design **109**, 73 (1988).

7.11. L.N. Salerno and R.C. Berglund et al., "PRISM Concept, Modular LMR Reactors," Nuclear Engineering and Design **109**, 79 (1988).

7.12. G.L. Gyorey, R.W. Hardy, and P.M.Magere, "Safety Design for the Advanced Liquid-Metal-Cooled Reactor," Nuclear Safety **31**, 323 (1990).

7.13. A.J. Neylan, D.V. Graf, and A. C. Millunzi, "The Modular High Temperature Gas Cooled Reactor (MHTGR) in the U.S.," Nuclear Engineering and Design **109**, 99 (1988).

7.14. F.A. Silady and L.L. Parme, "The Safety Approach of the Modular High-Temperature Gas-Cooled Reactor (MHTGR)," Energy **16**, 407 (1991).

7.15. P.R. Kasten, "The Safety of Modular High-Temperature Gas-Cooled Reactors," Energy **16**, 359 (1991).

7.16. J. Mandrekas and W.M. Stacey Jr., "Evaluation of Different Control Methods for the Thermal Stability of the International Thermonuclear Experimental Reactor," Fusion Technol. **19**, 57 (1991).

7.17. W.A. Houlberg and R.W. Conn, "Space-Dependent Thermal Stability of Reacting Tokamak Plasmas," Nuclear Fusion **19**, 81 (1979).

7.18. S.K. Ho., L.J. Perkins, S.W. Haney, and R.B. Campbell, "Assessment of Emergency Plasma Shutdown Schemes for ITER," Fusion Technol. **19**, 1322 (1991).

7.19. J.E. Massidda and M.S. Kazimi, "Thermal Design Considerations for Passive Safety of Fusion Reactors," MIT Plasma Fusion Center Report PFC/RR-87-18, October 1987.

7.20. S.J. Piet, E.T. Cheng, S. Fetter, and J.S. Herring, "Initial Integration of Accident, Safety, Waste Management, Effluents and Maintenance Considerations for Low-Activation Materials," Fusion Technol. **19**, 148 (1991).

7.21. R.W. Conn, et al., "Lower Activation Materials and Magnetic Fusion Reactors," Nuclear Technol./Fusion **5**, 291 (1984).

7.22. G.J. Butterworth, "Low Activation Structural Materials for Fusion," Fusion Engineering Design **11**, 231 (1989).

7.23. E.T. Cheng, et al, "International Fusion Activation Calculation Comparison Study," TSI Research Report TSIR-12, Solana Beach, CA., Jan. 1991.

7.24. L. Lidsky, "Safe Nuclear Power," The New Republic, Dec 18, 1987.

7.25. S.J. Piet, "Approaches to Achieving Inherently Safe Fusion Power Plants," Fusion Technol. **10**, 7 (1986).

8. PROGRAM INTERACTIONS

The Berkeley Fusion Environmental and Safety Group maintains close coordinations with the ITER and ARIES projects.

Contact with ITER has been sustained through the Lawrence Livermore National Laboratory (LLNL). Dr. L. John Perkins at LLNL, active in ITER systems analysis, is a regular participant in our group meetings, and Dr. Shu K. Ho in our group regularly attends informal ITER meetings at LLNL. Dr. Ho has participated in plasma burn control and emergency shutdown studies for ITER through LLNL and he attended the workshop on this subject in Garching in July 1990. Prof. Fowler was a member of the ITER Scientific and Technical Advisory Committee (ISTAC) during the three-year Conceptual Design Activity (CDA). Prof. Holdren participated in the U.S. review of the CDA Final Report and is a member of the Secretary of Energy's Fusion Energy Advisory Committee. He also has been a regular participant in the workshops of the Technical Committee on Fusion Reactor Safety of the International Atomic Energy Agency.

Contact with ARIES has been maintained by the regular participation of Dr. Ho in ARIES bi-monthly meetings. He is a contributing author to the ARIES-I and ARIES-III reports. He has performed comprehensive calculations of radioactive inventories and radiological hazard indices for an ARIES-I-like design candidate, including a comparison of environmental and safety aspects of that design with ESECOM cases. Through such studies, we have gained much experience in executing our computational tools and in comprehending the impacts of environmental and safety on fusion reactor design.

In addition, the principal investigators have maintained a strong interest in the environmental and safety aspects of fusion development through activities not funded by the contract. For example, Prof. Holdren served as a consultant to the Fusion Program Directorate of the European Community on fusion environmental and safety matters during the period of new fusion policy formulation in 1989-90, and Prof. Fowler presented an invited paper on environmental and safety aspects of ITER at the OECD conference on energy and greenhouse gases in Paris, 1989.

9. PUBLICATIONS AND THESES

9.1 THESES COMPLETED

1. Dimosthenis Sarigiannis, "Dynamic Simulation of the Tritium Inventory in a Fusion Power Plant," M.S. Thesis, Energy and Resources Group, University of California, Berkeley, December 1990.

2. Paul J. Hibbard, "The Display of Fusion-Reactor Radiological Hazards," M.S. Thesis, Energy and Resources Group, University of California, Berkeley, December 1990.

9.2 PAPERS AND REPORTS

1. T.K. Fowler, "Fusion Power: Expected Environmental Characterisitcs and Status of R&D," Proceedings of IEA/OECD Experts Seminar on Energy Technologies for Reducing Greenhouse Gases, Paris, April 12-14, 1989; and UCRL-100623 Preprint, March 24, 1989.

2. "Status Report -- Code Development Incorporating Environmental, Safety, and Economic Aspects of Fusion Reactors," Report UC-BFE-001, University of California, Berkeley, April 1989.

3. J.P. Holdren and T.K. Fowler, "Fusion's Future" (Letter to the Editor), Scientific American, Vol. 260, No. 5, pp 8-9, May 1989.

4. John P. Holdren, "Safety, Environment, and Licensing Issues for Fusion Energy: An Overview," Working Paper for the U.S. Submission to the International Fusion Research Council, Energy and Resources Group, University of California, Berkeley, May 1989. Revised version accepted October 1990 for publication in Annual Review of Energy.

5. R.W. Conn, J.P. Holdren, S. Sharafat, and D. Steiner, et al., " Economic, Safety, and Environmental Prospects of Fusion Reactors," U.S. Submission to the International Fusion Research Council, August 1989; Nucl. Fusion **30**, 1919 (1990).

6. W. Kozukue, Y. Chiba, and L. Grossman, "The Fusion Reactor Design and Cost Calculation Code GENEROMAK," Report UC-BFE-004, University of California, Berkeley, October 1989.

7. "Status Report -- Code Development Incorporating Environmental, Safety, and Economic Aspects of Fusion Reactors," Report UC-BFE-006, University of California, Berkeley, October 1989.

8. S.K. Ho, "An Estimation of Radiological Hazards of Current Tokamak Reactor Concepts," Proc. 13th Symp. Fusion Engineering, Knoxville, Tennessee, IEEE Catalog No. 89CH2820-9, (1989).

9. E. Greenspan and S.K. Ho, "Blanket Energy Multiplication Enhancement without Afterheat Safety Hazards," Proc. 13th Symp. Fusion Engineering, Knoxville, Tennessee, IEEE Catalog No. 89CH2820-9, (1989).

10. John P. Holdren, "Comments on 'Environmental, Safety-Related, and Economic Potential of Fusion Power' (Report of the EEF Study Group, Commission of the European Economic Communities, December 1989)," Manuscript report to the Office of Fusion Energy, U.S. Department of Energy, January 1990.

11. "Status Report -- Code Development Incorporating Environmental, Safety, and Economic Aspects of Fusion Reactors," Report UC-BFE-009, University of California, Berkeley, April 1990.

12. S.K. Ho and L.J. Perkins, "Operating Point Control, Fractional Power Operation, and Sensitivity to Confinement Assumptions," ITER Plasma Operational Control Workshop, Garching, FRG, July 1990.

13. R.B. Campbell, L.J. Perkins, S.W. Haney, and S.K. Ho, "Emergency Shutdown Control and Implications for ITER," ITER Plasma Operational Control Workshop, Garching, FRG, July 1990.

14. John P. Holdren, Invited testimony on "Nuclear Fusion" for the Committee on Research of the German Bundestag, September 19, 1990.

15. S.K. Ho and L.J. Perkins, "Plasma Operating Point Control for ITER," Bull. Am. Phys. Soc. **35**, 1923 (1990).

16. K. Borrass, et al., "Plasma Operation Control in ITER," 13th International Conference on Plasma Physics and Controlled Nuclear Fusion Research. International Atomic Energy Agency, IAEA-CN-53/F-3-6, Washington, D.C. (1990).

17. "Status Report -- Code Development Incorporating Environmental, Safety, and Economic Aspects of Fusion Reactors," Report UC-BFE-016, University of California, Berkeley, November 1990.

18. S.K. Ho, "Empirical Formula to Evaluate Activation Radioactivity for Various First Wall Designs of A Fusion Reactor," Fusion Technol. **19**, 1368 (1981).

19. S.K. Ho, R.B. Campbell, L.J. Perkins, and S.W.Haney, "Assessment of Emergency Plasma Shutdown Schemes for ITER," Fusion Technol. **19**, 1322 (1981).

20. L.J. Perkins, H.W. Haney, S.K. Ho, and J. Mandrekas, "US Burn Control Studies for the International Thermonuclear Experimental Reactor (ITER)," Lawrence Livermore National Laboratory, UCRL-ID-105546 (1991).

21. S.K. Ho, T.K. Fowler, L.M. Grossman, and J.P. Holdren, "Modeling of Fusion Reactor Environmental and Safety Aspects," Trans. Am. Nucl. Soc. **63**, 104 (1991).

22. D.E. Baldwin, J.L. Anderson, C.C. Baker, R.J. Briggs, D.L. Cook, J.P. Holdren, J.L. Luxon, D.B. Montgomery, G.A. Navratil, R.R. Parker, F.A. Puhn, P. Rutherford, J. Sheffield, W.M. Stacey, K.I. Thomassen, and A. Glass, "Report of the U.S. National ITER-CDA Design Review," U.S. ITER Review Panel Report, March 1991.

23. "Status Report -- Code Development Incorporating Environmental, Safety, and Economic Aspects of Fusion Reactors," Report UC-BFE-024, University of California, Berkeley, May 1991.

24. D. Sarigiannis, "Dynamic Simulation of Tritium Processing Systems in Magnetic Fusion Reactors," 22th Symp. of the Working Party on Use of Computers in Chemical Engineering, European Federation of Chemical Engineering, Barcelona, Spain, October 1991.

END

DATE FILMED

01/27/92